Multi-Messenger Signals from Stellar Evolution

by

Ebraheem Farag

A Dissertation Presented in Partial Fulfillment
of the Requirement for the Degree
Doctor of Philosophy

Approved May 2024 by the
Graduate Supervisory Committee:

F.X. Timmes, Chair
Patrick Young
Michael Line
Evgenya Shkolnik
Steven Desch

ARIZONA STATE UNIVERSITY

August 2024

ABSTRACT

Stars generate a variety of multi-messenger signals throughout their evolution. They radiate photons from their stellar surface, neutrinos from their interior, and recently-discovered gravitational waves during binary mergers. These signals give us important clues about the composition, nuclear physics, and energy transport in stellar interiors, enabling us to constrain the efficiency of convection, strength of nuclear reactions, and the ultimate structure of white dwarf and pre-supernova stars. In this thesis, I focus on analyzing the multi-messenger signals produced during or as a result of stellar evolution. I evolve thousands of stellar models of low-mass and high-mass stars to their final fate and explore how global features of stellar evolution are reflected in their multi-messenger signals. I present a novel method for analyzing stellar neutrino emission in a neutrino Hertzsprung-Russell diagram. I then discuss neutrino emissions from stars of all masses and metallicities to provide stellar targets for current and forthcoming neutrino detectors. I also discuss the evolution of the most massive stars which result in pair-instability supernovae and make predictions for the black hole (BH) mass spectrum. These predictions are currently being probed with gravitational wave detections of merging binary BHs by the LIGO/VIRGO/KAGRA collaboration. I then show how these gravitational wave signals can be used to constrain the most uncertain nuclear reaction rates in all of astrophysics: the $^{12}C(\alpha,\gamma)^{16}O$ and triple-α helium burning nuclear reactions which set the C and O composition of the cosmos.

DEDICATION

To my family, friends, colleagues, and advisor F.X. Timmes.

ACKNOWLEDGEMENTS

I'd like to thank everyone in my life who has supported me.

The research in chapter 2 and 4 was supported by the National Science Foundation (NSF) under grant PHY-1430152 for the "Joint Institute for Nuclear Astrophysics - Center for the Evolution of the Elements", and by the NSF under the Software Infrastructure for Sustained Innovation grants ACI-1663684, ACI-1663688, and ACI-1663696 for the `MESA` Project. This research in chapter 3 is supported by the National Science Foundation (NSF) under grant 2154339 entitled "Neutrino Emission From Stars".

I would like to personally thank Thomas Steindal for his helpful discussions throughout my academic career. I'd like to thank James Deboer for sharing the $^{12}C(\alpha, \gamma)^{16}O$ probability distribution function.

I acknowledge using ChatGPT (OpenAI, 2023) to polish the language of one paragraph (Vishniac, 2023) in Chapter 4.This thesis made extensive use of the SAO/NASA Astrophysics Data System (ADS).

TABLE OF CONTENTS

CHAPTER Page

LIST OF TABLES

LIST OF FIGURES

Figure Page

Figure Page

Figure Page

Figure Page

Figure Page

Figure Page

Chapter 1

INTRODUCTION

1.1 Overview

"*The lives and deaths of the stars seem impossibly remote from human experience, and yet we are related in the most intimate way to their life cycles. The very matter that makes us up was generated long ago and far away in red giant stars…The nitrogen in our DNA, the calcium in our teeth, the iron in our blood, the carbon in our apple pies were made in the interiors of collapsing stars. We are made of star stuff*" (Carl Sagan).

Understanding the composition, structure, and evolution of the stars is an essential component in uncovering our cosmic origins. In this way, studying the life cycles of the stars is a journey of self discovery.

For most of human history our primary method of contact with the stars other than the Sun has been through visual observations of the night sky. Stars radiate photons across space and time, and we capture them with eyes and more recently, telescopes. Peering into the interiors of stars was never thought possible until the advent of multi-messenger astronomy. Today, we know stars radiate photons from their stellar surface, neutrinos from their interior, and recently-discovered gravitational waves during binary mergers.

In 1930, Wolfgang Pauli first proposed the existence of a new very light particle which rarely interacted with matter. Enrico Fermi later named this particle the "*neutrino*" meaning "*little neutral one*". We now understand that in the core of stars the process of transmutation, by which many chemical elements are synthesized through nuclear fusion, also produces neutrinos as a byproduct. Since neutrinos interact feebly with normal baryonic matter, they can escape the cores of stars unhindered under circumstances where photons are trapped. Hence, The neutrinos radiated from the cores of stars carry with them information about the structures and energies of the stellar interior, making them a useful diagnostic of stellar cores.

In 1915 Albert Einstein first proposed his General Theory of Relativity through which he uncovered the coupling between space, time, and gravity. In 1916, he used this new theory of gravity to make the first prediction of gravitational waves, which would not be directly detected until 2015, a century later. The first direct detection came from the Laser Interferometer Gravitational Wave Observatory (LIGO) in Hanford, Washington and Livingston, Louisiana which observed the gravitational waves resulting from the in-spiral of two compact objects. An estimated 30 $M_\odot$ and 35$M_\odot$ black hole (BH) merging together to form an estimated 62 $M_\odot$ BH, with roughly 3 $M_\odot$ of being emitted in gravitational wave radiation during the merger. These BHs likely formed as the final fates of massive stars, and their progenitor masses and spins provide a host of information which can be used to constrain the stellar physics of massive stars in their late burning phases.

To better understand stellar sources of photons, neutrinos, and gravitational waves and how they can be used to inform stellar evolution as whole, we must first discuss the general physical processes stars undergo in their interiors and their resulting evolutionary phases.

1.2 Stellar Evolution

Our best models of the formation of the universe predict an initial composition of $\sim 75.1\%$ hydrogen $\sim 24.9\%$ helium, and $10^{-7}\%$ lithium. Most first generation stars in the universe (population III) formed from this initial composition near the beginning of cosmic time, re-ionizing the cosmos as it expanded and cooled from the big bang. Heavier elements were synthesized and recycled through multiple generations of stars, enriching the cosmos with metals.

A typical approach is to identify generations of stars by their metallicity. We denote their hydrogen mass fraction X, helium mass fraction Y, and metal mass fraction Z which encompasses all heavier chemical elements and isotopes. Each star has a unique set of chemical isotopes that compose Z determined by it's age, environment, and progenitors. The Sun is a later generation (population I) star with $X \sim 0.71$, $Y \sim 0.27$, and $Z \sim 0.02$, although the exact composition of the Sun is a subject of debate in the solar physics community.

In essence, the Sun and other stars are massive balls of hot gas powered by a heart of nuclear fire. The evolution of a star is a dance with gravity. Stars typically form from cold molecular clouds of gas and dust contracting under the force of gravity. As the core begins to form, its contraction under the force of gravity leads to an increase in the central temperature and pressure until nuclear fusion can begin. The energy produced from nuclear fusion, primarily in the form of photons diffusing through the stellar interior, provides the pressure necessary to counter the force of gravity and prevent further contraction. This condition of stability is called hydro-static equilibrium, when the radiation and gas pressure from the interior of star counters the pressure of gravity, resulting in a a dynamically stable object. Section **??** describes how we model such objects.

1.2.1 Hydrogen Burning

The first sources of nuclear burning in a newly forming star are from ^{2}H and ^{7}li at $T = 1 \times 10^{6}$ K and $T = 3 \times 10^{6}$ K, respectively. These energy sources only briefly halt the contraction of the stellar core, until the initial reservoir of ^{12}C and ^{13}N is converted to ^{14}N via The reaction sequence ^{12}C(p,γ)^{13}N(,$e^{+}\nu_{e}$)^{13}C(p,γ)^{14}N. CN burning occurs at lower temperatures than when the full CNO cycle operates. Once the temperature in the core reaches $T \sim 10^{7}$ K, the star enters what is called the main-sequence (MS) where the main hydrogen fuel source ^{1}H begins to fuse. Hydrogen burning is occurs through two separate nuclear two reaction chains, the proton-proton (pp) chain and the (CNO) cycles listed below.

Proton-Proton Chains:

$$PP-I \begin{cases} ^{1}H +^{1} H \rightarrow \ ^{2}H + e^{+} + \nu_{e} \\ ^{2}H +^{1} H \rightarrow \ ^{3}He + \gamma \\ ^{3}He +^{3} He \rightarrow \ ^{4}He +^{1} H +^{1} H \end{cases}$$

$$PP-II \begin{cases} ^{3}He +^{4} He \rightarrow^{7} Be + \gamma \\ ^{7}Be + e^{-} \rightarrow^{7} Li + \nu(+\gamma) \\ ^{7}Li +^{1} H \rightarrow^{4} He +^{4} He \end{cases}$$

$$PP-III \begin{cases} ^{7}Be +^{1} H \rightarrow^{8} B + \gamma \\ ^{8}B \rightarrow^{8} Be + e^{+} + \nu_{e} \\ ^{8}Be \rightarrow^{4} He +^{4} He \end{cases}$$

CNO cycle reactions:

$$CN\ cycle \begin{cases} ^{12}C +^{1} H \rightarrow^{13} N + \gamma \\ ^{13}N \rightarrow^{13} C + e^{+} + \nu_e \\ ^{13}C +^{1} H \rightarrow^{14} N + \gamma \\ ^{14}N +^{1} H \rightarrow^{15} O + \gamma \\ ^{15}O \rightarrow^{15} N + e^{+} + \nu_e \\ ^{15}N +^{1} H \rightarrow^{12} C +^{4} He \end{cases}$$

$$CNO\ full \begin{cases} ^{14}N +^{1} H \rightarrow^{16} O + \gamma \\ ^{16}O +^{1} H \rightarrow^{17} F + \gamma \\ ^{17}F \rightarrow^{17} O + e^{+} + \nu_e \\ ^{17}O +^{1} H \rightarrow^{14} N +^{4} He \end{cases}$$

The CNO cycle is not limited to these reactions but contains and contains larger nuclear reaction chains with heavier isotopes that dominate at higher temperatures. Stars with masses $\mathrm{M} \lesssim 1.1\mathrm{M}_{\odot}$ primarily burn hydrogen through pp reactions, whereas more massive stars primarily burn hydrogen via CNO cycle reactions. The transition from pp to CNO burning is primarily a result of the temperature dependence of each cycle:

$$\epsilon_{\mathrm{pp}} \propto X^2 \rho T^4,$$

$$\epsilon_{\mathrm{CNO}} \propto XZ\rho T^{17},$$

The pp reactions have a higher initial cross-section since they depend on the square of the hydrogen mass fraction, X, but a weaker temperature dependence, hence CNO reactions dominate the energy generation rate in more massive stars where the core temperatures are higher.

The main result of hydrogen burning is the conversion the initial core ^{1}H into ^{4}He. At the end of core-hydrogen burning, ^{1}H is depleted from the core marking the end of the main-sequence evolution of the star. The star is now termed a terminal age main-sequence (TAMS) star. The inert ^{4}He continues to contract and heat up as hydrogen burning propagates into the ^{1}H-rich shell around the core. The hydrogen shell burning phase of evolution continues until helium core ignition.

1.2.2 Helium Burning and beyond

As stars evolve, the ashes of nuclear burning usually have a heavier mean atomic number and lie interior to the unburned fuel. For example, the He core is interior to the H-burning shell, and the CO core is interior to the He-burning shell. One class of exceptions occurs when a combination of electron degeneracy and thermal neutrino losses lead to cooler temperatures in the central regions and the fuel ignites off-center.

The core He-burning phase of stellar evolution is characterized by a competition between the (3-α) process $^{4}\mathrm{He}(\alpha,)^{8}\mathrm{Be}(\alpha,)^{12}\mathrm{C}^{*}(,2\gamma)^{12}\mathrm{C}$ and $^{12}\mathrm{C}(\alpha,\gamma)^{16}\mathrm{O}$ which establish the C/O ratio of the stellar core for later phases.

The He core flash phase, which occurs in $M_{\mathrm{ZAMS}} \lesssim 2\,M_{\odot}$ stars, is characterized by a series of subflashes that propagate toward the stellar center (Thomas, 1967; Serenelli and Weiss, 2005; Bildsten *et al.*, 2012; Gautschy, 2012; Serenelli *et al.*, 2017). The number of subflashes decreases as the stellar mass increases, and the initial flash takes place closer to the stellar center. After the He core flash phase, which burns very little helium, core He-burning then proceeds quiescently (e.g., deBoer *et al.*, 2017) to produce an electron degenerate CO core. $M_{\mathrm{ZAMS}} \gtrsim 2\,M_{\odot}$ stars ignite helium under non degenerate condition.

After core Helium depletion in stars with $M < 8M_{\odot}$, a thin He shell grows as material from the adjacent H-burning shell is processed, causing the He shell to increase in temperature and pressure. Once the mass in the He shell reaches a critical value, He ignition causes a thermal pulse. low mass stars leave the thermal pulse phase when the envelope mass above the still active H and He burning shells is reduced to $\simeq 0.01$ $M_{\odot}$ by stellar winds. Nuclear burning extinguishes as these post-AGB stars enters the white dwarf (WD) cooling track as cooling degenerate CO core.

High mass stars ($M \gtrsim 8$ $M_{\odot}$) reach high enough temperatures to ignite C and O, fueling the evolution into a presupernova star. The evolution of massive stars through advanced burning stages depends sensitively on the C/O ratio at He-depletion. The evolution beyond core helium depletion high mass stars ($M \gtrsim 8$ $M_{\odot}$) is dominated by the energy losses from thermal neutrino sources. Free streaming neutrinos from thermal processes, primarily pair annihilation, dominate a star's energy loss budget from the core C-burning phase to core Si depletion. This dominance over photons as the primary energy loss mechanism sets a rapid evolutionary timescale (years to hours) for the advanced stages of nuclear fusion in presupernova stars (Woosley *et al.*, 2002).

1.3 Neutrino signals

In the stellar interiors, weak reactions produce electron neutrinos by thermal processes, electron and positron captures on nuclei, and nuclear decays. Neutrinos are produced during H-burning on the main-sequence (MS) from the proton-proton (pp) chain reactions $p(p,e^{+}\nu_e)^{2}H$, $p(e^{-}p,\nu_e)^{2}H$, $^{3}He(p,e^{+}\nu_e)^{4}He$, $^{7}Be(e^{-},\nu_e)^{7}Li$, $^{8}B(,e^{+}\nu_e)^{8}Be$, and the CNO cycle reactions $^{13}N(,e^{+}\nu_e)^{13}C$, $^{13}N(e^{-},\nu_e)^{13}C$, $^{15}O(,e^{+}\nu_e)^{15}N$, $^{15}O(e^{-},\nu_e)^{15}N$, $^{17}F(,e^{+}\nu_e)^{17}O$, $^{17}F(e^{-},\nu_e)^{17}O$, $^{18}F(,e^{+}\nu_e)^{18}O$, where electron capture reactions on CNO nuclei are included (Stonehill *et al.*, 2004). The slowest step in the H-burning CNO cycle is the proton capture onto ^{14}N. This results in all the CNO catalysts piling up into ^{14}N when core H-burning is complete. During He-burning all of the ^{14}N is converted in ^{22}Ne by the reaction sequence ^{14}N(α,γ)^{18}F(,$e^{+}\nu_{e}$)^{18}O(α,γ)^{22}Ne. Higher temperatures can trigger the production of nuclear reaction neutrinos from the H-burning hot CNO, Ne-Na, and Mg-Al cycles, especially in massive stellar cores.

Neutrinos are also thermally excited from a variety of processes that occur in hot-dense stellar interiors. The three most dominant thermal neutrino processes are plasmon decay ($\gamma_{\rm plasmon} \rightarrow \nu_e + \bar{\nu}_e$), photoneutrino production ($e^- + \gamma \rightarrow e^- + \nu_e + \bar{\nu}_e$), and pair annihilation ($e^- + e^+ \rightarrow \nu_e + \bar{\nu}_e$). The bremsstrahlung ($e^- + {}^{\rm A}{\rm Z} \rightarrow e^- + {}^{\rm A}{\rm Z} + \nu_e + \bar{\nu}_e$) and recombination ($e^-_{\rm continuum} \rightarrow e^-_{\rm bound} + \nu_e + \bar{\nu}_e$) channels play smaller roles. photoneutrino production is the dominant thermal neutrino process during H-burning, plasmon decay dominates in electron-degenerate cores typically encountered in the cooling He or CO WDs, and pair annihilation dominates in the hot interiors of massive stars evolving from C burning to core-collapse.

1.4 Gravitational wave signals

Stellar evolution of high mass stars seed the cosmic neutron star and black hole (BH) mass spectrum. Through gravitational wave detections of merging binary compacts objects we can place limits on abundance particular BH masses and the peak stellar BH mass. The spectrum of final BH masses resulting from massive star evolution depends sensitively on the C/O composition of a massive star at He-depletion. This is set by the competition between the $3-\alpha$ and ^{12}C(α,γ)^{16}O, the two most uncertain nuclear reaction rates in all of astrophysics. Therefore, constraining the shape of the BH mass spectrum in comparison to observations from the LIGO-VIRGO-KAGRA (LVK) collaboration can inform nculear theory calculations of the low-energy cross-section strengths for these important helium burning nuclear reactions. In particular, the standard theory of stellar evolution predicts a gap in the distribution of BH masses owing to the effects of pair-instability, which depend sensitively on the C/O composition of these stellar cores.

1.5 Software Instruments

This Thesis relied primarily on the open-source stellar evolution toolkit Modules for Experimentation in Stellar Astrophysics (`MESA`) (Paxton *et al.*, 2011, 2013, 2015, 2018, 2019; Jermyn *et al.*, 2023).

1.6 Outline

This Thesis largely explores various neutrino and gravitational wave signals with stellar evolution models. Chapter 2 explores stellar evolution in the novel neutrino Hertzsprung-Russell diagram, chapter 3 investigates stellar neutrino emission across stars a range of masses and metallicities and makes predictions for the neutrino emission from simple stellar populations, chapter 4 explores the sensitivity of stellar evolution models and predictions of the upper BH mass gap to uncertainties in the 3-α process and $^{12}C(\alpha,\gamma)^{16}O$ reaction rate, and chapter 5 summarizes the take-aways of this Thesis.

Chapter 2

ON STELLAR EVOLUTION IN A NEUTRINO HERTZSPRUNG-RUSSELL DIAGRAM

Below is the published work of Ebraheem Farag et al 2020 ApJ 893 133.

2.1 Abstract

We explore the evolution of a select grid of solar metallicity stellar models from their pre-main sequence phase to near their final fates in a neutrino Hertzsprung-Russell diagram, where the neutrino luminosity replaces the traditional photon luminosity. Using a calibrated MESA solar model for the solar neutrino luminosity ($L_{\nu,\odot}$ $= 0.02398 \cdot L_{\gamma,\odot} = 9.1795 \times 10^{31}$ erg s^{-1}) as a normalization, we identify $\simeq$0.3 MeV electron neutrino emission from helium burning during the helium flash (peak $L_\nu/L_{\nu,\odot} \simeq 10^9$, flux $\Phi_{\nu,\mathrm{He\ flash}} \simeq 1.7{\times}10^7$ (10 pc/d)^2 cm^{-2} s^{-1} for a star located at a distance of d parsec, timescale $\simeq$ 3 days)and the thermal pulse (peak $L_\nu/L_{\nu,\odot} \simeq 10^6$, flux $\Phi_{\nu,\mathrm{TP}} \simeq 1.7{\times}10^4$ (10 pc/d)^2 cm^{-2} s^{-1}, timescale $\simeq$ 0.1 yr) phases of in low mass stars as potential probes for stellar neutrino astronomy. We also delineate the contribution of neutrinos from nuclear reactions and thermal processes to the total neutrino loss along the stellar tracks in a neutrino Hertzsprung-Russell diagram. We find, broadly but with exceptions, that neutrinos from nuclear reactions dominate whenever hydrogen and helium burn, and that neutrinos from thermal processes dominate otherwise.

2.2 Introduction

Stars radiate energy by releasing photons from the stellar surface and neutrinos from the stellar interior. In the interior, weak reactions produce electron neutrinos by thermal processes, electron and positron captures on nuclei, and nuclear decays. Neutrinos interact feebly with baryonic matter, with typical cross sections of $\simeq 10^{-44}$ cm^2 as opposed to typical photon cross sections of $\simeq 10^{-24}$ cm^2, escaping from the star unhindered in circumstances where photons are trapped.

Neutrino losses play key roles on the main-sequence in the case of the Sun (Bahcall and Pinsonneault, 1992; Bahcall *et al.*, 2005; Haxton *et al.*, 2013), during the helium flash in red giants (Ramadurai, 1976; Sweigart and Gross, 1978; Raffelt and Weiss, 1992; Catelan *et al.*, 1996), in the conversion of ^{14}N to ^{22}Ne during core helium burning (Serenelli and Fukugita, 2005), for the cooling of white dwarfs (van Horn, 1971; Kawaler *et al.*, 1986; Fontaine *et al.*, 2001; Althaus *et al.*, 2010; Bischoff-Kim and Montgomery, 2018), during core carbon burning (Ramadurai, 1984; Aufderheide, 1993; Meakin and Arnett, 2007; Cristini *et al.*, 2017, 2019), for pre-supernova stars (Odrzywolek, 2009; Kutschera *et al.*, 2009; Patton *et al.*, 2017a,b), for both core-collapse supernovae (e.g., Janka, 2017) and electron-capture supernovae (Ray *et al.*, 1984; Jones *et al.*, 2013), for the cooling of neutron stars (Nomoto and Tsuruta, 1981; Potekhin *et al.*, 2015), during X-Ray bursts, (Fujimoto *et al.*, 1987; Goodwin *et al.*, 2019), for accretion disks around black holes (Birkl *et al.*, 2007; Fryer *et al.*, 2014; Uribe Suárez and Rueda Hernandez, 2019) during neutron star mergers (Albert *et al.*, 2017; Kyutoku and Kashiyama, 2018a), and for nucleosynthesis from the ν-process (Woosley *et al.*, 1990), νp process (McLaughlin and Fuller, 1995; Fröhlich *et al.*, 2006), and r-process (e.g., Kajino *et al.*, 2019).

Neutrino production from thermal processes mainly depends on the ambient thermodynamic conditions (Fowler and Hoyle, 1964; Beaudet *et al.*, 1967; Schinder *et al.*, 1987; Itoh *et al.*, 1996a). Neutrino production from electron/positron captures and nuclear decays have a stronger dependence on the isotopic composition (Fuller *et al.*, 1980, 1982b,a, 1985; Langanke and Martínez-Pinedo, 2000, 2014; Misch *et al.*, 2018), and thus on the network of nuclear reactions that take place in the stellar interior. These two classes of neutrino production thus carry complementary information about the interior of stars (Patton *et al.*, 2017a,b).

Neutrino astronomy has been limited, so far, to the Sun (Borexino Collaboration *et al.*, 2018), supernova 1987A (Hirata *et al.*, 1987, 1988; Bionta *et al.*, 1987; Alekseev *et al.*, 1987), and the blazar TXS 0506+056 (IceCube Collaboration *et al.*, 2018a,b). However, the *Super-Kamiokande with Gadolinium* (Simpson *et al.*, 2019), *Jiangmen Underground Neutrino Observatory* (Li, 2014; Brugière, 2017), and *XENON* (Newstead *et al.*, 2019) experiments usher in a new generation of multi-purpose neutrino detectors designed to open new avenues for potentially observing currently undetected neutrinos.

This article is novel in exploring the evolution of stellar models in a neutrino Hertzsprung-Russell (HR) diagram, where the traditional photon luminosity is replaced with the neutrino luminosity. This exploration provides targets for current, forthcoming, and future generations of neutrino detectors as well as providing estimates of the stellar neutrino background signal. In Section 2.3 we describe the input physics and solar normalization of the stellar models. In Section 2.4 we present our main results, and in Section 2.5 we discuss and summarize our results.

2.3 Stellar Models

2.3.1 Input Physics

We model the evolution of stars with initial masses M = 1, 2, 3, 15, 25, 30, 35, and 40 $M_\odot$ from the pre-main sequence (PMS) to a white dwarf (WD) for the lower masses, or the onset of core-collapse for the higher masses. These masses are chosen to delineate features in a forthcoming neutrino HR diagram. We use `MESA` revision r12115 to construct our stellar models (Paxton *et al.*, 2011, 2013, 2015, 2018, 2019). Each star is modeled as a single, non-rotating, mass losing, solar metallicity object. The files to reproduce our work are publicly available at `https://doi.org/10.5281/zenodo.3634068`.

We use the built-in `MESA` nuclear reaction network `mesa_49` for low mass stars and `mesa_204` for high mass stars. Relatively large nuclear networks are required to fully capture the energy generation rate, and thus the neutrino luminosity from β-processes, in neutron-rich compositions. The current defaults for nuclear reaction rates are described in Appendix A.2 of Paxton *et al.* (2019). Rates are taken from a combination of NACRE (Angulo *et al.*, 1999) and the Joint Institute for Nuclear Astrophysics REACLIB library (default version, dated 2017-10-20) (Cyburt *et al.*, 2010a). The `MESA` screening corrections are from Chugunov *et al.* (2007), which includes a physical parameterization for the intermediate screening regime and reduces to the familiar weak (Dewitt *et al.*, 1973; Graboske *et al.*, 1973) and strong (Alastuey and Jancovici, 1978; Itoh *et al.*, 1979) limits at small and large values of the plasma coupling parameter. All the weak reaction rates are based (in order of precedence) on the tabulations of Langanke and Martínez-Pinedo (2000), Oda *et al.* (1994), and Fuller *et al.* (1985).

The three most dominant thermal neutrino processes are plasmon decay ($\gamma_{\rm plasmon} \rightarrow$

$\nu_e + \bar{\nu}_e$), photoneutrino production ($e^- + \gamma \rightarrow e^- + \nu_e + \bar{\nu}_e$), and pair annihilation ($e^- + e^+ \rightarrow \nu_e + \bar{\nu}_e$). The bremsstrahlung ($e^- + {}^{\mathrm{A}}\mathrm{Z} \rightarrow e^- + {}^{\mathrm{A}}\mathrm{Z} + \nu_e + \bar{\nu}_e$) and recombination ($e^-_{\mathrm{continuum}} \rightarrow e^-_{\mathrm{bound}} + \nu_e + \bar{\nu}_e$) channels play smaller roles. The total emissivities of all these processes, over a range of temperatures and densities, are discussed in Itoh *et al.* (1989, 1992, 1996a,b) and implemented in the MESA thermal neutrino loss module. Differential rates and emissivities of selected thermal neutrino processes are discussed in Ratković *et al.* (2003); Dutta *et al.* (2004); Misiaszek *et al.* (2006a); Odrzywołek (2007); Kato *et al.* (2015); Patton *et al.* (2017a,b).

The models approximate convection using the recipes described in Paxton *et al.* (2019, 2018). The adopted values of the mixing-length parameter, α and overshooting parameter f_{ov}, as well as the initial hydrogen fraction X, helium fraction Y, and metallicity Z and are determined from our calibrated Solar model.

2.3.2 Solar Neutrino Luminosity Normalization

We perform a Solar model calibration to reproduce the present day neutrino flux (Villante *et al.*, 2014). We iterate on differences between the final model at $t_\odot = 4.568$ Gyr (Bouvier and Wadhwa, 2010) and the solar radius, $R_\odot = 6.9566 \times 10^{10}$ cm, solar luminosity, $L_{\gamma,\odot} = 3.828 \times 10^{33}$ erg s^{-1} (Prša *et al.*, 2016a), and surface heavy element abundance Z/X. We use the built-in MESA simplex module to iteratively vary the mixing-length parameter, α, and the initial composition X, Y, and Z, including the effects of element diffusion (Thoul *et al.*, 1994; Paxton *et al.*, 2018). This calibration is performed for two estimates of the heavy element abundance at the surface of the Sun, Z/X = 0.0181 (Asplund *et al.*, 2009) and Z/X = 0.0229 (Grevesse and Sauval, 1998). We adopt a small amount of exponential convective overshooting (Herwig, 2000a) by choosing $f_{ov} = 0.016$ as used in the MIST isochrones (Choi *et al.*, 2016a). Separate implementations of convective overshooting at the base of the solar convection zone can be found in Christensen-Dalsgaard *et al.* (2011) and Zhang *et al.* (2019). Our calibrated solar models do not include the structural effects of rotational deformation or the effects of rotational mixing. Calibrated parameters are listed in Table 4.1. We use the abbreviations AGSS09 = Asplund *et al.* (2009) photospheric abundances mixture and GS98 = Grevesse and Sauval (1998) meteoric abundance mixture in all Tables. The AGSS09 solar model is calculated using OPAL opacities (Iglesias and Rogers, 1996a), and the GS98 solar model is calculated using the Opacity Project (OP) opacities (?). See Vinyoles *et al.* (2017) for updated approaches toward standard solar models.

Component	AGSS09	GS98
X_o	0.7200	0.7108
Y_o	0.2654	0.2710
α_{mlt}	2.120	2.155
$(Z/X)_{surf}$	0.0181	0.0229
$L_{\nu,\odot}/L_{\gamma,\odot}$	0.02398	0.02422

Table 2.1: Solar Calibration Parameters

Component	AGSS09	GS98	Observed[a]
$R_{cz,b}/R_{\odot}$	0.7256	0.7178	0.713 ± 0.001
Y_{surf}	0.2396	0.2460	0.2485 ± 0.0035

Table 2.2: Properties of the Solar Calibrated Model

Figure 2.1 shows the fractional difference in sound speed, δc, and density, $\delta\rho$, between our calibrated solar models and the inferred helioseismic values, see Basu *et al.* (2009). Calculated values for helioseimic quantities are shown in Table 4.3.

Component	AGSS09	GS98	Observed[a]
$\Phi_{\rm pp}$	6.01	5.98	$6.05(1^{+0.003}_{-0.011})$
$\Phi_{\rm Be}$	4.71	4.95	$4.82(1^{+0.05}_{-0.04})$
$\Phi_{\rm B}$	4.62	5.09	$5.00(1 \pm 0.03)$
$\Phi_{\rm N}$	2.25	2.91	≤ 6.7
$\Phi_{\rm O}$	1.67	2.21	≤ 3.2

Table 2.3: Solar Neutrino Fluxes

Disagreements arise from differences in the solar abundance profiles, equation of state, opacities, model atmospheres, treatment of convection, and the absence of rotational mixing. The task of correcting these disagreements is the subject of ongoing research, see Bergemann and Serenelli (2014) and Serenelli (2016). Nonetheless, our seismic results appear similar to those in Villante *et al.* (2014) and Asplund *et al.* (2009).

Neutrinos are produced during H-burning on the main-sequence (MS) from the proton-proton (pp) chain reactions: $\rm p(p,e^+\nu_e)^2H$, $\rm p(e^-p,\nu_e)^2H$, $\rm ^3He(p,e^+\nu_e)^4He$, $\rm ^7Be(e^-,\nu_e)^7Li$, $\rm ^8B(,e^+\nu_e)^8Be$, and the CNO cycle reactions: $\rm ^{13}N(,e^+\nu_e)^{13}C$, $\rm ^{13}N(e^-,\nu_e)^{13}C$, $\rm ^{15}O(,e^+\nu_e)^{15}N$, $\rm ^{15}O(e^-,\nu_e)^{15}N$, $\rm ^{17}F(,e^+\nu_e)^{17}O$, $\rm ^{17}F(e^-,\nu_e)^{17}O$, $\rm ^{18}F(,e^+\nu_e)^{18}O$, where electron capture reactions on CNO nuclei are included (Stonehill *et al.*, 2004). Higher temperatures can trigger the production of nuclear reaction neutrinos from the H-burning hot CNO, Ne-Na, and Mg-Al cycles.

The neutrino flux in the solar interior is strongly dependent on the core temperature (see Bahcall and Ulmer, 1996). Standard solar models that accurately predict temperatures near the solar core should also generate comparable neutrino fluxes to solar neutrino data. Neutrino fluxes are calculated from each solar model and compared to observations in Table 2.3. Our predicted neutrino fluxes are similar to

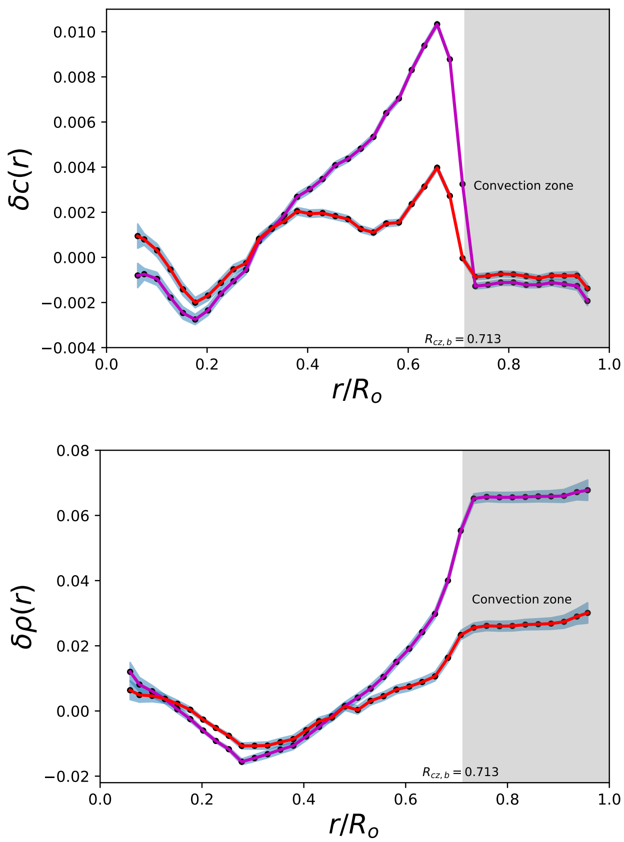

Figure 2.1: Fractional sound speed and density differences, $\delta c = (c_{\rm obs}$ - $c(r))/c(r)$ and $\delta\rho = (\rho_{\rm obs}$ - $\rho(r))/\rho(r)$, between the values predicted by the calibrated `MESA` standard solar model, $c(r)$ and $\rho(r)$, and the values inferred from helioseismic data (Basu *et al.*, 2009), $c_{\rm obs}$ and $\rho_{\rm obs}$. Black dots mark locations where δc and $\delta\rho$ are evaluated. Purple curves are for AGSS09 and red curves are for GS98. The gray band shows the convective region, with the radius at the base of the convection zone $\rm R_{cz,b}$ marked. The 3σ uncertainties are shown as the blue bands.

Villante *et al.* (2014) and Haxton *et al.* (2013). We adopt the AGSS09 `MESA` model, calculated using OPAL opacities, as the standard in this article. Specifically, we use $L_{\nu,\odot} = 0.02398 \cdot L_{\gamma,\odot} = 9.1795 \times 10^{31}$ erg s^{-1} as the normalization for the neutrino HR diagram.

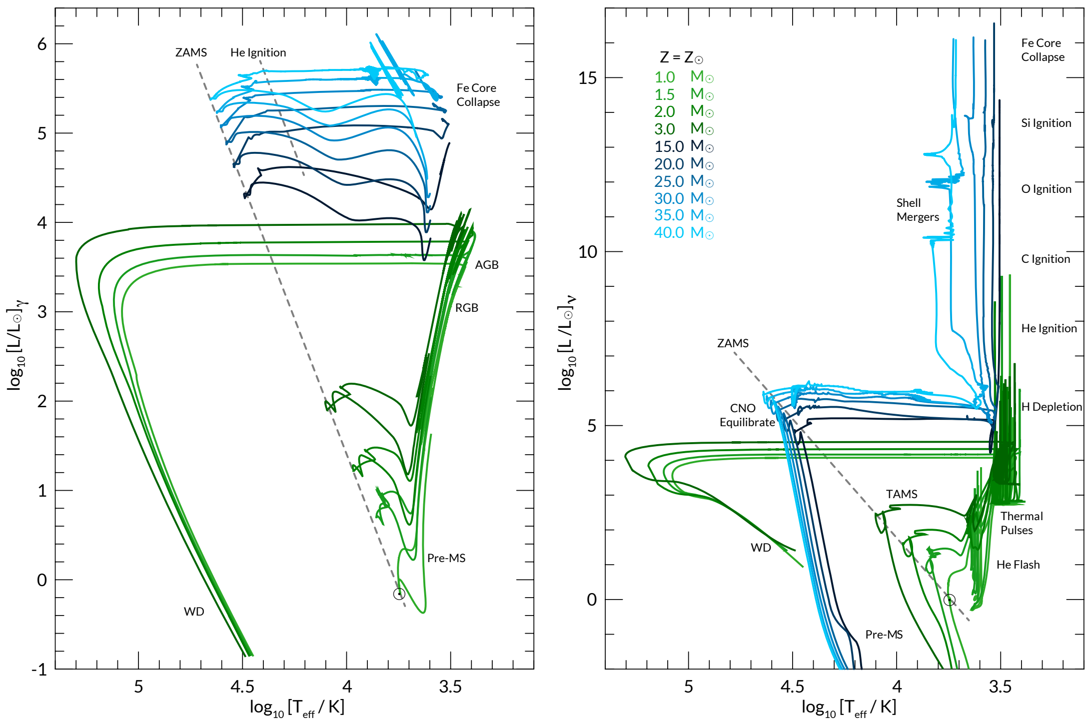

Figure 2.2: Stellar evolution tracks in a photon HR diagram (left) and a neutrino HR diagram (right). Tracks for low mass stars are shades of green and those for high mass stars are shades of blue. Luminosities are normalized by their respective current solar values, $L_{\gamma,\odot} = 3.828 \times 10^{33}$ erg s^{-1} (Prša *et al.*, 2016a) and $L_{\nu,\odot} = 0.02398 \cdot L_{\gamma,\odot} = 9.1795 \times 10^{31}$ erg s^{-1} (see Section 2.3.2), and key evolutionary phases are labeled.

2.4 Evolution in A Neutrino HR Diagram

Stars are powered mainly by fusion reactions throughout their life, but weak reactions play a key role in determining their structure, energy budget, and nucleosynthesis. A fundamental aspect of weak reactions for stellar evolution is that they facilitate hydrogen fusion into helium (for Universes and stellar evolution without the weak force see Grohs *et al.*, 2018). They affect the interior structure because the pressure is mostly due to free electrons and in some cases (e.g., electron capture supernovae) weak reactions change the number of free electrons. Neutrino losses modify the energy budget, and dominate for C-burning and beyond. Finally, they affect the nucleosynthesis because the production of most nuclei is sensitive to the electron to baryon ratio.

Figure 2.2 shows the stellar evolution tracks of the models considered in a photon and neutrino HR diagram. A photon HR diagram uses two surface properties, the effective temperature $T_{\rm eff}$ and photon luminosity L_γ. A neutrino HR diagram uses the $T_{\rm eff}$ surface property and an interior property, the neutrino luminosity L_ν. We next discuss the key phases of evolution that are labeled in the neutrino HR diagram.

Each pre-main sequence (PMS) model begins with a uniform composition and central temperature that is low enough that nuclear burning is inconsequential. The central temperature and density then increase as the stellar model undergoes gravitational contraction. The initial CNO abundances for solar metallicity stars is not equal to the CNO abundances when the CNO cycle is operating in equilibrium. Nuclear reactions replace gravitational contraction as the major source of L_γ and L_ν by burning the ^{12}C abundance to a value that is commensurate with CNO equilibrium values (Iben, 1965).

The reactions ^{12}C(p,γ)^{13}N(,$e^+\nu_e$)^{13}C(p,γ)^{14}N can occur at lower temperatures than when the full CNO cycle competes with the pp-chain. They produce a nuclear energy $E_{\rm nuc} \simeq N_A Q \rho X_c/{\rm A}_c$, where N_A is the Avogadro number, ρ is the mass density, X_c is the mass fraction of ^{12}C, ${\rm A}_c$ is the number of nucleons in ^{12}C, and $Q \simeq 11$ MeV is the nuclear binding energy release. The thermal energy is $E_{\rm th} \simeq 3/2 N_A \rho k_B T$, where k_B is the Boltzmann constant and T is the temperature. The ratio at solar metallicity and $T = 10^7$ K is $E_{\rm nuc}/E_{\rm th} \simeq Q X_c/(18 k_B T) \simeq 1.5$ (Bildsten, 2019). That is, the star can delay gravitational contraction for about one Kelvin-Helmholtz by reducing ^{12}C. This transition from the PMS to the zero-age main sequence (ZAMS) is visible in the neutrino HR diagram of Figure 2.2 as the loop prior to landing on the ZAMS.

For all of the models considered, core H-burning powers L_ν on the ZAMS by the weak reactions given in Section 2.3.2. As H in the core depletes, all the models enter the terminal-age main sequence (labeled TAMS in Figure 2.2) and continue to evolve toward cooler T_{eff}. Further evolution is now divided into low mass stars (Section 3.5) and high mass stars (Section 3.6).

2.4.1 Low Mass Stars

Low mass stars (M $\lesssim$ 8 M$_\odot$) ascend the red giant branch (labeled RGB in Figure 2.2) as they evolve to cooler T_{eff} in the photon HR diagram, and evolve at approximately constant L_ν from shell H-burning in the neutrino HR diagram.

As stars evolve, the ashes of nuclear burning usually have a heavier mean atomic number and lie interior to the unburned fuel. For example, the He core is interior to the H-burning shell, and the CO core is interior to the He-burning shell. One class of exceptions occurs when a combination of electron degeneracy and thermal neutrino losses lead to cooler temperatures in the central regions and the fuel ignites off-center. Examples include He ignition in $M_{\mathrm{ZAMS}} \lesssim 2M_\odot$ stars (i.e., the "helium flash") and C ignition in Super-AGB stars. Fuels that ignite off-center develop convection behind the nuclear burning (towards the surface of the star) and propagate towards the center. These convectively bounded flames have relatively slow speeds (Timmes *et al.*, 1994; García-Berro *et al.*, 1997; Schwab *et al.*, 2020), due to the propagation being driven by thermal conduction under semi-degenerate conditions.

Helium ignition occurs at the tip of the RGB in the photon HR diagram and in the lower-right in the neutrino HR diagram. The slowest step in the H-burning CNO cycle is the proton capture onto ^{14}N. This results in all the CNO catalysts piling up into ^{14}N when core H-burning is complete. During He-burning all of the ^{14}N is converted in ^{22}Ne by the reaction sequence ^{14}N(α,γ)^{18}F(,$e^+\nu_e$)^{18}O(α,γ)^{22}Ne. It is the weak reaction in this sequence that powers L_ν throughout this phase of evolution (e.g., Serenelli and Fukugita, 2005).

The He core flash phase, which occurs in $M_{\rm ZAMS} \lesssim 2\,M_\odot$ stars, is characterized by a series of subflashes that propagate toward the stellar center (Thomas, 1967; Serenelli and Weiss, 2005; Bildsten *et al.*, 2012; Gautschy, 2012; Serenelli *et al.*, 2017). For example, the 1 M$_\odot$ model in Figure 2.2 undergoes five subflashes with the first subflash occurring at $\simeq$ 0.18 M$_\odot$and reaching $L_\nu \simeq 10^4\ L_{\nu,\odot}$. The number of subflashes decreases as the stellar mass increases, and the initial flash takes place closer to the stellar center. These subflashes, with their dependence on the stellar mass, are visible in the neutrino HR diagram of Figure 2.2 as the spikes in the region labeled "He Flash". After the He core flash phase, which burns very little helium, core He-burning then proceeds quiescently (e.g., deBoer *et al.*, 2017) to produce an electron degenerate CO core.

Helium ignition in $M_{\rm ZAMS} \gtrsim 2M_\odot$ stars occurs under non-degenerate conditions, without flashes or subflashes, and leads to a different, smoother, signature in the production of neutrinos from ^{18}F decay. For the 2 M$_\odot$ model, from Figure 2, L_ν=0.8 $L_{\gamma,\odot}$ and L_γ=16 $L_{\gamma,\odot}$ on the MS, L_ν=4330 $L_{\gamma,\odot}$ and L_γ=1750 $L_{\gamma,\odot}$ at He-ignition (tip of the RGB), L_ν=5.1 $L_{\gamma,\odot}$ and L_γ=110 $L_{\gamma,\odot}$ at core He-depletion (mass fraction of ^{4}He less than 0.001), L_ν=420 $L_{\gamma,\odot}$ and L_γ=6100 $L_{\gamma,\odot}$ after the thermal pulses when the envelope mass is 0.01 M$_\odot$, L_ν=1.8 $L_{\gamma,\odot}$ when L_γ=1.0 $L_{\gamma,\odot}$ on the WD cooling track.

Asymptotic giant branch (AGB) stars are the final stage of evolution driven by nuclear burning. This phase is characterized by H and He burning in geometrically thin shells on top of the CO core (Herwig, 2005). For the more massive super-AGB stars a ONeMg core is produced from a convectively bounded carbon flame that propagates toward the center (Becker and Iben, 1979, 1980; García-Berro *et al.*, 1997;

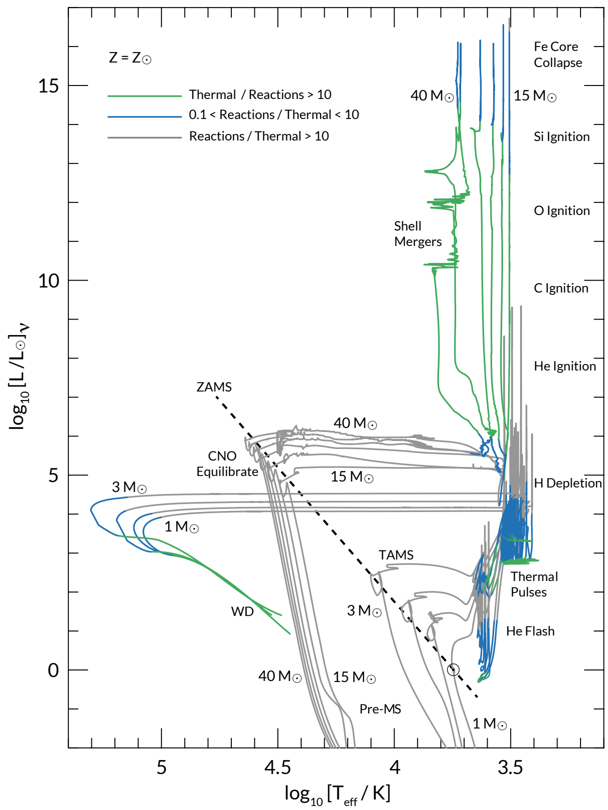

Figure 2.3: Ratio of the nuclear reaction neutrino luminosity to the thermal neutrino luminosity plotted along stellar evolution tracks in a neutrino HR diagram. Gray curves indicate where nuclear reaction neutrinos dominate, green curves where thermal neutrinos dominate, and blue curves where the reaction and thermal neutrino luminosities are within a factor of 10. The neutrino luminosity is normalized by the current solar value $L_{\nu,\odot} = 0.02398 \cdot L_{\gamma,\odot} = 9.1795 \times 10^{31}$ erg s^{-1} (see Section 2.3.2).

Siess, 2007; Denissenkov *et al.*, 2015; Farmer *et al.*, 2015; Lecoanet *et al.*, 2016).

A thin He shell grows as material from the adjacent H-burning shell is processed, causing the He shell to increase in temperature and pressure. Once the mass in the He shell reaches a critical value, He ignition causes a thermal pulse. For example, the 3 $M_\odot$ model goes through a series of six thermal pulses, with an interpulse period of $\simeq 10^5$ yr. The number of thermal pulses a model undergoes is poorly determined as the number is sensitive to the mass resolution, the stellar mass loss rate, and the treatment of convective boundaries. These thermal pulses are visible in the neutrino HR diagram of Figure 2.2 as the spikes in the region labelled "Thermal Pulses".

The stellar models leave the thermal pulse phase when the envelope mass above the still active H and He burning shells is reduced to $\simeq$ 0.01 $M_\odot$ by stellar winds. All the low mass models then evolve toward larger $T_{\rm eff}$ at nearly constant L_ν and L_γ. Nuclear burning extinguishes as the post-AGB model enters the WD cooling track. Plasmon neutrino emission then dominates the energy loss budget for average-mass CO WDs with $T_{\rm eff} \gtrsim$ 25,000 K (Vila, 1966; Kutter and Savedoff, 1969; Bischoff-Kim and Montgomery, 2018). As the WD continues to cool, photons leaving the surface begin to dominate the cooling as the electrons transition to a strongly degenerate plasma (van Horn, 1971; Córsico *et al.*, 2019). The low mass models in Figure 2.2 are arbitrarily chosen to terminate when the WD reaches $L_\gamma = 0.1\ L_{\gamma,\odot}$. With $T_{\rm eff} \simeq$ 30,000 K at this arbitrary termination point, the WD models are still dominated by thermal neutrino cooling, $L_\nu/L_\gamma \simeq 3$ (Winget *et al.*, 2004). For calculating the integrated neutrino background from stellar sources, especially if WDs are abundant, these models should be further evolved to $T_{\rm eff} \lesssim$ 12,000 K to drive $L_\nu/L_\gamma \leq 10^{-5}$ (e.g., Figure 5 in Timmes *et al.*, 2018a).

2.4.2 High Mass Stars

High mass stars (M $\gtrsim$ 8 $M_\odot$) in Figure 2.2 evolve at nearly constant L_ν and L_γ as hydrogen depletes in the core and the models evolve to cooler $T_{\rm eff}$. Free streaming neutrinos from thermal processes, primarily pair annihilation, dominate a star's energy loss budget from the core C-burning phase to core Si depletion. For the 30 $M_\odot$ model, from Figure 2.2, L_ν=8.2×10^3 $L_{\gamma,\odot}$ and L_γ=1.2×10^5 $L_{\gamma,\odot}$ on the MS, L_ν=1.3×10^4 $L_{\gamma,\odot}$ and L_γ=3.0×10^5 $L_{\gamma,\odot}$ at core He-ignition, L_ν=5.3×10^3 $L_{\gamma,\odot}$

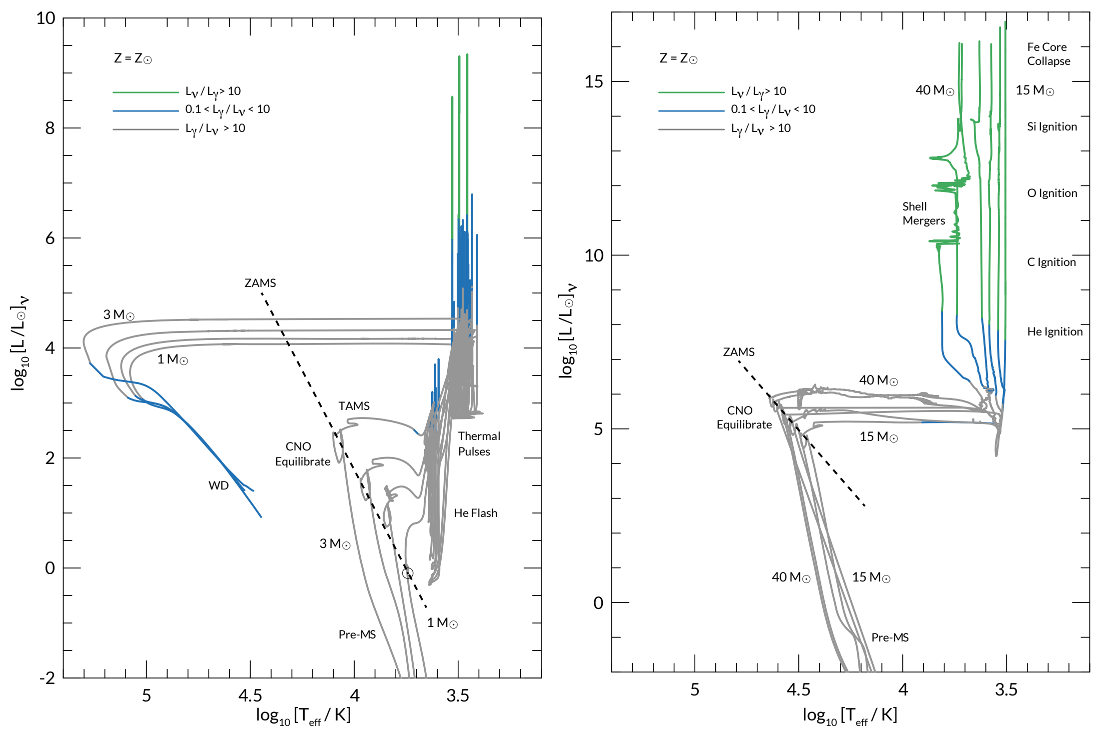

Figure 2.4: Ratio of the photon luminosity to the neutrino luminosity in a neutrino HR diagram. Low mass stars are on the left, high mass stars on the right. Gray curves indicate where photons dominate, green curves where neutrinos dominate, and blue curves where the photon and neutrino luminosities are within a factor of 10. The neutrino luminosity is normalized by the current solar value $L_{\nu,\odot} = 0.02398 \cdot L_{\gamma,\odot} = 9.1795 \times 10^{31}$ erg s^{-1} (see Section 2.3.2).

and L_γ=2.7×10^5 $L_{\gamma,\odot}$ at core He-depletion (mass fraction of ^{4}He less than 0.001), L_ν=3.2×10^7 $L_{\gamma,\odot}$ and L_γ=3.1×10^5 $L_{\gamma,\odot}$ at core C-ignition. This dominance over photons as the primary energy loss mechanism sets a rapid evolutionary timescale (years to hours) for the advanced stages of nuclear fusion in presupernova stars (Woosley *et al.*, 2002). This rapid evolution is visible in the neutrino HR diagram of Figure 2.2 as the nearly vertical curves at approximately constant $T_{\rm eff}$.

Weak reactions that increase the electron to baryon ratio during C-burning include

β-processes involving ^{23}Mg and ^{21,22}Na. The composition continues to become more neutron-rich during O-burning from β-processes on ^{30,33}P, ^{33}P, ^{35}Cl, and ^{37}Ar Core Si-burning is the last exothermic burning stage and produces the Fe-peak nuclei. Many isotopes in this stage of evolution undergo β-processes that continue to make the material more neutron-rich (see Heger *et al.*, 2001; Odrzywolek, 2009; Patton *et al.*, 2017b).

Dynamical large-scale mixing on nuclear burning timescales occurs during the late stages of evolution in massive stars. Stellar evolution models suggest that merging occurs between the C, Ne, O, and Si shells. These shell mergers are beginning to be explored with 3D hydrodynamic simulations (e.g., Ritter *et al.*, 2018). The approximate location of these shell mergers is labeled in the neutrino HR diagram. In addition, the energetics of nuclear burning tightly couples to turbulent convection during O-burning and Si-burning. This strong coupling must be modeled with 3D simulations (Meakin and Arnett, 2007; Couch *et al.*, 2015; Müller *et al.*, 2017; Fields and Couch, 2020) to assess the fidelity of the convection approximations made by 1D models.

When the Fe core reaches its finite-temperature Chandrasekhar mass, electron capture and photodisintegration drive collapse of the Fe core, with the largest infall speeds usually occurring near the outer edge of the Fe core. The massive star models in Figure 2.2 terminate when any mass coordinate within the Fe core exceeds an inward velocity of 300 km sec^{-1}.

2.4.3 Reaction and Thermal Neutrino Luminosities

Figure 2.3 shows the ratio of nuclear reaction neutrinos to thermal neutrinos along the stellar evolution tracks in the neutrino HR diagram. Broadly, neutrinos from reactions dominate during H and He burning, and thermal neutrinos dominate for C-burning onwards. There are exceptions to this general scenario. One exception is between the subflashes of the He flash for low mass stars, where thermal neutrinos become comparable or larger than neutrino losses from reactions. Another exception are between thermal pulses on the AGB where thermal neutrinos are again comparable or larger than nuclear reaction neutrinos. Conversely, nuclear reaction neutrinos are comparable to, but less than, thermal neutrinos during the final phases of massive star evolution.

2.4.4 Photon and Neutrino Luminosities

Figure 2.4 shows the L_γ/L_ν ratio along the stellar evolution tracks in the neutrino HR diagram. Photons dominate over most of star's lifetime (e.g., Barkat, 1975), except in the advanced stages of evolution, where neutrinos dominate on the early portions of the WD cooling tracks for low mass stars and for carbon burning to the onset of core collapse for high mass stars.

2.5 Discussion and Summary

Using a `MESA` solar calibrated model for the Sun's neutrino luminosity as a normalization (Section 2.3.2), we have explored the evolution of a select grid of stellar models from their pre-main sequence phase to near their final fates in a neutrino HR diagram (Figure 2.2). We also delineated the contributions from reaction and thermal neutrinos during a model's evolution (Figure 2.3). This is the first time, to our knowledge, that such an exploration with a different messenger, neutrinos, has been presented in the literature.

Neutrino astronomy is a unique tool that can yield insights into otherwise hidden aspects of stellar astrophysics (Bahcall, 1989; Beacom, 2010). However, the small cross section between neutrinos and baryonic matter, which allows neutrinos to escape from the star in the first place, means it is unlikely that near-future neutrino detectors will be able to probe the neutrino luminosity tracks shown in Figure 2.2.

A possible exception is the evolution of a pre-supernova star on timescales of a $\simeq$10 hr before Fe core-collapse. For a normal neutrino mass hierarchy, more than 200 events could be detected before core collapse for a 15-30 $M_\odot$ star at $\simeq$ 200 pc (e.g., α Orionis, Betelgeuse), and neutrino emission may be detectable within $\simeq$ 600 pc with the improved sensitivity of Super-Kamiokande with Gadolinium (Patton *et al.*, 2017b; Simpson *et al.*, 2019).

Another possible exception is the detection of neutrinos from the He flash and thermal pulses of low mass stars. Figures 2 and 3 suggest the He flash reaches peaks of $L_\nu \simeq 10^9\ L_{\nu,\odot}$ and is driven by the ^{18}F($,e^+\nu_e$)^{18}O reaction (Serenelli and Fukugita, 2005). The maximum energy of neutrinos emitted by this reaction is $\simeq$ 0.6 MeV and the average energy is $\simeq$ 0.3 MeV. The neutrino flux is thus $\Phi_{\nu,\mathrm{He\ flash}} \simeq 1.7\times10^7$ (10 pc/d)^2 cm^{-2} s^{-1} for a star located at a distance of d parsec. The timescale of this peak emission is $\simeq$ 3 days, depending chiefly on the initial ZAMS mass. Figures 2 and 3 also suggest that the He-burning driven thermal pulses reach peaks of $L_\nu \simeq 10^6\ L_{\nu,\odot}$ from the same ^{18}F($,e^+\nu_e$)^{18}O reaction with an average energy of $\simeq$ 0.3 MeV. This gives a neutrino flux of $\Phi_{\nu,\mathrm{TP}} \simeq 1.7\times10^4$ (10 pc/d)^2 cm^{-2} s^{-1} on timescales of $\simeq$ 0.1 yr, depending on the mass of the stellar envelope, uncertain mass loss rate, and pulse number. Finally, integration of the neutrino luminosity stellar evolution tracks may be useful for refining estimates of the diffuse stellar neutrino background (Horiuchi *et al.*, 2009; Beacom, 2010).

Chapter 3

STELLAR NEUTRINO EMISSION ACROSS THE MASS-METALLICITY PLANE

Below is the published work of Ebraheem Farag et al 2024 ApJS 270 5.

3.1 Abstract

We explore neutrino emission from nonrotating, single star models across six initial metallicities and seventy initial masses from the zero-age main sequence to the final fate. Overall, across the mass spectrum, we find metal-poor stellar models tend to have denser, hotter and more massive cores with lower envelope opacities, larger surface luminosities, and larger effective temperatures than their metal-rich counterparts. Across the mass-metallicity plane we identify the sequence (initial CNO $\rightarrow$ ^{14}N $\rightarrow$ ^{22}Ne $\rightarrow$ ^{25}Mg $\rightarrow$ ^{26}Al $\rightarrow$ ^{26}Mg $\rightarrow$ ^{30}P $\rightarrow$ ^{30}Si) as making primary contributions to the neutrino luminosity at different phases of evolution. For the low-mass models we find neutrino emission from the nitrogen flash and thermal pulse phases of evolution depend strongly on the initial metallicity. For the high-mass models, neutrino emission at He-core ignition and He-shell burning depends strongly on the initial metallicity. Anti-neutrino emission during C, Ne, and O burning shows a strong metallicity dependence with ^{22}Ne(α,n)^{25}Mg providing much of the neutron excess available for inverse-β decays. We integrate the stellar tracks over an initial mass function and time to investigate the neutrino emission from a simple stellar population. We find average neutrino emission from simple stellar populations to be 0.5–1.2 MeV electron neutrinos. Lower metallicity stellar populations produce slightly larger neutrino luminosities and average β decay energies. This study can provide targets for neutrino detectors from individual stars and stellar populations. We provide convenient fitting

formulae and open access to the photon and neutrino tracks for more sophisticated population synthesis models.

3.2 Introduction

The next core-collapse (CC) supernova in the Milky Way or one of its satellite galaxies will be an opportunity to observe the explosion of a massive star across the electromagnetic, gravitational, and particle spectrums. For example, neutrinos with energies $\lesssim$10 MeV have played a prominent role in stellar physics (Hirata *et al.*, 1987, 1988; Bionta *et al.*, 1987; Alekseev *et al.*, 1987; Bahcall, 1989; Borexino Collaboration *et al.*, 2014, 2018, 2020) and particle physics (Bahcall, 1989; Ahmad *et al.*, 2002; Ackermann *et al.*, 2022). Maps of $\geq$1 TeV neutrinos from the Galactic plane are consistent with a diffuse emission model of neutrinos whose analysis includes the supernova remnant and pulsar wind nebula outcome(s) of CC events (IceCube Collaboration, 2023).

Ongoing technological improvements in detector masses, energy resolution, and background abatement will allow the global *SuperNova Early Warning System* network (Al Kharusi *et al.*, 2021) to observe new signals from different stages of the lifecycle of individual stars or the aggregate signal from a stellar population with multi-kiloton detectors such as *SuperKamiokande* (Simpson *et al.*, 2019; Harada *et al.*, 2023), *SNO+* (Allega *et al.*, 2023), *KamLAND* (Abe *et al.*, 2023), *Daya Bay* (An *et al.*, 2023), *DUNE* (Acciarri *et al.*, 2016), *JUNO* (Yang and JUNO Collaboration, 2022) and the upcoming *HyperKamiokande* (Abe *et al.*, 2016).

Examples of ongoing stellar neutrino searches include pre-supernova neutrinos which allow new tests of stellar and neutrino physics (e.g., Odrzywolek *et al.*, 2004; Kutschera *et al.*, 2009; Odrzywolek, 2009; Patton *et al.*, 2017a,b; Kato *et al.*, 2017, 2020a; Kosmas *et al.*, 2022) and enable an early alert of an impending CC supernova to the electromagnetic and gravitational wave communities (Beacom and Vogel, 1999; Vogel and Beacom, 1999; Mukhopadhyay *et al.*, 2020; Al Kharusi *et al.*, 2021). Other ongoing explorations include the diffuse supernova neutrino background (Hartmann and Woosley, 1997; Bisnovatyi-Kogan and Seidov, 1984; Krauss *et al.*, 1984; Ando and Sato, 2004; Horiuchi *et al.*, 2009; Beacom, 2010; Anandagoda *et al.*, 2020; Suliga, 2022; Anandagoda *et al.*, 2023), and neutrinos from the helium-core nitrogen flash (Serenelli and Fukugita, 2005), compact object mergers (Kyutoku and Kashiyama, 2018b; Lin and Lunardini, 2020), tidal disruption of stars (Lunardini and Winter, 2017; Winter and Lunardini, 2022; Reusch *et al.*, 2022), and pulsational pair-instability supernovae (Leung *et al.*, 2020).

Farag *et al.* (2020) introduced the idea of a neutrino Hertzsprung–Russell Diagram (νHRD) with a sparse grid of models. Each model started from the zero-age main sequence (ZAMS) and ended at a final fate but only at solar metallicity. They found all masses produce a roughly constant neutrino luminosity L_ν during core H burning on the main-sequence (MS), and confirmed that low-mass ($M_{\rm ZAMS} < 8\ {\rm M}_\odot$) Red Giant Branch (RGB) models with $M_{\rm ZAMS} \leq 2\ {\rm M}_\odot$ undergo large increases in L_ν during the helium flash (nitrogen flash for neutrinos, Serenelli and Fukugita, 2005) and subsequent sub-flashes. They also found He burning in asymptotic giant branch (AGB) models undergo sharp increases in L_ν from thermal pulses (TPs), and significantly larger L_ν from the hotter and denser cores of later evolutionary stages culminating at the onset of CC in high-mass ($M_{\rm ZAMS} \geq 8\ {\rm M}_\odot$), non-rotating, single star models. A photon Hertzsprung–Russell Diagram (γHRD) provides information about the stellar surface, a νHRD can serve as a diagnostic tool of the stellar interior.

Changes in the initial metallicity Z of a model changes the structure of the model through the equation of state (EOS Saumon *et al.*, 1995; Timmes and Swesty, 2000; Rogers and Nayfonov, 2002; Irwin, 2004; Potekhin and Chabrier, 2010; Jermyn *et al.*, 2021; Bauer, 2023), radiative opacity (Iglesias and Rogers, 1993, 1996b; Ferguson *et al.*, 2005; Ferguson and Dotter, 2008; Poutanen, 2017), conductive opacity (Cassisi *et al.*, 2007; Blouin *et al.*, 2020), nuclear energy generation rate (Angulo *et al.*, 1999; Cyburt *et al.*, 2010b; Sallaska *et al.*, 2013; deBoer *et al.*, 2017; Farag *et al.*, 2022), gravitational sedimentation (Bauer *et al.*, 2020), and mass-loss by line driven winds (Sanyal *et al.*, 2017; VandenBerg *et al.*, 2022).

The coupling between these pieces of stellar physics and neutrino production from thermal (Itoh *et al.*, 1996a) and weak reaction processes (Fuller *et al.*, 1985; Oda *et al.*, 1994; Langanke and Martínez-Pinedo, 2000; Nabi *et al.*, 2021) suggests that changes in Z can cause changes in a νHRD, and upon integration, the neutrino emission from a simple stellar population model.

This article is novel in exploring stellar neutrino emission across the mass-metallicity plane. This study can provide targets for neutrino detectors from individual stars and stellar populations. Section 3.3 describes the mass-metallicity grid and stellar physics, § 3.4 presents overall features and drivers across the mass-metallicity plane, § 3.5 analyzes low-mass tracks, § 3.6 details high-mass tracks, § 3.7 explores neutrino emission from a simple stellar population model, and § 4.6 summarizes our results.

Important symbols are defined in Table 3.1 and Table 3.2. Acronyms and terminology are defined in Table 3.3.

3.3 Mass-Metallicity Plane and Stellar Physics

We model the evolution of single, non-rotating stars over a wide range of initial masses and metallicities, from the pre-main sequence (PMS) to the final fate. Figure 3.1 shows the mass-metallicity plane for 70 $M_{\rm ZAMS}$ models distributed in the range $0.2\,{\rm M}_\odot \leq M_{\rm ZAMS} \leq 150\,{\rm M}_\odot$ for six initial metallicities $\log({\rm Z}/Z_\odot) = 0.5$, 0, -0.5, -1, -2, -3, where we choose $Z_\odot = 0.0142$ (Asplund *et al.*, 2009). This mass-metallicity

Name	Description	Appears
A	Atomic number	3.3
D	Element diffusion coefficient	3.3
E	Energy	3.4.2
ϵ	Average neutrino energy	3.6.1
g	Gravitational acceleration	3.4.2
H	Pressure scale height	3.4.2
κ	Opacity	3.4.2
k_{B}	Boltzmann constant	3.4.2
L	Luminosity	4.2
M	Stellar mass	4.2
μ	Mean molecular weight	3.3
n	Number density	3.3
η	Neutron excess	3.3
R	Stellar Radius	3.5.2
ρ	Mass density	3.4.2
P	Pressure	3.4.2

Table 3.1: Important symbols.

plane spans the range of single stars found in the Galaxy (Edvardsson *et al.*, 1993; Ratcliffe *et al.*, 2023; Almeida-Fernandes *et al.*, 2023), and aids estimates of the neutrino emission from simple stellar population models.

We use `MESA` version r15140 to construct our stellar models (Paxton *et al.*, 2011, 2013, 2015, 2018, 2019; Jermyn *et al.*, 2023). We follow MIST (Choi *et al.*, 2016b) to

Name	Description	Appears
P	Pressure	3.4.2
T	Temperature	3.3
τ	Time or Timescale	3.5.2
X	Mass fraction	3.3
X	Hydrogen mass fraction	3.3
Y	Abundance	3.3
Y	Helium mass fraction	3.3
Y_e	Electron fraction	3.3
Z	Metal mass fraction	4.2
Z	Atomic charge	3.3

Table 3.2: Important symbols.

scale the H mass fraction X, He mass fraction Y, and metallicity Z

$$\mathrm{Y} = \mathrm{Y_p} + \left(\frac{\mathrm{Y_\odot} - \mathrm{Y_p}}{\mathrm{Z_\odot}}\right)\mathrm{Z} \tag{3.1}$$

$$\mathrm{X} = 1 - \mathrm{Y} - \mathrm{Z} \ , \tag{3.2}$$

where we adopt the primordial He abundance $\mathrm{Y_p} = 0.249$ (Planck Collaboration *et al.*, 2016), $Y_\odot = 0.2703$ and $Z_\odot = 0.0142$ with mass fractions from Asplund *et al.* (2009).

For the low-mass models, we chose the Riemers wind mass loss scheme (Reimers, 1977) with an efficiency of 0.5 on the RGB, and Blöckers wind mass loss scheme (Blöcker, 2001) with an efficiency of 1.0 on the AGB. All low-mass models terminate as a white dwarf (WD) at $L = 10^{-3}\,\mathrm{L_\odot}$, even if the evolution is longer than the age of the universe.

For the high-mass models, we choose the "Dutch" wind loss scheme (Nieuwenhuijzen and de Jager, 1990; Nugis and Lamers, 2000; Vink *et al.*, 2001; Glebbeek

Acronym	Description	Appears
AGB	Asymptotic Giant Branch	4.2
CC	Core Collapse	4.2
CHeB	Core Helium Burning	3.4
CHeD	Core Helium Depletion	3.4
CO	Carbon-Oxygen	3.4.1
EOS	Equation of State	4.2
γHRD	Photon Hertzsprung Russell Diagram	4.2
νHRD	Neutrino Hertzsprung Russell Diagram	4.2
HB	Horizontal Branch	3.5
IMF	Initial mass function	3.7
MLT	Mixing Length Theory	3.3
PMS	Pre-Main Sequence	3.3
RGB	Red Giant Branch	4.2
RSG	Red Supergiant	3.6
TP	Thermal Pulse	4.2
WD	White Dwarf	3.3
ZAMS	Zero Age Main Sequence	4.2
TAMS	Terminal Age Main Sequence	3.4
Low-mass	$M_{\rm ZAMS} < 8$ M$_{\odot}$	4.2
High-mass	$M_{\rm ZAMS} \geq 8$ M$_{\odot}$	4.2

Table 3.3: Acronyms and Terminology.

et al., 2009) with an efficiency of 1.0 to generate stripped models. All models use an Eddington-grey iterated atmosphere as an outer boundary condition. We apply an extra pressure to the surface (see Section 6.1 of Jermyn *et al.*, 2023) of our AGB and high-mass models to maintain stability of the surface layer in super Eddington regimes where the surface of the model can otherwise run away. The termination age for all high-mass models is at the onset of CC when the infall velocity of the Fe core reaches 100 km s^{-1}. A subset of our models halted prematurely: at core C-depletion ($M_{\rm ZAMS} = 8$–$10\ M_\odot$), a stalled Ne/O flame in a degenerate core ($M_{\rm ZAMS} = 11$–$14\ M_\odot$), the onset of pair-instability (C-ignition with $M_{\rm He} \gtrsim 45\ M_\odot$), or due to numerical difficulties near the onset of CC.

We adopt a minimum chemical diffusive mixing coefficient of $D_{\rm min} = 10^{-2}$ cm^2 s^{-1} from C-ignition to the onset of CC to aid the convergence properties of our high-mass models (Farag *et al.*, 2022). To reduce the numerical cost we use operator splitting to decouple the hydrodynamics from the nuclear burning for temperatures above $T = 1{\times}10^9$ K (Jermyn *et al.*, 2023).

We also adopt $\alpha = 1.5$ for the convective mixing-length parameter, and $f_{ov} = 0.016$, $f_{0,ov} = 0.008$ for the convective overshooting parameters in all convective regions (Herwig, 2000b; Choi *et al.*, 2016b). All stellar models use the MLT++ treatment for superadiabatic convection in the envelopes (Sabhahit *et al.*, 2021). We also damp the velocities in the envelopes of our low-mass AGB models and high-mass models during the advanced burning stages to inhibit the growth of radial pulsations.

Figure 3.1 illustrates the 52 isotope nuclear reaction network used for low-mass stars and the 136 isotope reaction network used for high-mass models. Extended networks are required to accurately capture the nuclear energy generation, composition and stellar structure profiles, and the neutrino luminosity and spectra from β-processes (Farmer *et al.*, 2016; Patton *et al.*, 2017a,b; Kato *et al.*, 2020a). The 136 isotope network is reliable up to the onset of Si-shell burning, $T \lesssim 4{\times}10^9$ K. At higher temperatures, the paucity of Fe group isotopes in this reaction network cannot fully capture the nuclear burning (Farmer *et al.*, 2016; Patton *et al.*, 2017a).

Nuclear reaction rates are a combination of NACRE (Angulo *et al.*, 1999) and JINA REACLIB (Cyburt *et al.*, 2010a). We use the median ^{12}C(α,γ)^{16}O reaction rate from the experimental probability distribution function provided by deBoer *et al.* (2017), updated in Mehta *et al.* (2022), and publicly released in Chidester *et al.* (2022). Reaction rate screening corrections are from Chugunov *et al.* (2007), which includes a physical parameterization for the intermediate screening regime and reduces to the weak (Dewitt *et al.*, 1973; Graboske *et al.*, 1973) and strong (Alastuey and Jancovici, 1978; Itoh *et al.*, 1979) screening limits at small and large values of the plasma coupling parameter. Weak reaction rates are based, in order of precedence, on Langanke and Martínez-Pinedo (2000), Oda *et al.* (1994), and Fuller *et al.* (1985).

Baryon number is conserved in nuclear reactions. Define the abundance of species Y_i by

$$Y_i = \frac{n_i}{n_B} \tag{3.3}$$

where n_i is the number density of isotope i and n_B is baryon number density. The number of baryons in isotope i divided by the total number of baryons of all isotopes is the baryon fraction (mass fraction)

$$X_i = \frac{n_i\ A_i}{n_B} = Y_i\ A_i\ , \tag{3.4}$$

where A_i is the atomic mass number, the number of baryons in an isotope. The mean atomic number is

$$\overline{A} = \frac{\sum n_i A_i}{\sum n_i} = \frac{n_B}{\sum n_i} = \frac{\sum Y_i A_i}{\sum Y_i} = \frac{1}{\sum Y_i}\ , \tag{3.5}$$

the mean charge is

$$\overline{Z} = \frac{\sum n_i Z_i}{\sum n_i} = \frac{\sum Y_i Z_i}{\sum Y_i} = \overline{A} \sum Y_i Z_i\ , \tag{3.6}$$

the electron to baryon ratio (electron fraction) is

$$Y_e = \frac{n_e}{n_B} = \frac{\sum n_i Z_i}{n_B} = \sum Y_i Z_i = \frac{\overline{Z}}{\overline{A}} \ , \tag{3.7}$$

where n_e is the free electron number density and the second equality assumes full ionization. The related neutron excess is

$$\eta = \sum (\mathrm{N}_i - \mathrm{Z}_i) Y_i = 1 - 2Y_e \ , \tag{3.8}$$

the mean ion molecular weight is

$$\mu_{\mathrm{ion}} = \overline{A} \ , \tag{3.9}$$

the mean electron molecular weight is

$$\mu_{\mathrm{ele}} = \frac{1}{Y_e} = \frac{\overline{A}}{\overline{Z}} \ , \tag{3.10}$$

and the mean molecular weight is

$$\mu = \left[\frac{1}{\mu_{\mathrm{ion}}} + \frac{1}{\mu_{\mathrm{ele}}} \right]^{-1} = \frac{\overline{A}}{\overline{Z} + 1} = \frac{n_B}{\sum n_i + n_e} \ . \tag{3.11}$$

Across the mass-metallicity plane the dominant thermal neutrino processes in our models are plasmon decay ($\gamma_{\mathrm{plasmon}} \rightarrow \nu + \bar{\nu}$) which scales with the composition as Y_e^3, photoneutrino production ($e^- + \gamma \rightarrow e^- + \nu + \bar{\nu}$) which scales as Y_e, and pair annihilation ($e^- + e^+ \rightarrow \nu + \bar{\nu}$) which also scales as Y_e. All else being equal, as material becomes more neutron rich the neutrino emission from these three dominant processes decrease.

Bremsstrahlung ($e^- + {}^A Z \rightarrow e^- + {}^A Z + \nu + \bar{\nu}$), which scales with the composition as $Y_e \overline{Z}$, and recombination ($e^-_{\mathrm{continuum}} \rightarrow e^-_{\mathrm{bound}} + \nu + \bar{\nu}$) , which scales as $\overline{Z}^{14}/\overline{A}$, play smaller roles. Neutrino emission from these five processes are discussed in Itoh *et al.* (1989, 1992, 1996a,b); Kantor and Gusakov (2007) and implemented, with partial first derivatives, in the `MESA` module `neu`. Differential thermal neutrino emission rates are discussed in Ratković *et al.* (2003); Dutta *et al.* (2004); Misiaszek *et al.* (2006a); Odrzywołek (2007); Kato *et al.* (2015); Patton *et al.* (2017a); Dzhioev *et al.* (2023).

Each of the 420 stellar models in the mass-metallicity grid use between 2000–3500 mass zones (lower values occur at ZAMS where there are no composition gradients) with ≃3000 mass zones over the evolution being typical. Each low-mass model uses $1{\times}10^5 - 3{\times}10^5$ timesteps depending on the number of thermal pulses (TPs), and each high-mass model uses $2{\times}10^4 - 5{\times}10^4$ timesteps. Each model executes on a 16 core node with 2 GHz AMD Epyc 7713 CPUs, with low-mass models consuming 14–21 days and high-mass models using 10-21 days. The uncompressed total data set size is ≃ 730 GB.

The `MESA` files to reproduce our models, and open access to the photon and neutrino tracks, are available at `https://doi.org/10.5281/zenodo.8327401`.

3.4 Overall Mass-Metallicity Features

Here we present features and drivers of the neutrino emission, first at one metallicity in Section 3.4.1 and then for all six metallicities in Section 3.4.2.

3.4.1 One Metallicity

Figure 3.2 shows the photon and neutrino light curves for all 70 calculated masses at $Z = 1\,Z_{\odot}$. Both plots begin at the ZAMS, defined when the luminosity from nuclear reactions $L_{\rm nuc}$ is 99% of the total luminosity L, marking a transition from evolution on thermal timescale to a nuclear timescale.

MS evolution is characterized by stable core H-burning, where neutrinos are produced by weak reactions in the proton-proton (pp) chains $\rm p(p,e^+\nu_e)^2H$, $\rm p(e^-p,\nu_e)^2H$, $\rm ^3He(p,e^+\nu_e)^4He$, $\rm ^7Be(e^-,\nu_e)^7Li$, $\rm ^8B(,e^+\nu_e)^8Be$, and the CNO cycles $\rm ^{13}N(,e^+\nu_e)^{13}C$, $\rm ^{13}N(e^-,\nu_e)^{13}C$, $\rm ^{15}O(,e^+\nu_e)^{15}N$, $\rm ^{15}O(e^-,\nu_e)^{15}N$, $\rm ^{17}F(,e^+\nu_e)^{17}O$, $\rm ^{17}F(e^-,\nu_e)^{17}O$,

^{18}F(,e$^{+}\nu_e$)^{18}O, where electron capture reactions on CNO nuclei are included (Stonehill *et al.*, 2004).

Models with $M_{\rm ZAMS} \lesssim 1.2$ M$_\odot$ have a central temperature $T_{\rm c} \lesssim 18{\times}10^7$ K and burn H in their cores primarily through the pp chains, with a small fraction from the CNO cycles. For example, based on observations of solar neutrinos CNO burning accounts for around 1.6% of the current energy generation of the Sun (Naumov, 2011; Borexino Collaboration *et al.*, 2020). Models with $M_{\rm ZAMS} \gtrsim 1.2$ M$_\odot$ have $T_{\rm c} \gtrsim 18{\times}10^7$ K and maintain their stability primarily from the CNO cycles (Wiescher *et al.*, 2010). Metal-poor models can produce their own carbon to begin CNO cycle H-burning (Mitalas, 1985; Wiescher *et al.*, 1989; Weiss *et al.*, 2000; Tompkins *et al.*, 2020). In addition, most of a model's initial Z comes from the CNO and ^{56}Fe nuclei inherited from its ambient interstellar medium. The slowest step in the CNO cycle is proton capture onto ^{14}N, resulting in all the CNO catalysts accumulating into ^{14}N during core H-burning.

All light curves in Figure 3.2 proceed to the terminal age main sequence (TAMS), defined by core H-depletion ($X_{\rm c} \leq 10^{-6}$). The He-rich core contracts as a H-burning shell forms. The higher temperatures of shell H-burning can activate the Ne-Na, and Mg-Al cycles (Salpeter, 1955; Marion and Fowler, 1957; Arnould *et al.*, 1999; José *et al.*, 1999; Izzard *et al.*, 2007; Boeltzig *et al.*, 2022). The light curves then bifurcate depending on $M_{\rm ZAMS}$.

During He-burning the accumulated ^{14}N is converted into the neutron-rich isotope ^{22}Ne through the reaction sequence ^{14}N(α,γ)^{18}F(,$e^{+}\nu_e$)^{18}O(α,γ)^{22}Ne, also shown in Figure 3.2. This sequence is the source of neutrinos powering L_ν through all phases of He-burning (Serenelli and Fukugita, 2005; Farag *et al.*, 2020).

Usually the ashes of nuclear burning have a larger $\overline{A}$ and lie interior to the unburned fuel. For example, a He core is interior to a H-burning shell, and a carbon-oxygen (CO) core is interior to a He-burning shell. Exceptions occur when electron degeneracy and thermal neutrino losses lead to a temperature inversion with cooler temperatures in the central regions and hotter temperatures exterior to the core. The fuel ignites off-center and a burning front propagates towards the center.

For example, the $0.9\,\mathrm{M}_\odot \leq M_{\mathrm{ZAMS}} \leq 2\,\mathrm{M}_\odot$ light curves in Figure 3.2 undergo off-center He ignition, the He Flash (Thomas, 1967; Bildsten *et al.*, 2012; Gautschy, 2012; Serenelli *et al.*, 2017). The accompanying nitrogen flash for neutrinos (Serenelli and Weiss, 2005) are prominent and labeled. In contrast, the $M_{\mathrm{ZAMS}} \geq 2\,\mathrm{M}_\odot$ light curves undergo central He burning. The $0.9\,\mathrm{M}_\odot \leq M_{\mathrm{ZAMS}} \leq 7\,\mathrm{M}_\odot$ light curves undergo TPs on the AGB, generating neutrinos first from H burning, and subsequently from He burning. A few light curves show a late TP during the transition to a cool WD.

Neutrino emission from nuclear reactions dominate whenever H and He burn, otherwise neutrinos from thermal processes generally dominate (Farag *et al.*, 2020). For example, light curves for $M_{\mathrm{ZAMS}} \geq 8$ $\mathrm{M}_\odot$ in Figure 3.2 have the minimum mass for C ignition and those for $M_{\mathrm{ZAMS}} \geq 10$ $\mathrm{M}_\odot$ have the minimum mass for Ne ignition (Becker and Iben, 1979, 1980; García-Berro *et al.*, 1997; Farmer *et al.*, 2015; De Gerónimo *et al.*, 2022). For these advanced burning stages L_ν in Figure 3.2 become nearly vertical and greatly exceeds L_γ. Thermal neutrinos from pair-production dominate until the last few hours before CC when neutrinos from nuclear processes contribute (Odrzywolek *et al.*, 2004; Odrzywolek and Heger, 2010; Patton *et al.*, 2017a,b; Kato *et al.*, 2020a,b).

3.4.2 Six Metallicities

The top panel of Figure 3.3 shows the total energy emitted in photons E_γ and neutrinos E_ν, obtained by integrating L_γ and L_ν over the lifetime of a model. Metal-poor models tend to have larger E_γ and E_ν than the metal-rich models. Homology relations with power-law expressions for a bound-free Kramers opacity $\kappa \propto$ Z(1 + X)$\rho T^{-3.5}$, pp-chain energy generation rate $\epsilon_{\rm pp} \propto$ X$^2\rho T^4$, and mean molecular weight $\mu \propto$ X$^{-0.57}$ lead to (Sandage, 1986; Hansen *et al.*, 2004)

$$E_\gamma \simeq L_\gamma\, \tau_{\rm MS} \propto (Z^{-1.1} X^{-5.0} M^{5.5})\, \tau_{\rm MS}\ , \tag{3.12}$$

where $\tau_{\rm MS}$ is the MS lifetime. Similarly, for a Thomson electron scattering opacity $\kappa \propto 1 +$ X and CNO cycle energy generation rate $\epsilon_{\rm CNO} \propto$ XZρT^{17},

$$E_\gamma \simeq L_\gamma\, \tau_{\rm MS} \propto (Z^{-1.0} X^{-4.3} M^{5.1})\, \tau_{\rm MS}\ . \tag{3.13}$$

These expressions suggest that displacement on the MS due to a lower Z is partially offset by a shift to a larger X (Demarque, 1960). In addition, a lower Z requires higher $T_{\rm c}$ to produce the same L_γ and L_ν. This is mainly why the low-Z high-mass models in Figure 3.3 produce only a marginally larger L_γ and L_ν on the MS while possessing larger $T_{\rm c}$. In turn, a larger L_γ implies a larger radiative gradient, and thus a larger core mass.

L_γ and L_ν in the core is primarily set by the mass of the model. Envelope opacities affect the rate of nuclear reactions in the core insofar as the envelope has a large mass. The hotter the model is overall (e.g., the more massive), the less mass in the envelope will be cold enough to provide bound-free or bound-bound opacity. The largest differences due to the opacity occur in the low-mass models because they are colder, both in the core and the envelope. The models adjust the structure to accommodate a change in Z at a fixed luminosity.

Overall, across the mass spectrum, metal-poor stellar models tend to have denser, hotter and more massive cores with lower envelope opacities, larger surface luminosities and larger effective temperatures $T_{\rm eff}$ than their metal-rich counterparts (Demarque, 1960; Iben, 1963; Demarque, 1967; Iben and Rood, 1970; Vandenberg, 1983;

Sandage, 1986; Hansen *et al.*, 2004; Georgy *et al.*, 2013; Young, 2018; Groh *et al.*, 2019; Kemp *et al.*, 2022). These are the main drivers of changes to the thermal and nuclear reaction neutrino emission as the initial Z changes.

The bottom panel of Figure 3.3 shows the ratio E_γ/E_ν. A maximum of $E_\gamma/E_\nu \simeq 20$ at $M_{\rm ZAMS} \simeq 0.9\,{\rm M}_\odot$ occurs at the transition between models that ignite He and those that do not, between the most massive He WD and the least massive CO WD. As $M_{\rm ZAMS}$ increases the resulting electron degenerate cores, first CO then ONeMg, become progressively more massive, denser, and hotter (also see Woosley and Heger, 2015). This increases production of thermal neutrinos from the plasmon, photoneutrino, and pair annihilation channels faster than the production of reaction neutrinos or photons. Thus $E_\gamma/\ E_\nu$ decreases with $M_{\rm ZAMS}$ as shown in Figure 3.3.

A minimum of $E_\gamma/E_\nu \simeq 8$ at $M_{\rm ZAMS} \simeq 12\,{\rm M}_\odot$ in Figure 3.3 occurs at the transition between models that produce the most massive WD and those that go to CC. As $M_{\rm ZAMS}$ further increases, thermal neutrinos from pair annihilation increases slower than reaction neutrinos or photons, and thus E_ν is smaller than E_γ in more massive models (pulsational pair-instability supernovae models are suppressed). The ratio E_γ/E_ν thus rises from the minimum and develops a roughly linear trend for $M_{\rm ZAMS} \gtrsim 12\,{\rm M}_\odot$. Overall, both extrema of E_γ/E_ν of Figure 3.3 correlate with transitions in the final fate.

Another trend in the bottom panel of Figure 3.3 is the metallicity dependence of $M_{\rm ZAMS}$ models that become CO WD, the blue shaded region. More metal-rich models have a larger E_γ/E_ν than metal-poor models. A larger initial Z produces a larger accumulation of ^{14}N during CNO cycle H-burning, thus a larger mass fraction of ^{22}Ne during He-burning, and hence a smaller Y_e as the CO WD becomes more neutron-rich. Plasmon neutrino rates scale as Y_e^3 leading to a smaller E_ν, hence more metal-rich models have a larger E_γ/E_ν than metal-poor models in this $M_{\rm ZAMS}$ range.

The dependence of CO WD on the ^{22}Ne mass fraction, the degree of neutronization, may have implications for the progenitors Type Ia supernova (Timmes *et al.*, 2003; Townsley *et al.*, 2009; Bravo *et al.*, 2010; Piersanti *et al.*, 2022) and the pulsation periods of variable WD (Campante *et al.*, 2016; Chidester *et al.*, 2021; Althaus and Córsico, 2022).

Farag *et al.* (2020) showed $L_\gamma/L_\nu \simeq 40$ for a standard solar model. As this model evolves off the MS the inert He core becomes denser, more electron degenerate, thermal neutrino production rise, L_ν increases, and thus L_γ/L_νdecreases. Integrated over the lifetime of the model, E_γ/E_ν decreases to $\simeq 20$ as shown in Figure 3.3.

For any $M_{\rm ZAMS}$, what is the impact of changing Z on the neutrino emission at any evolutionary stage?

Figure 3.4 compares L_ν to L_ν of the $\mathrm{Z} = 1\,Z_\odot$ model across the mass-metallicity plane at three evolutionary stages in the top three panels. As for Figure 3.3, at the ZAMS there is generally a small dependence on the initial Z but there are interesting features. For example, the dip at $M_{\rm ZAMS} \simeq 1.2\,\mathrm{M}_\odot$ corresponds to the transition from pp-chain dominated to CNO cycle dominated H-burning. Another feature is the stronger Z dependence for $M_{\rm ZAMS}$ models that become CO WD. As low-Z models tend to have denser, hotter and more massive H-burning cores, thermal and reaction neutrino contributions to L_ν is larger relative to high-Z models.

At the TAMS, the 0.2 $\mathrm{M}_\odot \leq M_{\rm ZAMS} \leq$ 8.0 $\mathrm{M}_\odot$ models in Figure 3.4 have a partially degenerate He-rich core. As low-Z models have denser, hotter and more massive cores than high-Z models, the thermal plasmon neutrino contributions to L_ν are larger. More massive $M_{\rm ZAMS}$ models do not develop degenerate He-rich cores, and the small dependence on the initial Z continues. The most metal-rich track decreases due to the larger mass loss.

At core He-depletion (CHeD), the $0.9\,\mathrm{M}_\odot \leq M_{\rm ZAMS} \leq 8.0\,\mathrm{M}_\odot$ models have a partially electron-degenerate CO-rich core. The denser, hotter and more massive cores of the low-Z models means larger thermal neutrino contributions, and thus L_ν is larger in lower Z models.

The $M_{\rm ZAMS} \geq 60$ $M_\odot$ models at CHeD in Figure 3.4 show sawtooth profiles with the lowest Z models disrupting a metallicity trend. This occurs because the convective boundary mixing model, exponential overshooting (Herwig, 2000b), is based on the pressure scale height $H = P/(\rho g) \simeq k_B T/(\mu_{\rm ion} g)$, where P is the pressure, $k_{\rm B}$ is the Boltzmann constant, and g is the gravitational acceleration. All else being equal, a smaller Z means a smaller $\mu_{\rm ion}$, a larger H, and thus the chemical mixing region in low-Z models is larger than in high-Z models. If two burning shells are within H, they are mixed. For masses with low L_ν, the H-shell mixes into the burning He core repeatedly. This delays core He burning until there is a homogeneous stripped CO core with a little He on the surface. By CHeD there is no H-shell to undergo CNO burning and all the ^{14}N is depleted, ergo L_ν is very low.

Overall, for fixed overshooting parameters, metal-poor models have larger amounts of chemical mixing. This is a secondary driver of changes to the thermal and nuclear reaction neutrino emission as the initial metallicity changes. Other specific examples of overshooting dominating are shown for low-mass models in Section 3.5 and for high-mass models in Section 3.6. The overshooting prescription may have an additional metallicity dependence that is not captured by these models.

Figure 3.4 also compares E_ν at each $M_{\rm ZAMS}$ to E_ν of the $Z = 1\, Z_\odot$ model on a linear scale at three evolutionary stages in the bottom three panels. At the TAMS, models across the mass spectrum reflect the Z dependence of L_ν shown in the top two panels. At CHeD, the denser, hotter and more massive cores of the low-Z models, plus contributions from the conversion of ^{14}N into ^{22}Ne, also show larger E_ν with decreasing Z.

Tracks in the bottom panel of Figure 3.4 are the same neutrino tracks in Figure 3.3 but normalized to the solar metallicity track. The $M_{\rm ZAMS}$ range for He WD and CO WD have the metallicity signature of having had an inert, electron-degenerate core during their evolution. The ONeMg WD region shows a sawtooth pattern because these models had numerical challenges completing the propagation of their off-center, convectively bounded flame fronts to the center. The $M_{\rm ZAMS}$ region for CC events show a weak dependence of E_ν on Z.

3.5 Low-Mass Stars

Here we analyze the neutrino emission from the low-mass stellar tracks at one metallicity in Section 3.5.1, and then for all six metallicities in Section 3.5.2.

3.5.1 One Metallicity

Figure 3.5 shows the 0.2 $\rm M_\odot \leq M_{\rm ZAMS} \leq 7.0\ M_\odot$ tracks in a γHRD and a νHRD for $\rm Z = 1\ \it Z_\odot$. The cores are progressively enriched with the ashes of H-burning as the models begin to evolve beyond the MS. The H-burning reactions increase μ and thus ρ in the core. To maintain hydrostatic equilibrium the central temperature $T_{\rm c}$ rises with the central density $\rho_{\rm c}$, increasing the rate of nuclear fusion and thus L_γ and L_ν. This slow increase of $T_{\rm c}$ is reflected in the γHRD and νHRD of Figure 3.5 as an increase in their respective luminosities until core H-depletion at the terminal-age main-sequence (TAMS).

The He-rich core contracts as an H-burning shell forms and the tracks in Figure 3.5 evolve across both HRDs on a thermal timescale. Both L_γ and L_ν increase along the RGB until core He-ignition at the tip of the RGB. All tracks that reach this point have a semi electron degenerate He core with 0.5 $\rm M_\odot \leq M_{\rm He} \leq 1.7\ M_\odot$, and a similar L_γ, L_ν, and $T_{\rm eff}$ (Cassisi and Salaris, 2013; Serenelli *et al.*, 2017). Photons from the tip of the RGB provide a standard candle distance indicator (Da Costa and Armandroff, 1990; Lee *et al.*, 1993; Madore *et al.*, 2023), and offer constraints on the neutrino magnetic dipole moment (Capozzi and Raffelt, 2020; Franz *et al.*, 2023).

He ignition by the triple-α process in the 0.9 $M_\odot \leq M_{\rm ZAMS} \leq 2.1$ $M_\odot$ tracks of Figure 3.5 occur off-center (on-center in the 2.1 $M_\odot$) and under semi-electron-degenerate conditions in a helium flash (Thomas, 1967; Bildsten *et al.*, 2012; Gautschy, 2012; Serenelli *et al.*, 2017). A He burning front propagates towards the center by conduction, with burning behind the front driving convection. The helium flash and the sub-flashes that follow burn very little He; the nuclear energy generated mainly goes into lifting the electron degeneracy in the core. The last sub-flash reaches and heats the center allowing stable convective core He-burning under non-degenerate conditions.

During each helium flash, a nitrogen flash also occurs from the conversion of all of the accumulated ^{14}N to ^{22}Ne, sharply increasing L_ν via ^{18}F$(,e^+\nu_e)^{18}$O (Serenelli and Weiss, 2005). For example, Figure 3.6 shows that a $M_{\rm ZAMS} = 1$ $M_\odot$, $Z = 1$ $Z_\odot$ track undergoes 7 flashes. The first flash is the strongest, occurring at $M \simeq 0.2 M_\odot$ and reaches $L_\nu \simeq 2 \times 10^7$ $L_\odot$ for $\simeq 3$ days.

Tracks with $M_{\rm ZAMS} \geq 2.1\, M_\odot$ reach a high enough $T_{\rm c}$ at the tip of the RGB to ignite He in the center quiescently under non-degenerate conditions. For example, Figure 3.6 shows a $M_{\rm ZAMS} = 3$ $M_\odot, 1$ $Z_\odot$ track produces a smoother L_ν signature during core He burning than a $M_{\rm ZAMS} = 1$ $M_\odot, 1$ $Z_\odot$ track. Tracks in this mass-metallicity range also experience a blue loop (Hayashi *et al.*, 1962; Hofmeister *et al.*, 1964; Xu and Li, 2004; Zhao *et al.*, 2023) in the γHRD and νHRD of Figure 3.5.

Post He ignition, the tracks in Figure 3.5 migrate to the horizontal branch (HB), becoming less luminous with larger $T_{\rm eff}$. All the He cores have approximately the same mass, regardless of the total stellar mass, and thus about the same helium fusion luminosity $L_{\rm He}$. These stars form the red clump at $T_{\rm eff} \simeq 5{,}000$ K, $L_\gamma \simeq 50$ L$_\odot$ and $L_\nu \simeq 20$ L$_\odot$ (Alves and Sarajedini, 1999; Sarajedini, 1999; Girardi, 1999; Hawkins *et al.*, 2017; Wang and Chen, 2021). Less massive H envelopes shift the tracks to hotter $T_{\rm eff}$ and smaller L_γ on the HB. This effect occurs more readily at lower Z (see §3.5.2) with old metal-poor clusters showing pronounced HB in a γHRD (Casamiquela *et al.*, 2021; Dondoglio *et al.*, 2021).

Core He-burning produces an electron-degenerate CO core with a semi-electron-degenerate He shell encased in a larger H-rich envelope. These AGB stars are the final stage of evolution driven by nuclear burning, characterized by H and He burning in geometrically thin shells on top of the CO core (Herwig, 2005). Larger $M_{\rm ZAMS}$ yield super-AGB models, where an Oxygen-Neon-Magnesium (ONeMg) core forms from a convectively bounded carbon flame propagating toward the center (Becker and Iben, 1979, 1980; Timmes *et al.*, 1994; García-Berro *et al.*, 1997; Siess, 2007; Denissenkov *et al.*, 2015; Farmer *et al.*, 2015; Lecoanet *et al.*, 2016).

During the AGB phase a thin He shell grows in mass as material from the adjacent H-burning shell is processed, causing the He shell to increase in temperature and pressure. When the mass in the He shell reaches a critical value (Schwarzschild and Härm, 1965; Giannone and Weigert, 1967; Siess, 2010; Gautschy, 2013; Lawlor, 2023), He ignition causes a thermal pulse (TP).

For example, Figure 3.6 shows the L_ν of a 3 M$_\odot$, 1 $Z_\odot$ track experiencing a series of 21 TPs, with an interpulse period of $\simeq 10^5$ yr. Like the helium flash, each TP is composed of a primary flash followed by a series of weaker sub-flashes. These TP sequences appear as spikes in the νHRD of Figure 3.5. The primary flash produces the largest $L_\nu \simeq 4.6 \times 10^4$ L$_\odot$ from ^{18}F$(,e^+\nu_e)^{18}$O. The sub-flashes do not produce neutrino emissions from this process, as nearly all of the ^{14}N is converted to ^{22}Ne during the primary flash. The number of TPs a track undergoes is uncertain as the number is sensitive to the mass and time resolution, the stellar mass loss rate, and the treatment of convective boundaries.

3.5.2 Six Metallicities

Figure 3.7 shows the evolution of $M_{\rm ZAMS} = 1$ M$_\odot$ and 3 M$_\odot$ in a γHRD and a νHRD across all six metallicities. Overall, the low-Z models show the trend of having denser, hotter and more massive cores with lower envelope opacities, larger surface luminosities and larger effective temperatures $T_{\rm eff}$ than the high-Z counterparts. Features in the νHRD between core H depletion and the end of the TP-AGB phase are analyzed below.

The tracks in Figure 3.7 leave the TP-AGB phase when the envelope mass above the H and He burning shells is reduced to $\simeq 0.01$ M$_\odot$ by stellar winds. All the tracks then evolve toward larger $T_{\rm eff}$ at nearly constant L_ν and L_γ. The $M_{\rm ZAMS} = 1$ M$_\odot$ and 3 M$_\odot$ tracks, in both the γ-HRD and ν-HRD, show late TPs for some metallicities. These are the result of a strong He flash (and nitrogen flash) that occurs after the AGB phase but before the WD cooling phase (Iben *et al.*, 1983; Bloecker and Schoenberner, 1997; Lawlor, 2023). A candidate late TP star is V839 Ara, the central star of the Stingray Nebula (Reindl *et al.*, 2017; Peña *et al.*, 2022). The more dramatic very late TP stars, also visible in Figure 3.7, include Sakurai's Object, V605 Aql, and perhaps HD 167362 the central star of planetary nebula SwSt 1 (Clayton and De Marco, 1997; Herwig, 2002; Miller Bertolami and Althaus, 2007; Hajduk *et al.*, 2020; Lawlor, 2023).

Plasmon neutrino emission then dominates the energy loss budget in Figure 3.7 for average-mass $\simeq 0.6$ M$_\odot$ CO WDs with $T_{\rm eff} \gtrsim 25{,}000$ K (Vila, 1966; Kutter and Savedoff, 1969; Bischoff-Kim and Montgomery, 2018). As the WD continues to cool, photons dominate the cooling as the electrons transition to a strongly degenerate plasma (van Horn, 1971; Córsico *et al.*, 2019). The tracks in Figure 3.7 are arbitrarily chosen to terminate when the WD reaches $L \leq 10^{-3}$L$_\odot$. This is sufficient (see Figure 5 of Timmes *et al.*, 2018b) for calculating the integrated neutrino background from a simple stellar population.

Figure 3.8 shows the fraction of L_ν from specific reaction sequences and weak reactions over the lifetime of the 1 M$_\odot$ models for all six metallicities. Fractions whose components do not sum to unity indicate the contribution of thermal neutrinos to L_ν.

The green shaded regions correspond to shell H-burning. The fraction of L_ν from the CNO cycles in this phase steadily increases with metallicity from the Z$\,=10^{-3}$ $Z_\odot$ in the bottom panel to Z$\,=10^{0.5}$ $Z_\odot$ in the top panel. Since the CNO nuclei catalyze H-burning, L_γ and L_ν depend directly on the initial metallicity.

The blue shaded regions represent core He-burning. In this phase, the fraction of L_ν from the ^{19}F $\rightarrow$ ^{18}O reaction dominates during the nitrogen flash. Neutrino emission from the H-burning pp-chain and CNO cycles appear during this phase of evolution for all six metallicities due to convective boundary mixing processes ingesting fresh H-rich material into the hotter core region. For the Z $\geq 10^{-0.5}$ $Z_\odot$ tracks, the convective boundary mixing processes and hotter temperatures drive the H-burning Mg-Al cycles (red curves) and the appearance of ^{26}Al $\rightarrow$ ^{26}Mg between sub-flashes.

Shell He-burning and the TP-AGB phase of evolution are shown by the pink shaded regions in Figure 3.8. The Z$\,=10^{-1,-0.5,0}$ $Z_\odot$ tracks show traditional TPs, with the fractions contributing to L_ν oscillating between successive TPs. Neutrino emission is initially from CNO burning before a TP, and then from ^{19}F $\rightarrow$ ^{18}O during the ensuing He-burning TP.

The Z$\,=10^{-3}$ $Z_\odot$ and Z$\,=10^{-2}$ $Z_\odot$ tracks in Figure 3.8 do not show traditional TPs. Instead they show a single event from a merger of their H-shells and He-shells that is driven by convective boundary mixing. As analyzed in Section 3.2, this is because metal-poor models have larger chemical convective boundary mixing regions than metal-rich models for fixed overshooting parameters. The Z$\,=\,10^{0.5}$ $Z_{\odot}$ tracks in Figure 3.8 also do not show traditional TPs due their thinner envelopes, caused by the metallicity dependent line driven wind mass loss prescriptions removing more envelope mass ($\dot{M} \propto Z$). During the WD cooling phase (purple shaded regions) late TPS are visible in the Z$\,=\,10^{-1,0}$ $Z_{\odot}$ tracks by the rise of L_{ν} from CNO burning and subsequently ^{19}F $\rightarrow$ ^{18}O.

Figure 3.9 is the same as Figure 3.8 but for the lifetime of the 3 $M_{\odot}$ models for all six metallicities. The fraction of L_{ν} from CNO processing during shell H-burning (green regions) is larger for the 3 $M_{\odot}$ tracks than the corresponding 1 $M_{\odot}$ tracks of Figure 3.8 at all metallicities. Core He-burning (blue shaded regions) proceeds smoothly under non-degenerate conditions at all metallicities. The spikes from ^{19}F $\rightarrow$ ^{18}O in the Z$\,=\,10^{0.5}$ $Z_{\odot}$ track during core He-burning are due to overshooting injecting fresh H-rich fuel into the core. Shell He-burning and the TP-AGB phase of evolution (pink regions) show a trend of stronger and more numerous TPs as the metallicity increases from Z$\,=\,10^{-3}$ $Z_{\odot}$ to Z$\,=\,10^{0.5}$ $Z_{\odot}$. Hotter temperatures in the 3 $M_{\odot}$ models cause neutrino emission from ^{26}Al $\rightarrow$ ^{26}Mg during the H burning Ne-Na cycle (red curves) and from the inverse beta decay ^{24}Na $\rightarrow$ ^{24}Mg reaction (purple curves). While ^{24}Na is not part of the H burning Mg-Al cycle, this isotope is synthesized at low abundance levels during the Mg-Al cycle. A late TP occurs during the WD cooling phase (purple regions) for the Z$\,=\,10^{0,-1}$ $Z_{\odot}$ tracks.

Figure 3.10 shows L_{ν}, L_{γ}, and the He-burning luminosity $L_{\rm He}$ during the nitrogen flash in 1 $M_{\odot}$ models. Across all metallicities the first flash has the largest L_{ν} and $L_{\rm He}$ with $L_{\rm He} > L_{\nu}$. The maximum neutrino luminosity $L_{\nu,\rm max}$, marked by the red circles and labels, spans $\simeq 2$ orders of magnitude as the initial metallicity varies from

$Z = 10^{-3}\ Z_\odot$ to $Z = 10^{0.5}\ Z_\odot$. Note $L_{\nu,\rm max}$ is larger for the $Z = 1\ Z_\odot$ model than the $Z = 10^{0.5}$ model. This is due to mass loss. If the metallicity was $10^{0.3}\ Z_\odot$, then $L_{\nu,\rm max}$ at the He flash would be larger than the $Z = 1\ Z_\odot$ model. At $Z = 10^{0.5}\ Z_\odot$, mass-loss hampers the strength of the He flash. The $Z = 10^{0.5}\ Z_\odot$ model has $M = 0.6\ \rm M_\odot$ at the onset of He-flash, while the $Z = 1\ Z_\odot$ model has $M = 0.66\ \rm M_\odot$. The smaller shell burning temperatures is sufficient to weaken $L_{\nu,\rm max}$. Note the duration of the peak in the $Z = 10^{0.5}\ Z_\odot$ model is significantly longer than in the $Z = 1\ Z_\odot$ model, ensuring more neutrinos are produced overall from the larger ^{14}N reservoir, but with a $L_{\nu,\rm max}$ of similar magnitude.

Figure 3.10 shows the average neutrino energy at $L_{\nu,\rm max}$ is insensitive to the initial Z. The neutrino fluxes at $L_{\nu,\rm max}$ span $\simeq 2$ orders of magnitude across metallicity and can serve as target values for neutrino observations of the nitrogen flash. The duration where $L_\nu \geq 1/2\ L_{\nu,\rm max}$ increases steadily from $\simeq 0.8$ days at $Z = 10^{-3}\ Z_\odot$ to $\simeq 11$ days at $Z = 10^{0.5}\ Z_\odot$. The duration where $L_\nu \geq 1/3\ L_{\nu,\rm max}$ increases from $\simeq 1.2$ days at $Z = 10^{-3}\ Z_\odot$ to $\simeq 17$ days at $Z = 10^{0.5}\ Z_\odot$. In addition, the time period between sub-flashes increases from $\simeq 10^5$ yr at $Z = 10^{-3}\ Z_\odot$ to $\simeq 2\times10^5$ yr at $Z = 10^{0.5}\ Z_\odot$ while the number of sub-flashes ranges between 8 at the lowest initial Z to 5 at the largest initial Z.

Figure 3.11 shows L_ν, L_γ, and $L_{\rm He}$ during the TP-AGB phase of evolution in 1 $\rm M_\odot$ models for all six metallicities. As discussed for Figure 3.8, the tracks for the lowest initial Z show a single H-shell and He-shell merger event instead of a traditional TP. For these models L_ν is dominated by $^{13}\rm N \rightarrow {}^{13}C$ from non-equilibrium hot CNO cycle burning. At the peak of the merger $T \simeq 2\times10^8$ K and $\rho \simeq 10^4$ g cm^{-3}. At these conditions the first half of the CNO cycle, $^{12}{\rm C}(p,\gamma)^{13}{\rm N}(,e^+\nu)^{13}{\rm C}(p,\gamma)^{14}{\rm N}$, is sufficiently energetic to cause a rapid expansion that self-quenches the second half of the CNO cycle, $^{14}{\rm N}(p,\gamma)^{15}{\rm O}(,e^+\nu)^{15}{\rm N}(p,\alpha)^{12}{\rm C}$. For example, the stellar radius R of the Z = 10^{-3} $Z_\odot$ model rapidly increases from 68 R$_\odot$ to 465 R$_\odot$ during the merger and the number of reactions per second from ^{13}N $\rightarrow$ ^{13}C is $\simeq$ 3 orders of magnitude larger than from ^{15}O $\rightarrow$ ^{15}N. Thus, these 1 M$_\odot$ low-Z models do not undergo a TP because a violent shell merger causes the model to quickly lose most of the H envelope. These mergers, driven by convective boundary mixing, produce the largest $L_{\nu,\mathrm{max}}$ events over the entire evolution. They are also prominent and labeled in the νHRD of Figure 3.7. The Z = $10^{0.5}$ $Z_\odot$ track also does not show TPs due to their thinner envelopes from wind mass loss. For the other metallicities, $L_{\nu,\mathrm{max}}$ during the TPs is $\simeq$ 3 orders of magnitude smaller than $L_{\nu,\mathrm{max}}$ from the nitrogen flash shown in Figure 3.10.

Figure 3.12 shows L_ν, L_γ, and L_{He} during the TP-AGB phase in the 3 M$_\odot$ models. The number of L_ν peaks (6 to 21), the L_ν peaks (2×10^3 L$_\odot$ to 2×10^5 L$_\odot$), and time between L_ν peaks (2×10^4 yr to 4×10^4 yr) increase with Z, with evidence of saturation by Z = 1 $Z_\odot$. Each successive TP releases more nuclear energy, thus $L_{\nu,\mathrm{max}}$ occurs at the end of the tracks (red circles and labels) across all metallicities. The Z = 10^{-3} $Z_\odot$ model has a larger $L_{\nu,\mathrm{max}}$ than the Z = 10^{-2} $Z_\odot$ model due to ^{13}N $\rightarrow$ ^{13}O (instead of the usual ^{18}F $\rightarrow$ ^{18}O) from a shell merger that is driven by convective boundary mixing.

Figure 3.13 compares the fraction of the total energy emitted by neutrinos at five phases of evolution across the mass-metallicity plane. Models with 0.2 M$_\odot$ $\leq$ M_{ZAMS} $\leq$ 0.8 M$_\odot$ emit $\simeq$ 80% of their neutrinos during shell H-burning (second panel) with a slight trend towards high-Z tracks making larger contributions than low-Z tracks. A $\simeq$ 10% contribution originates from core H-burning (top panel), and a $\simeq$ 10% contribution occurs during the He WD cooling phase (bottom panel). These models do not go through shell He-burning phase, as indicated by the empty region in the fourth panel, and the shorter tracks in the γHRD and νHRD of Figure 3.7.

Models whose final fate is a CO WD emit $\simeq$ 20–80% of their neutrinos during core

H-burning, $\simeq$20–40% during core He-burning, and $\simeq$10–30% during the TP-AGB phase. The percentages increase with $M_{\rm ZAMS}$, and with Z for more massive models.

3.6 High-mass Stars

We present features of the neutrino emission from high-mass models for one metallicity in Section 3.6.1, and then for all six metallicities in Section 3.6.2.

3.6.1 One Metallicity

Tracks from the ZAMS to the onset of CC for the $8\,{\rm M}_\odot \leq M_{\rm ZAMS} \leq 150\,{\rm M}_\odot$ models in a γHRD and νHRD is shown in Figure 3.14. All tracks evolve at roughly constant L_γ and L_ν during core H-burning and He-burning as the tracks evolve from ZAMS to cooler $T_{\rm eff}$. Neutrinos from the CNO cycles and $^{14}{\rm N} \rightarrow {}^{22}{\rm Ne}$ power L_ν through these phases of evolution. From CHeD onwards, the dominance of L_ν from the core over L_γ from the surface results in a rapid reduction in evolutionary timescales from years to hours to seconds (Fowler and Hoyle, 1964; Deinzer and Salpeter, 1965; Woosley *et al.*, 2002). This escalating rapidity appears in the νHRD as the nearly vertical curves at approximately constant $T_{\rm eff}$.

For $M_{\rm ZAMS} \lesssim 50\,{\rm M}_\odot$, the nearly vertical tracks at cooler $T_{\rm eff}$ in the νHRD end their lives as red supergiants (RSG). The $M_{\rm ZAMS} \gtrsim 50\,{\rm M}_\odot$ models evolve through the advanced stages at increasingly hotter $T_{\rm eff}$ with thinner H envelopes, until wind driven mass-loss strips the H-envelope, creating a Wolf–Rayet model. The nearly vertical tracks at hotter $T_{\rm eff}$ in the νHRD end their lives as a blue supergiants. This transition mass is the Humphrey-Davidson limit in our models (Humphreys and Davidson, 1979; Davies *et al.*, 2018; Davies and Beasor, 2020; Sabhahit *et al.*, 2021). The conversion of a mass limit to a luminosity limit depends on assumptions. For example, Sabhahit *et al.* (2021) adopt the luminosity limit as the luminosity above which a massive star model spends <5% of it's lifetime or above the luminosity limit while the model is a yellow/red supergiant. This transition mass is sensitive to the mass and time resolution, mass-loss prescription, and treatment of super adiabatic convection in the outer envelope (Sabhahit *et al.*, 2021).

Another feature in the νHRD of Figure 3.14 is the radial pulsations in the 35 $M_{\odot} \lesssim M_{\rm ZAMS} \lesssim 50$ $M_{\odot}$ tracks that develop during He shell or C-burning, models with thin H envelopes, and $3.9 \lesssim \log(T_{\rm eff}) \lesssim 4.1$.

C-burning sets the entropy for the continued evolution to CC, by proceeding either convectively or radiatively (Murai *et al.*, 1968; Arnett, 1972; Lamb *et al.*, 1976). If the energy released by nuclear reactions is slightly larger than pair production neutrino losses, then net energy produced is transported by convection (e.g., Cristini *et al.*, 2017). Otherwise, the core burns carbon radiatively in balanced power (Woosley *et al.*, 2002; El Eid *et al.*, 2004; Limongi and Chieffi, 2018), where the mass averaged nuclear energy release nearly balances the mass averaged neutrino losses. For $Z = 1$ $Z_{\odot}$, tracks for $M_{\rm ZAMS} \leq 20$ $M_{\odot}$ burn carbon convectively (black circles in Figure 3.14) and tracks with $M_{\rm ZAMS} \geq 21$ $M_{\odot}$ burn carbon radiatively (red circles in Figure 3.14).

The decrease in entropy from thermal neutrino emission that occurs during convective core C-burning is missing during radiative core C-burning (Weaver and Woosley, 1993). For the $M_{\rm ZAMS} \geq 21$ $M_{\odot}$ tracks that undergo radiative C-burning, the subsequent burning phases occur at higher entropy, $s \propto T^3/\rho \propto (M/M_{\odot})^2$, at higher temperatures and lower densities. The larger entropy, in turn, drives shallower and more extended density gradients, larger effective Chandrasekhar masses at core-collapse, smaller compactness parameters, and thus are more challenging to explode as CC events (Woosley and Weaver, 1986; Nomoto and Hashimoto, 1988; Sukhbold and Woosley, 2014; Sukhbold *et al.*, 2016, 2018; Limongi and Chieffi, 2018; Sukhbold and Adams, 2020; Burrows and Vartanyan, 2021). This entropy bifurcation at C-burning may seed a bimodal compact object distribution for single stars that undergo convective C-burning forming one peak in the compact object initial mass function (neutron stars) and single stars that undergo radiative C-burning forming a second peak (black holes) (e.g., Timmes *et al.*, 1996; Heger *et al.*, 2003; Zhang *et al.*, 2008; Piro *et al.*, 2017; Sukhbold *et al.*, 2018; Vartanyan *et al.*, 2018; Takahashi *et al.*, 2023).

In the terminal phases Y_e and μ act as guides to the evolution and culminating fate. A dwindling Y_e, catalyzed by electron captures, hastens the core's contraction and amplifies energy depletion through neutrino emissions, thereby altering the core's structural equilibrium. Concurrently, as $Y_e \propto 1/\mu$, an ascending μ signifies a shift towards fusing isotopically heavier nuclei, requiring ever larger core temperatures and densities to maintain hydrostatic equilibrium.

In addition, dynamical large-scale mixing on nuclear burning timescales can occur, as can mergers between the He, C, Ne, O, and Si shells. These shell mergers are sensitive to the mixing scheme adopted and particularly the treatment of convective boundary mixing across shell boundaries (e.g., Ritter *et al.*, 2018; Fields and Couch, 2021). An approximate location of these shell mergers is labeled in the νHRD of Figure 3.14. Strong coupling between nuclear burning and turbulent convection develop during late O-burning which requires 3D simulations to establish the fidelity of the 1D convection approximations (Meakin and Arnett, 2007; Couch *et al.*, 2015; Müller *et al.*, 2017; Fields and Couch, 2020, 2021). As the Fe core approaches its effective Chandrasekhar mass, electron capture and photodisintegration of nuclei drive the onset of CC.

Figure 4.7 shows the components L_ν for each phase of evolution in the $M_{\rm ZAMS}$= 20 $M_\odot$ Z = 1 $Z_\odot$ model, from shell He-burning on the left to CC on the right. After CHeD the CO core cools and contracts as a convective He-burning shell forms. The first panel on the left shows the energy budget becomes increasingly dominated by photoneutrino production with $L_\nu \simeq 10^5$ L$_\odot$.

At $t_{\rm cc} \simeq 574$ yr, carbon ignites with $L_\nu \simeq 10^6$ L$_\odot$ and the energy budget becomes dominated by pair annihilation (second panel) . Thermal neutrinos from plasmon decay, bremsstrahlung, and recombination have luminosities several orders of magnitude smaller.

At $t_{\rm cc} \simeq 13.6$ yr the C-shell ignites (third panel), with a sharp increase in $L_{\nu,\rm nuc}$ $= L_{\nu,\beta+} + L_{\nu,\beta-} \simeq 10^{6.7}$ L$_\odot$. At $t_{\rm cc} \simeq 1.5$ yr Ne ignites (fourth panel) also with a second sharp increase in $L_{\nu,\beta-}$ and $L_{\nu,\rm nuc}/L_\nu \simeq 5\%$. At $t_{\rm cc} \simeq 0.5$ yr (fifth panel) core O ignites. Convection mixes some of the Ne-shell into the core inducing a third spike in $L_{\nu,\beta-}$ and $L_{\nu,\rm nuc}/L_\nu \simeq 15\%$. At $t_{\rm cc} \simeq 11.5$ day (sixth panel) the O-Neon shell ignites, producing a fourth spike with L$_{\nu,nuc} \sim 10^9$ and L$_\nu \sim 10^{11}$, followed shortly by a subdued fifth spike marking the depletion of the Ne-shell and the ignition of shell O-burning. The common reason for these sharp increases (^{22}Ne) is analyzed in detail below. At $t_{\rm cc} \simeq 11.5$ day (seventh panel) the Si-core ignites, yielding another phase where $L_{\nu,\rm nuc}/L_\nu \simeq 15\%$. At $t_{\rm cc} \simeq 10$ hr (last panel) the Si-shell ignites and ^{56}Fe begins to form through α-capture channels. Shortly after, electron capture and endothermic burning in the Fe core leads to the onset of CC.

Overall, Figure 4.7 shows thermal processes are the dominant form of neutrino production until Si-depletion, when neutrinos from β-processes in Fe-group nuclei become a comparable portion of energy-loss budget until CC. In models which include more Fe-group nuclei in the nuclear network than we do here, neutrinos from β-processes surpass thermal neutrino production at the onset of CC (Patton *et al.*, 2017a,b; Farag *et al.*, 2020).

We calculate an approximate pair-neutrino spectrum (Misiaszek *et al.*, 2006b;

Leung *et al.*, 2020) from

$$\phi_{\rm pair}(\epsilon) = \frac{A}{k_B T}\left(\frac{\epsilon}{k_B T}\right)^{\gamma} \exp\left(\frac{-a\epsilon}{k_B T}\right) \ , \tag{3.14}$$

where $\phi(\epsilon)$ is the number of emissions with energy ϵ, and the fitting parameters are $\alpha = 3.180657028$, $a = 1.018192299$, $A = 0.1425776426$. This expression assumes the matter is relativistic and non-degenerate. We also assume all of the neutrinos are produced at the $T_{\rm c}$ of a model, so our estimates serve as upper limits. The average pair-neutrino energy is then

$$\langle\epsilon\rangle_{\rm pair} = \int_0^{1000} \epsilon\phi_{\rm pair}(\epsilon){\rm d}\epsilon \ , \tag{3.15}$$

where the integral limits are in MeV. We also cumulatively integrate over the pair-neutrino spectrum to find the lower 10% and upper 90% of neutrino energies of the pair-neutrino spectrum.

We also calculate the average electron neutrino energy ϵ_{ν_e} from β^+ processes and average electron antineutrino energy $\epsilon_{\bar{\nu}_e}$ from β^- processes as the sum of the energy released per second $\dot{\epsilon}_i$ of each weak reaction i divided by the number luminosity $L_{N,i}$

$$\epsilon_\nu = \sum_{i=1}^{N}(\dot{\epsilon}_i) \Big/ \sum_{i=1}^{N}(L_{N,i}) \ , \tag{3.16}$$

where N=40 for the low-mass reaction network and N=148 for the high-mass reaction network of Figure 3.1.

Figure 4.8 shows ϵ_{ν_e} and $\epsilon_{\bar{\nu}_e}$ versus $T_{\rm c}$ for different $M_{\rm ZAMS}$ at Z = 1 $Z_\odot$. During H and He burning, $\epsilon_{\nu_e} \lesssim 1$ MeV while $\epsilon_{\bar{\nu}_e} \simeq 1$–1.5 MeV. From C-burning to the onset of CC, $\langle\epsilon\rangle_{\rm pair}$ remains well below ϵ_{ν_e} and $\epsilon_{\bar{\nu}_e}$.

During C and Ne burning β^+ processes are dominated by ^{21,22}Na→^{21,22}Ne from the Ne-Na cycle, ^{26}Al→^{26}Mg from the Mg-Al cycle, and supplemented by ^{23}Mg→^{23}Na. These reactions decrease Y_e in the core, and produce ν_e with average energies $\epsilon_{\nu_e} \simeq 1.6$, 1.8, and 1.7 MeV respectively. During this phase β^- decays are dominated by ^{28}Si←^{28}Al, ^{24}Mg←^{24}Na, and ^{27}Al←^{27}Mg, producing $\bar{\nu}_e$ with average energies $\epsilon_{\bar{\nu}_e} \simeq 1.6$, 2.7, and 0.9 MeV respectively. The total β^- neutrino emission grows from $\simeq 20\%$ of the total β emission during C burning to $\simeq 50\%$ during Ne burning, with ϵ_{ν_e} between 1.6–2 MeV independent of $M_{\rm ZAMS}$.

During Ne and O-burning there are windows where the $\epsilon_{\bar{\nu}_e}$ exceeds the $\simeq 1.8$ MeV detection threshold to inverse beta decay of current neutrino detectors (e.g., Simpson *et al.*, 2019; Harada *et al.*, 2023). Table 2.3 lists the dominant electron anti-neutrino luminosity sources for the $M_{\rm ZAMS} = 20{\rm M}_\odot$ model during the windows where $\bar{\nu}_e$ exceeds current detector thresholds.

The core continues to become more neutron-rich during O-burning primarily from ^{31}S→^{31}P, supplemented by ^{30}P→^{30}Si, ^{36}Ar→^{36}Cl, producing ν_e with average energies $\epsilon_{\nu_e} \simeq$ 2.2–2.4, 2.4–3.0, and 1.4 MeV respectively. β-processes in the He, C, and Ne shells remain active.

Core and shell Si-burning are the last exothermic burning stages and produce the Fe-peak nuclei. Initially ^{31,32}S→^{31,32}P and ^{35,36}Ar→^{35,36}Cl are the main β-decay channels, but are quickly replaced by ^{53,54,55}Fe→^{53,54,55}Mn, ^{51,52,53,54}Mn→^{51,52,53,54}Cr, ^{51,52,53,54}Mn→^{51,52,53,54}Cr, ^{55,56,57}Co→^{55,56,57}Fe, ^{48,49}Cr→^{48,49}V, and ^{56,57,58,60}Ni→^{56,57,58,60}Co. Many of the isotopes formed during the final stages undergo β-processes that continue to make the core more neutron-rich (e.g., Heger *et al.*, 2001; Odrzywolek, 2009; Patton *et al.*, 2017b) with $\epsilon_{\nu_e} \simeq 2.2$ MeV and $\epsilon_{\bar{\nu}_e} \simeq 1.8$ MeV.

3.6.2 Six Metallicities

Figure 3.17 shows the tracks of a $M_{\rm ZAMS} = 20$ M$_\odot$ model in a γHRD and a νHRD across all six metallicities. Overall, the low-Z models show the trend of having denser, hotter and more massive cores with lower envelope opacities, larger surface luminosities and larger effective temperatures $T_{\rm eff}$ than the high-Z counterparts. The hotter yet more massive H cores extends their MS lifetimes. High-Z models show significantly shorter lifetimes than low-Z models due to their smaller H abundance at the ZAMS. For example, at the ZAMS, X = 0.75 for Z = 10^{-3} $Z_{\odot}$ and X = 0.637 for Z = $10^{0.5}$ $Z_{\odot}$. The Z = $10^{0.5}$ $Z_{\odot}$ model also possesses a significantly smaller H reservoir to burn, due to the large line-driven wind mass-loss prescription ($\dot{M} \propto Z$) which drives the already less massive H-burning region to retreat further inward during the MS evolution, resulting in a significantly shorter MS lifetime than any other model. Metal-poor tracks have lower envelope opacities and do not evolve to as low an $T_{\rm eff}$ as their metal-rich counterparts. This behavior is especially prominent in the Z = 10^{-3} $Z_{\odot}$ model, the purple curve in Figure 3.17, which has a much shorter track in the γHRD and is prominently offset from the lower-Z models in the νHRD.

The first and second vertical panels in Figure 3.18 show the primary source of neutrinos during H-burning and He-core burning in a 20 $M_{\odot}$ model is CNO β^{+} decays. At CHeD and the onset of shell He-burning (third vertical panel) L_{ν} from β decays decreases while the CO core contracts and heats up. In higher Z models, the dominant source of β neutrinos are from ^{14}N$\rightarrow$^{22}Ne in the growing He-burning shell. In lower Z models where less ^{14}N is present, the dominant source of β neutrinos continues to be from CNO β^{+} decays in the active H-burning shell. In all models, thermally excited photoneutrinos in the hot contracting CO core begin to dominate the neutrino emission until temperatures are high enough, $T_{\rm c} \geq 7 \times 10^{8}$ K, for pair-neutrinos to become the dominant energy loss mechanisms.

The accumulation of isotopically heavy ^{22}Ne during He-burning provides the neutron excess η necessary for β^{-} decays to occur during advanced burning stages. A fraction of the ^{22}Ne undergoes ^{22}Ne(α,n)^{25}Mg and to a lesser extent ^{22}Ne(α,γ)^{26}Mg. Through CHeD and into C-burning ^{22}Ne(α,n)^{25}Mg is a neutron source for s-process nucleosynthesis (Peters, 1968; Couch *et al.*, 1974; Prantzos *et al.*, 1990; Raiteri *et al.*, 1991b; Kappeler *et al.*, 1989; Gallino *et al.*, 1998; Pignatari *et al.*, 2010; Käppeler *et al.*, 2011; Wiescher *et al.*, 2023).

The fate of neutron-rich ^{25}Mg evolves during C-burning (Raiteri *et al.*, 1991a), which is the fusion of two ^{12}C nuclei to form an excited ^{24}Mg* nucleus which decays in three channels (e.g., Woosley *et al.*, 2002)

$$
\begin{aligned}
{}^{12}\mathrm{C} + {}^{12}\mathrm{C} \rightarrow \ {}^{24}\mathrm{Mg}^{*} \rightarrow & \ {}^{20}\mathrm{Ne} + \alpha + \gamma \\
\rightarrow & \ {}^{23}\mathrm{Na} + p + \gamma \\
\rightarrow & \ {}^{23}\mathrm{Mg} + n + \gamma \ .
\end{aligned}
\tag{3.17}
$$

The α- and p-channels occur at similar rates while the $n-$channel branching ratio of $\sim 1\,\%$ (Dayras *et al.*, 1977). Uncertainties in the branching ratios and temperature dependant rates can alter the nucleosynthetic yields during C-burning through the Ne-Na or Mg-Al cycles and the amount ^{20}Ne available for Ne-melting (Bennett *et al.*, 2012; Pignatari *et al.*, 2013; Zickefoose *et al.*, 2018; Tan *et al.*, 2020; Monpribat *et al.*, 2022).

The fourth vertical panel in Figure 3.18 shows ^{26}Al$\rightarrow$^{26}Mg (red curve) makes a primary contribution to L_ν from nuclear reactions at all metallicities during C-burning. The p-channel powers the Ne-Na cycle, producing a neutrino signal through ^{21,22}Na$\rightarrow$^{21,22}Ne and ^{23}Mg$\rightarrow$^{23}Na β^{+} decays. ^{24}Mg is then produced via ^{23}Na(p,γ)^{24}Mg, and ^{23}Na(p,α)^{20}Ne creates stable ^{20}Ne – now available for a later stage of Ne-melting into ^{24}Mg and ^{28}Si. The Mg-Al cycle is weakly powered by the p-channel ^{24}Mg(p,γ)^{25}Al reaction. Instead the α-channel powers the Mg-Al cycle by providing the He nuclei necessary for ^{22}Ne(α,n)^{25}Mg for the cycle to operate. Instead of ^{25}Mg then being consumed by ^{25}Mg(n,γ)^{26}Mg, protons from the p-channel power ^{25}Mg(p,γ)^{26}Al which undergoes β^{+} decay ^{26}Al$\rightarrow$^{26}Mg, dominating the nuclear neutrino production during C-burning.

The larger T_c of low-Z models results in a stronger expression of ^{21,22}Na$\rightarrow$^{21,22}Ne during C-burning. High-Z models also show a larger β^- luminosity during C-burning than their low-Z counterparts. This results from differences in the neutron excess across metallicities. High-Z models enter C-burning with a larger ^{22}Ne abundance available for ^{22}Ne(α,n)^{25}Mg, which provides most of the free neutrons for an s-process (Raiteri *et al.*, 1991a; The *et al.*, 2007; Choplin *et al.*, 2018).

Another feature during C-burning is the β^- luminosity declines from $\simeq 50\%$ of the total β neutrino luminosity in the Z $= 10^{0.5}$ $Z_\odot$ model, to $\simeq 25\%$ in the Z $=1$ $Z_\odot$ model, and $\leq 10\%$ in lower Z models. Independent of metallicity, these β^- decays are primarily ^{28}Al$\rightarrow$^{28}Si, ^{27}Mg$\rightarrow$^{27}Al, and ^{24}Na$\rightarrow$^{24}Mg.

Neon melting is characterized by photodisintegration of Neon into α particles, which recapture onto a second Neon nucleus to form ^{16}O and ^{24}Mg. The fifth vertical panel in Figure 3.18 shows α-capture onto the remaining ^{22}Ne in the core provides a spike in the β^- luminosity, and a neutron source for an s-process. A metallicity dependence on the initial ^{22}Ne content of the core affects the strength of β^- decays at the onset of Ne-melting. A significant fraction of the ^{26}Mg also undergoes ^{26}Mg(α,n)^{30}P which then decays to ^{30}P$\rightarrow$^{30}Si.

O-burning is the fusion of two ^{16}O nuclei to form an excited state of ^{32}S*, which promptly decays to

$$\begin{aligned} {}^{16}\mathrm{O} + {}^{16}\mathrm{O} \rightarrow\ {}^{32}\mathrm{S}^* &\rightarrow\ {}^{28}\mathrm{Si} + \alpha + \gamma \\ &\rightarrow\ {}^{31}\mathrm{P} + p + \gamma \\ &\rightarrow\ {}^{31}\mathrm{S} + n + \gamma \\ &\rightarrow\ {}^{30}\mathrm{P} + d - \gamma\ . \end{aligned} \tag{3.18}$$

Branching ratios for the α, p n, and d channels are $\simeq 34\%$, 56%, 5%, and $\leq 5\%$ respectively, and the products of O-burning include ^{28}Si, ^{32,33,34}S, ^{35,36,37}Cl, ^{36,37,38}Ar,

^{39,40,41}K, and ^{40,41,42}Ca (Woosley *et al.*, 2002). The limited extent of neutron rich isotopes in the high-mass nuclear reaction network of Figure 3.1 means we do not capture all these isotopes, including ^{35}S and ^{33}P.

The sixth vertical panel in Figure 3.18 shows ^{31}S$\rightarrow$^{31}P makes a primary contribution to L_ν from nuclear reactions at all metallicities during O-burning. The accumulation of ^{36}Ar leads to a growing neutrino signal from ^{36}Ar$\rightarrow$^{36}Cl. After core O-depletion, shell Ne-melting occurs before O-shell burning. The α-captures onto the remaining ^{22}Ne nuclei in the shell provides a second spike in the β^- luminosity in Figure 3.18.

From Si burning (Si-α) until CC, the seventh and eighth vertical panel in Figure 3.18, there are little differences in the relative strength of individual β decays. At this stage of evolution, the expression of Fe-group β decays is metallicity independent, and β^- decays remain subdominant until $t_{cc} \lesssim 10^{-1}$ hr (Patton *et al.*, 2017a,b; Kato *et al.*, 2017, 2020a; Kosmas *et al.*, 2022).

In Figure 3.19 the average neutrino and anti-neutrino energies are, to first-order, similar across metallicities for β^+ and β^- decays in a 20 $M_\odot$ model. The largest differences in anti-neutrino energies occur during C-shell and Ne-core burning, when the neutron excess provided by ^{22}Ne is most important. Metal-poor tracks possess lower L_{β^-}, but higher overall average anti-neutrino energy, since the signal is increasingly dominated by ^{24}Mg$\leftarrow$^{24}Na as opposed to ^{28}Si$\leftarrow$^{28}Al. Windows where $\bar{\nu}_e$ exceeds current detector thresholds are listed in Table 2.3 for the Z = 1 $Z_\odot$ model.

Figure 3.20 shows the fraction of the total neutrino energy produced during different phases of evolution in the mass-metallicity plane. The spread reflects the different fates experienced by stellar models of differing mass-metallicity. Larger spreads occur for the high-mass models where wind-driven mass-loss and shell-core mergers contribute.

Across metallicities in Figure 3.20, the chief nuclear neutrino production in high-mass models come from the CNO cycle during H-burning, accounting for $\simeq$40–90% of the total neutrino emission with a trend towards larger fractions with increasing $M_{\rm ZAMS}$. Typical fractions for He-burning are $\lesssim$ 8%, with an exception for some very massive models that produce $\simeq$10–20% from recurrent mixing of the shell-H into the He core before CHeD. Typical fractions for C-burning and O-burning are $\simeq$5–20% and $\simeq 5-30\%$ respectively, with a negative trend toward higher masses. From core-Si ignition to CC, $\simeq$2–10% of the total neutrino emission occurs with a negative trend toward increasing masses. Overall, most neutrinos are produced during H and He burning from β^+ decays, especially in the most massive models.

3.7 Integrated Stellar Photon and Neutrino Emission

We explore the time-integrated photon and neutrino emission of a simple stellar population model. We assume a burst cluster population where all models are born at the same time and evolve together.

$$N_0 = \frac{1}{M_\odot} \int_{M_{min0}}^{M_{max}} \frac{dN}{dm} M_* \, dm \ , \tag{3.19}$$

$$\Phi(t) = \frac{1}{N_0} \int_{M_{min}}^{M_{max}} \frac{dN}{dm} \phi(m,t) \, dm \ , \tag{3.20}$$

We adopt the normalized broken power law initial mass function (IMF) from Kroupa (2001) for the number of stars per unit mass dN/dm. We integrate over the IMF in Equation 3.19 to solve for a normalization coefficient such that a cluster of mean mass 1 $M_\odot$ is formed in the burst of star formation. The minimum mass $M_{\rm min0} = 0.01$ $M_\odot$ and the maximum mass $M_{\rm max} = 150$ $M_\odot$ of the IMF set the integration limits for the 1 $M_\odot$ stellar cluster. We then solve Equation 3.20 for $\Phi(t)$ the resultant integrated quantity, where $\phi(t)$ is the quantity we source along an isochrone. The minimum mass $M_{\rm min0} = 0.2$ $M_\odot$ and the maximum mass $M_{\rm max} = 150$ $M_\odot$ of the mass-metallicity plane set the integration limits.

Figure 3.21 shows L_γ and L_ν light curves for each population synthesis model, sampled at 600,000 points in log(Age) for each metallicity. We overlay a quadratic power law for each population synthesis model to provide a convenient fitting formulae for L_γ and L_ν as a function of the stellar cluster age and mass

$$\log\left(\frac{L}{\mathrm{L}_\odot}\right) = \left[a\log\left(\frac{\mathrm{Age}}{\mathrm{yr}}\right)^2 - b\log\left(\frac{\mathrm{Age}}{\mathrm{yr}}\right) + c\right] + \log\left(\frac{M}{\mathrm{M}_\odot}\right) \tag{3.21}$$

where the fit coefficients (a,b,c) are listed in Table 3.4.

Figure 3.22 shows the cluster L_γ and L_ν light curves and their ratio of L_γ/L_ν. Both L_γ and L_ν are slightly larger in low-Z models until $\sim 10^{10.5}$ Gyr when low-Z models are depleted of most H-burning and He-burning stellar tracks, and L_γ and L_ν become comparable across all metallicities (except for Z = $10^{0.5}$ $Z_\odot$). Low-Z stellar population fits show an overall larger L_γ/L_ν than high-Z fits until $\sim 10^{10.5}$ Gyr, when the population synthesis models are dominated by very low-mass models $M_{\mathrm{ZAMS}} \leq 0.8$ $\mathrm{M}_\odot$.

Figure 3.23 shows the $\epsilon_{\bar{\nu}_e}$, $\epsilon_{\bar{\nu}_e}$, B-V color, V-K color, and the light to mass ratio in the V-band versus cluster age for all six metallicities. Photon and neutrino emission at early times $\simeq 10^7$ yr is indicative of high-mass model emissions. By $\simeq 10^8$ yr, all high-mass models have reached their final fate, leaving only low-mass models in the stellar population. Most of a star's life is spent during H and He burning in which neutrino emission is dominated by β processes, therefore it is reasonable to approximate the average neutrino energy of a simple stellar population by β processes alone.

The top panel in Figure 3.23 shows the average neutrino energy from a simple stellar population model ranges from 0.5–1 MeV. Average neutrino energies show a slight metallicity trend, with low-Z models producing up to 0.5 MeV larger signal

	a	b	c
For Z = $10^{0.5}$ $Z_\odot$			
L_γ	0.0454	1.8499	12.1782
L_ν	0.0157	1.4109	9.3456
For Z = $10^{0.0}$ $Z_\odot$			
L_γ	0.0640	2.1469	13.4535
L_ν	0.0368	1.7576	10.8520
For Z = $10^{-0.5}$ $Z_\odot$			
L_γ	0.0484	1.8839	12.4324
L_ν	0.0198	1.4757	9.7766
For Z = $10^{-1.0}$ $Z_\odot$			
L_γ	0.0408	1.7563	11.9527
L_ν	0.0100	1.3157	9.1845
For Z = $10^{-2.0}$ $Z_\odot$			
L_γ	0.0442	1.8098	12.1904
L_ν	0.0056	1.2368	8.9000
For Z = $10^{-3.0}$ $Z_\odot$			
L_γ	0.0452	1.8212	12.2151
L_ν	-0.0065	1.0227	8.0339

Table 3.4: Fit coefficients of Equation 3.21.

than high-Z models between ages of 10^7 – $10^{9.5}$ yr, then decreasing to $\simeq 0.5$ MeV at $10^{10.5}$ yr. The second panel shows the average anti-neutrino energy ranging from 0.6 – 1.8 MeV. The anti-neutrino emission at early times, $\simeq 10^7$ yr, is dominated by high-mass models reaching up to $\sim$ 1.8 MeV. By $\simeq 10^8$ yr, the anti-neutrino energy has reduced to $\simeq$0.6 MeV, and remains roughly constant until $10^{10.5}$ yr.

The third and fourth panels in Figure 3.23 shows the Johnson-Cousins B-V and V-K colors respectively, calculated using the tabulations from Lejeune *et al.* (1998). At early times, $\simeq 10^7$ yr, there is a slight excess in B-V and a relatively large jump in V-K from the high-Z population models, roughly at the onset of the RSG phase in the high-mass models (Choi *et al.*, 2016b). The bump in V-K is suppressed in the lowest metallicity models, which do not evolve toward the RSG branch and instead remain relatively blue, with RSG color spectra similar to the MS. At late times, $\gtrsim 10^9$ yr when the population contains only low-mass stars, the B-V and V-K colors show an overall reddening in high-Z stellar populations.

The V band light to mass ratio in the bottom panel of Figure 3.23 shows a weak but distinct metallicity trend. At early times, L_V/M is larger in the lower metallicity populations. This is due to the increased L_γ in low-Z models. At late times, the trend is inverted with larger L_V/M the high-Z population models. This is due to the longer MS lifetimes in the high-Z population models.

3.8 Summary

We explored the evolution of stellar neutrino emission with 420 models spanning the initial mass $0.2\,\mathrm{M}_\odot \leq M_{\mathrm{ZAMS}} \leq 150\,\mathrm{M}_\odot$ and initial metallicity $-3 \leq \log(\mathrm{Z}/Z_\odot) \leq 0.5$ plane. We found lower metallicity models are more compact, hotter, and produce larger L_ν with two exceptions. At He-core ignition on the RGB and He-shell burning on the AGB, the birth metallicity determines the amount of ^{14}N available for the nitrogen flash $^{14}\mathrm{N}(\alpha,\gamma)^{18}\mathrm{F}(,e^+\nu_e)^{18}\mathrm{O}$. In high-mass models, the birth metallicity determines the amount of ^{14}N and therefore ^{22}Ne available for $^{22}\mathrm{Ne}(\alpha,n)^{25}\mathrm{Mg}$, providing a neutron excess to power anti-neutrino emission during C, Ne and O burning. Overall, across the mass-metallicity plane we identify the sequence ($\mathrm{Z}_{\mathrm{CNO}} \rightarrow {}^{14}\mathrm{N} \rightarrow$

^{22}Ne $\rightarrow$ ^{25}Mg $\rightarrow$ ^{26}Al $\rightarrow$ ^{26}Mg $\rightarrow$ ^{30}P $\rightarrow$ ^{30}Si) as making primary contributions to L_ν at different phases of evolution.

Simple stellar populations with lower birth metallicities have higher overall L_ν than their metal-rich counterparts. We find that most neutrinos from simple stellar populations are emitted in the form of electron-neutrinos through β^+ decays, with average energies in the range 0.5 – 1.2 MeV. Lastly, we find that metal-poor stellar populations produce larger average β^+ neutrino energies (up to 0.5 MeV), though this trend is much weaker, if resolved, for β^- neutrino emission.

We close this article by pointing out that there are many potential sensitivities that we have not investigated. Examples include choosing different convective mixing prescriptions, mass loss algorithms, and nuclear reaction rate probability distribution functions (especially ^{12}C(α,γ)^{16}O and triple-α). We also neglected rotation, their associated magnetic fields, and binary interactions. Future uncertainty quantification studies could also explore potential couplings between simultaneous variations in uncertain parameters. We caution that these uncertainties, or missing physics, could alter the neutrino emission properties of our models.

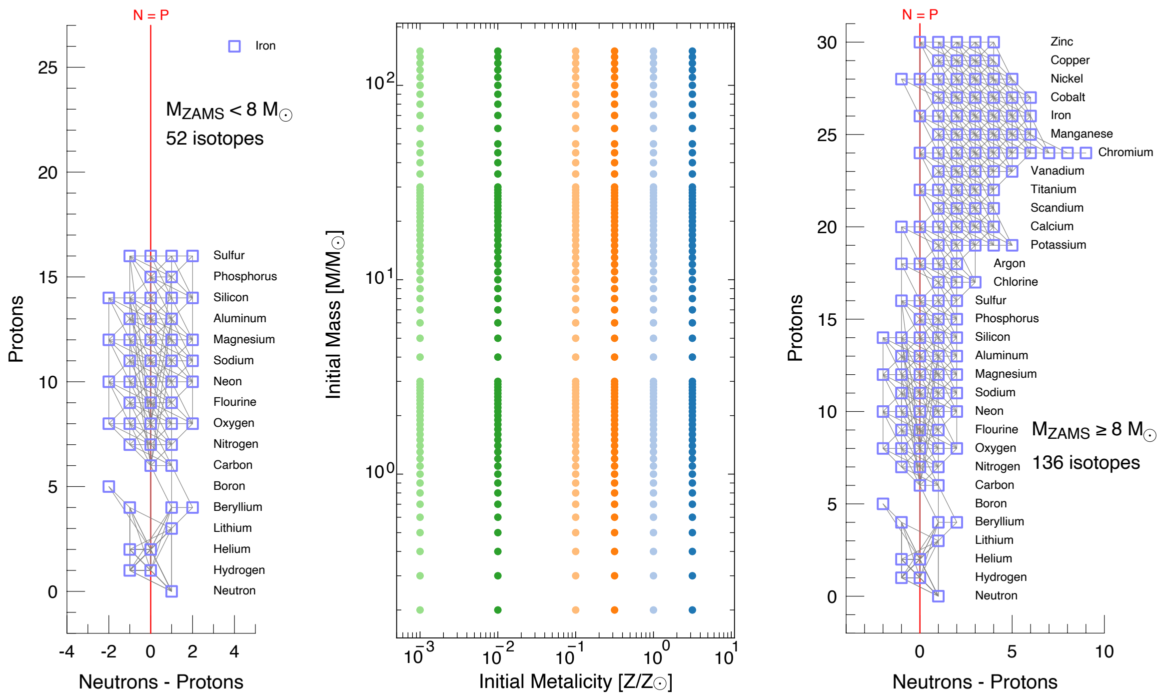

Figure 3.1: Coverage in the mass-metallicity plane (center). The x-axis is the initial Z of a model relative to solar, and the y-axis is $M_{\rm ZAMS}$ of a model relative to solar. Six metallicities, each marked with a different color, and 70 masses at each metallicity (circles) span the mass-metallicity plane. The nuclear reaction network for low-mass (left) and high-mass (right) models is illustrated. These x-axes are the difference in the number of neutrons and protons in an isotope. Positive values indicate neutron-rich isotopes, the zero value is marked by the red vertical line, and negative values indicate proton-rich isotopes. These y-axes are the number of protons in an isotope, labelled by their chemical element names. Isotopes in the reaction network are shown by purple squares. Reactions between isotopes are shown by gray lines. Note Fe in the low-mass reaction network does not react with other isotopes. Fe is included for a more consistent specification of the initial composition, hence any microphysics that depends upon the composition including the opacity, equation of state, element diffusion, and neutrino emission.

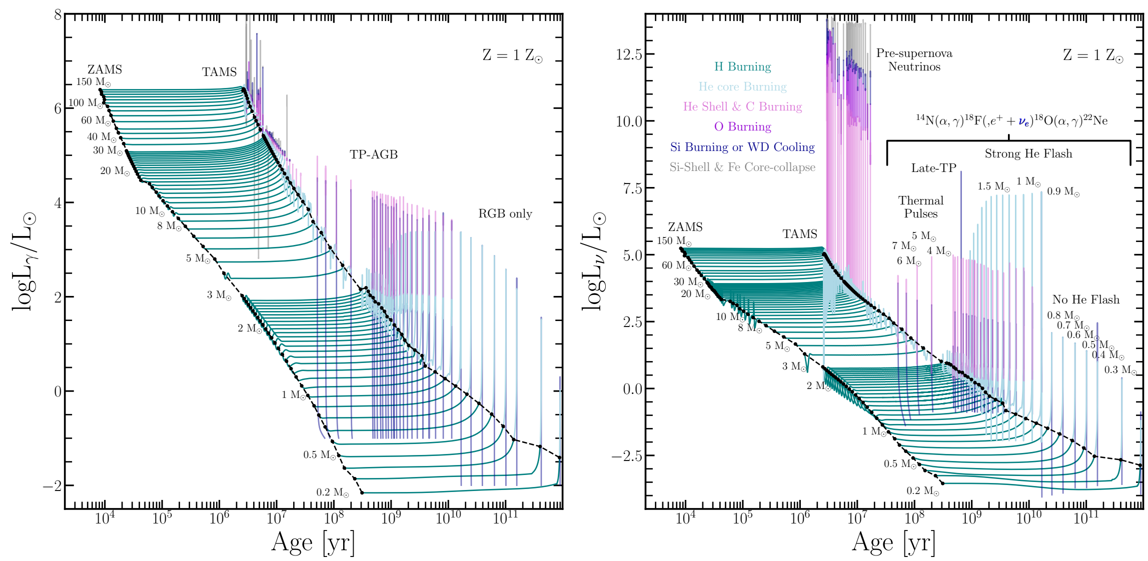

Figure 3.2: Light curves for photons (left) and neutrinos (right). Tracks span 0.2–150 $M_{\odot}$ for $Z = 1\,Z_{\odot}$ and are labeled. Key phases of evolution including the ZAMS (black circles), TAMS (black circles), core He flashes (light green), thermal pulses, and pre-supernova stage are also labeled. The PMS light curves are suppressed for visual clarity. L_ν during the nitrogen flash (He flash for photons) and thermal pulses for the $M < 8\,M_{\odot}$ light curves can exceed L_γ. At and beyond core C-burning L_ν dominates the evolution of the $M \geq 8\,M_{\odot}$ light curves. Luminosities are normalized to $L_{\odot} = 3.828 \times 10^{33}$ erg s^{-1} (Prša *et al.*, 2016b).

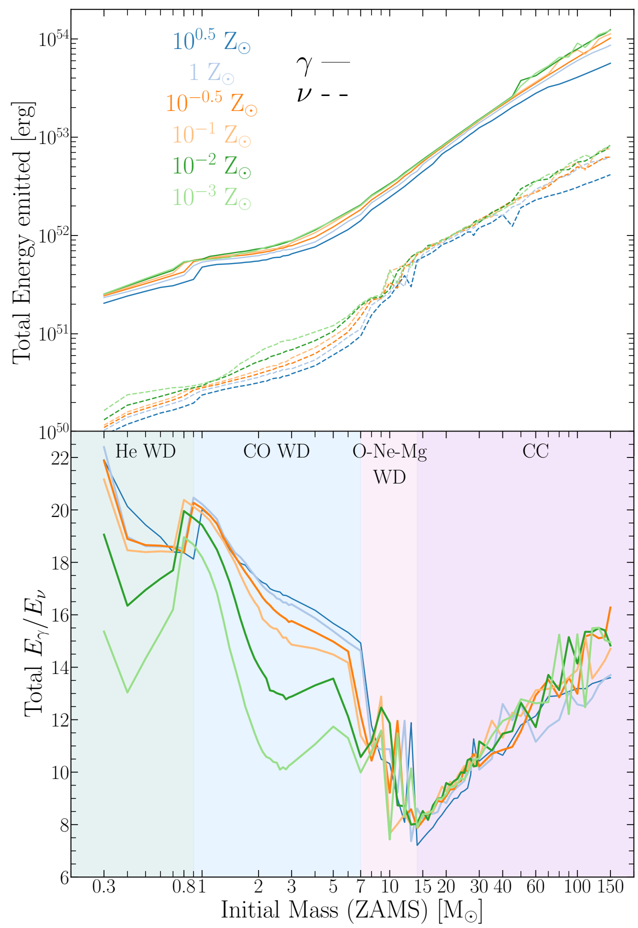

Figure 3.3: Total energy emitted in photons and neutrinos over the lifetime of a model (top) and their ratio (bottom) across the mass-metallicity plane. Transitions between different final fates occur at local extrema, indicated by the colored panels and labels.

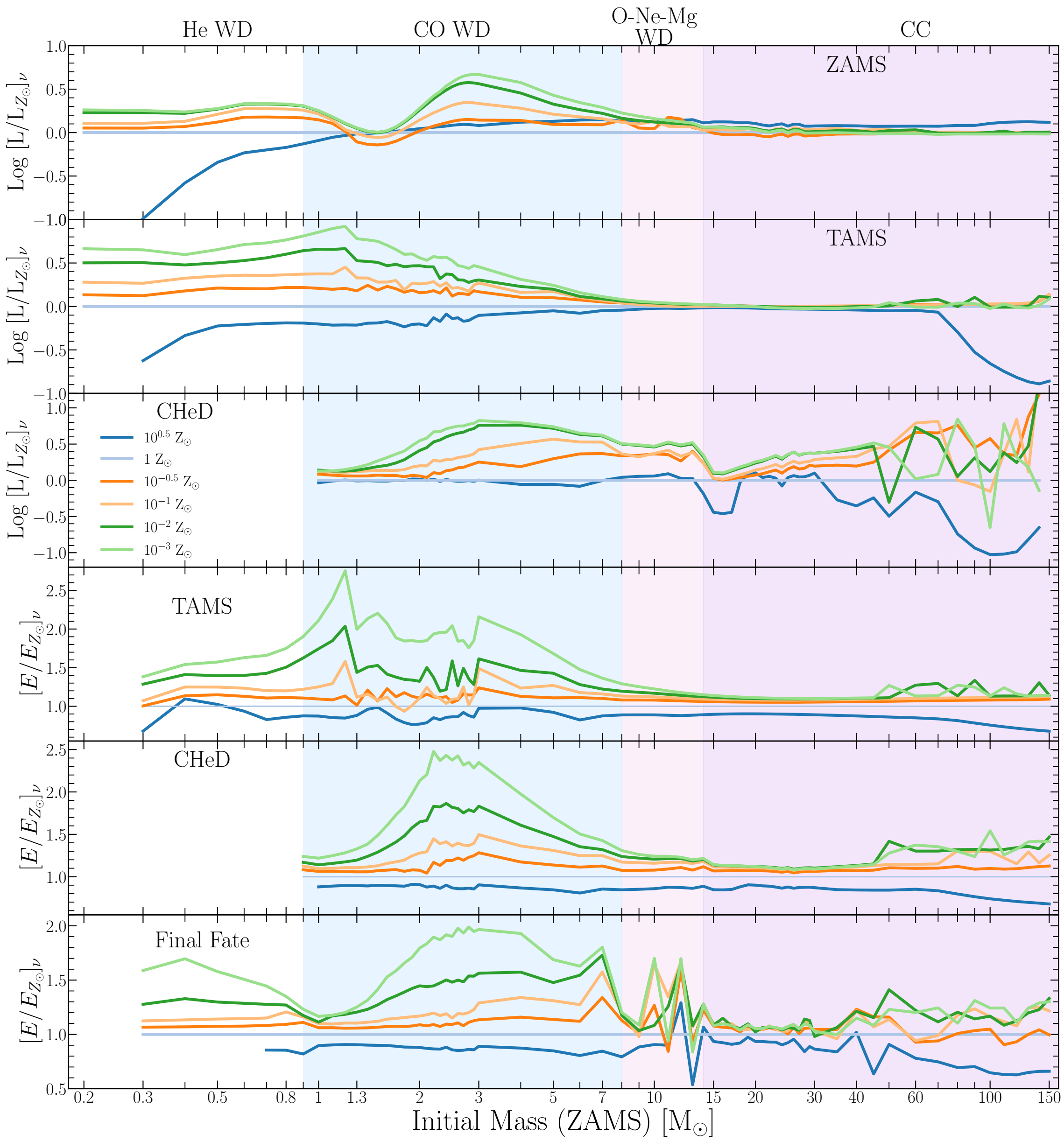

Figure 3.4: Ratio of L_ν to L_ν of the $Z = 1\,Z_\odot$ model versus $M_{\rm ZAMS}$ for all six metallicities at ZAMS (top panel), TAMS (second panel) and CHeD (third panel). The ratio of E_ν to E_ν of the $Z = 1\,Z_\odot$ model versus $M_{\rm ZAMS}$ for all six metallicities at TAMS (fourth panel), CHeD (fifth panel) and final fate (bottom panel). Each panel is colored by the final fate given by the legend.

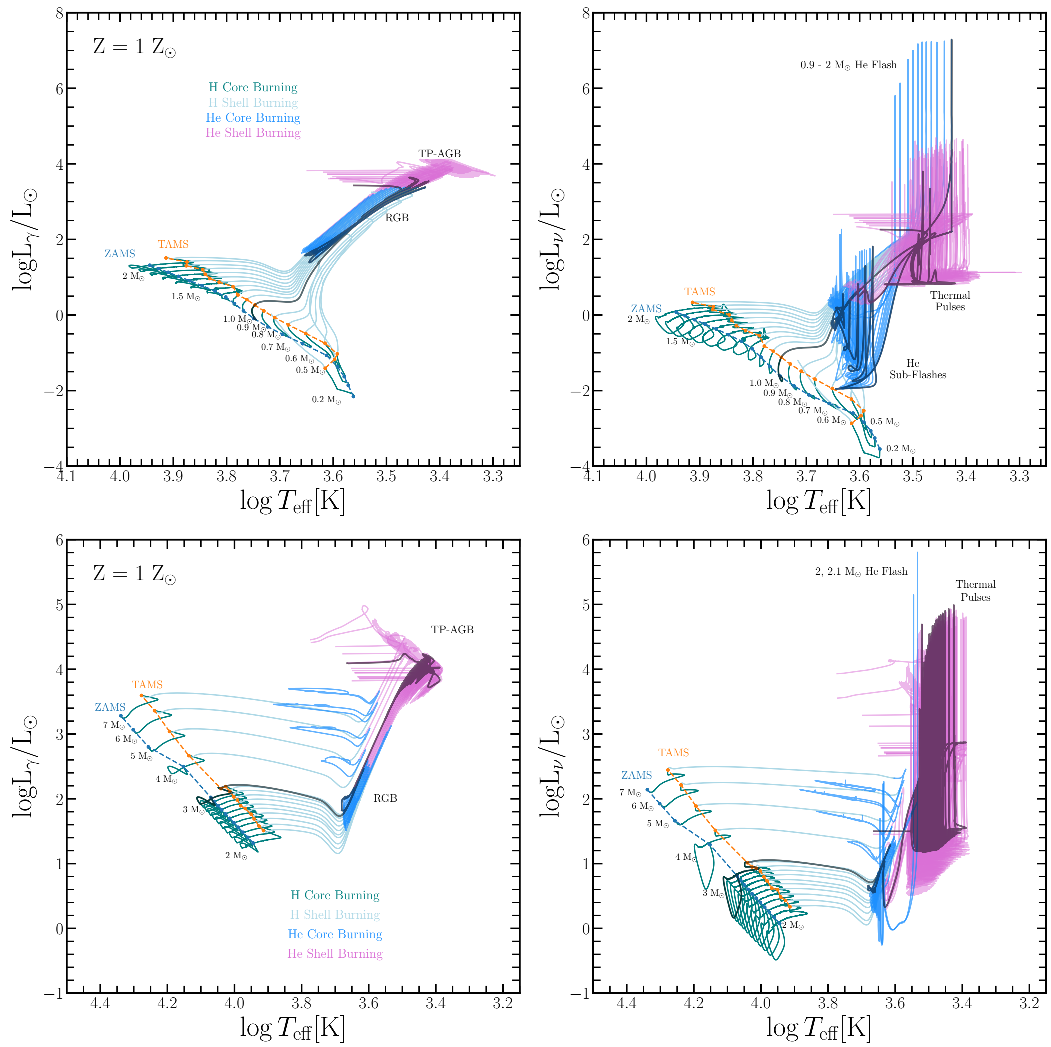

Figure 3.5: Low-mass tracks in a γHRD (left panels) and a νHRD (right panels) for $\mathrm{Z} = 1\, Z_{\odot}$ over 0.2–2.0 $\mathrm{M}_{\odot}$ (top row) and 2.0–7.0 $\mathrm{M}_{\odot}$(bottom row). Tracks are colored by evolutionary phase and labeled. WD cooling tracks are suppressed for visual clarity. Luminosities are normalized to $\mathrm{L}_{\odot} = 3.828 \times 10^{33}$ erg s^{-1} (Prša *et al.*, 2016b). The 1 $\mathrm{M}_{\odot}$ and 3 $\mathrm{M}_{\odot}$ tracks are highlighted in black as they are analyzed in detail as examples of low-mass models that do and do not undergo the He flash, respectively.

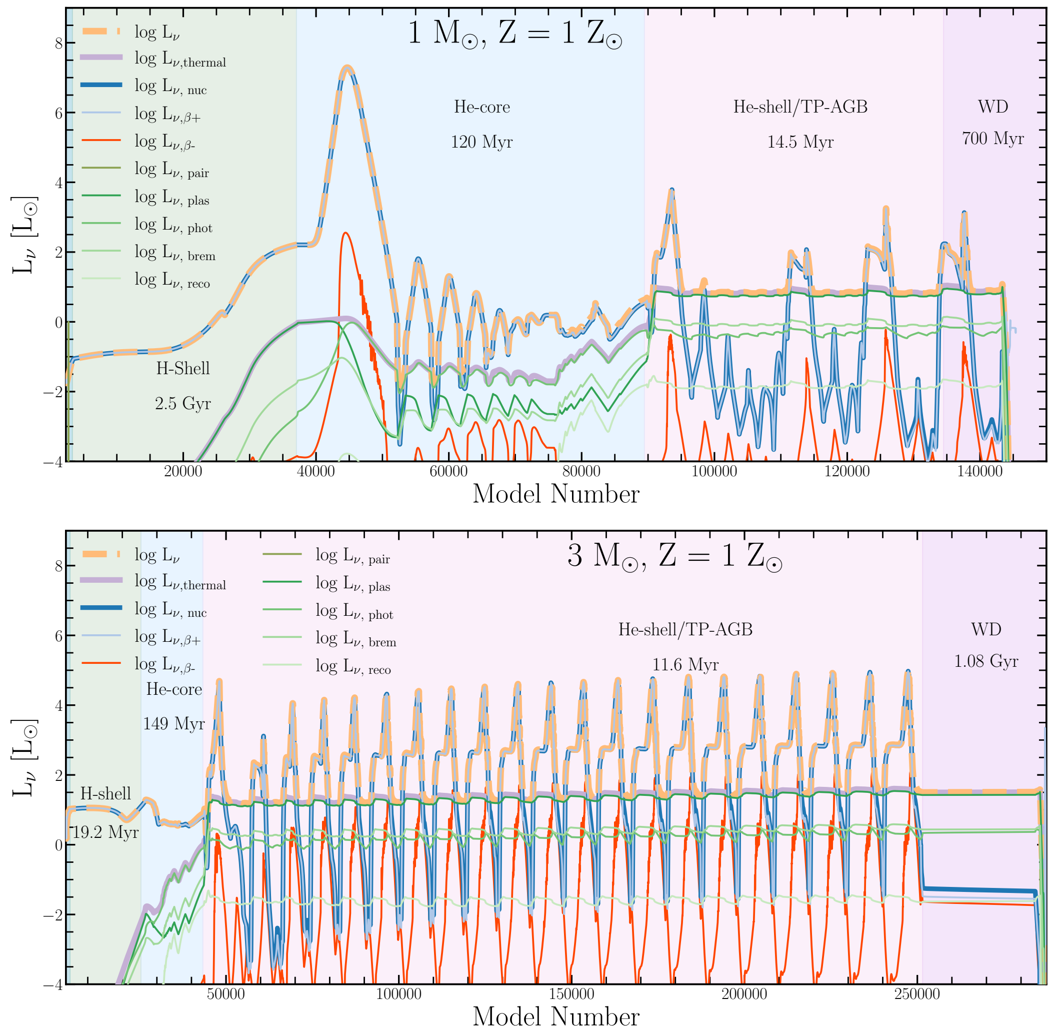

Figure 3.6: Components of L_ν over the lifetimes of a 1 M$_\odot$, 1 $Z_\odot$ model (top) and a 3 M$_\odot$, 1 $Z_\odot$ model (bottom). The x-axis is the sequential model number, a non-linear proxy for time, which begins on the left at core H-depletion and ends on the right as a cool WD at each metallicity. Phases of evolution are marked by the colored regions and the time spent in each phase is labeled. Curves show the luminosities from nuclear and thermal processes and their sub-components, and are smoothed with a 50 model moving average filter. Luminosities are normalized to L$_\odot$ = 3.828×10^{33} erg s^{-1} (Prša *et al.*, 2016b).

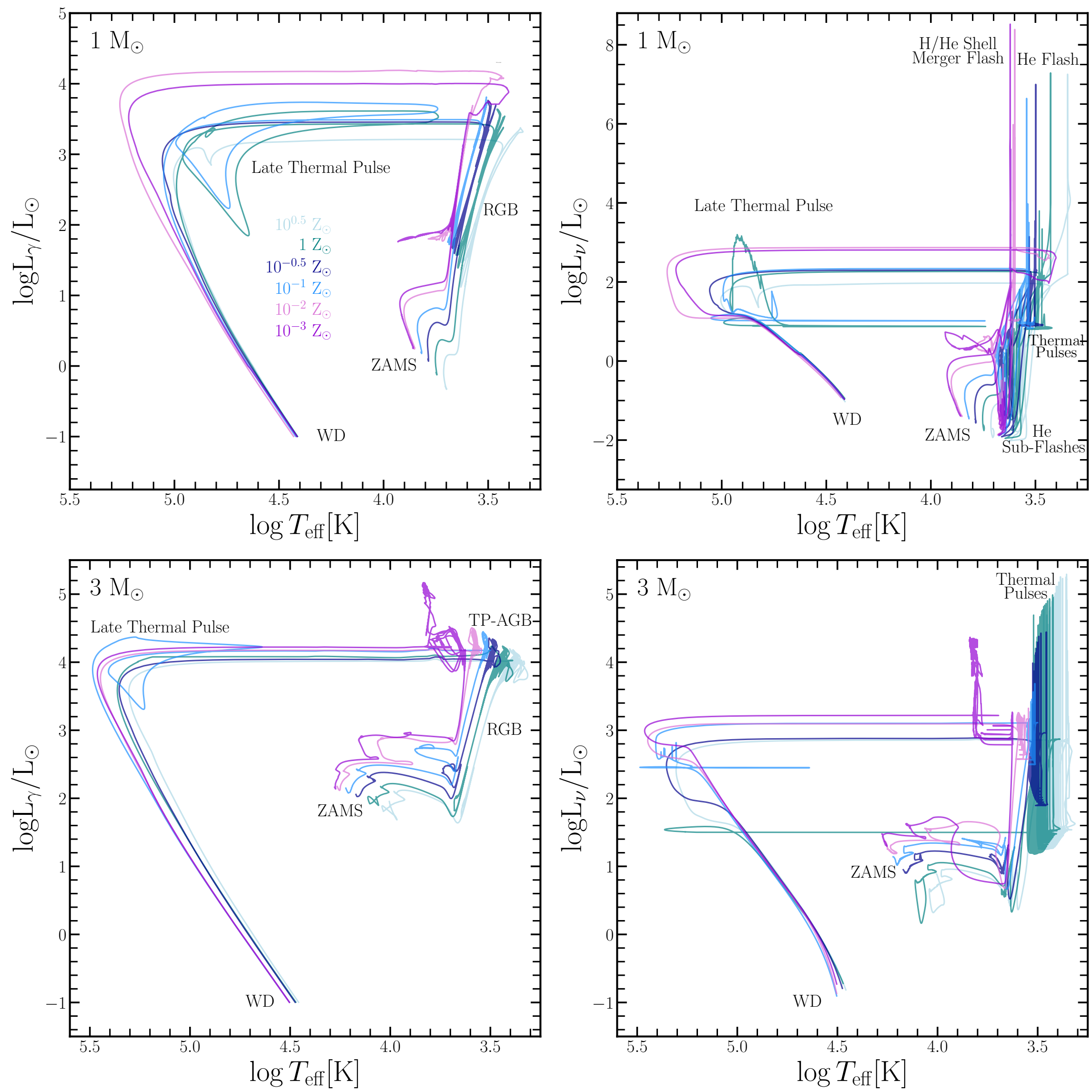

Figure 3.7: Tracks in a γHRD (left panels) and νHRD (right panels) for $M_{\rm ZAMS} = 1$ M$_\odot$ (top row) and 3 M$_\odot$ (bottom row) across all six metallicities. Luminosities are normalized to the current solar photon luminosity L$_\odot$ = 3.828 $\times 10^{33}$ erg s^{-1} (Prša *et al.*, 2016b). Metal-poor tracks are generally bluer and more luminous than metal-rich tracks.

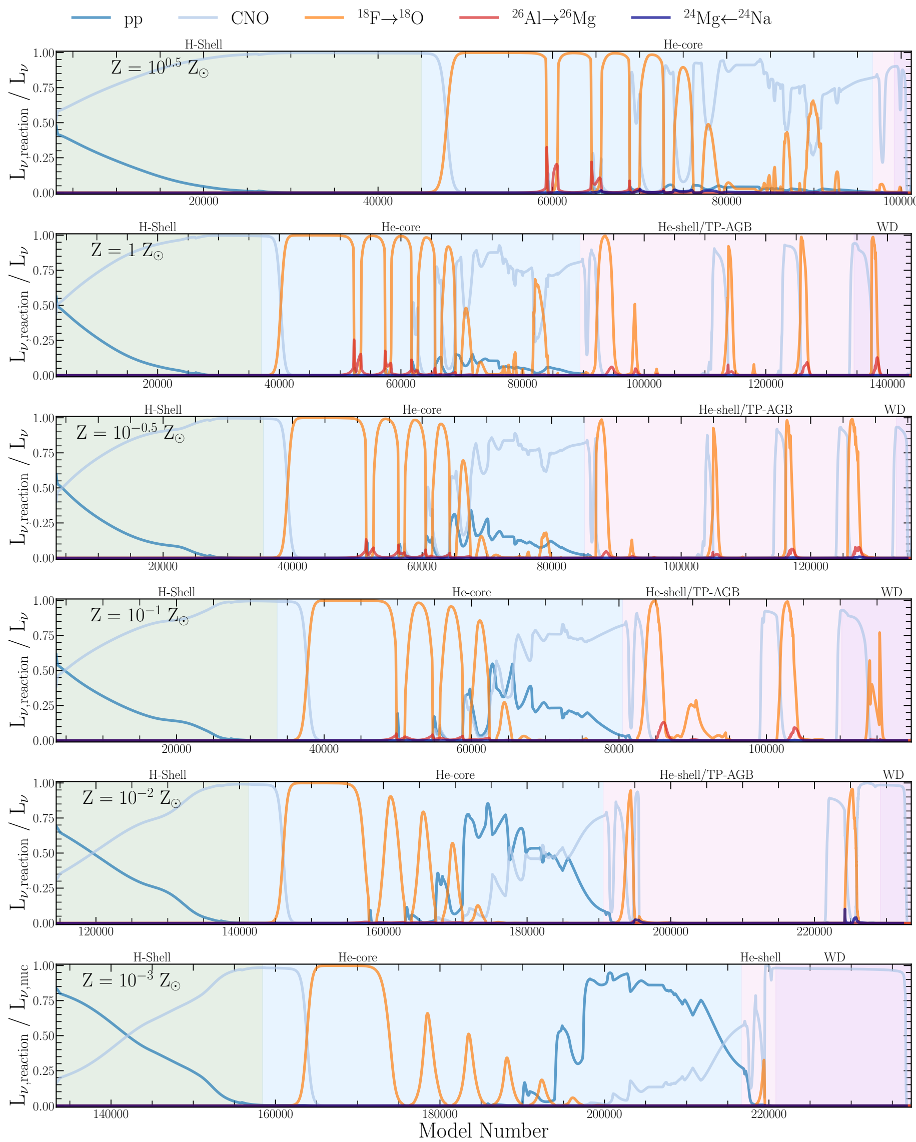

Figure 3.8: Components of L_ν from nuclear reactions over the lifetime of a $M_{\mathrm{ZAMS}}=$ 1 $\mathrm{M}_\odot$ model for all six metallicities. The x-axis is the sequential model number, a proxy for time, beginning at core H-depletion (left) and ending as a cool WD (right). Curves are smoothed with a 50 model moving average filter. Evolutionary phases are shown by the colored regions and labelled. Reactions emitting neutrinos in the pp-chain and CNO cycles are listed in Section 3.4.1.

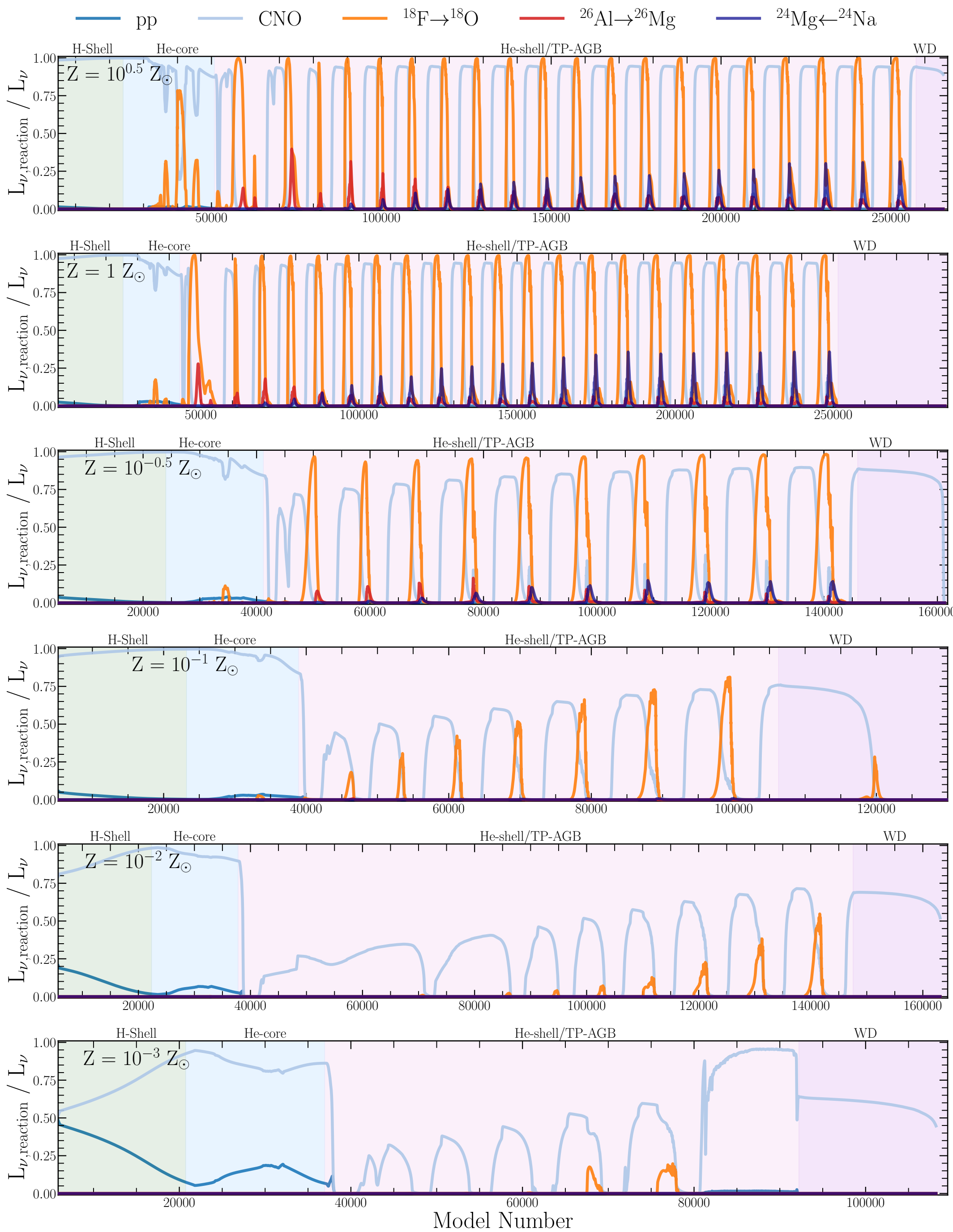

Figure 3.9: Same as Figure 3.8 for 3 $M_\odot$ models.

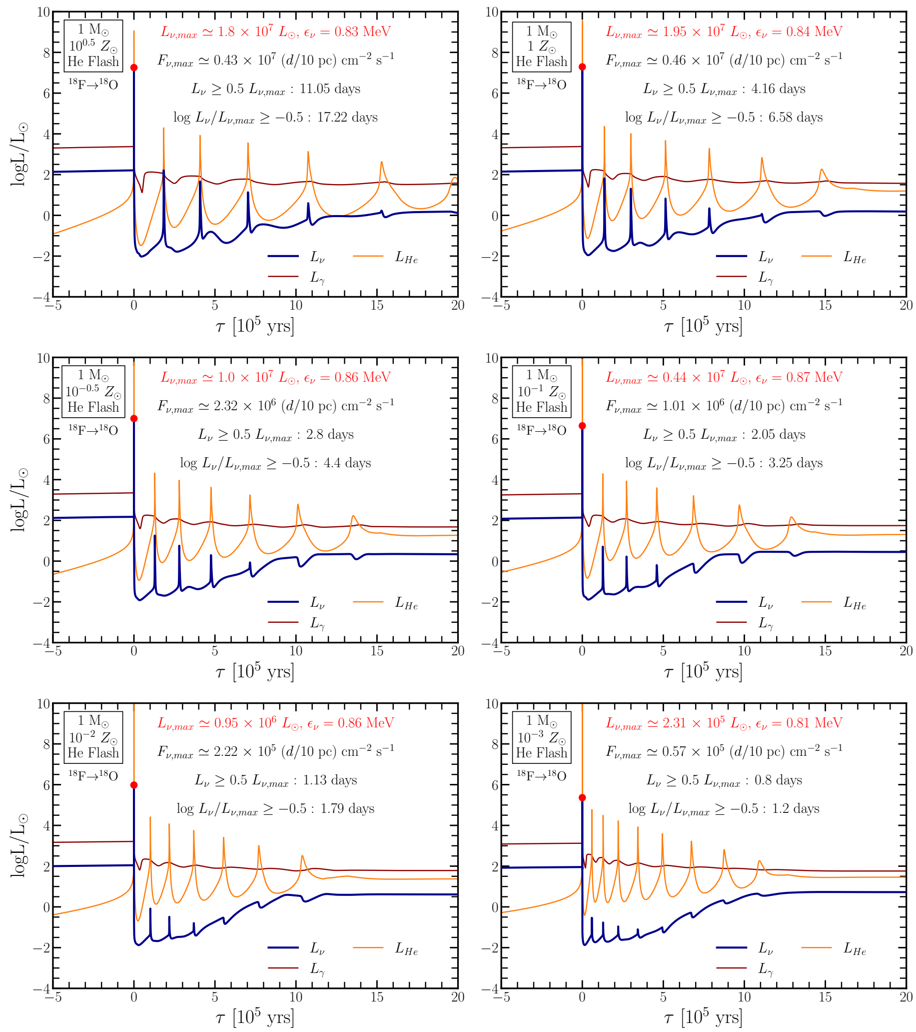

Figure 3.10: Neutrino targets for the nitrogen flash in 1 $M_\odot$ models for all six metallicities. The x-axis is the time since the first, and strongest, nitrogen flash. The y-axis is a luminosity relative to $L_\odot = 3.828 \times 10^{33}$ erg s^{-1} (Prša *et al.*, 2016b). Colored curves show the ν, γ, and He-burning luminosity. The red circle marks the maximum L_ν and the red label gives the value of $L_{\nu,\rm max}$ and the average neutrino energy. Labelled are the maximum flux at a distance d in parsec, and the duration for the L_ν to be larger than 1/2 and 1/3 $L_{\nu,\rm max}$. Metal-rich models have larger $L_{\nu,\rm max}$ and longer periods between flashes.

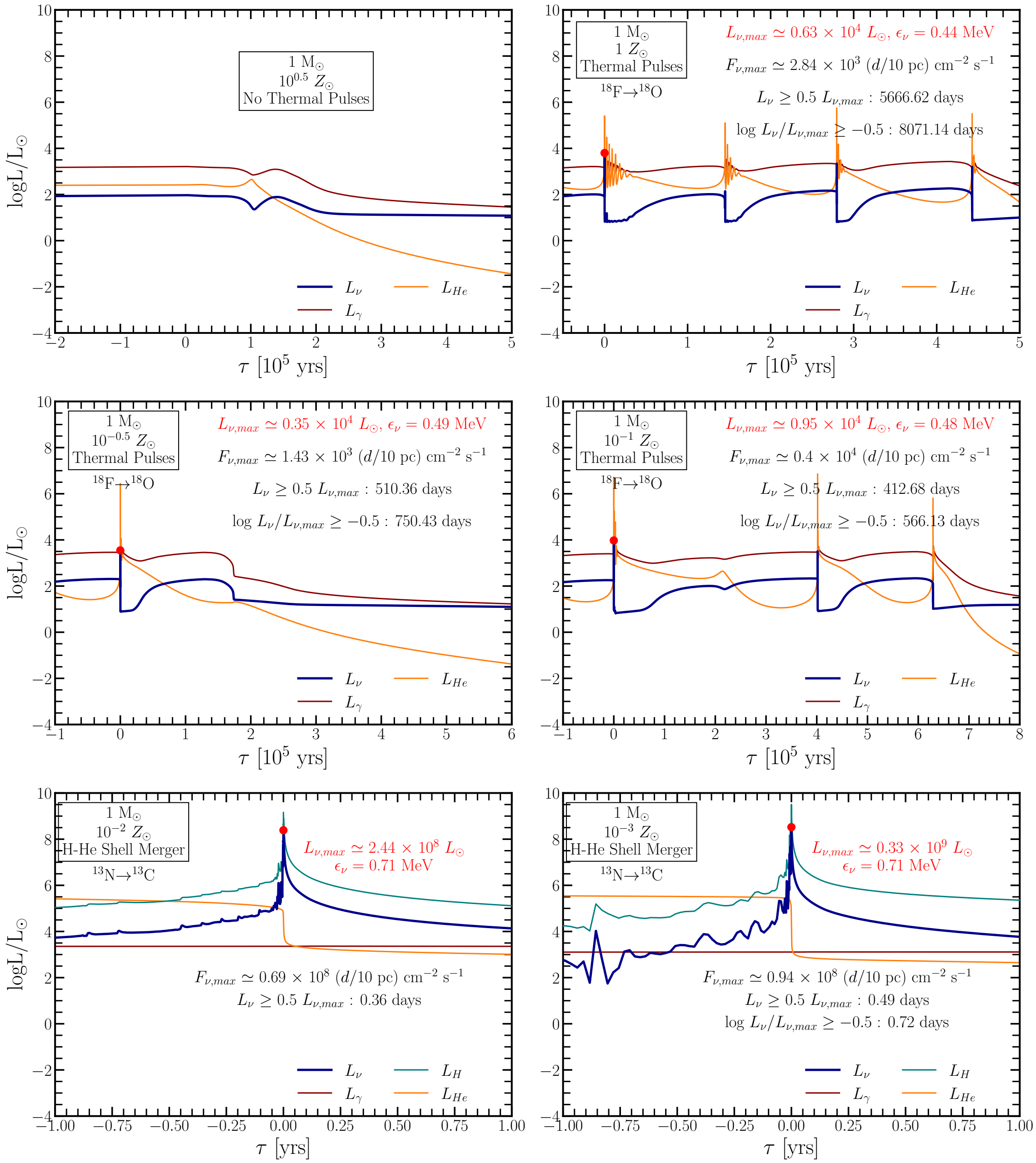

Figure 3.11: Same format as Figure 3.10 but for the TP-AGB phase of evolution.

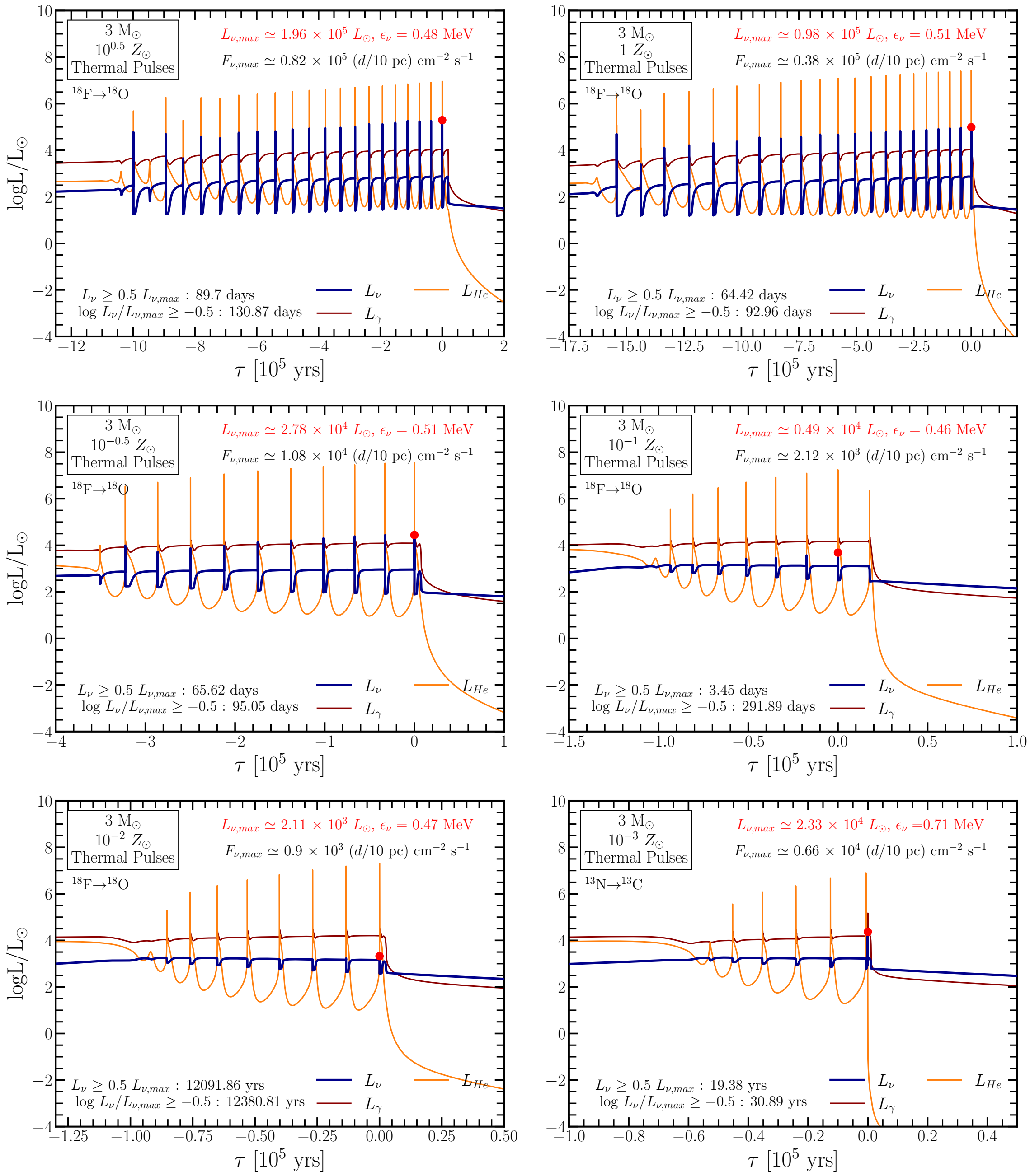

Figure 3.12: Same format as Figure 3.11 but for 3 M$_\odot$ models across all six metallicities.

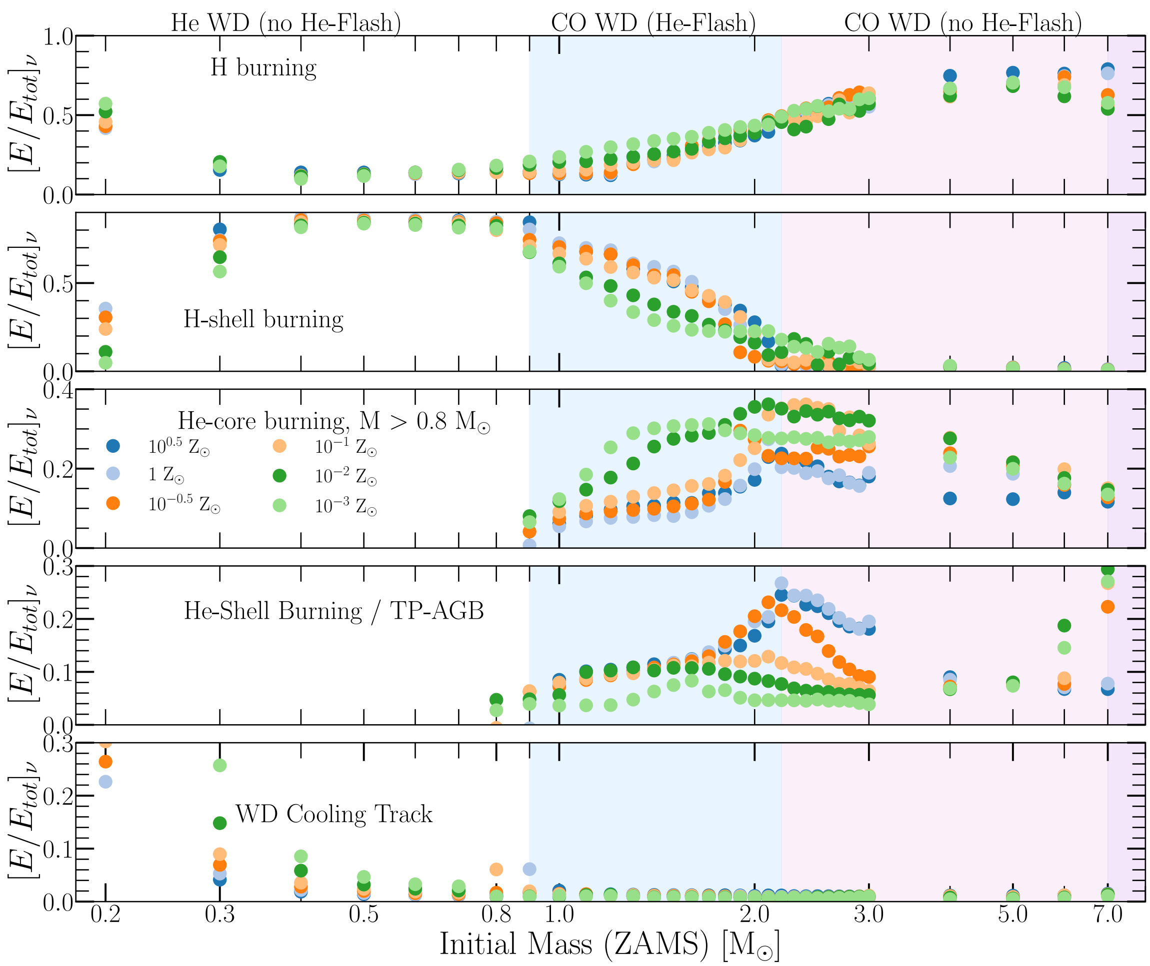

Figure 3.13: Fraction of E_ν emitted at different phases of evolution for all six metallicities (colored circles). From top to bottom, the panels show $[E/E_{\rm tot}]_\nu$ for core H-burning, shell H-burning, core He-burning prior to any TP-AGB phase, He-burning through the TP-AGB phase, and during the WD cooling phase.

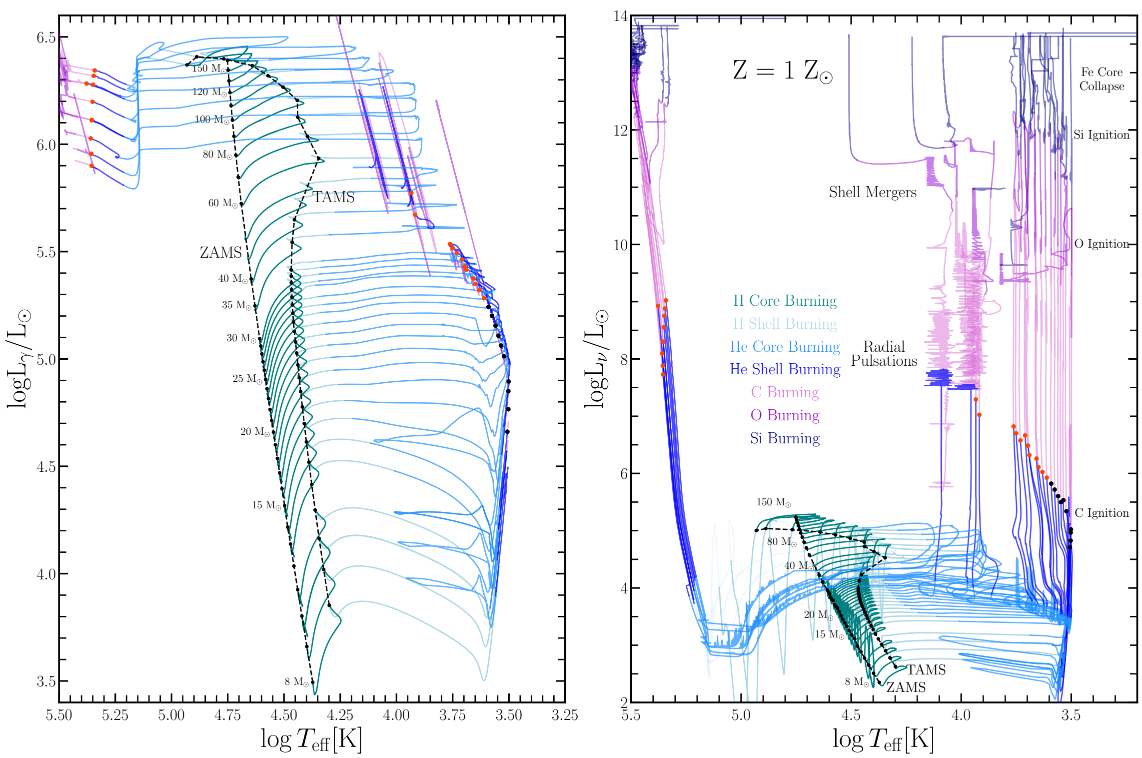

Figure 3.14: Tracks in a γHRD (left panels) and a νHRD (right panels) for $\mathrm{Z} = 1\,Z_{\odot}$ over $M_{\mathrm{ZAMS}} = 8$–$150\ \mathrm{M}_{\odot}$. Tracks are colored by evolutionary phase and labeled. Black circles mark convective core C-burning, red circles mark radiative core C-burning. Luminosities are normalized to $\mathrm{L}_{\odot} = 3.828 \times 10^{33}$ erg s^{-1} (Prša *et al.*, 2016b).

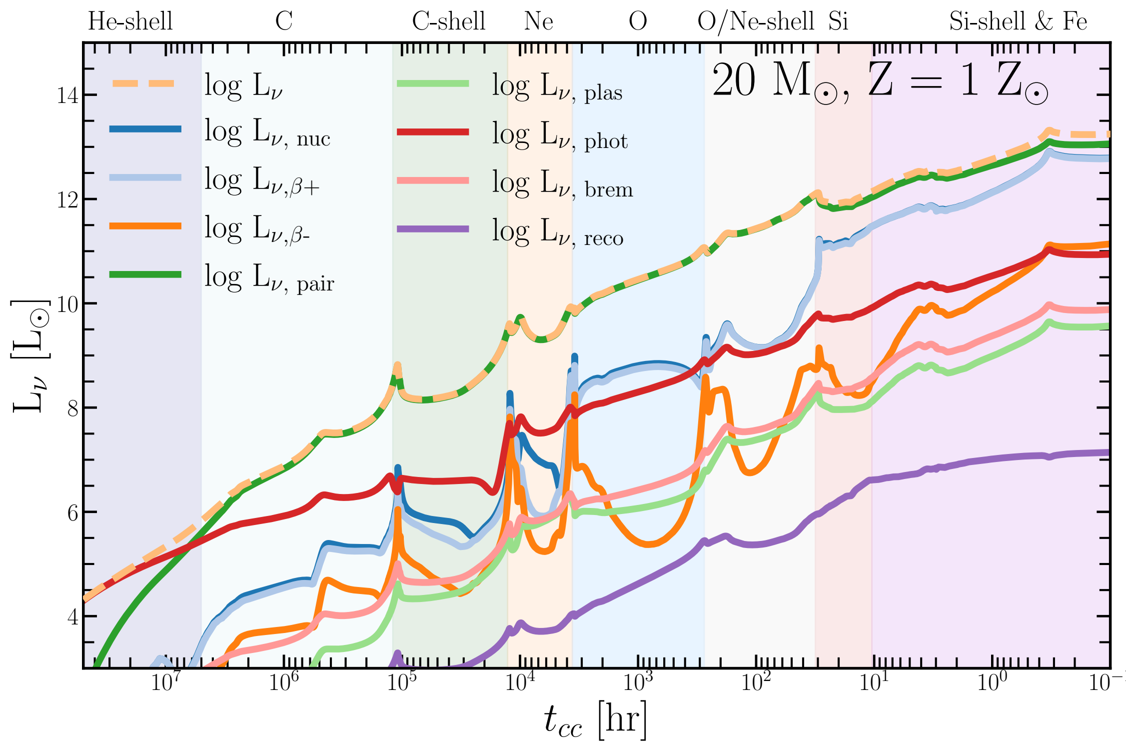

Figure 3.15: Components of L_ν for each phase of evolution of a $M_{\text{ZAMS}} = 20$ $M_\odot$, 1 $Z_\odot$model. The x-axis is the time to the onset of CC. Curves show the contributions from nuclear and thermal neutrinos, and are smoothed with a 50 timestep moving average filter. Phases of evolution are shown by the colored regions and labeled above the plot. Boundaries between phases are defined by the ignition of the next fuel source, when the central mass fraction of the next fuel source decreases by 10^{-3}.

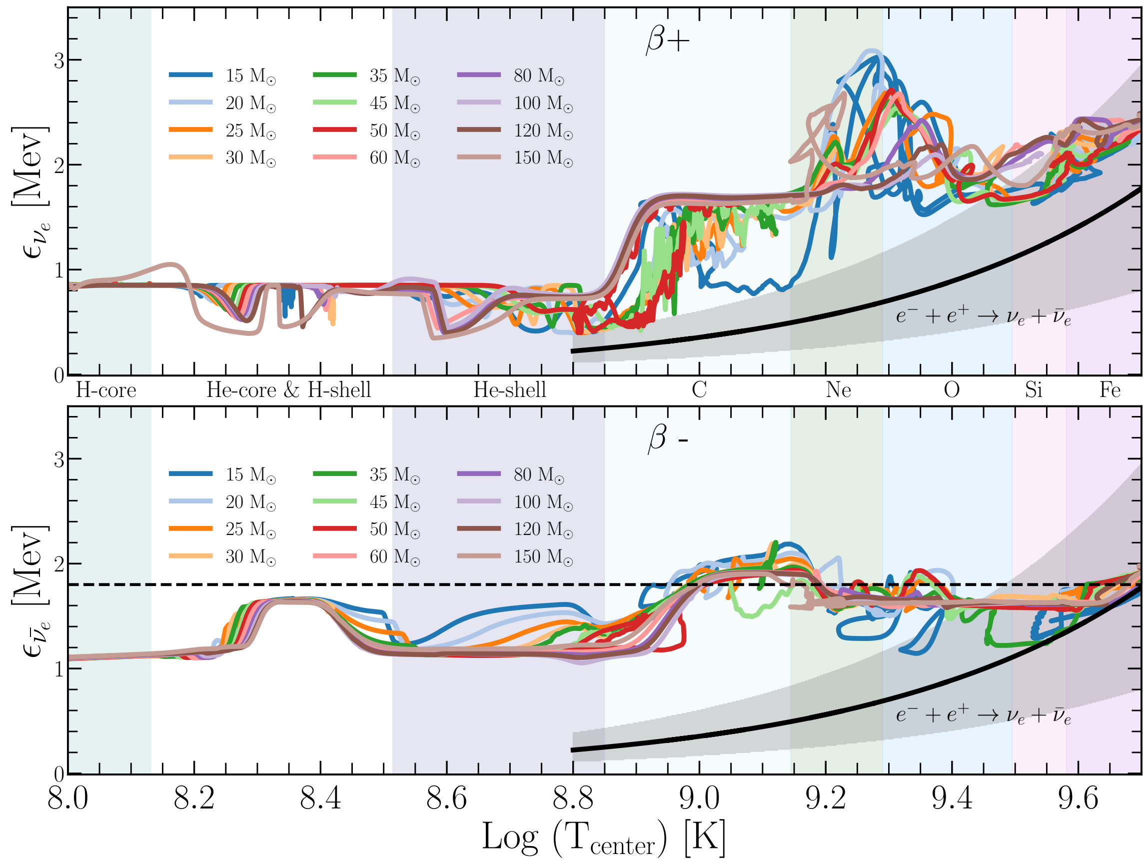

Figure 3.16: Average electron neutrino energy for beta decays (top), and average electron anti-neutrino energy for inverse-beta decays (bottom) for the 1 $Z_{\odot}$ models across a range of $M_{\rm ZAMS}$. Curves are smoothed with a 50 timestep moving average filter. The average pair-neutrino energy is shown by the black curve, with the gray band giving the lower 10% and upper 90% of pair-neutrino energies. Phases of evolution are shown by the colored panels and labeled. The horizontal dashed line shows a representative $\simeq$1.8 MeV detection threshold to inverse beta decay of current neutrino detectors (e.g., Simpson *et al.*, 2019; Harada *et al.*, 2023). The average electron neutrino and anti-neutrino energies are approximately independent of $M_{\rm ZAMS}$.

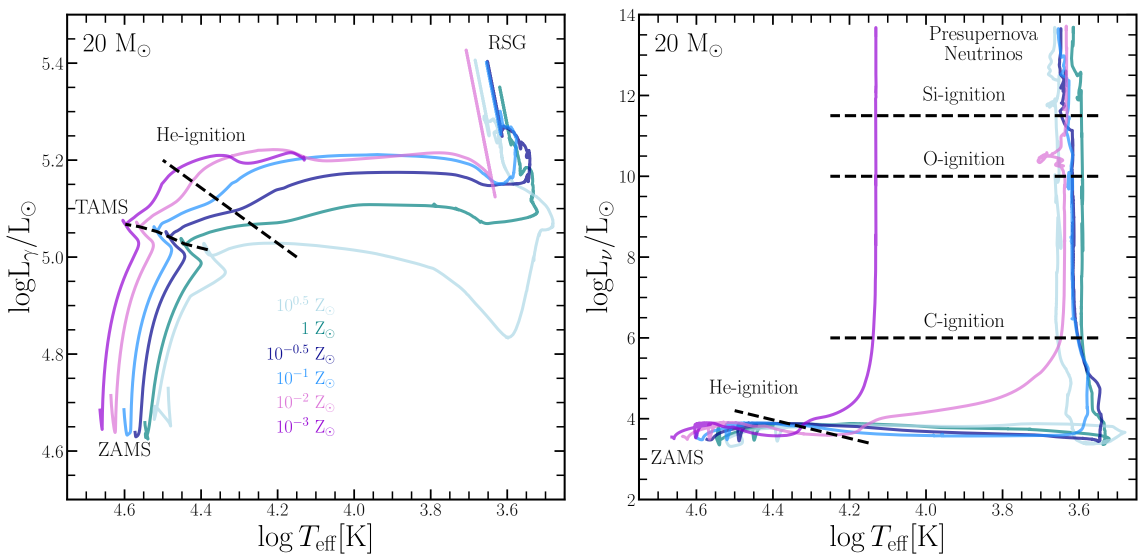

Figure 3.17: Tracks in a γHRD (left) and νHRD (right) from ZAMS to the onset of CC for the $M_{\rm ZAMS} = 20$ M$_\odot$ models across all six metallicities. Approximate locations of evolutionary phases are labeled or marked with a black dashed line. Luminosities are normalized to L$_\odot$ = 3.828 $\times 10^{33}$ erg s^{-1} (Prša *et al.*, 2016b).

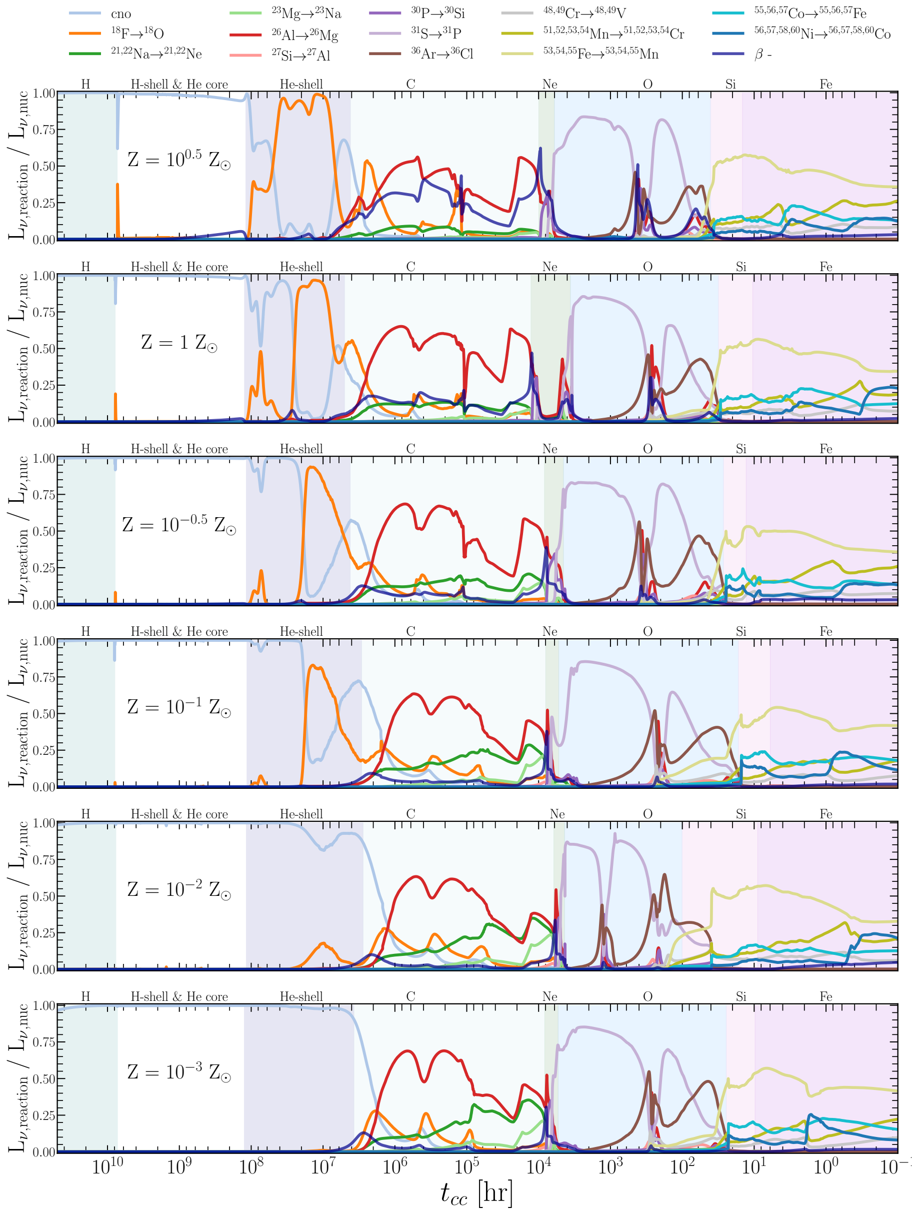

Figure 3.18: Components of L_ν from nuclear reactions over the lifetime of a M_{ZAMS}= 20 M$_\odot$ model for all six metallicities. The x-axis is the time to the onset of CC. Evolutionary phases are shown by the colored regions and labelled. Curves show the largest contributions by the burning processes and weak reactions listed in the legend.

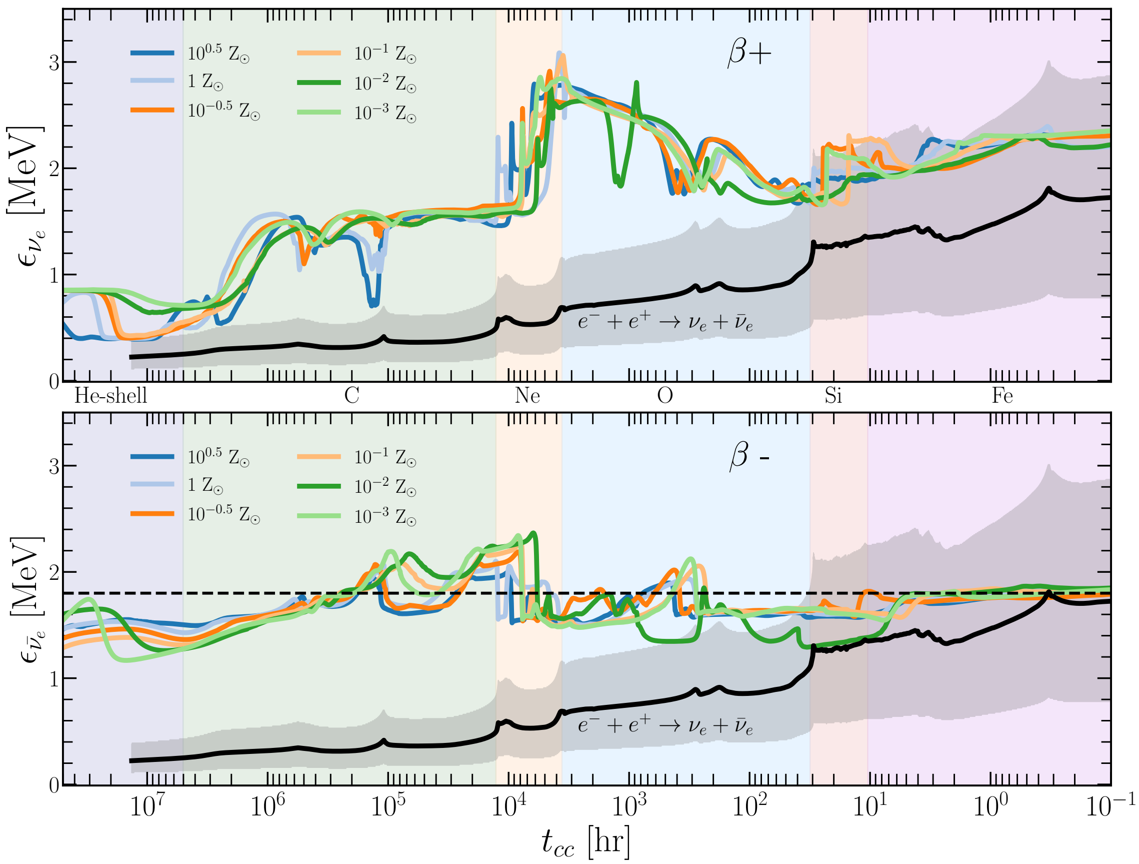

Figure 3.19: Average electron neutrino energy for beta decays (top), and average electron anti-neutrino energy for inverse-beta decays (bottom) for the $M_{\rm ZAMS} = 20\ \rm M_\odot$ models across all six metallicities. Curves are smoothed with a 50 timestep moving average filter. The average pair-neutrino energy is shown by the black curve, with the gray band giving the lower 10% and upper 90% pair-neutrino energies. Phases of evolution are shown by the colored panels and labeled. The horizontal dashed line shows a representative $\simeq 1.8$ MeV detection threshold to inverse beta decay of current neutrino detectors (e.g., Simpson *et al.*, 2019; Harada *et al.*, 2023). The average electron neutrino and anti-neutrino energies are to first-order independent of Z.

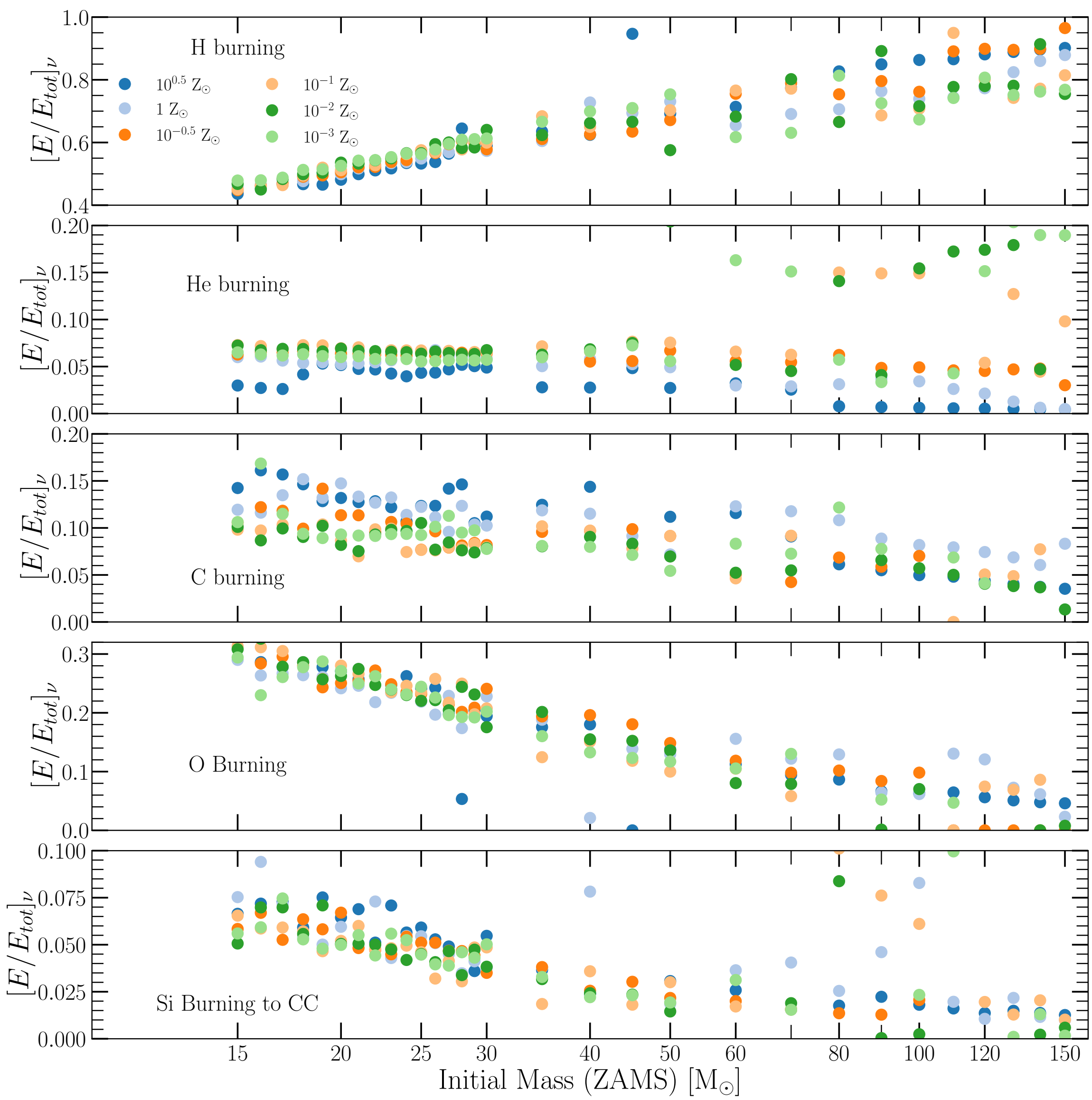

Figure 3.20: Fraction of E_ν emitted at different phases of evolution for all six metallicities (colored circles). From top to bottom, the panels show $[E/E_{\rm tot}]_\nu$ for H-burning, He-burning, C-burning, O-burning and Si-burning to the onset of CC.

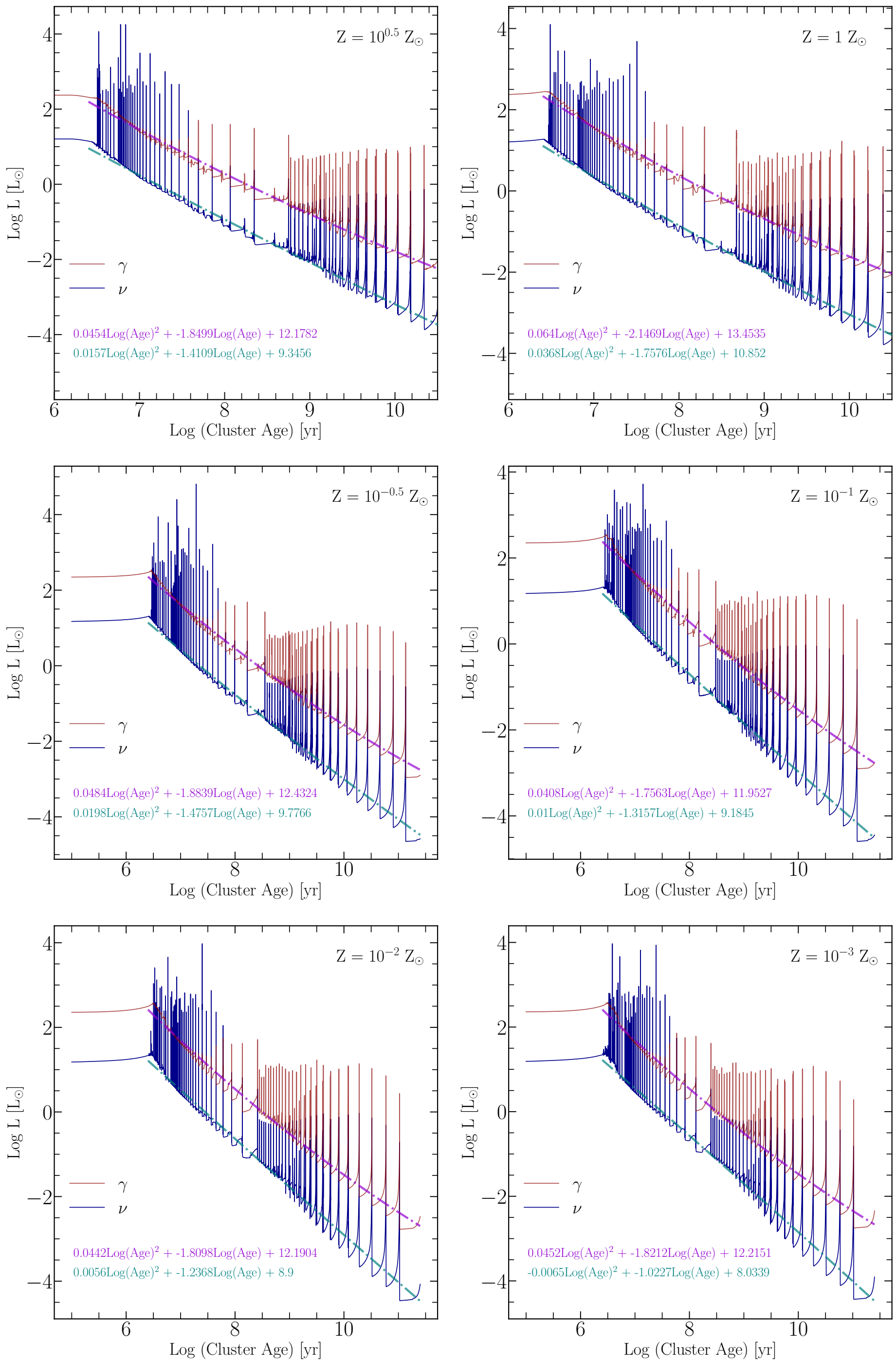

Figure 3.21: Cluster L_γ and L_ν light curves from the evolution models for all six metallicities. Overlayed are quadratic fitting functions with the coefficients for each metallicity listed (see Equation 3.21).

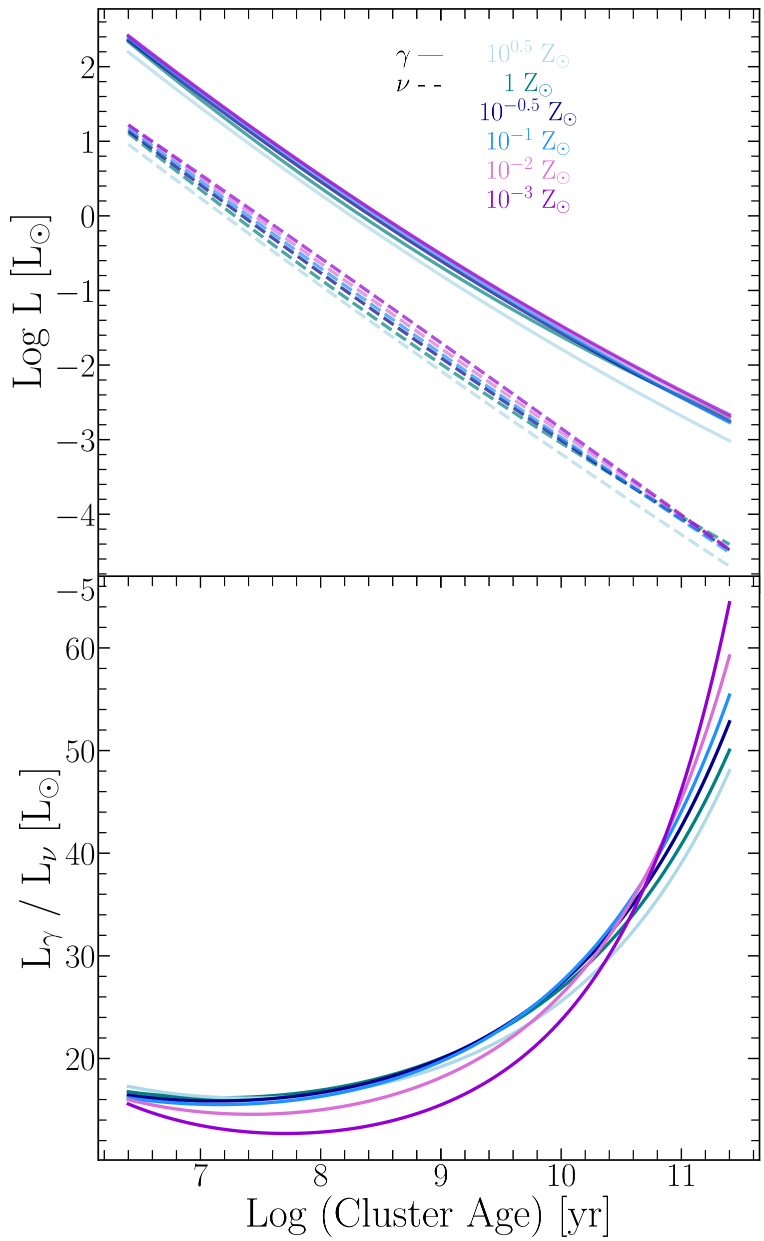

Figure 3.22: Cluster L_γ and L_ν light curves (top) and the ratio L_γ/L_ν (bottom) using Equation 3.21 with $M = 1$ $M_\odot$ for all six metallicities.

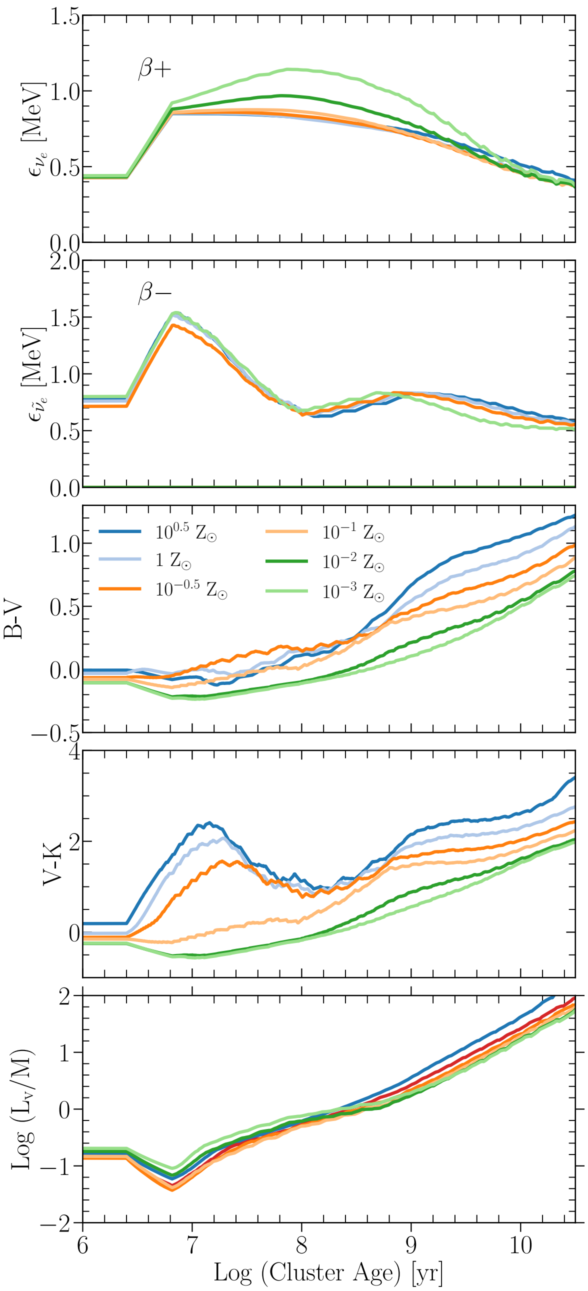

Figure 3.23: Average electron neutrino energies for beta decay processes (top panel), average electron anti-neutrino energies for inverse-beta decay processes (second panel), Johnson-Cousins B-V and V-K colors (third and fourth panels), and neutrino light to mass ratio for a simple stellar population (bottom panel) for all six metallicities.

Chapter 4

RESOLVING THE PEAK OF THE BLACK HOLE MASS SPECTRUM

Below is the published work of Ebraheem Farag et al 2022 ApJ 937 112.

4.1 Abstract

Gravitational wave (GW) detections of binary black hole (BH) mergers have begun to sample the cosmic BH mass distribution. The evolution of single stellar cores predicts a gap in the BH mass distribution due to pair-instability supernova (PISN). Determining the upper and lower edges of the BH mass gap can be useful for interpreting GW detections from merging BHs. We use MESA to evolve single, non-rotating, massive helium cores with a metallicity of $Z = 10^{-5}$ until they either collapse to form a BH or explode as a PISN without leaving a compact remnant. We calculate the boundaries of the lower BH mass gap for S-factors in the range S(300 keV) = (77,203) keV b, corresponding to the $\pm 3\sigma$ uncertainty in our high resolution tabulated $^{12}C(\alpha,\gamma)^{16}O$ reaction rate probability distribution function. We extensively test the temporal and mass resolution to resolve the theoretical peak of the BH mass spectrum across the BH mass gap. We explore the convergence with respect to convective mixing and nuclear burning, finding that significant time resolution is needed to achieve convergence. We also test adopting a minimum diffusion coefficient to help lower resolution models reach convergence. We establish a new lower edge of the upper mass gap as $M_{lower} \simeq 60^{+32}_{-14}\,M_\odot$ from the $\pm 3\sigma$ uncertainty in the $^{12}C(\alpha,\gamma)^{16}O$ rate. We explore the effect of a larger 3-α rate on the lower edge of the upper mass gap, finding $M_{lower} \simeq 69^{+34}_{-18}\,M_\odot$. We compare our results with BHs reported in the Gravitational-Wave Transient Catalog.

The BH initial mass function from single star evolutionary models predict three physics-driven transitions in the distribution. In order of increasing mass, the first transition is set by the maximum possible neutron star mass, the second by electron-positron pair production from energetic photons in the stellar interior of a massive star, and the third by exothermic photodisintegration reactions which absorb enough energy in a high temperature stellar core for the model star to, once again, reach core collapse.

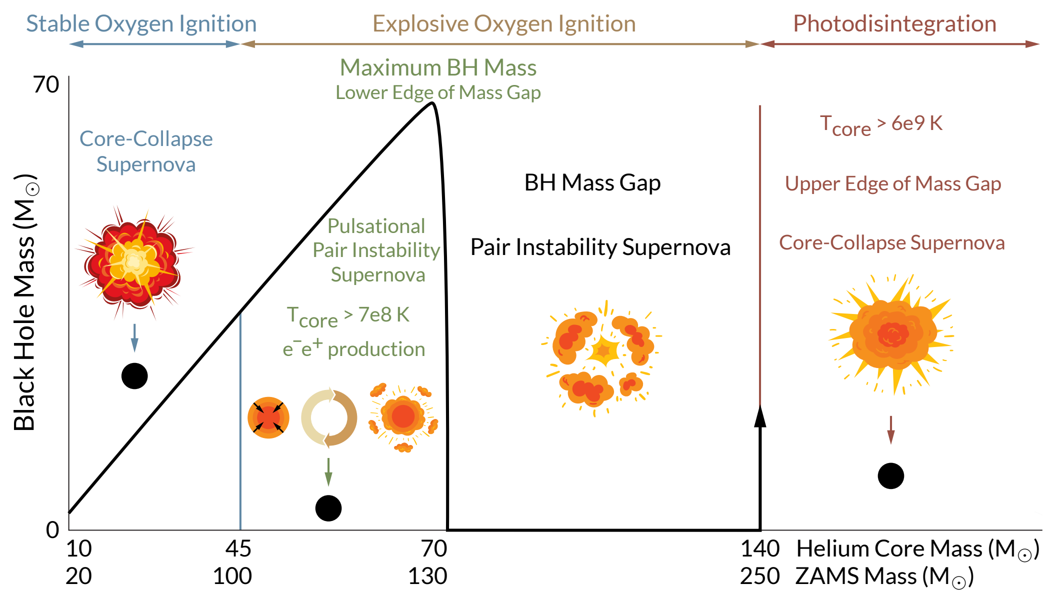

Figure 4.1: Illustration of a single star BH mass spectrum.

On the first transition, the maximum observed masses of neutron stars include about 2.01 $M_\odot$ for PSR J0348+0432 (Antoniadis *et al.*, 2013), about 2.08-2.14 $M_\odot$ for PSR J0740+6620 (Cromartie *et al.*, 2020; Farr and Chatziioannou, 2020; Riley *et al.*, 2021; Miller *et al.*, 2021; Fonseca *et al.*, 2021), and about 2.16 $M_\odot$ for GW170817 (Abbott *et al.*, 2017a,b; Rezzolla *et al.*, 2018). Integration of the general relativistic equations of hydrostatic equilibrium with a nuclear equation of state predict a restricted range of allowed gravitational neutron star masses, with currently favored equations of state giving $\simeq 0.1$–$2.5\,\mathrm{M}_\odot$ (Banik *et al.*, 2014; Marques *et al.*, 2017; Ferreira and Providência, 2021; Lattimer, 2021). The lower bound is the minimum stable neutron star mass (Oppenheimer and Serber, 1938; Colpi *et al.*, 1989; Haensel *et al.*, 2002; Koliogiannis and Moustakidis, 2021), although a more relevant minimum mass stems from a neutron star's origin in a supernova (Timmes *et al.*, 1996; Zhang *et al.*, 2008; Sukhbold *et al.*, 2016; Richers *et al.*, 2017; Sukhbold *et al.*, 2018; Ghosh *et al.*, 2022; Patton *et al.*, 2022) or accretion induced collapse of a white dwarf (Fryer *et al.*, 1999; Schwab, 2021; Wang *et al.*, 2022). Less massive neutron star masses can undergo explosive decompression (Page, 1982; Colpi *et al.*, 1993; Sumiyoshi *et al.*, 1998; Nixon *et al.*, 2020) while more massive ones overcome the repulsive strong force and neutron degeneracy pressure to collapse into BHs.

In addition, there is an apparent paucity of observed BH candidates in the $\simeq 2.5$–$5\,\mathrm{M}_\odot$ mass range (Bailyn *et al.*, 1998; Özel *et al.*, 2010; Belczynski *et al.*, 2012), hinting at the possible existance of a contested "lower mass gap" (Farr *et al.*, 2011; Wyrzykowski and Mandel, 2020; Zevin *et al.*, 2020; Mandel and Farmer, 2022). The "lower edge" of the lower mass gap is set by the maximum possible neutron star mass while the "upper edge" is set by the minimum observed BH mass. The upper edge of the lower mass gap, if it exists, is currently uncertain as BHs found in this mass range may have been created by changes in the growth time of convection during a SN explosion (Fryer *et al.*, 2022), or by binary neutron star mergers (Thompson *et al.*, 2019; Abbott *et al.*, 2020; Gupta *et al.*, 2020; Yang *et al.*, 2020; Ye and Fishbach, 2022).

The second and third transitions form the "upper mass gap", see Figure 4.1. Models with zero-age main sequence (ZAMS) masses $M_{\mathrm{ZAMS}} \gtrsim 100\,\mathrm{M}_\odot$ reach central temperatures of $T_{\mathrm{c}} \gtrsim 7\times10^8$ K. This allows for the production of electron–positron pairs from photons, $\gamma+\gamma \rightarrow e^- + e^+$, that soften the equation of state (Fowler and Hoyle, 1964; Barkat *et al.*, 1967; Rakavy and Shaviv, 1967). These models become dynamically unstable before core O-depletion as the pair production leads to regions where the adiabatic index $\Gamma_1 \leq 4/3$ (Fraley, 1968; Ober *et al.*, 1983; Bond *et al.*, 1984).

The ensuing dynamical collapse results in explosive O-burning, with a variety of possible outcomes (Glatzel *et al.*, 1985; Woosley *et al.*, 2002; Heger *et al.*, 2003; Takahashi, 2018; Farmer *et al.*, 2019; Marchant *et al.*, 2019; Marchant and Moriya, 2020; Renzo *et al.*, 2020a; Woosley and Heger, 2021; Mehta *et al.*, 2022; Renzo *et al.*, 2022). The energy injected can cause a cyclic pattern of entering the pair-instability region, contracting, burning, and expanding; eventually leading to pulsational pair-instability supernovae (PPISN) and a BH remnant. The energy injected by a single strong pulse can also unbind the model without leaving a BH remnant in a pair-instability supernova (PISN). This transition to a PISN defines the "lower edge" of the upper mass gap. Models with $M_{\rm ZAMS} \gtrsim 250\,\rm M_\odot$ reach $T_{\rm c} \gtrsim 6\times10^9$ K, where endothermic photodisintegration reactions absorb enough energy to prevent the star from unbinding (Bond *et al.*, 1984; Heger *et al.*, 2003). This third transition defines the "upper edge" of the upper mass gap.

The ZAMS mass of the second and third transitions depend on the He core-to-ZAMS mass mapping and thus the rotation, convective boundary mixing, and mass loss adopted (Vink *et al.*, 2015, 2021; Higgins *et al.*, 2021; Woosley, 2019). Since roughly half of all massive stars are found in binaries (Sana and Evans, 2011; Sana *et al.*, 2012), a simple assumption is that binary interactions will strip the H envelope revealing bare He cores, before He burning commences. This can occur from Roche lobe overflow and or formation and ejection of a common envelope. All low-metallicity stars, including those with H-rich envelopes, are also expected to undergo

PPISN/PISN and lose part or all of their envelope in the pulses (Woosley, 2017; Renzo *et al.*, 2020b). We are only interested in determining peak BH masses from GW sources in isolated systems, so we assume their progenitors are He cores.

While the three transitions are set by nuclear and particle physics, the total number of BHs as well as their distribution with mass is a consequence of stellar evolution. A number of uncertain factors make a straightforward determination challenging. For example, current estimates of the BH initial mass function from single stars chiefly rely on parameterized explosion models (Spera *et al.*, 2015; Patton and Sukhbold, 2020; Zapartas *et al.*, 2021; Patton *et al.*, 2022; Fryer *et al.*, 2012, 2022; Renzo *et al.*, 2022). Models for the evolution from the ZAMS also still rely on effective mixing length theories for convection, including ours. Finally, BHs in either mass gap may occur through mechanisms other than those involving a single star. Examples include isolated binary star evolution (de Mink and Mandel, 2016; Spera *et al.*, 2019; Breivik *et al.*, 2020; Belczynski, 2020; Santoliquido *et al.*, 2021; Fuller and Lu, 2022; van Son *et al.*, 2020), dynamical formation in dense star clusters (Portegies Zwart and McMillan, 2000; Di Carlo *et al.*, 2020; Fragione *et al.*, 2022; Renzo *et al.*, 2020a), mergers in higher multiplicity systems (Antonini and Perets, 2012; Liu and Lai, 2018; Hamers and Samsing, 2019), mergers of compact binaries in galactic nuclei (O'Leary *et al.*, 2009; Bartos *et al.*, 2017; Wang *et al.*, 2021), and mass loss from putative progenitors above the PISN regime (i.e., super-kilonova Siegel *et al.*, 2021). Contributions from the different populations may be unraveled as the number of detected gravitational wave events increase (Perna *et al.*, 2019; Zevin *et al.*, 2021; Renzo *et al.*, 2021; Mandel and Broekgaarden, 2022).

This article focuses on the second transition, the lower edge of the upper mass gap. The predicted BH mass at the lower edge from single naked He core models are generally robust with respect to model uncertainties (Takahashi, 2018; Farmer *et al.*, 2019; Marchant and Moriya, 2020; Farmer *et al.*, 2020; Renzo *et al.*, 2020c), but depend sensitively on the $^{12}C(\alpha,\gamma)^{16}O$ reaction rate (Farmer *et al.*, 2020). The masses and spins of merging binary BHs from LIGO/Virgo/Karga (LVK, LIGO Scientific Collaboration *et al.*, 2015; Acernese *et al.*, 2015; Akutsu *et al.*, 2021) observations probe the location of the lower edge of the upper mass gap. The observed lower edge can then be used to place a constraint on the $^{12}C(\alpha,\gamma)^{16}O$ reaction rate (Farmer *et al.*, 2020). However, we caution that LVK merging BHs might have a very complex astrophysical history (e.g., binary evolution and stellar dynamics) which might blur the mass gap, and the mass gap may not appear at all with the LVK BHs. Furthermore, we caution that there are competing effects at the lower edge of the mass gap (e.g., overshooting, collapse of the H-envelope) that might have the same effect as varying $^{12}C(\alpha,\gamma)^{16}O$ reaction rates.

The main novelty of this article is a new effort, initiated by Farmer *et al.* (2020) and refined in Mehta *et al.* (2022), aimed at showing convergence in the sequence of models used to define the lower edge of the upper mass gap as a function of the He-burning reaction rates. Section 4.3 describes our models, Sections 4.4 and 4.5 describe our results, and Section 4.6 summarizes our conclusions.

4.3 Models

We use `MESA` version r11701 to evolve single, non-rotating, massive He cores with a metallicity of $Z = 10^{-5}$ until they either collapse to form a BH or explode as a PISN without leaving a compact remnant. We adopt a low metallicity so that stellar winds are irrelevant (Farmer *et al.*, 2019), and to avoid the possible numerical complications of resolving models with winds (Renzo *et al.*, 2017). Low metallicity environments are also likely to form some of the most massive stellar mass BHs that can be detected as GW sources (Mapelli, 2021; Vink *et al.*, 2021; Mandel and Farmer, 2022; Spera *et al.*, 2022). Metallacities as low as $Z = 0.02\,Z_{\odot}$ are enough to yield final He core masses of up to $140\,M_{\odot}$ when adopting recently updated and physically motivated Wolf-rayet mass loss schemes (Higgins *et al.*, 2021).

We use the same `MESA` inlists and run_star_extras.f90 used in Farmer *et al.* (2020) and Mehta *et al.* (2022) to calculate BH mass spectrum across the lower edge of the upper mass gap. We also use a 21-isotope nuclear network with nuclear reactions rates from the NACRE compilation (Angulo *et al.*, 1999) and JINA reaclib database (Cyburt *et al.*, 2010a). The tabulated $^{12}C(\alpha,\gamma)^{16}O$ reaction rates were originally provided by deBoer *et al.* (2017) and refined in Mehta *et al.* (2022). A total of 1750 models were run that consumed $\simeq$3,000,000 core-hours. Full details of the `MESA` models and reaction rate files to reproduce our results are available at doi: `https://doi.org/10.5281/zenodo.6930577`.

Preceding any individual pulse, we use `MESA`'s implicit hydrodynamic solver. As a model evolves into the pair-instability region we switch to `MESA`'s Hartan-Lax-van Leer-Contact hydrodynamic solver (HLLC, Toro *et al.*, 1994; Paxton *et al.*, 2018) to resolve shocks during the dynamic phase of evolution. The switch generally occurs when central temperatures exceed 10^9 K and the volumetric pressure-weighted average adiabatic index $\langle \Gamma_1 \rangle - 4/3 < 0.01$ (Stothers, 1999; Marchant *et al.*, 2019; Farmer *et al.*, 2019). We then follow the core as it gravitationally unbinds on the first pulse as a PISN, or contracts and rebounds repeatedly until all shocks have reached the surface of the model (Yoshida *et al.*, 2016; Woosley, 2017; Marchant *et al.*, 2019; Renzo *et al.*, 2020c). Individual pulses can eject between $\simeq 0.01\,M_{\odot}$ and $\simeq 30\,M_{\odot}$ with surface velocities up to 20000 km s^{-1}.

Once hydrostatic equilibrium is reached again, the unbound material is removed, the remaining mass is relaxed to a new stellar model with an identical entropy and chemical profile. This is possible since the removed mass is already moving at speeds beyond both the escape velocity and the surface sound speed, so no back-reaction on the remaining material is expected (Marchant *et al.*, 2019). The evolution then continues with the implicit solver. The new model contracts as it loses energy due to radiation and neutrino emission until it undergoes an additional pulse or collapses to form a BH. At the onset of core collapse (CC), the HLLC solver is activated to capture the dynamics of the infalling core. We define CC to occur when any part of the model begins collapsing with velocities $v > 8000$ km s^{-1}, so as to capture any pulse that might be ejected during CC. The mass of the BH is defined as the mass of bound material at CC (Renzo *et al.*, 2020c). These BHs masses are upper limits due to uncertainties in BH formation (Fryer *et al.*, 2001; Branch and Wheeler, 2017; Uchida *et al.*, 2019; Mandel and Broekgaarden, 2022; Renzo *et al.*, 2022) and weak shock generation (Nadezhin, 1980; Fernández *et al.*, 2018; Ivanov and Fernández, 2021; Rahman *et al.*, 2022).

4.4 Convergence of the Peak BH Mass Spectrum

Mapping the final evolutionary phases of massive stars remains challenging given the difficulty in resolving the interplay between convection, nuclear burning, rotation, convective-core overshooting, radiative transport, internal waves, mass loss eruptions, and binary interactions (Quataert and Shiode, 2012; Shiode and Quataert, 2014; Matzner and Ro, 2021; Vink *et al.*, 2021; Tanikawa *et al.*, 2021; Jacobson-Galán *et al.*, 2022; Wu and Fuller, 2022). All else equal, mass resolution is an important consideration to accurately control for changes in stellar structure (Farmer *et al.*, 2016). Assessing the sensitivity to mass resolution is a necessary practice to ensure robust predictions. The evolution of PPISN stars are characterized by short episodes of strong nuclear burning in their core rapidly changing their composition and density. We will control changes in the central density for temporal resolution. PPISN stars also eject large amounts of material at and beneath escape velocity. We will control the spatial mesh resolution of our models to resolve this material.

The goal of this section is to assess the numerical convergence the `MESA` models used to determine the lower edge of the upper mass gap with respect to spatial and temporal resolution. During hydrostatic phases of evolution when the implicit solver is active, we control the number of cells with `max_dq`, the maximum fractional mass in a cell. That is, the minimum number of cells is 1/`max_dq`. During the dynamic phases of evolution when the HLLC solver is active, we control the number of cells with `split_merge_amr_nz_baseline`. For both phases of evolution we primarily control the timestep with `delta_lgRho_cntr_limit` which limits the timestep such that the change in the logarithm of the central density is less than a specified fraction.

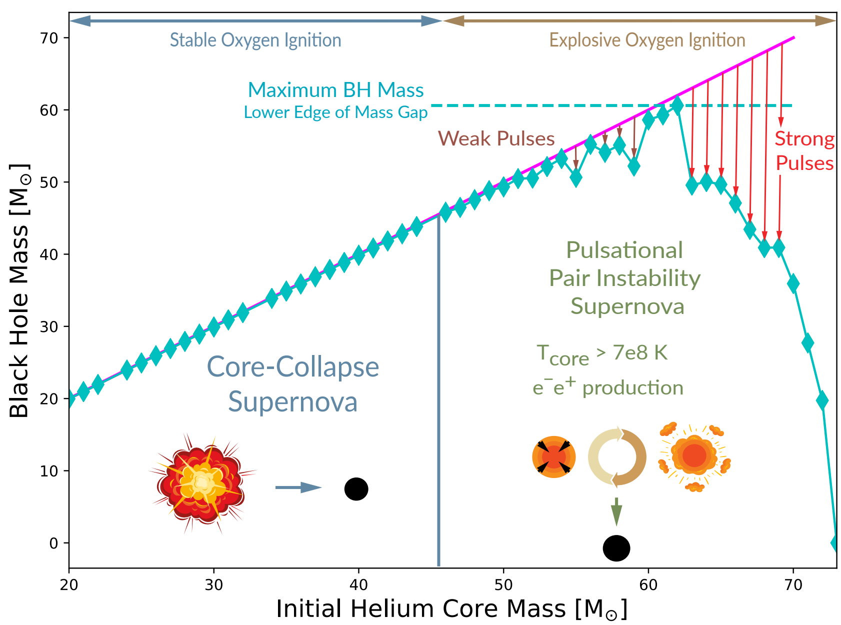

Figure 4.2: As in Figure 4.1, but with an example of a calculated BH mass spectrum (teal line and diamonds). A magenta line marks $M_{\rm BH} = M_{\rm He}$. The peak BH mass is labeled. Smaller masses, just left of the peak, show weak pulses. Larger masses, just right, show strong pulses.

In the following sections we indicate a “strong” pulse as a single pulse that arises from $\langle \Gamma_1 - 4/3 \rangle < 0$ and results in the ejection of $>0.1\,\mathrm{M}_\odot$ of material. We indicate “weak” pulses as any rebounding pulse formed while the model relaxes from a strong pulse. Weak pulses also arise at or just above $\langle \Gamma_1 - 4/3 \rangle = 0$ from dynamical behavior that is not strong enough to remove $>0.1\,\mathrm{M}_\odot$ of material with a single shock, yet can remove $\gg 0.1\,\mathrm{M}_\odot$ in a series of several or significantly more weak pulses which compound shocks near the surface. Strong pulses typically develop on a timescale of ≤ 50 seconds, while typical periods for the contraction and bounce of a single weak pulse can range between, but are not limited to, 10^2–10^3 seconds. In this paper, a PPISN is any model in which a single strong pulse or a series of weak pulses is able to remove $\geq 0.1\,\mathrm{M}_\odot$ of material from the surface. Figure 4.2 illustrates a sample BH mass spectrum with weak and strong pulses.

4.4.1 Global mixing floors

Because of the finite-size of the Lagrangian mesh representing a star in numerical models, sharp gradients (e.g., in chemical composition or thermal properties) can be hard to resolve. This can lead to unphysical “spikes” that can have an oversized and resolution-dependent effect on stellar processes depending on those gradients (e.g., mixing instabilities). To mitigate this effect, a global minimum chemical mixing diffusion coefficient D_{min} can be used. Physically, D_{min} may be interpreted as a small amount of mixing arising from small scale perturbations not captured in one-dimensional models. The global evolution of a model is unaffected when the associated diffusive mixing timescale $\tau = L^2/D_{\mathrm{min}}$, where L is the characteristic length-scale over which the mixing is active, is significantly longer than the lifetime of the stellar model. Choosing $D_{\mathrm{min}} = 10^{-2}\ \mathrm{cm}^2\ \mathrm{s}^{-1}$, `min_D_mix` in `MESA`, and a typical PPISN radius of $R_{\mathrm{He}} = 1$-$10\,\mathrm{R}_\odot$, the global mixing timescale is $\tau \simeq 10^{17}$ yr. A $50\,\mathrm{M}_\odot$ He

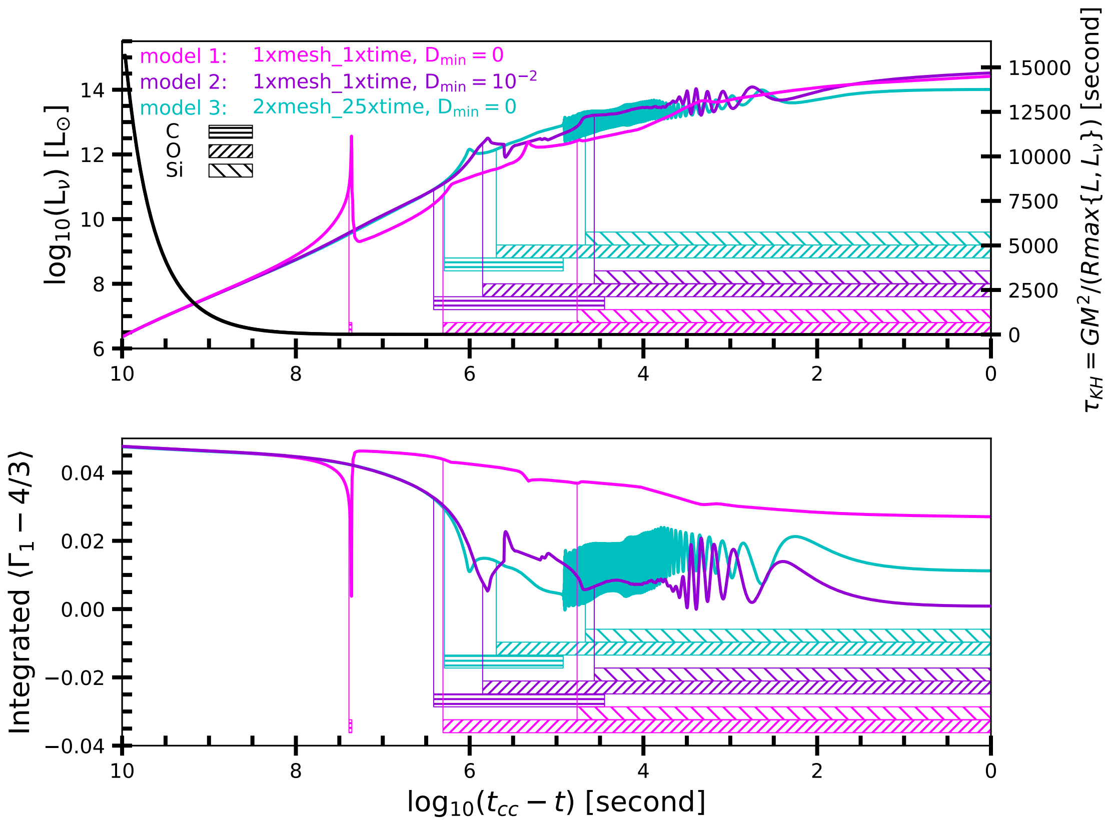

Figure 4.3: Both panels share the same x-axis, the logarithmic time to core-collapse (CC) in seconds. The top panel shows the neutrino luminosity and Kelvin-Helmholtz timescale, normalized to account for the energy lost to neutrinos, which dominates over photon cooling in the evolutionary phases shown. The integrated $\langle \Gamma_1 - 4/3 \rangle$ is shown in the bottom panel to illustrate when the models are evolving dynamically. Hatched regions indicate where C-shell, O-core, and Si-core burning take place.

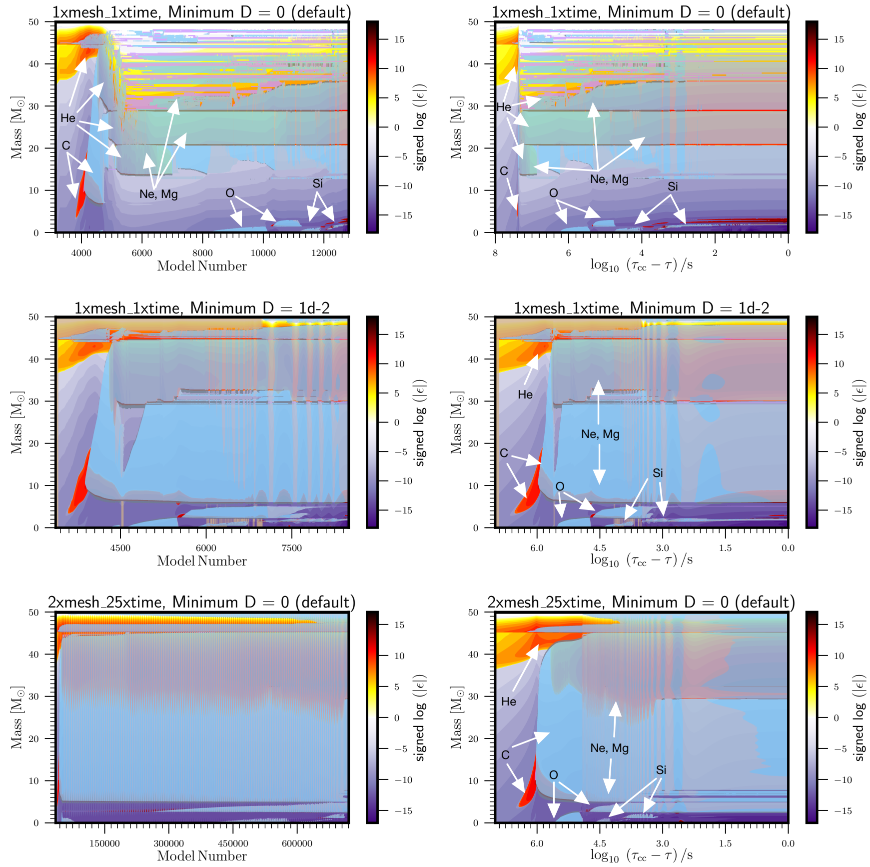

Figure 4.4: Difference in convection and nuclear burning between three stellar models in Section 4.4.1. Figures in the left column are shown versus model number from He-burning to CC. Figures in the right column are shown versus logarithm of the time to CC, beginning at the onset of shell C-burning. The different fuels burning are labelled. Each figure shows the signed logarithm of the net specific power, $\mathrm{sign}(\epsilon_{\mathrm{nuc}} - \epsilon_{\nu}) \log_{10}(\max(1.0, |\epsilon_{\mathrm{nuc}} - \epsilon_{\nu}|))$, where ϵ_{nuc} is the specific energy generation rate and ϵ_{ν} is the specific energy loss from neutrinos. Purple regions denote strong neutrino cooling and red regions denote regions of strong nuclear burning. Light blue regions indicate standard mixing length convection, grey regions indicate convection with reduced mixing because of shorter convective timescales, and for model 2 beige-orange regions (e.g. near the surface) indicate where the diffusive mixing coefficient is set to D $= 10^{-2}$ cm^2/s.

core has a lifetime of $\simeq 10^5$ yr, about 12 orders of magnitude smaller than this global mixing timescale. Thus, we do not anticipate a significant *global* impact with this value of $D_{\rm min}$, while it smooths *local* composition gradients. Nevertheless, models at the boundaries of different physical behaviors (e.g., core-collapse or pulsational pair-instability) may differ qualitatively.

Figure 4.3 and 4.4 illustrate the difference in evolutionary behavior between three $M_{\rm He} = 50\,{\rm M}_\odot$ models from the advent of shell C-burning to CC. The thermal evolution of these models is dominated by neutrino cooling and therefore all three models remain in local thermodynamic equilibrium. Figure 4.3 compares the luminosities, timescales, energies, and integrated $\langle \Gamma_1 - 4/3 \rangle$ of three $50\,{\rm M}_\odot$ He core models as they evolve to CC. Figure 4.4 displays the convective and nuclear burning behavior of these models. Model 1 uses the same mass and temporal resolution as Farmer *et al.* (2020):

```
max_dq = 1d-3
split_merge_amr_nz_baseline = 6000
delta_lgRho_cntr_limit = 2.5d-3
min_D_mix = 0.
```

Model 1 uses $\simeq$2000–3000 cells during the hydrostatic phases, $\simeq$2500–3500 cells during the dynamic phases, and $\simeq$13000 timesteps to reach CC. Model 2 is the same as Model 1, but sets `min_D_mix`= 1d-2. Model 2 uses $\simeq$2000–3000 cells during the hydrostatic phases, $\simeq$2500–4200 cells during the dynamic phases, and $\simeq$9000 timesteps to reach CC. Model 3 is the same as Model 1, but with about twice the mass resolution and 25 times the temporal resolution: `max_dq = 2d-4`

```
split_merge_amr_nz_baseline = 12000
delta_lgRho_cntr_limit = 1d-4
min_D_mix = 0.
```

Model 3 uses $\simeq$3500–4000 cells during the hydrostatic phases, $\simeq$5000–10,000 cells during the dynamic phases, and $\simeq$740,000 timesteps to reach CC.

In model 1, 2, and 3 off-center C-ignition occurs at $\log(t_{cc}-t) \simeq 7.4$, $\log(t_{cc}-t) \simeq 6.5$, $\log(t_{cc}-t) \simeq 6.4$. In model 1, the chemical evolution of the core is interrupted by a dynamical episode at $\log(t_{cc}-t) \simeq 7.3$. Shell C-burning is an insufficient energy source to combat the dynamical instability as only a fraction of the ^{12}C in the shell in burned before a Γ_1 instability leads to a core contraction. During this contraction the He-burning shell propagates inward, mixing and burning alongside Ne, Mg, and Si in the O-rich shell, stabilizing the core until CC.

Models 2 and 3 smoothly evolve through shell C-burning and undergoing weak dynamical behavior, and a steady decrease in total energy as their cores smoothly evolve toward CC. With $D_{\rm min} = 10^{-2}$ cm^2 s^{-1}, model 2 experiences minimal mixing between the He-rich shell and the C-O core commensurate with model 3. Models 2 and 3 both smoothly burn through most of the ^{12}C in the C-O shell while their cores burn through oxygen. This convective C-burning shell stabilizes the star long enough to prevent a dynamical contraction that disrupts core burning, unlike model 1. When the mass fraction of carbon, $X(^{12}\rm C)$, in the shell drops below $\sim 10^{-2}$, shell burning is no longer strong enough to prevent Γ_1 instability from pair-production. The shell begins to contract outward-in rebounding off the core from brief episodes of explosive O-burning. These explosive burning episodes drive weak shocks outward, momentarily stabilizing the shell until the shocks reach the surface and the shell contracts again. During each contraction, the temperatures and densities increase causing Ne and Mg burning in the outer shell to reach deeper within the model with every contraction, and recede back toward the surface during each pulse. As the core evolves further toward CC, Si-burning contributes to each episode. These pulsations can be seen in the oscillations of $\langle \Gamma_1 - 4/3 \rangle$ and the oscillatory convection in Figures

4.3 and 4.4. Model 2 manages to resolve a few pulsations before core-collapse, each ejecting a small amount of mass, resulting in $M_{eject} \simeq 0.01\,M_\odot$. The higher resolution of model 3 is able to resolve > 140 pulses before reaching CC, each pulse releasing a small amount of mass, resulting in $M_{eject} \simeq 0.45\,M_\odot$.

Adopting $D_{min} = 10^{-2}$ cm^2 s^{-1} improves the rate of numerical convergence of low resolution models akin to a slight increase in temporal resolution. While model 2 can resolve core burning reasonably well, the timesteps are too large to fully resolve nuclear burning in the shell or the coupling between the core and shell that generates oscillatory burning in the core during later stages, as in model 3. Because our timesteps are primarily limited by `delta_lgRho_cntr_limit`, small changes in central density resulting from the dynamical contraction between each core and shell burning episode can be fully resolved in model 3 but not in models 1 or 2. Only the strongest, largest core-shell contractions can be resolved at the lower resolution of model 2. Since each contraction does not change the core density at an appreciably large level, timesteps taken by model 2 skip or smooth over many of these pulsations. This suggests that $D_{min} = 10^{-2}$ cm^2 s^{-1} improves the rate of convergence of models run with lower resolutions, but cannot fully recover the convective behavior generated by models which use significantly greater temporal resolutions. Next we continue our exploration of $D_{min} = 10^{-2}$ cm^2 s^{-1} at higher resolutions to better characterize the impact across the entire BH mass spectrum.

4.4.2 Resolution Testing The Single Star BH Mass Spectrum

In Farmer *et al.* (2019), Marchant *et al.* (2019), Renzo *et al.* (2020a) and Mehta *et al.* (2022), brief explorations of enhanced mass and temporal resolution were conducted, but further work was needed to assess the convergence of these models across the entire BH mass spectrum. In this section we take on the challenge of exploring

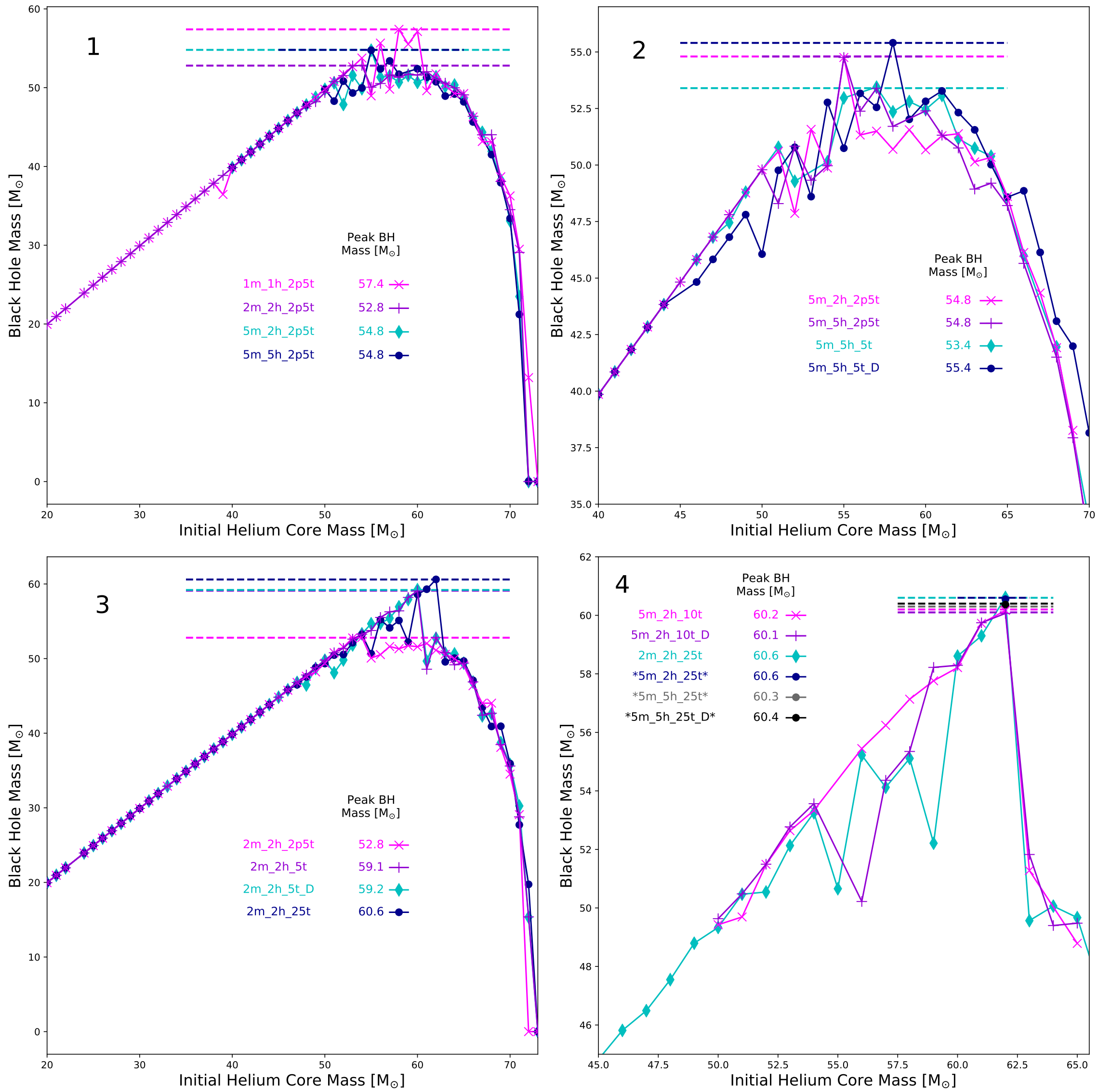

Figure 4.5: BH mass spectrums for the resolutions in Table 4.1 and Table 4.2. All panels share a similar x-axis, Initial He Core Mass M_{He} in $M_{\odot}$, and y axis, BH Mass in $M_{\odot}$. Resolutions only shown at their respective peak BH mass are labeled with asterisks. Horizontal dashed and solid lines indicate the location of the peak BH mass for each resolution.

Name	min D	max_dq	split_nz	$\delta_{\log\rho_c}$	$M_{He}(M_\odot)$	M_{CO}	$X(^{12}C)_{He}$
1m_1h_1t[a]	0	1d-3	6000	2.5d-3	53	47.59	0.1807
2m_1h_2p5t[b]	0	5d-4	6000	1d-3	60	54.51	0.1699
1m_1h_2p5t	0	1d-3	6000	2.5d-3	58	52.53	0.1730
2m_2h_2p5t	0	5d-4	12000	2.5d-3	54	53.76	0.1757
2m_2h_5t	0	5d-4	12000	5d-4	60	54.50	0.1696
2m_2h_5t_D	1d-2	5d-4	12000	5d-4	60	54.15	0.1694
2m_2h_25t	0	5d-4	12000	1d-4	62	56.24	0.1670
5m_2h_2p5t	0	2d-4	30000	1d-3	55	48.92	0.1687
5m_5h_2p5t	0	2d-4	30000	1d-3	55	48.92	0.1687
5m_5h_5t	0	2d-4	30000	5d-4	57	50.34	0.1688
5m_5h_5t_D	1d-2	2d-4	30000	5d-4	57	50.28	0.1719
5m_2h_10t	0	2d-4	12000	2.5d-4	62	56.29	0.1672
5m_2h_10t_D	1d-2	2d-4	12000	2.5d-4	62	56.39	0.1673
5m_2h_25t	0	2d-4	12000	1d-4	62	56.17	0.1674
5m_5h_25t	0	2d-4	30000	1d-4	62	56.17	0.1674
5m_5h_25t_D	1d-2	2d-4	30000	1d-4	62	56.17	0.1674

Table 4.1: Initial He core mass, composition at He depletion, and resolution controls for the models producing the peak BH mass below the upper mass gap. [a](Farmer *et al.*, 2020), [b](Mehta *et al.*, 2022)

the numerical convergence of MESA stellar models computed across the BH mass spectrum. The goal of this section is to achieve convergence in the peak BH mass at the $< 1\,M_\odot$ level. We focus on resolution testing the BH mass spectrum for He cores with the $\sigma = 0$ $^{12}C(\alpha,\gamma)^{16}O$ reaction rate provided by deBoer *et al.* (2017) and updated

Name	Pulses	$M_{BH}(M_\odot)$
1m_1h_1t[a]	0	52.77
2m_1h_2p5t[b]	1 strong, 6 weak	59.17
1m_1h_2p5t	1 strong, $\sim$ 6 weak	57.40
2m_2h_2p5t	4 strong, $>$ 50 weak	52.3
2m_2h_5t	1 strong, $\sim$ 7 weak	59.07
2m_2h_5t_D	1 strong, $\sim$ 7 weak	59.23
2m_2h_25t	1 strong, $\sim$ 9 weak	60.61
5m_2h_2p5t	0	54.76
5m_5h_2p5t	0	54.76
5m_5h_5t	1 strong, $\sim$ 10 weak	53.43
5m_5h_5t_D	1 strong, $\sim$ 5 weak	55.41
5m_2h_10t	1 strong, $\sim$ 10 weak	60.17
5m_2h_10t_D	1 strong, $\sim$ 10 weak	60.07
5m_2h_25t	1 strong, $\sim$ 10 weak	60.55
5m_5h_25t	1 strong, $\sim$ 10 weak	60.32
5m_5h_25t_D	1 strong, $\sim$ 10 weak	60.37

Table 4.2: Extension of table 4.1. [a](Farmer *et al.*, 2020), [b](Mehta *et al.*, 2022)

to 2015 temperature points in Mehta *et al.* (2022), corresponding to an approximate astrophysical S-factor S(300 keV) = 140 keV b. We also investigate the inclusion of a minimum diffusive mixing floor $D_{\rm min}$ on the BH mass spectrum.

Our testing consists of 16 different model resolutions, each modified using some variation of `max_dq`, `split_merge_amr_nz_baseline`, and `delta_lgRho_cntr_limit` to control for mass and temporal resolution. In Table 4.1 and Table 4.2 we summarize the adopted resolution and associated peak BH spectrum mass. In Figure 4.5 we plot the BH mass spectrum for each resolution listed in Table 4.1 and Table 4.2. The baseline resolution of `1m_1h_1t` represents the resolution adopted in Farmer *et al.* (2020). All other models are scaled up from `1m_1h_1t`. Generally models with `1m`, `2m`, and `5m` have between 2000-3000, 3500-4000, and 7000-8000 cells respectively during the hydrostatic phase of evolution. Models with `1h`, `2h`, and `5h` have between 2500-4500, 5000-10000, and 12000-25000 cells respectively during the hydrodynamic phase of evolution. The number of cells typically increases from the lower bound to the higher bound as a model evolves and the average density of the model generally increases (except during pulses). Models with timesteps set by `1t`, `2p5t`, `5t`, `10t`, and `25t` generally take between 8000-40000, 15000-150,000, 20,000-200,000, 40,000-500,000, and 100,000-1,800,000 timesteps to reach CC depending on the number of pulses encountered during the evolution. Models that produce the peak of the BH mass spectrum tend to be the most stable and undergo less pulsational behavior than neighboring models to the left and right of the peak. At `2m_2h_25t`, models with $M_{He} = 50–58\,M_\odot$ undergo many weak and some strong pulsations reducing the BH mass and deviating from a linear growth in the BH mass. $M_{He} = 60–62\,M_\odot$ models are the most stable resulting few pulsations, and at $M_{He} \geq 63\,M_\odot$, strong pulses mixed with weak pulses result in much less massive BH masses.

All models were run on 8-core nodes and allotted 32GB of RAM. Wall-clock times are generally between 1–4 days for low resolution models (e.g. `1m_1h_1t - 2m_2h_5t`), 1–3 weeks for intermediate resolution models (e.g. `5m_5h_2p5t - 5m_2h_10t`), and 1–10 weeks for the highest resolution models (e.g. `2m_2h_25t`). The highest resolution models take between 1–3 weeks near the BH mass spectrum peak, between 3–10 weeks to the left of the peak where hundreds of weak pulsations occur, and 3–10 weeks to the right of the peak where strong pulsations are intermixed with weak pulsation episodes. The computational cost of `2m_2h_25t` limited us from computing full spectrums at higher mass resolutions such as `5m_5h_25t`. These models could not feasibly be calculated anywhere except at the BH spectrum peak in this work as they would take between 3–9 months to complete. Any model which did not reach CC or result in a PISNe is not included in this work.

In Table 4.1 and Table 4.2 all models except `1m_1h_t` possess central $X(^{12}C)_{He}$ mass fractions within 0.01 of each other at core He-depletion, regardless of the initial He core mass M_{He}. The C-O core mass M_{CO_He} at He-depletion primarily depends on M_{He}. Models with similar initial M_{He} develop values of M_{CO_He} within $1\,M_\odot$ of each other regardless of the adopted resolution. Our CO and He core mass boundaries are defined as the outermost location where $X(^4He) \leq 0.01$ and $X(^1H) \leq 0.01$, respectively.

Across all resolutions, the behavior of each PPISN model shown in Figure 4.5 is similar. Regardless of He core mass, each model undergoes He core burning followed by shell He-burning as the core beneath contracts. In all cases, the contracting core is momentarily stabilized by central C-ignition radiatively burning outward and leaving behind an O-Mg rich core, with traces of Si. The next evolutionary phase is primarily determined by the total mass of the C-O core at the end of He-burning which scales linearly with M_{He}, and $X(^{12}C)$ of the shell which is identical to $X(^{12}C)_{He}$, the $X(^{12}C)$ mass fraction at He-depletion. If the core is not massive enough or $X(^{12}C)_{He}$ is large enough, a convectively burning Carbon shell will form and the core will undergo stable convective O-ignition to maintain hydrostatic equilibrium. This sort of evolution is characterized by a smooth transition from C to O/Ne/Mg and then Si/S/Ar and eventually Fe-burning in the core. This leads the star to CC without any dynamical contractions or pulses driven by Γ_1 instability. These stellar models only lose mass through winds during He-burning, $M_{eject} \leq 0.3\,M_\odot$, and thus produce a linear growth in the BH spectrum in correspondence with the initial He core mass. For

$\sigma[^{12}C(\alpha,\gamma)^{16}O]= 0$ the left side of the BH mass spectrum is stable up to $M_{He} \simeq 47\,M_\odot$, at which point the lower edge of the pulsational pair-instability strip is encountered. Models that are slightly more massive than $M_{He} \simeq 47\,M_\odot$ and or with slightly lower $X(^{12}C)_{He}$ begin to suffer from pair-instability in their interiors fueling a dynamic evolution toward CC. Just above $M_{He} \simeq 47\,M_\odot$, pair-production in the interior of these stellar cores softens the equation of state, and dynamical contractions begin to drive weak pulses that remove material from the surface of these models. As M_{He} increases, weak pulses increase in frequency and number until strong pulses develop, unbinding $M_{eject} \geq 1\,M_\odot$until the peak of the BH mass spectrum is encountered. More detail on the characteristics of weak pulsations encountered before the peak have been discussed in Woosley (2017); Renzo *et al.* (2020a), although not at the highest resolutions explored in this work. Weak pulsations begin to develop when convective shell C-burning can not supply the energy needed to stabilize the shell long enough for smooth O-ignition in the center. The onset of this instability has been discussed in detail in the behavior of the $50\,M_\odot$ He cores from section 4.4.1. stronger pulsations near to and at the peak of the BH mass spectrum typically involve a short episode of convective shell C-burning while a portion of the central O-core convectively burns. Once ^{12}C is nearly depleted from the shell, Γ_1 instability leads to a dynamical contraction followed by a thermonuclear explosion of a significant mass fraction of the O-rich core. When the shock reaches the surface of the model, multiple contractions and bounces occur as the star relaxes back to hydrostatic equilibrium. After a dynamical episode, stable O-burning can ensue in the core, followed by burning of heavier isotopes and eventually CC.

To the right of the BH mass spectrum peak, all models with larger M_{He} are unable to develop sufficient pressure from shell C-burning to enable smooth O-ignition in the core. The convective growth of the C-burning shell is undercut by a Γ_1 instability resulting in an infalling core that radiatively burns through most of its neon on a timescale of $\lesssim 50-70$ seconds followed by explosive burning of the central O-core in the next $\lesssim 50$ seconds. Nearly all of the central ^{16}O is burned in this explosive burning episode, removing between $\simeq$5–30 $M_\odot$ of material after just one strong pulse and the weak pulses that follow. These pulses are so strong they temporarily perturb the model for $1-10^3$ years. After the model relaxes back into hydrostatic equilibrium, nuclear burning recommences and one or several more strong and weak pulsing episodes may follow depending on the strength of the initial pulse and the amount of unburnt ^{16}O remaining in the core. For models with $M_{He} \geq 72\,M_\odot$, the O-rich core explodes in a single thermonuclear pulse driving a supersonic shock with energy greater than the total binding energy of the model, disrupting the entire model after a single pulse, and leaving no compact remnant in a PISNe.

In panel 1 of Figure 4.5 we compare the BH mass spectrum at three resolutions with increasing mass resolution and otherwise equal temporal resolution. Models with $M_{He} \leq 47\,M_\odot$ do not appear to encounter pulsational pair-instability according to panel 1, as this appears to be the lower edge of the pair-instability strip. The first resolution to display PPISN behavior is `5m_5h_2p5t`, followed by `5m_2h_2p5t`, `2m_2h_2p5t`, and then `1m_1h_2p5t`. Increasing the mass resolution appears to smooth out the peak of the BH mass Spectrum, however this could be due to a lack of temporal resolution to accurately resolve models with greater mass resolution. The erratic behavior near the peak for `1m_1h_2p5t` is likely due to being slightly under-resolved. Convergence in the peak BH mass is observed between `5m_5h_2p5t` and `5m_2h_2p5t`. Both resolutions predict a BH mass peak of $M_{BH} \simeq 54.8\,M_\odot$ satisfying our criteria for convergence at the $< 1\,M_\odot$ level. This convergence is slightly suspect though, as both models evolved from a 55 $M_\odot$ He core that does not enter the hydrodynamic solver during core O-burning, remaining in the implicit hydrostatic solver until the

HLLC hyrodynamic solver is turned on at CC, refer to Marchant *et al.* (2019) for a discussion of the criterion to turn on the HLLC solver. Directly right of the peak, all the model resolutions appear to fall within 1–2 $M_\odot$ of one another.

In panel 2 of Figure 4.5 we compare our previously converged mass resolution models with two additional resolutions at twice the temporal resolution with and without a minimum diffusive mixing floor, `5m_5h_5t` and `5m_5h_5t_D`. This comparison illustrates that while the mass resolution might be converged, increasing the temporal resolution and including a minimum diffusive mixing floor changes the peak BH mass at >1 $M_\odot$ level indicating our models are not fully time resolved near the peak. There is a wide spread in BH mass across the entire peak, another indication that increasing the temporal resolution of these models might be warranted.

In panel 3 we conduct a test of the temporal resolution of these models by controlling for changes in the central density per timestep. Increasing from `2m_2h_2p5t` to `2m_2h_25t`, an order of magnitude increase in temporal resolution, leads to a change in the BH mass of $\simeq 8 M_\odot$. This is a significant increase in the peak BH mass demonstrating the importance of time resolution in resolving the convective burning behavior of our PPISN models. To the left of the peak, the number of weak pulses resolved is also particularly sensitive to time resolution. This is one of the primary reasons `2m_2h_25t` takes >1,000,000 time steps in models between 50–58 $M_\odot$. These models are able to resolve hundreds of weak pulses creating small shocks that unbind between 0.5–1 $M_\odot$ of material. In several cases (e.g. $M_{He} = 53, 54, 55, 59\,M_\odot$) these weak shocks precede the development of an episode of strong shocks which can go entirely unresolved at resolutions lower than `2m_2h_25t`, straying from the trend of linear growth in M_{BH} observed at lower resolutions. Hundreds of weak shocks are also observed on the right side of the BH mass spectrum peak. Between each strong shock hundreds of weak shocks can remove multiple $M_\odot$ of additional material.

In panel 4, we show the resolved peak of the BH spectrum from our highest temporal resolution models and confirm its existence at our highest adopted mass resolution. By comparing our highest temporal resolution `2m_2h_25t` with `5m_2h_10t` and `5m_2h_10t_D` we confirm that 10x the temporal resolution is needed to resolve the BH mass spectrum peak to within $\leq 1\,\mathrm{M}_{\odot}$. We confirm the convergence of these models by including the peak BH masses from `5m_2h_25t`, `5m_5h_25t`, `5m_5h_25t_D`. In conjunction with Table 4.1 and Table 4.2, Panel 4 illustrates that the adoption of a minimum diffusion coefficient D_{min} changes the peak BH mass at the $\leq 0.1\,\mathrm{M}_{\odot}$ level. Models with D_{min} also tend to be more numerically stable than models run without, encountering less overall crashes, and typically achieving their final fate in less timesteps and therefore a generally lower wall-clock time, even for similar BH masses.

Looking at all four panels, we are able to differentiate between the importance of mass and temporal resolution. The amount of mass resolution needed to resolve the peak is limited by the amount of temporal resolution available. For example, models run with `2m_2h_5t` are more stable than models run with `5m_5h_5t` displaying respective peak BH masses of $\mathrm{M}_{\mathrm{BH}} \simeq 59.1\,\mathrm{M}_{\odot}$ and $\mathrm{M}_{\mathrm{BH}} \simeq 53.4\,\mathrm{M}_{\odot}$. We find that an adequate amount of temporal resolution is necessary to resolve the peak at a given mass resolution. Models with large mass and low time resolution tend to produce the most smeared peaks with the lowest overall peak BH mass, where as models with the low mass resolution and high temporal resolution display the largest overall peak BH mass. This explains why `1m_1h_2p5t` is able to resolve a larger peak BH mass than at any other mass resolution with similar time resolution. Increasing mass resolution in a vacuum is not advised, without comparable increases in temporal resolution. Panel 4 indicates that time steps limited by at least $\delta_{\mathtt{log}\rho_c} \leq 2.5 \times 10^{-4}$ are needed to resolve the peak BH mass, and $\delta_{\mathtt{log}\rho_c} \leq 10^{-4}$ is needed to accurately resolve the shape of the

BH mass spectrum, while the amount of mass resolution needed is rather unclear.

Marchant and Moriya (2020) and Woosley and Heger (2021) found that the efficiency of angular-momentum transport changes the lower edge of the BH's mass gap at the $\simeq 10\%$ level. Farmer *et al.* (2019) found that the lower edge of mass gap was robust at the $\simeq 10\%$ level to changes in the metallicity, wind mass loss prescription, and treatment of chemical mixing. In Renzo *et al.* (2020c) on convection during pulses, we showed that the treatment of time-dependent convection does not directly affect the maximum BH mass. In Mehta *et al.* (2022), we claimed our models for the peak BH mass were robust with respect to mass and temporal resolution at the $\simeq 10\%$ level. In this section we have gone further to show that by adopting a resolution of `5m_2h_10t` or `5m_2h_10t_D` our peak BH mass models are robust to mass and temporal resolution at the $\simeq 1\%$ level at $\sigma[^{12}\mathrm{C}(\alpha,\gamma)^{16}\mathrm{O}] = 0$.

4.5 The Rate Dependent Single Star BH Mass Gap

During the core He-burning phase of stellar evolution, a competition between the (3-α) process $^{4}\mathrm{He}(\alpha,)^{8}\mathrm{Be}(\alpha,)^{12}\mathrm{C}^{*}(,2\gamma)^{12}\mathrm{C}$ and $^{12}\mathrm{C}(\alpha,\gamma)^{16}\mathrm{O}$ establishes the C/O ratio of the stellar core for later C and O burning phases. The evolution of He cores through advanced burning stages depends sensitively on the C/O ratio of these models at He-depletion. Reducing the uncertainty in the $^{12}\mathrm{C}(\alpha,\gamma)^{16}\mathrm{O}$ reaction rate probability distribution function is a goal of forthcoming experiments (deBoer *et al.*, 2017; Smith *et al.*, 2021). A common approach to investigating the C/O ratio of differing stellar cores is to explore a modified $^{12}\mathrm{C}(\alpha,\gamma)^{16}\mathrm{O}$ during He-burning, and tracing it's effect on the BH mass distribution (Takahashi, 2018; Farmer *et al.*, 2020; Costa *et al.*, 2021; Mehta *et al.*, 2022). In this section, we will continue with a similar exploration of this rate albeit at a significantly higher model resolution than similar works previously conducted in `MESA`. We will explore variations in the $^{12}\mathrm{C}(\alpha,\gamma)^{16}\mathrm{O}$ at

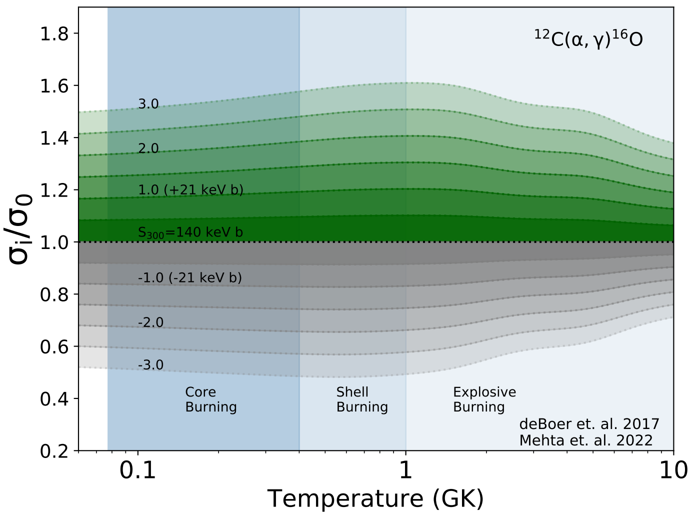

Figure 4.6: ^{12}C(α,γ) reaction rate ratios, σ_i/σ_0, as a function of temperature. σ_i spans -3.0 to 3.0 in 0.5 step increments, with σ_0 being the current nominal rate. Negative σ_i are gray curves and positive σ_i are green curves. The $\pm 1, 2, 3$ σ_i curves are labeled. The blue band show the range of temperatures encountered during core and shell He burning.

the 0.5σ level, with the ^{12}C(α,γ)^{16}O rate provided by deBoer *et al.* (2017) and updated in Mehta *et al.* (2022), see Figure 4.6. σ_o represents the median rate consistent with an astrophysical S-factor of S(300 keV) = 140 keV b with a $\pm 1\sigma$ = 21 keV b uncertainty. By exploring $\pm 3\sigma$, we effectively explore the range S(300 keV) = (77,203) keV b, where positive and negative σ indicate a stronger and weaker rate than the median value, respectively.

In this Section, we will explore a range of `MESA` stellar model resolutions across the rate dependant upper mass gap. In section 4.5.1 we extend our resolution study to resolve the tip of the BH mass spectrum at the $\leq 2\,\mathrm{M}_\odot$ level at $\sigma[^{12}\mathrm{C}(\alpha,\gamma)^{16}\mathrm{O}] = -3, +3$ and we recompute a new resolved lower edge to the BH mass gap. In section 4.5.2, we discuss the impact of a newly calculated ^{4}He$(2\alpha,)^{12}$C (3-α) reaction rate on the location of the lower edge of the ^{12}C(α,γ)^{16}O rate-dependant mass gap. We then recompute a resolved lower edge to the rate-dependent mass gap with inclusion of this revised 3-α rate. We end this section by comparing our new lower BH mass gap edge with recent measurements of binary black holes (BBH) mergers detected in the third Gravitational-Wave Transient Catalogue (GWTC-3) by (The LIGO Scientific Collaboration *et al.*, 2021a).

4.5.1 Resolving the ^{12}C(α,γ)^{16}O Dependant BH Mass Gap

By varying the ^{12}C(α,γ)^{16}O rate, we probe the convergence of models with differing C/O cores. We then establish a new resolved lower edge of the upper mass gap as $M_{\rm lower} \simeq 60^{+32}_{-14}\,M_\odot$ from the $\pm 3\sigma$ uncertainty in the ^{12}C(α,γ)^{16}O. In Figure 4.7 we compute the BH mass spectrum and their associated peak BH masses at five different resolutions found in Table 4.1. In each panel we display the BH mass spectrums produced by adopting the model resolutions found in Farmer *et al.* (2020) (`1m_1h_1t`), Mehta *et al.* (2022) (`2m_1h_2p5t`), our highest feasible temporal resolution `2m_2h_25t`, and `5m_2h_10t_D` which we've shown to reproduce the BH mass spectrum peak to within $\leq 1\,M_\odot$ at σ[^{12}C(α,γ)^{16}O] = 0. We opt to only compute BH mass spectrums across the peak for `5m_2h_10t_D` as these models tend to be much more numerically stable than models run with `5m_2h_10t`, encountering less overall crashes than models which do not adopt $D_{\rm min}$. In each panel only the peak BH mass is shown for `5m_2h_10t` to illustrate similar agreement with `5m_2h_10t_D`.

In the top panel of Figure 4.7, we show the BH mass spectrum for models with σ[^{12}C(α,γ)^{16}O] = -3. These models possess larger C/O mass fractions with typical X(^{12}C)$\sim$ 0.32. The larger ^{12}C mass fraction of these He cores allows for the development of strong convective shell C-burning which manages to counter the affects of pair-instability in these cores long enough for them to reach CC (Takahashi,

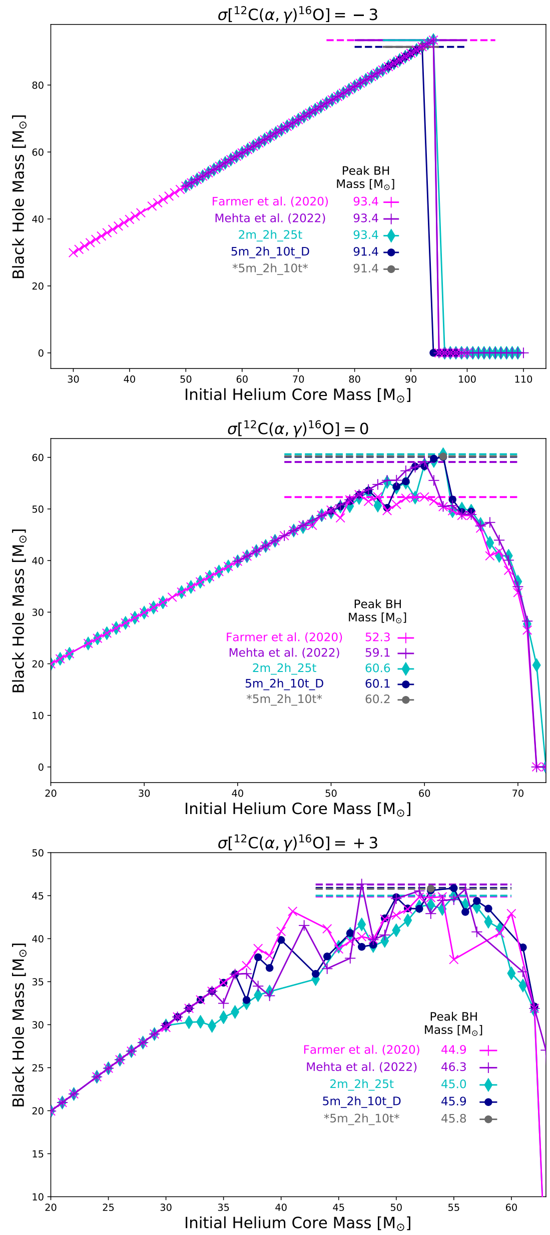

Figure 4.7: The BH mass spectrum for different values of the $^{12}C(\alpha,\gamma)^{16}O$ rate; left ($\sigma = -3$), right ($\sigma = +3$), and center ($\sigma = 0$), for five of the resolutions listed in Table 4.1. All panels share a similar x-axis, Initial He Core Mass M_{He} in $M_\odot$, and y axis, BH Mass in $M_\odot$. Resolutions that are only shown at their respective peak BH mass are labeled with asterisks on either side. Horizontal dashed and solid lines indicate the location of the peak BH mass for each resolution.

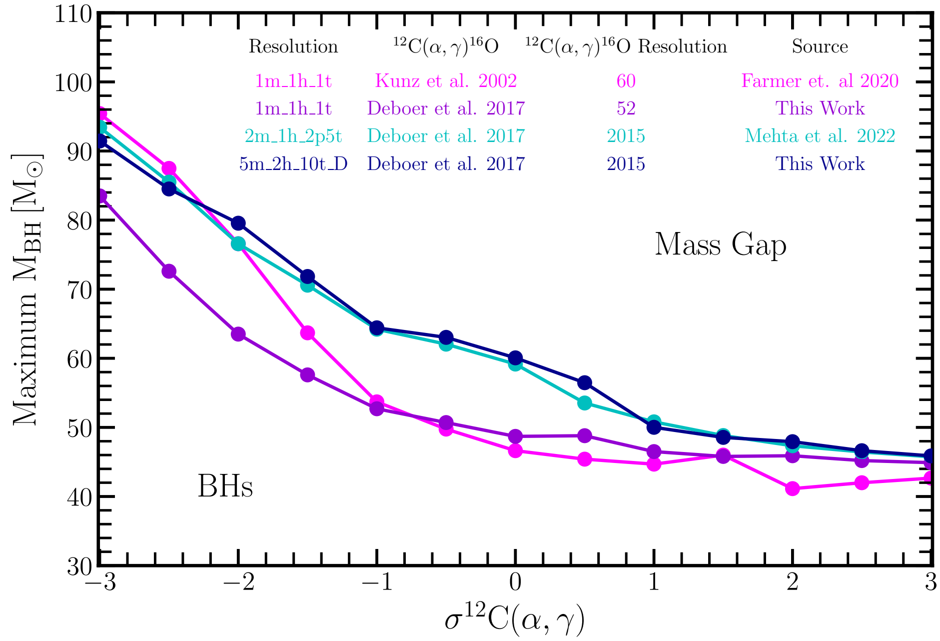

Figure 4.8: The location of the lower edge of the BH mass gap as a function of the temperature-dependent uncertainty in the ^{12}C(α,γ)^{16}O reaction rate. Each line marks the lower mass-gap boundary predicted by the adopted ^{12}C(α,γ)^{16}O rate uncertainties. The magenta/pink line mark the lower mass-gap boundary, as found in Figure 5 of Farmer *et al.* (2020), predicted by the Kunz *et al.* (2002) rate as expressed in the `STARLIB` reaction-rate library (Sallaska *et al.*, 2013). The dark purple line marks the lower mass-gap boundary predicted by models adopting the resolution from Farmer *et al.* (2020) and the original 52 temperature point ^{12}C(α,γ)^{16}O rate provided by deBoer *et al.* (2017). The coral blue line marks the lower mass-gap boundary using the updated ^{12}C(α,γ)^{16}O calculated and implemented in Mehta *et al.* (2022). The dark blue line marks the revised lower mass-gap boundary calculated in this work using the updated ^{12}C(α,γ)^{16}O adopted in Mehta *et al.* (2022). Note that σ[^{12}C(α,γ)^{16}O] represent different astrophysical S-factor's for each rate source.

2018; Woosley and Heger, 2021). There is little shape to this spectrum as models are stable up until they undergo PISNe. If the true cosmic $^{12}C(\alpha,\gamma)^{16}O$ rate was in fact this weak, we would not expect to observe any PPISN stars as the lower edge of the pair instability strip is synchronous with the lower edge of the BH mass gap. Here, Farmer *et al.* (2020) (`1m_1h_1t`), Mehta *et al.* (2022) (`2m_1h_2p5t`), and `2m_2h_25t` produce BHs of identical mass, $M_{BH} \simeq 93.4\,M_\odot$. Models `5m_2h_10t` and `5m_2h_10t_D` appear to agree with one another, producing BHs with identical masses $M_{BH} \simeq 91.4\,M_\odot$. Interestingly our lowest resolution illustrates better agreement with out highest resolution than our moderate resolution models. As a check, we have computed an additional model with `5m_2h_25t` and found the peak BH mass remains $M_{BH} \simeq 93.4\,M_\odot$. It is unclear why our lowest resolution models agree with our highest resolution models here, however in a stellar evolution model there are many choices that are made which interact highly non-linearly with one another. It is possible that our experiment varying only a few parameters does not capture all the possible variations necessary. Nonetheless, the location of the BH mass spectrum peak is sensitive to temporal resolution due to its discontinuous nature. In this case, we are able to resolve the peak BH mass spectrum at lower resolutions, but we can only be confident in our peak BH mass estimate to within $\leq 2\,M_\odot$ with `5m_2h_10t_D`.

In the middle panel of Figure 4.7, we show the BH mass spectrum for models with $\sigma[^{12}C(\alpha,\gamma)^{16}O] = 0$. The behavior of models with these C/O mass fractions, $X(^{12}C) \sim 0.17$, were previously discussed in section 4.4.2. Within the context of our `MESA` models, Mehta *et al.* (2022) has shown the dependence of the BH mass spectrum on the tabulated temperature resolution of the $\sigma = 0$ $^{12}C(\alpha,\gamma)^{16}O$ reaction rate at `2m_1h_2p5t`. When the reaction rate was defined by 52 temperature points, the BH mass spectrum reaches a maximum BH mass of $49.6\,M_\odot$ at an initial He core mass of $55.0\,M_\odot$. When the reaction rate is defined by 2015 temperature points, the BH mass spectrum reaches a maximum BH mass of 59.1 $M_\odot$ at an initial He core mass of 60.0 $M_\odot$. In this work, we have confirmed the maximum BH mass to be 60.3–60.4 $M_\odot$ with an initial He core mass of 62 $M_\odot$ at our highest resolution, `5m_5h_25t`. Mehta *et al.* (2022) happened to choose a combination of mass and temporal resolution to be able to resolve the peak of the BH mass to within 2 $M_\odot$ of the resolved value. As a result, the ability of the 2015 point rate to produce models which sustain a linear trend of larger BH masses with larger initial He core masses was not just a result of the improved tabulated resolution of the $^{12}C(\alpha,\gamma)^{16}O$ reaction rate, but also largely due to the resolution of the models used to calculate the peak in Mehta *et al.* (2022). In this work, the peak of the $\sigma[^{12}C(\alpha,\gamma)^{16}O] = 0$ BH mass spectrum can only be resolved to within $\leq 1\,M_\odot$ with `5m_2h_10t_D` or greater resolutions.

In the bottom panel of Figure 4.7, we show the BH spectrum for models with $\sigma[^{12}C(\alpha,\gamma)^{16}O] = +3$. These models possess the lowest overall C/O mass fractions with typical $X(^{12}C) \sim 0.07$. Given the small C/O mass fractions present in these cores, most of these models undergo at least one strong pulse. At the lower end of the BH mass spectrum a notable difference in the location of the lower edge of the pair-instability strip can be seen between `2m_2h_25t` and all other resolutions. From this panel, we find that the lower edge of the pair instability strip is $\simeq 32\,M_\odot$ at `2m_2h_25t`, $\simeq 5\,M_\odot$ lower than at any other resolution. Temporal resolution appears to be of critical importance in establishing the lower edge of the pair-instability strip for models with low C/O mass fractions. Models with low temporal resolution are unable to resolve the hundreds of weak pulses which which culminate in a strong pulse for models with M_{He} as low as 32 $M_\odot$. Across the mass spectrum, a large spread in the BH masses is found at varying resolutions with the primary difference being owed to the shear number of weak pulsation episodes intermixed between strong pulses. Models run at `2m_2h_25t` are able to resolve many more weak pulses than at any other resolution, leading to BH masses which are typically lower than those predicted by lower resolutions. At $\sigma[^{12}\mathrm{C}(\alpha,\gamma)^{16}\mathrm{O}] = +3$, we are able to resolve the peak BH mass to within $\leq 1\,\mathrm{M}_\odot$ with `5m_2h_10t_D`, although we cannot resolve the entire shape of the BH mass spectrum.

Figure 4.7 shows that the temporal resolution during the hydrodynamic phase of evolution is most important for resolving the peak of the BH mass spectrum. This is due to a tight coupling between the nuclear burning and convection at each timestep. Models with $\sigma[^{12}\mathrm{C}(\alpha,\gamma)^{16}\mathrm{O}] = -3$ spend the least amount of time in the hydrodynamic phase, while models with $\sigma[^{12}\mathrm{C}(\alpha,\gamma)^{16}\mathrm{O}] = +3$ spend the most. The BH mass spread between different temporal resolutions is larger the longer these models spend in the hydrodynamic phase. Models with stronger $^{12}\mathrm{C}(\alpha,\gamma)^{16}\mathrm{O}$ rates undergo stronger nuclear burning episodes and convection, requiring the highest temporal resolutions to resolve.

Given the large computational cost of computing models with `2m_2h_25t`, we adopt `5m_2h_10t_D` as our highest resolution moving forward, with numerical convergence in peak BH mass at the $\leq (2,\ 1,\ 1)\,\mathrm{M}_\odot$ level for $\sigma[^{12}\mathrm{C}(\alpha,\gamma)^{16}\mathrm{O}] = -3, 0, +3$. More specifically, models run with `5m_2h_10t_D` appear to underestimate the peak BH mass by $\leq 2\,\mathrm{M}_\odot$ at $\sigma = -3$ and overestimate the peak BH mass by $\leq 1\,\mathrm{M}_\odot$ at $\sigma = 3$. In Figure 4.8 we compute the lower edge of a resolved $^{12}\mathrm{C}(\alpha,\gamma)^{16}\mathrm{O}$ rate-dependant BH mass gap and compare to previous work. In Farmer *et al.* (2020), using a default resolution of `1m_1h_1t`, a 60 temperature point $^{12}\mathrm{C}(\alpha,\gamma)^{16}\mathrm{O}$ from STARLIB (Kunz *et al.*, 2002) was calculated and discussed along with the deBoer *et al.* (2017) $^{12}\mathrm{C}(\alpha,\gamma)^{16}\mathrm{O}$ rate at $\sigma = -1, 0, 1$. In this work we extend that calculation across the lower edge of the mass gap to show the result of adopting the original 52 temperature point deBoer *et al.* (2017) $^{12}\mathrm{C}(\alpha,\gamma)^{16}\mathrm{O}$ rate at `1m_1h_1t`. While the agreement between (deBoer *et al.*, 2017) and (Kunz *et al.*, 2002) was $\leq 3\,\mathrm{M}_\odot$ at $\sigma = -1, 0, 1$, the difference be-

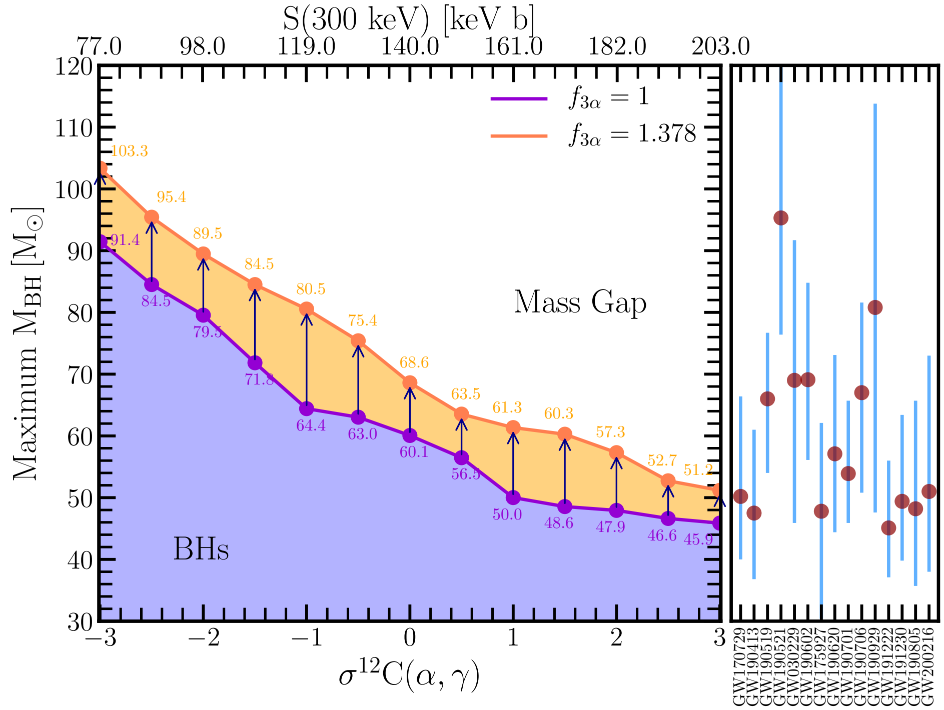

Figure 4.9: The location of the lower edge of the BH mass gap as a function of the temperature-dependent uncertainty in the ^{12}C(α,γ)^{16}O reaction rate. The dark purple line marks the revised lower mass-gap boundary calculated in this work using the updated ^{12}C(α,γ)^{16}O adopted in Mehta *et al.* (2022) and $f_{3\alpha} = 1$ (Angulo *et al.*, 1999). The orange line marks the revised lower mass-gap boundary calculated in this work using the updated ^{12}C(α,γ)^{16}O adopted in Mehta *et al.* (2022) and $f_{3\alpha} = 1.378$ (Kibédi *et al.*, 2020). The white region denotes the mass gap and the yellow-orange regions highlight differences between models computed with $f_{3\alpha} = 1$ and $f_{3\alpha} = 1.378$ at the same uncertainty in ^{12}C(α,γ)^{16}O. All BH masses with $M_{BH} \geq 45\,M_\odot$ included in GWTC-3 are shown with dark red points and blue error bars showing the uncertainty in their inferred mass. The approximate astrophysical S-factor corresponding to each probability distribution function sourced σ value is labeled on the top x axis.

tween both rates grows appreciably large between $\sigma = -1, -3$. This is due to the fact that σ does not represent the same physical quantity, the astrophysical S-factor, for different sources of the reaction rate.

In Mehta *et al.* (2022), a revised deBoer *et al.* (2017) reaction rate probability distribution function defined by 2015 temperature points at each σ_i was adopted and implemented at an improved resolution of `2m_1h_2p5t`. This small improvement in model and reaction rate resolution substantially increased the lower edge of the BH mass gap between $\sigma = -2, +3$. The resolved lower edge computed with `5m_2h_10t` shows reasonable agreement with the results of Mehta *et al.* (2022) at the $\leq 4\,\mathrm{M}_\odot$ level across the lower edge of the BH mass gap.

4.5.2 The Impact of 3-α on the BH Mass Gap and GWTC-3

The 3-α process is primarily carried out by the fusion of three α particles to form ^{12}C in the Hoyle-state (Hoyle, 1954), a resonant 0^+ second excited state of ^{12}C at ~7.65 Mev, which then decays into the ground state. The currently adopted rate for 3-α in many stellar evolution codes currently comes from Nomoto *et al.* (1985) which adopted Γ_{rad}= 3.7 meV (i.e., $3.7{\times}10^{-3}$ ev) as the radiative branching ratio width of the Hoyle-state. All three 3α rates available for use in `MESA` adopt this value of Γ_{rad} in their calculation: CF88 (Caughlan and Fowler, 1988), NACRE (Angulo *et al.*, 1999), and JINA REACLIB (Cyburt *et al.*, 2010a). We have up to this point adopted the NACRE formulation for 3-α rate though it should be noted that the CF88 and JINA rate are always smaller than the NACRE rate at He-burning temperatures (0.2-0.4 GK), see Figure **??** in Appendix A. More recently Freer and Fynbo (2014) have performed an up to date review of the relevant literature to affirm the recommended value to as Γ_{rad}= 3.7 meV. Recent measurements of by Eriksen *et al.* (2020); Kibédi *et al.* (2020); Cook *et al.* (2021) have measured and proposed a revised width of

σ^{12}C(α,γ)	M_{He} ($M_\odot$)	M_{CO} ($M_\odot$)	X(^{12}C)	Pulses	M_{BH}($M_\odot$)
$f_{3\alpha} = 1$					
-3.0	92	82.80	0.3156	0	91.45
-2.5	85	76.57	0.2816	1 weak	84.51
-2.0	80	72.12	0.2510	0	79.55
-1.5	73	72.61	0.2278	1 strong, $\sim$ 10 weak	71.84
-1.0	65	58.93	0.2105	$>$ 100 weak	64.41
-0.5	65	59.03	0.1855	1 strong, $\sim$ 10 weak	63.03
0	62	56.39	0.1673	1 strong, $\sim$ 10 weak	60.07
0.5	58	52.37	0.1508	1 strong, $\sim$ 9 weak	56.47
1.0	56	49.73	0.1280	4 strong, $>$ 100 weak	50.01
1.5	56	50.10	0.1160	3 strong, $>$ 80 weak	48.55
2.0	56	49.69	0.0972	3 strong, $>$ 30 weak	47.94
2.5	55	49.07	0.0840	3 strong, $>$ 30 weak	46.63
3.0	55	48.89	0.0729	3 strong, $>$ 20 weak	45.88

Table 4.3: MESA BH mass gap He core explosive behavior for Figure 4.9

Γ_{rad}= 5.1(6) meV. If true, this would imply an upward revision in the 3α rate at the 37.8% level. An increase of this magnitude would warrant a large revision to the BH mass gap and could improve the overall agreement between recent gravitational wave detection of BBHs and the theorized existence of pair-instability stars. In Rolfs and Rodney (1988) the 3-α reaction rate is quoted as being known to a 15% accuracy, and to a 10% accuracy in West *et al.* (2013) and Austin *et al.* (2014).

We explore the impact of the 3-α reaction rate by implementing a 37.8% larger rate as a multiplicative factor on the currently adopted NACRE rate. Here, the

σ^{12}C(α,γ)	M$_{\texttt{He}}$(M$_\odot$)	M$_{\texttt{CO}}$(M$_\odot$)	X(^{12}C)	Pulses	M$_{\texttt{BH}}$(M$_\odot$)
$f_{3\alpha} = 1.378$					
-3.0	104	93.70	0.3689	0	103.34
-2.5	96	86.49	0.3356	0	95.41
-2.0	90	81.07	0.3061	0	89.47
-1.5	85	76.58	0.2800	0	84.51
-1.0	81	73.04	0.2564	0	80.54
-0.5	76	68.60	0.2370	$>$ 90 weak	75.41
0	70	63.27	0.2216	1 strong, $\sim$ 9 weak	68.61
0.5	65	59.03	0.2057	1 strong, $\sim$ 9 weak	63.53
1.0	63	57.31	0.1877	1 strong, $\sim$ 9 weak	61.35
1.5	62	56.42	0.1700	1 strong, $\sim$ 10 weak	60.27
2.0	60	54.57	0.1553	1 strong, $>$ 100 weak	57.29
2.5	57	51.70	0.1437	2 strong, $>$ 20 weak	52.73
3.0	55	48.72	0.1274	2 strong, $>$ 100 weak	51.18

Table 4.4: Extension of Table 4.3 showing MESA BH mass gap He core explosive behavior for Figure 4.9

NACRE rate is represented by $f_{3\alpha} = 1$, while the revised rate denoted by $f_{3\alpha} = 1.378$. Figure 4.9 shows the location of the lower edge to the ^{12}C$(\alpha,\gamma)^{16}$O rate-dependant BH mass gap at a resolution of 5m_2h_10t_D for $f_{3\alpha} = (1,\ 1.378)$, supplemented with the data provided in Table 4.3 and Table 4.4. Figure 4.9 also shows all BHs that with M $\geq 45\,\mathrm{M}_\odot$ in GWTC-3 (The LIGO Scientific Collaboration *et al.*, 2021b). Testing at a resolution of 5m_2h_25t for $\sigma = -3$ confirms that the peak BH mass of $\mathrm{M_{BH}} = 103.3\,\mathrm{M}_\odot$ for $f_{3\alpha} = 1.378$ remains within $\leq 2\,\mathrm{M}_\odot$ of $\mathrm{M_{BH}} = 105.3\,\mathrm{M}_\odot$, the value found by models calculated with `5m_2h_25t`. The BH mass gaps shown in Figure 4.9 are likely to be numerically resolved with $\lesssim 2\,\mathrm{M}_\odot$ as compared to models run at our highest temporal resolution. At $\sigma[^{12}\mathrm{C}(\alpha,\gamma)^{16}\mathrm{O}] = -3, 0, +3$, using $f_{3\alpha} = 1.378$ results in an increase in the lower edge of the upper stellar mass gap of $\mathrm{M}_{\mathrm{BH}} = (11.9,\, 8.4,\, 5.3)\,\mathrm{M}_\odot$ respectively, yielding $\mathrm{M}_{\mathrm{lower}} \simeq 69^{+34}_{-18}$ /Msun.

In rotating stars the pulsational instability region is shifted by the additional centrifugal force. This causes the BH masses to increase, depending on the efficiency of angular momentum transport. Marchant and Moriya (2020) showed that under assumptions that maximize the impact of rotation on the gap (no angular momentum transport and fast rigid rotation at He ignition), the shift in the peak BH mass is $\lesssim 10\%$, similar to the findings of Woosley and Heger (2021).

Assuming GW190521 formed as an isolated $\mathrm{M} = 95.3\,\mathrm{M}_\odot$ BH implies an S-factor of $\gtrsim 77$ keV b (or 88 keV b with an enhanced 3-α rate). This is consistent with the 73^{+11} keV b inferred by Farmer *et al.* (2020), which used the Kunz *et al.* (2002) $^{12}\mathrm{C}(\alpha,\gamma)^{16}\mathrm{O}$ reaction rate. The next most massive BH, GW190929 with $\mathrm{M} = 80.8\,\mathrm{M}_\odot$, implies an S-factor $\gtrsim 98$ keV b (or 119 keV b for an enhanced 3-α rate). This is consistent with Aadland *et al.* (2022) who suggest that observations of WO-type Wolf Rayet stars are best matched by models with a 25–50% reduced $^{12}\mathrm{C}(\alpha,\gamma)^{16}\mathrm{O}$ rate.

4.6 Conclusions

Three physics driven transitions in the BH initial mass function are predicted by single star stellar evolution. We have have focused this work on the lower edge of the upper BH mass gap, the second transition. By evolving He cores from He-ZAMS to their final fate we have explored physically motivated mixing floors, varying spatial and temporal resolutions, and a wide range of C/O core compositions to assess the numerical convergence of our `MESA` stellar evolution models. We find:

- The inclusion of $D_{\rm min} = 10^{-2}$ cm^2/s improves the rate of convergence of models run with lower temporal resolution, but cannot fully recover the convective behavior generated by models which use higher temporal resolutions.

- The mass resolution needed to resolve the peak of the BH mass spectrum is limited by the amount temporal resolution available. Models with high mass and low temporal resolution smear out the BH mass spectrum peak. Models with lower mass resolution and higher temporal resolution display the largest overall peak BH mass. In `MESA` timesteps limited by $\delta_{\log\rho_c} \leq 2.5 \times 10^{-4}$ are needed to resolve the peak BH mass to within $\leq 1\,\rm M_\odot$, and $\delta_{\log\rho_c} \leq 10^{-4}$ are needed to accurately resolve the shape of the BH mass spectrum.

- By adopting a resolution of `5m_2h_10t` or `5m_2h_10t_D` our peak BH mass models are robust to mass and temporal resolution at the $\simeq 1\%$ level at $\sigma[^{12}\rm C(\alpha,\gamma)^{16}O] = 0$ and $\simeq 2\%$ level across the mass gap. This resolution underestimates the peak BH mass by $\leq 2\,\rm M_\odot$ at $\sigma = -3$ and overestimate the peak BH mass by $\leq 1\,\rm M_\odot$ at $\sigma = 3$. The resolved lower edge shows reasonable agreement with the results of Mehta *et al.* (2022) at the $\leq 4\,\rm M_\odot$ level across the lower edge of the BH mass gap. We establish a new lower edge of the upper mass gap as $\rm M_{lower} \simeq 60^{+32}_{-14}\,M_\odot$ from the $\pm 3\sigma$ uncertainty in the $^{12}\rm C(\alpha,\gamma)^{16}O$ reaction rate probability distribution function (Mehta *et al.*, 2022).

- At $\sigma[^{12}\rm C(\alpha,\gamma)^{16}O] = -3$, the BH mass spectrum grows linearly with initial He core mass until models undergo PISNe. If the true $^{12}\rm C(\alpha,\gamma)^{16}O$ rate is in fact this weak, we do not expect to observe any $\rm Z = 10^{-5}$ PPISN stars as the lower edge of the pair instability strip is synchronous with the lower edge of the BH mass gap. At $\sigma[^{12}\rm C(\alpha,\gamma)^{16}O] = 0$, the lower edge of the pair instability strip is $\rm M_{He} \sim 47\,M_\odot$. At $\sigma[^{12}\rm C(\alpha,\gamma)^{16}O] = +3$, our highest resolution models

(`2m_2h_25t`) indicate the lower edge of the pair instability strip could be as low as $M_{He} \simeq 32\,M_\odot$, about $5\,M_\odot$ lower than at any other resolution. High temporal resolution is necessary to resolve the lower edge of the pair-instability strip for models with low C/O mass fractions.

- Increased temporal resolution is important during the hydrodynamic phase due to a tight coupling between the nuclear burning and time dependant convection. Models with larger $^{12}C(\alpha,\gamma)^{16}O$ rates yield cores with low C/O mass fractions which undergo stronger nuclear burning episodes and convection and experience hundreds of pulses.

- We explored stronger 3-α reaction rates by implementing a 37.8% larger rate as a multiplicative factor on the currently adopted NACRE rate. At $\sigma[^{12}C(\alpha,\gamma)^{16}O]$ $= -3, 0, +3$, adopting a stronger 3-α rate results in an increase in the lower edge of the Upper stellar mass gap of M_{BH} = 11.9, 8.4, 5.3 $M_\odot$ respectively, yielding $M_{lower} \simeq 69^{+34}_{-18}\,M_\odot$.

Future efforts to explore the resolved evolution of PPISN stars and their BH mass spectrum could consider coupling the temperature dependant uncertainties in the $^{12}C(\alpha,\gamma)^{16}O$ and 3-α rate probability distribution functions (e.g., Fields *et al.*, 2018), larger nuclear reaction networks, time dependent convection models (Kupka *et al.*, 2022; Jermyn *et al.*, 2022), and variations in the prescriptions for wind driven mass loss, angular momentum transport, convective-core overshooting (Vink *et al.*, 2021; Tanikawa *et al.*, 2021) and binary interactions.

A goal of forthcoming low-energy nuclear experiments is to further reduce the uncertainty in the $^{12}C(\alpha,\gamma)^{16}O$ reaction rate probability distribution (deBoer *et al.*, 2017; Smith *et al.*, 2021; Aliotta *et al.*, 2022). Partnering with this laboratory astrophysics quest are other avenues for placing astrophysical constraints on the $^{12}C(\alpha,\gamma)^{16}O$ reaction rate from the period spectrum of variable carbon-oxygen white dwarfs (Chidester *et al.*, 2022), lifetimes of He core burning stars (Imbriani *et al.*, 2001; Jones *et al.*, 2015), and the surface abundances of WO-type Wolf-Rayet stars (Aadland *et al.*, 2022).

Chapter 5

SUMMARY

Stars generate a variety of multi-messenger signals throughout their evolution. They radiate photons from their stellar surface, neutrinos from their interior, and recently-discovered gravitational waves during binary mergers. These signals give us important clues about the composition, nuclear physics, and convective transport in stellar interiors, enabling us to solve major problems such as identifying the efficiency of convection, strength of Helium burning nuclear reactions, and the ultimate structure of white dwarf and pre-supernova stars. My thesis has focused on analysing the multi-messenger signals resulting from stellar evolution.

I have calculated the neutrino emission from stars of all masses and metallicities to provide stellar targets for current and forthcoming neutrino detectors Farag *et al.* (2020, 2024). I've integrated these stellar tracks over an initial mass function and time to investigate the neutrino emission from a simple stellar population. I've studied the evolution of the most massive stars which result in pair-instability supernovae and made predictions for the cosmic BH mass spectrum. Current and future gravitational wave detectors will be able to sample from the BH mass spectrum and constrain the nuclear physics of BH progenitors. In particular, gravitational wave signals of merging binary black holes can be used in conjunction with my thesis work to constrain the most uncertain nuclear reaction rates in all of astrophysics: the $^{12}C(\alpha,\gamma)^{16}O$ and triple-α helium burning nuclear reactions which set the C and O composition of the cosmos (Mehta *et al.*, 2022; Farag *et al.*, 2022).

REFERENCES

Aadland, E., P. Massey, D. John Hillier, N. I. Morrell, K. F. Neugent and J. J. Eldridge, "WO-type Wolf-Rayet Stars: The Last Hurrah of Massive Star Evolution", *ApJ* **931**, 2, 157 (2022).

Abbott, B. P., R. Abbott, T. D. Abbott, F. Acernese, K. Ackley, C. Adams, T. Adams, P. Addesso, R. X. Adhikari, V. B. Adya, C. Affeldt, M. Afrough, B. Agarwal, M. Agathos, K. Agatsuma, N. Aggarwal, O. D. Aguiar, L. Aiello, A. Ain, P. Ajith, B. Allen, G. Allen, A. Allocca, P. A. Altin, A. Amato, A. Ananyeva, S. B. Anderson, W. G. Anderson, S. V. Angelova, S. Antier, S. Appert, K. Arai, M. C. Araya, J. S. Areeda, N. Arnaud, K. G. Arun, S. Ascenzi, G. Ashton, M. Ast, S. M. Aston, P. Astone, D. V. Atallah, P. Aufmuth, C. Aulbert, K. AultONeal, C. Austin, A. Avila-Alvarez, S. Babak, P. Bacon, M. K. M. Bader, S. Bae, P. T. Baker, F. Baldaccini, G. Ballardin, S. W. Ballmer, S. Banagiri, J. C. Barayoga, S. E. Barclay, B. C. Barish, D. Barker, K. Barkett, F. Barone, B. Barr, L. Barsotti, M. Barsuglia, D. Barta, S. D. Barthelmy, J. Bartlett, I. Bartos, R. Bassiri, A. Basti, J. C. Batch, M. Bawaj, J. C. Bayley, M. Bazzan, B. Bécsy, C. Beer, M. Bejger, I. Belahcene, A. S. Bell, B. K. Berger, G. Bergmann, J. J. Bero, C. P. L. Berry, D. Bersanetti, A. Bertolini, J. Betzwieser, S. Bhagwat, R. Bhandare, I. A. Bilenko, G. Billingsley, C. R. Billman, J. Birch, R. Birney, O. Birnholtz, S. Biscans, S. Biscoveanu, A. Bisht, M. Bitossi, C. Biwer, M. A. Bizouard, J. K. Blackburn, J. Blackman, C. D. Blair, D. G. Blair, R. M. Blair, S. Bloemen, O. Bock, N. Bode, M. Boer, G. Bogaert, A. Bohe, F. Bondu, E. Bonilla, R. Bonnand, B. A. Boom, R. Bork, V. Boschi, S. Bose, K. Bossie, Y. Bouffanais, A. Bozzi, C. Bradaschia, P. R. Brady, M. Branchesi, J. E. Brau, T. Briant, A. Brillet, M. Brinkmann, V. Brisson, P. Brockill, J. E. Broida, A. F. Brooks, D. A. Brown, D. D. Brown, S. Brunett, C. C. Buchanan, A. Buikema, T. Bulik, H. J. Bulten, A. Buonanno, D. Buskulic, C. Buy, R. L. Byer, M. Cabero, L. Cadonati, G. Cagnoli, C. Cahillane, J. Calderón Bustillo, T. A. Callister, E. Calloni, J. B. Camp, M. Canepa, P. Canizares, K. C. Cannon, H. Cao, J. Cao, C. D. Capano, E. Capocasa, F. Carbognani, S. Caride, M. F. Carney, J. Casanueva Diaz, C. Casentini, S. Caudill, M. Cavaglià, F. Cavalier, R. Cavalieri, G. Cella, C. B. Cepeda, P. Cerdá-Durán, G. Cerretani, E. Cesarini, S. J. Chamberlin, M. Chan, S. Chao, P. Charlton, E. Chase, E. Chassande- Mottin, D. Chatterjee, K. Chatziioannou, B. D. Cheeseboro, H. Y. Chen, X. Chen, Y. Chen, H. P. Cheng, H. Chia, A. Chincarini, A. Chiummo, T. Chmiel, H. S. Cho, M. Cho, J. H. Chow, N. Christensen, Q. Chu, A. J. K. Chua, S. Chua, A. K. W. Chung, S. Chung, G. Ciani, R. Ciolfi, C. E. Cirelli, A. Cirone, F. Clara, J. A. Clark, P. Clearwater, F. Cleva, C. Cocchieri, E. Coccia, P. F. Cohadon, D. Cohen, A. Colla, C. G. Collette, L. R. Cominsky, J. Constancio, M., L. Conti, S. J. Cooper, P. Corban, T. R. Corbitt, I. Cordero-Carrión, K. R. Corley, N. Cornish, A. Corsi, S. Cortese, C. A. Costa, M. W. Coughlin, S. B. Coughlin, J. P. Coulon, S. T. Countryman, P. Couvares, P. B. Covas, E. E. Cowan, D. M. Coward, M. J. Cowart, D. C. Coyne, R. Coyne, J. D. E. Creighton, T. D. Creighton, J. Cripe, S. G. Crowder, T. J. Cullen, A. Cumming, L. Cunningham, E. Cuoco, T. Dal Canton, G. Dálya, S. L. Danilishin, S. D'Antonio, K. Danzmann, A. Dasgupta, C. F. Da Silva Costa, V. Dattilo,

I. Dave, M. Davier, D. Davis, E. J. Daw, B. Day, S. De, D. DeBra, J. Degallaix, M. De Laurentis, S. Deléglise, W. Del Pozzo, N. Demos, T. Denker, T. Dent, R. De Pietri, V. Dergachev, R. De Rosa, R. T. DeRosa, C. De Rossi, R. DeSalvo, O. de Varona, J. Devenson, S. Dhurandhar, M. C. Díaz, L. Di Fiore, M. Di Giovanni, T. Di Girolamo, A. Di Lieto, S. Di Pace, I. Di Palma, F. Di Renzo, Z. Doctor, V. Dolique, F. Donovan, K. L. Dooley, S. Doravari, I. Dorrington, R. Douglas, M. Dovale Álvarez, T. P. Downes, M. Drago, C. Dreissigacker, J. C. Driggers, Z. Du, M. Ducrot, P. Dupej, S. E. Dwyer, T. B. Edo, M. C. Edwards, A. Effler, P. Ehrens, J. Eichholz, S. S. Eikenberry, R. A. Eisenstein, R. C. Essick, D. Estevez, Z. B. Etienne, T. Etzel, M. Evans, T. M. Evans, M. Factourovich, V. Fafone, H. Fair, S. Fairhurst, X. Fan, S. Farinon, B. Farr, W. M. Farr, E. J. Fauchon-Jones, M. Favata, M. Fays, C. Fee, H. Fehrmann, J. Feicht, M. M. Fejer, A. Fernandez-Galiana, I. Ferrante, E. C. Ferreira, F. Ferrini, F. Fidecaro, D. Finstad, I. Fiori, D. Fiorucci, M. Fishbach, R. P. Fisher, M. Fitz-Axen, R. Flaminio, M. Fletcher, H. Fong, J. A. Font, P. W. F. Forsyth, S. S. Forsyth, J. D. Fournier, S. Frasca, F. Frasconi, Z. Frei, A. Freise, R. Frey, V. Frey, E. M. Fries, P. Fritschel, V. V. Frolov, P. Fulda, M. Fyffe, H. Gabbard, B. U. Gadre, S. M. Gaebel, J. R. Gair, L. Gammaitoni, M. R. Ganija, S. G. Gaonkar, C. Garcia-Quiros, F. Garufi, B. Gateley, S. Gaudio, G. Gaur, V. Gayathri, N. Gehrels, G. Gemme, E. Genin, A. Gennai, D. George, J. George, L. Gergely, V. Germain, S. Ghonge, A. Ghosh, A. Ghosh, S. Ghosh, J. A. Giaime, K. D. Giardina, A. Giazotto, K. Gill, L. Glover, E. Goetz, R. Goetz, S. Gomes, B. Goncharov, G. González, J. M. Gonzalez Castro, A. Gopakumar, M. L. Gorodetsky, S. E. Gossan, M. Gosselin, R. Gouaty, A. Grado, C. Graef, M. Granata, A. Grant, S. Gras, C. Gray, G. Greco, A. C. Green, E. M. Gretarsson, B. Griswold, P. Groot, H. Grote, S. Grunewald, P. Gruning, G. M. Guidi, X. Guo, A. Gupta, M. K. Gupta, K. E. Gushwa, E. K. Gustafson, R. Gustafson, O. Halim, B. R. Hall, E. D. Hall, E. Z. Hamilton, G. Hammond, M. Haney, M. M. Hanke, J. Hanks, C. Hanna, M. D. Hannam, O. A. Hannuksela, J. Hanson, T. Hardwick, J. Harms, G. M. Harry, I. W. Harry, M. J. Hart, C. J. Haster, K. Haughian, J. Healy, A. Heidmann, M. C. Heintze, H. Heitmann, P. Hello, G. Hemming, M. Hendry, I. S. Heng, J. Hennig, A. W. Heptonstall, M. Heurs, S. Hild, T. Hinderer, D. Hoak, D. Hofman, K. Holt, D. E. Holz, P. Hopkins, C. Horst, J. Hough, E. A. Houston, E. J. Howell, A. Hreibi, Y. M. Hu, E. A. Huerta, D. Huet, B. Hughey, S. Husa, S. H. Huttner, T. Huynh- Dinh, N. Indik, R. Inta, G. Intini, H. N. Isa, J. M. Isac, M. Isi, B. R. Iyer, K. Izumi, T. Jacqmin, K. Jani, P. Jaranowski, S. Jawahar, F. Jiménez-Forteza, W. W. Johnson, D. I. Jones, R. Jones, R. J. G. Jonker, L. Ju, J. Junker, C. V. Kalaghatgi, V. Kalogera, B. Kamai, S. Kandhasamy, G. Kang, J. B. Kanner, S. J. Kapadia, S. Karki, K. S. Karvinen, M. Kasprzack, M. Katolik, E. Katsavounidis, W. Katzman, S. Kaufer, K. Kawabe, F. Kéfélian, D. Keitel, A. J. Kemball, R. Kennedy, C. Kent, J. S. Key, F. Y. Khalili, I. Khan, S. Khan, Z. Khan, E. A. Khazanov, N. Kijbunchoo, C. Kim, J. C. Kim, K. Kim, W. Kim, W. S. Kim, Y. M. Kim, S. J. Kimbrell, E. J. King, P. J. King, M. Kinley-Hanlon, R. Kirchhoff, J. S. Kissel, L. Kleybolte, S. Klimenko, T. D. Knowles, P. Koch, S. M. Koehlenbeck, S. Koley, V. Kondrashov, A. Kontos, M. Korobko, W. Z. Korth, I. Kowalska, D. B. Kozak, C. Krämer, V. Kringel, B. Krishnan, A. Królak, G. Kuehn, P. Kumar, R. Kumar, S. Kumar, L. Kuo, A. Kutynia, S. Kwang, B. D. Lackey, K. H. Lai, M. Landry, R. N. Lang, J. Lange,

B. Lantz, R. K. Lanza, S. L. Larson, A. Lartaux-Vollard, P. D. Lasky, M. Laxen, A. Lazzarini, C. Lazzaro, P. Leaci, S. Leavey, C. H. Lee, H. K. Lee, H. M. Lee, H. W. Lee, K. Lee, J. Lehmann, A. Lenon, M. Leonardi, N. Leroy, N. Letendre, Y. Levin, T. G. F. Li, S. D. Linker, T. B. Littenberg, J. Liu, R. K. L. Lo, N. A. Lockerbie, L. T. London, J. E. Lord, M. Lorenzini, V. Loriette, M. Lormand, G. Losurdo, J. D. Lough, C. O. Lousto, G. Lovelace, H. Lück, D. Lumaca, A. P. Lundgren, R. Lynch, Y. Ma, R. Macas, S. Macfoy, B. Machenschalk, M. MacInnis, D. M. Macleod, I. Magaña Hernandez, F. Magaña-Sandoval, L. Magaña Zertuche, R. M. Magee, E. Majorana, I. Maksimovic, N. Man, V. Mandic, V. Mangano, G. L. Mansell, M. Manske, M. Mantovani, F. Marchesoni, F. Marion, S. Márka, Z. Márka, C. Markakis, A. S. Markosyan, A. Markowitz, E. Maros, A. Marquina, P. Marsh, F. Martelli, L. Martellini, I. W. Martin, R. M. Martin, D. V. Martynov, K. Mason, E. Massera, A. Masserot, T. J. Massinger, M. Masso-Reid, S. Mastrogiovanni, A. Matas, F. Matichard, L. Matone, N. Mavalvala, N. Mazumder, R. McCarthy, D. E. McClelland, S. McCormick, L. McCuller, S. C. McGuire, G. McIntyre, J. McIver, D. J. McManus, L. McNeill, T. McRae, S. T. McWilliams, D. Meacher, G. D. Meadors, M. Mehmet, J. Meidam, E. Mejuto-Villa, A. Melatos, G. Mendell, R. A. Mercer, E. L. Merilh, M. Merzougui, S. Meshkov, C. Messenger, C. Messick, R. Metzdorff, P. M. Meyers, H. Miao, C. Michel, H. Middleton, E. E. Mikhailov, L. Milano, A. L. Miller, B. B. Miller, J. Miller, M. Millhouse, M. C. Milovich-Goff, O. Minazzoli, Y. Minenkov, J. Ming, C. Mishra, S. Mitra, V. P. Mitrofanov, G. Mitselmakher, R. Mittleman, D. Moffa, A. Moggi, K. Mogushi, M. Mohan, S. R. P. Mohapatra, M. Montani, C. J. Moore, D. Moraru, G. Moreno, S. R. Morriss, B. Mours, C. M. Mow-Lowry, G. Mueller, A. W. Muir, A. Mukherjee, D. Mukherjee, S. Mukherjee, N. Mukund, A. Mullavey, J. Munch, E. A. Muñiz, M. Muratore, P. G. Murray, K. Napier, I. Nardecchia, L. Naticchioni, R. K. Nayak, J. Neilson, G. Nelemans, T. J. N. Nelson, M. Nery, A. Neunzert, L. Nevin, J. M. Newport, G. Newton, K. K. Y. Ng, P. Nguyen, T. T. Nguyen, D. Nichols, A. B. Nielsen, S. Nissanke, A. Nitz, A. Noack, F. Nocera, D. Nolting, C. North, L. K. Nuttall, J. Oberling, G. D. O'Dea, G. H. Ogin, J. J. Oh, S. H. Oh, F. Ohme, M. A. Okada, M. Oliver, P. Oppermann, R. J. Oram, B. O'Reilly, R. Ormiston, L. F. Ortega, R. O'Shaughnessy, S. Ossokine, D. J. Ottaway, H. Overmier, B. J. Owen, A. E. Pace, J. Page, M. A. Page, A. Pai, S. A. Pai, J. R. Palamos, O. Palashov, C. Palomba, A. Pal- Singh, H. Pan, H.-W. Pan, B. Pang, P. T. H. Pang, C. Pankow, F. Pannarale, B. C. Pant, F. Paoletti, A. Paoli, M. A. Papa, A. Parida, W. Parker, D. Pascucci, A. Pasqualetti, R. Passaquieti, D. Passuello, M. Patil, B. Patricelli, B. L. Pearlstone, M. Pedraza, R. Pedurand, L. Pekowsky, A. Pele, S. Penn, C. J. Perez, A. Perreca, L. M. Perri, H. P. Pfeiffer, M. Phelps, O. J. Piccinni, M. Pichot, F. Piergiovanni, V. Pierro, G. Pillant, L. Pinard, I. M. Pinto, M. Pirello, M. Pitkin, M. Poe, R. Poggiani, P. Popolizio, E. K. Porter, A. Post, J. Powell, J. Prasad, J. W. W. Pratt, G. Pratten, V. Predoi, T. Prestegard, L. R. Price, M. Prijatelj, M. Principe, S. Privitera, G. A. Prodi, L. G. Prokhorov, O. Puncken, M. Punturo, P. Puppo, M. Pürrer, H. Qi, V. Quetschke, E. A. Quintero, R. Quitzow-James, F. J. Raab, D. S. Rabeling, H. Radkins, P. Raffai, S. Raja, C. Rajan, B. Rajbhandari, M. Rakhmanov, K. E. Ramirez, A. Ramos-Buades, P. Rapagnani, V. Raymond, M. Razzano, J. Read, T. Regimbau, L. Rei, S. Reid, D. H. Reitze, W. Ren, S. D. Reyes, F. Ricci, P. M. Ricker, S. Rieger, K. Riles, M. Rizzo,

N. A. Robertson, R. Robie, F. Robinet, A. Rocchi, L. Rolland, J. G. Rollins, V. J. Roma, R. Romano, C. L. Romel, J. H. Romie, D. Rosińska, M. P. Ross, S. Rowan, A. Rüdiger, P. Ruggi, G. Rutins, K. Ryan, S. Sachdev, T. Sadecki, L. Sadeghian, M. Sakellariadou, L. Salconi, M. Saleem, F. Salemi, A. Samajdar, L. Sammut, L. M. Sampson, E. J. Sanchez, L. E. Sanchez, N. Sanchis- Gual, V. Sandberg, J. R. Sanders, B. Sassolas, B. S. Sathyaprakash, P. R. Saulson, O. Sauter, R. L. Savage, A. Sawadsky, P. Schale, M. Scheel, J. Scheuer, J. Schmidt, P. Schmidt, R. Schnabel, R. M. S. Schofield, A. Schönbeck, E. Schreiber, D. Schuette, B. W. Schulte, B. F. Schutz, S. G. Schwalbe, J. Scott, S. M. Scott, E. Seidel, D. Sellers, A. S. Sengupta, D. Sentenac, V. Sequino, A. Sergeev, D. A. Shaddock, T. J. Shaffer, A. A. Shah, M. S. Shahriar, M. B. Shaner, L. Shao, B. Shapiro, P. Shawhan, A. Sheperd, D. H. Shoemaker, D. M. Shoemaker, K. Siellez, X. Siemens, M. Sieniawska, D. Sigg, A. D. Silva, L. P. Singer, A. Singh, A. Singhal, A. M. Sintes, B. J. J. Slagmolen, B. Smith, J. R. Smith, R. J. E. Smith, S. Somala, E. J. Son, J. A. Sonnenberg, B. Sorazu, F. Sorrentino, T. Souradeep, A. P. Spencer, A. K. Srivastava, K. Staats, A. Staley, M. Steinke, J. Steinlechner, S. Steinlechner, D. Steinmeyer, S. P. Stevenson, R. Stone, D. J. Stops, K. A. Strain, G. Stratta, S. E. Strigin, A. Strunk, R. Sturani, A. L. Stuver, T. Z. Summerscales, L. Sun, S. Sunil, J. Suresh, P. J. Sutton, B. L. Swinkels, M. J. Szczepańczyk, M. Tacca, S. C. Tait, C. Talbot, D. Talukder, D. B. Tanner, M. Tápai, A. Taracchini, J. D. Tasson, J. A. Taylor, R. Taylor, S. V. Tewari, T. Theeg, F. Thies, E. G. Thomas, M. Thomas, P. Thomas, K. A. Thorne, K. S. Thorne, E. Thrane, S. Tiwari, V. Tiwari, K. V. Tokmakov, K. Toland, M. Tonelli, Z. Tornasi, A. Torres-Forné, C. I. Torrie, D. Töyrä, F. Travasso, G. Traylor, J. Trinastic, M. C. Tringali, L. Trozzo, K. W. Tsang, M. Tse, R. Tso, L. Tsukada, D. Tsuna, D. Tuyenbayev, K. Ueno, D. Ugolini, C. S. Unnikrishnan, A. L. Urban, S. A. Usman, H. Vahlbruch, G. Vajente, G. Valdes, N. van Bakel, M. van Beuzekom, J. F. J. van den Brand, C. Van Den Broeck, D. C. Vander-Hyde, L. van der Schaaf, J. V. van Heijningen, A. A. van Veggel, M. Vardaro, V. Varma, S. Vass, M. Vasúth, A. Vecchio, G. Vedovato, J. Veitch, P. J. Veitch, K. Venkateswara, G. Venugopalan, D. Verkindt, F. Vetrano, A. Viceré, A. D. Viets, S. Vinciguerra, D. J. Vine, J. Y. Vinet, S. Vitale, T. Vo, H. Vocca, C. Vorvick, S. P. Vyatchanin, A. R. Wade, L. E. Wade, M. Wade, R. Walet, M. Walker, L. Wallace, S. Walsh, G. Wang, H. Wang, J. Z. Wang, W. H. Wang, Y. F. Wang, R. L. Ward, J. Warner, M. Was, J. Watchi, B. Weaver, L. W. Wei, M. Weinert, A. J. Weinstein, R. Weiss, L. Wen, E. K. Wessel, P. Wessels, J. Westerweck, T. Westphal, K. Wette, J. T. Whelan, S. E. Whitcomb, B. F. Whiting, C. Whittle, D. Wilken, D. Williams, R. D. Williams, A. R. Williamson, J. L. Willis, B. Willke, M. H. Wimmer, W. Winkler, C. C. Wipf, H. Wittel, G. Woan, J. Woehler, J. Wofford, K. W. K. Wong, J. Worden, J. L. Wright, D. S. Wu, D. M. Wysocki, S. Xiao, H. Yamamoto, C. C. Yancey, L. Yang, M. J. Yap, M. Yazback, H. Yu, H. Yu, M. Yvert, A. Zadrożny, M. Zanolin, T. Zelenova, J. P. Zendri, M. Zevin, L. Zhang, M. Zhang, T. Zhang, Y. H. Zhang, C. Zhao, M. Zhou, Z. Zhou, S. J. Zhu, X. J. Zhu, A. B. Zimmerman, M. E. Zucker, J. Zweizig, LIGO Scientific Collaboration, Virgo Collaboration, C. A. Wilson-Hodge, E. Bissaldi, L. Blackburn, M. S. Briggs, E. Burns, W. H. Cleveland, V. Connaughton, M. H. Gibby, M. M. Giles, A. Goldstein, R. Hamburg, P. Jenke, C. M. Hui, R. M. Kippen, D. Kocevski, S. McBreen, C. A. Meegan, W. S. Paciesas, S. Poolakkil, R. D. Preece, J. Racusin,

O. J. Roberts, M. Stanbro, P. Veres, A. von Kienlin, F. GBM, V. Savchenko, C. Ferrigno, E. Kuulkers, A. Bazzano, E. Bozzo, S. Brandt, J. Chenevez, T. J. L. Courvoisier, R. Diehl, A. Domingo, L. Hanlon, E. Jourdain, P. Laurent, F. Lebrun, A. Lutovinov, A. Martin-Carrillo, S. Mereghetti, L. Natalucci, J. Rodi, J. P. Roques, R. Sunyaev, P. Ubertini, INTEGRAL, M. G. Aartsen, M. Ackermann, J. Adams, J. A. Aguilar, M. Ahlers, M. Ahrens, I. A. Samarai, D. Altmann, K. Andeen, T. Anderson, I. Ansseau, G. Anton, C. Argüelles, J. Auffenberg, S. Axani, H. Bagherpour, X. Bai, J. P. Barron, S. W. Barwick, V. Baum, R. Bay, J. J. Beatty, J. Becker Tjus, E. Bernardini, D. Z. Besson, G. Binder, D. Bindig, E. Blaufuss, S. Blot, C. Bohm, M. Börner, F. Bos, D. Bose, S. Böser, O. Botner, E. Bourbeau, J. Bourbeau, F. Bradascio, J. Braun, L. Brayeur, M. Brenzke, H. P. Bretz, S. Bron, J. Brostean-Kaiser, A. Burgman, T. Carver, J. Casey, M. Casier, E. Cheung, D. Chirkin, A. Christov, K. Clark, L. Classen, S. Coenders, G. H. Collin, J. M. Conrad, D. F. Cowen, R. Cross, M. Day, J. P. A. M. de André, C. De Clercq, J. J. DeLaunay, H. Dembinski, S. De Ridder, P. Desiati, K. D. de Vries, G. de Wasseige, M. de With, T. DeYoung, J. C. Díaz-Vélez, V. di Lorenzo, H. Dujmovic, J. P. Dumm, M. Dunkman, E. Dvorak, B. Eberhardt, T. Ehrhardt, B. Eichmann, P. Eller, P. A. Evenson, S. Fahey, A. R. Fazely, J. Felde, K. Filimonov, C. Finley, S. Flis, A. Franckowiak, E. Friedman, T. Fuchs, T. K. Gaisser, J. Gallagher, L. Gerhardt, K. Ghorbani, W. Giang, T. Glauch, T. Glüsenkamp, A. Goldschmidt, J. G. Gonzalez, D. Grant, Z. Griffith, C. Haack, A. Hallgren, F. Halzen, K. Hanson, D. Hebecker, D. Heereman, K. Helbing, R. Hellauer, S. Hickford, J. Hignight, G. C. Hill, K. D. Hoffman, R. Hoffmann, B. Hokanson-Fasig, K. Hoshina, F. Huang, M. Huber, K. Hultqvist, M. Hünnefeld, S. In, A. Ishihara, E. Jacobi, G. S. Japaridze, M. Jeong, K. Jero, B. J. P. Jones, P. Kalaczynski, W. Kang, A. Kappes, T. Karg, A. Karle, M. Kauer, A. Keivani, J. L. Kelley, A. Kheirandish, J. Kim, M. Kim, T. Kintscher, J. Kiryluk, T. Kittler, S. R. Klein, G. Kohnen, R. Koirala, H. Kolanoski, L. Köpke, C. Kopper, S. Kopper, J. P. Koschinsky, D. J. Koskinen, M. Kowalski, K. Krings, M. Kroll, G. Krückl, J. Kunnen, S. Kunwar, N. Kurahashi, T. Kuwabara, A. Kyriacou, M. Labare, J. L. Lanfranchi, M. J. Larson, F. Lauber, M. Lesiak-Bzdak, M. Leuermann, Q. R. Liu, L. Lu, J. Lünemann, W. Luszczak, J. Madsen, G. Maggi, K. B. M. Mahn, S. Mancina, R. Maruyama, K. Mase, R. Maunu, F. McNally, K. Meagher, M. Medici, M. Meier, T. Menne, G. Merino, T. Meures, S. Miarecki, J. Micallef, G. Momenté, T. Montaruli, R. W. Moore, M. Moulai, R. Nahnhauer, P. Nakarmi, U. Naumann, G. Neer, H. Niederhausen, S. C. Nowicki, D. R. Nygren, A. Obertacke Pollmann, A. Olivas, A. O'Murchadha, T. Palczewski, H. Pandya, D. V. Pankova, P. Peiffer, J. A. Pepper, C. Pérez de los Heros, D. Pieloth, E. Pinat, P. B. Price, G. T. Przybylski, C. Raab, L. Rädel, M. Rameez, K. Rawlins, I. C. Rea, R. Reimann, B. Relethford, M. Relich, E. Resconi, W. Rhode, M. Richman, S. Robertson, M. Rongen, C. Rott, T. Ruhe, D. Ryckbosch, D. Rysewyk, T. Sälzer, S. E. Sanchez Herrera, A. Sandrock, J. Sandroos, M. Santander, S. Sarkar, S. Sarkar, K. Satalecka, P. Schlunder, T. Schmidt, A. Schneider, S. Schoenen, S. Schöneberg, L. Schumacher, D. Seckel, S. Seunarine, J. Soedingrekso, D. Soldin, M. Song, G. M. Spiczak, C. Spiering, J. Stachurska, M. Stamatikos, T. Stanev, A. Stasik, J. Stettner, A. Steuer, T. Stezelberger, R. G. Stokstad, A. Stössl, N. L. Strotjohann, T. Stuttard, G. W. Sullivan, M. Sutherland, I. Taboada, J. Tatar, F. Tenholt, S. Ter- Antonyan, A. Terliuk,

G. Tešić, S. Tilav, P. A. Toale, M. N. Tobin, S. Toscano, D. Tosi, M. Tselengidou, C. F. Tung, A. Turcati, C. F. Turley, B. Ty, E. Unger, M. Usner, J. Vandenbroucke, W. Van Driessche, N. van Eijndhoven, S. Vanheule, J. van Santen, M. Vehring, E. Vogel, M. Vraeghe, C. Walck, A. Wallace, M. Wallraff, F. D. Wandler, N. Wandkowsky, A. Waza, C. Weaver, M. J. Weiss, C. Wendt, J. Werthebach, B. J. Whelan, K. Wiebe, C. H. Wiebusch, L. Wille, D. R. Williams, L. Wills, M. Wolf, T. R. Wood, E. Woolsey, K. Woschnagg, D. L. Xu, X. W. Xu, Y. Xu, J. P. Yanez, G. Yodh, S. Yoshida, T. Yuan, M. Zoll, IceCube Collaboration, A. Balasubramanian, S. Mate, V. Bhalerao, D. Bhattacharya, A. Vibhute, G. C. Dewangan, A. R. Rao, S. V. Vadawale, AstroSat Cadmium Zinc Telluride Imager Team, D. S. Svinkin, K. Hurley, R. L. Aptekar, D. D. Frederiks, S. V. Golenetskii, A. V. Kozlova, A. L. Lysenko, P. P. Oleynik, A. E. Tsvetkova, M. V. Ulanov, T. Cline, IPN Collaboration, T. P. Li, S. L. Xiong, S. N. Zhang, F. J. Lu, L. M. Song, X. L. Cao, Z. Chang, G. Chen, L. Chen, T. X. Chen, Y. Chen, Y. B. Chen, Y. P. Chen, W. Cui, W. W. Cui, J. K. Deng, Y. W. Dong, Y. Y. Du, M. X. Fu, G. H. Gao, H. Gao, M. Gao, M. Y. Ge, Y. D. Gu, J. Guan, C. C. Guo, D. W. Han, W. Hu, Y. Huang, J. Huo, S. M. Jia, L. H. Jiang, W. C. Jiang, J. Jin, Y. J. Jin, B. Li, C. K. Li, G. Li, M. S. Li, W. Li, X. Li, X. B. Li, X. F. Li, Y. G. Li, Z. J. Li, Z. W. Li, X. H. Liang, J. Y. Liao, C. Z. Liu, G. Q. Liu, H. W. Liu, S. Z. Liu, X. J. Liu, Y. Liu, Y. N. Liu, B. Lu, X. F. Lu, T. Luo, X. Ma, B. Meng, Y. Nang, J. Y. Nie, G. Ou, J. L. Qu, N. Sai, L. Sun, Y. Tan, L. Tao, W. H. Tao, Y. L. Tuo, G. F. Wang, H. Y. Wang, J. Wang, W. S. Wang, Y. S. Wang, X. Y. Wen, B. B. Wu, M. Wu, G. C. Xiao, H. Xu, Y. P. Xu, L. L. Yan, J. W. Yang, S. Yang, Y. J. Yang, A. M. Zhang, C. L. Zhang, C. M. Zhang, F. Zhang, H. M. Zhang, J. Zhang, Q. Zhang, S. Zhang, T. Zhang, W. Zhang, W. C. Zhang, W. Z. Zhang, Y. Zhang, Y. Zhang, Y. F. Zhang, Y. J. Zhang, Z. Zhang, Z. L. Zhang, H. S. Zhao, J. L. Zhao, X. F. Zhao, S. J. Zheng, Y. Zhu, Y. X. Zhu, C. L. Zou, Insight-HXMT Collaboration, A. Albert, M. André, M. Anghinolfi, M. Ardid, J. J. Aubert, J. Aublin, T. Avgitas, B. Baret, J. Barrios- Martí, S. Basa, B. Belhorma, V. Bertin, S. Biagi, R. Bormuth, S. Bourret, M. C. Bouwhuis, H. Brânzaş, R. Bruijn, J. Brunner, J. Busto, A. Capone, L. Caramete, J. Carr, S. Celli, R. Cherkaoui El Moursli, T. Chiarusi, M. Circella, J. A. B. Coelho, A. Coleiro, R. Coniglione, H. Costantini, P. Coyle, A. Creusot, A. F. Díaz, A. Deschamps, G. De Bonis, C. Distefano, I. Di Palma, A. Domi, C. Donzaud, D. Dornic, D. Drouhin, T. Eberl, I. El Bojaddaini, N. El Khayati, D. Elsässer, A. Enzenhöfer, A. Ettahiri, F. Fassi, I. Felis, L. A. Fusco, P. Gay, V. Giordano, H. Glotin, T. Grégoire, R. G. Ruiz, K. Graf, S. Hallmann, H. van Haren, A. J. Heijboer, Y. Hello, J. J. Hernández-Rey, J. Hössl, J. Hofestädt, C. Hugon, G. Illuminati, C. W. James, M. de Jong, M. Jongen, M. Kadler, O. Kalekin, U. Katz, D. Kiessling, A. Kouchner, M. Kreter, I. Kreykenbohm, V. Kulikovskiy, C. Lachaud, R. Lahmann, D. Lefèvre, E. Leonora, M. Lotze, S. Loucatos, M. Marcelin, A. Margiotta, A. Marinelli, J. A. Martínez-Mora, R. Mele, K. Melis, T. Michael, P. Migliozzi, A. Moussa, S. Navas, E. Nezri, M. Organokov, G. E. Păvălaş, C. Pellegrino, C. Perrina, P. Piattelli, V. Popa, T. Pradier, L. Quinn, C. Racca, G. Riccobene, A. Sánchez-Losa, M. Saldaña, I. Salvadori, D. F. E. Samtleben, M. Sanguineti, P. Sapienza, C. Sieger, M. Spurio, T. Stolarczyk, M. Taiuti, Y. Tayalati, A. Trovato, D. Turpin, C. Tönnis, B. Vallage, V. Van Elewyck, F. Versari, D. Vivolo, A. Vizzoca, J. Wilms, J. D. Zornoza,

J. Zúñiga, ANTARES Collaboration, A. P. Beardmore, A. A. Breeveld, D. N. Burrows, S. B. Cenko, G. Cusumano, A. D'Aì, M. de Pasquale, S. W. K. Emery, P. A. Evans, P. Giommi, C. Gronwall, J. A. Kennea, H. A. Krimm, N. P. M. Kuin, A. Lien, F. E. Marshall, A. Melandri, J. A. Nousek, S. R. Oates, J. P. Osborne, C. Pagani, K. L. Page, D. M. Palmer, M. Perri, M. H. Siegel, B. Sbarufatti, G. Tagliaferri, A. Tohuvavohu, The Swift Collaboration, M. Tavani, F. Verrecchia, A. Bulgarelli, Y. Evangelista, L. Pacciani, M. Feroci, C. Pittori, A. Giuliani, E. Del Monte, I. Donnarumma, A. Argan, A. Trois, A. Ursi, M. Cardillo, G. Piano, F. Longo, F. Lucarelli, P. Munar-Adrover, F. Fuschino, C. Labanti, M. Marisaldi, G. Minervini, V. Fioretti, N. Parmiggiani, F. Gianotti, M. Trifoglio, G. Di Persio, L. A. Antonelli, G. Barbiellini, P. Caraveo, P. W. Cattaneo, E. Costa, S. Colafrancesco, F. D'Amico, A. Ferrari, A. Morselli, F. Paoletti, P. Picozza, M. Pilia, A. Rappoldi, P. Soffitta, S. Vercellone, AGILE Team, R. J. Foley, D. A. Coulter, C. D. Kilpatrick, M. R. Drout, A. L. Piro, B. J. Shappee, M. R. Siebert, J. D. Simon, N. Ulloa, D. Kasen, B. F. Madore, A. Murguia-Berthier, Y. C. Pan, J. X. Prochaska, E. Ramirez-Ruiz, A. Rest, C. Rojas-Bravo, The 1M2H Team, E. Berger, M. Soares-Santos, J. Annis, K. D. Alexander, S. Allam, E. Balbinot, P. Blanchard, D. Brout, R. E. Butler, R. Chornock, E. R. Cook, P. Cowperthwaite, H. T. Diehl, A. Drlica-Wagner, M. R. Drout, F. Durret, T. Eftekhari, D. A. Finley, W. Fong, J. A. Frieman, C. L. Fryer, J. García-Bellido, R. A. Gruendl, W. Hartley, K. Herner, R. Kessler, H. Lin, P. A. A. Lopes, A. C. C. Lourenço, R. Margutti, J. L. Marshall, T. Matheson, G. E. Medina, B. D. Metzger, R. R. Muñoz, J. Muir, M. Nicholl, P. Nugent, A. Palmese, F. Paz-Chinchón, E. Quataert, M. Sako, M. Sauseda, D. J. Schlegel, D. Scolnic, L. F. Secco, N. Smith, F. Sobreira, V. A. Villar, A. K. Vivas, W. Wester, P. K. G. Williams, B. Yanny, A. Zenteno, Y. Zhang, T. M. C. Abbott, M. Banerji, K. Bechtol, A. Benoit-Lévy, E. Bertin, D. Brooks, E. Buckley-Geer, D. L. Burke, D. Capozzi, A. Carnero Rosell, M. Carrasco Kind, F. J. Castander, M. Crocce, C. E. Cunha, C. B. D'Andrea, L. N. da Costa, C. Davis, D. L. DePoy, S. Desai, J. P. Dietrich, T. F. Eifler, E. Fernandez, B. Flaugher, P. Fosalba, E. Gaztanaga, D. W. Gerdes, T. Giannantonio, D. A. Goldstein, D. Gruen, J. Gschwend, G. Gutierrez, K. Honscheid, D. J. James, T. Jeltema, M. W. G. Johnson, M. D. Johnson, S. Kent, E. Krause, R. Kron, K. Kuehn, O. Lahav, M. Lima, M. A. G. Maia, M. March, P. Martini, R. G. McMahon, F. Menanteau, C. J. Miller, R. Miquel, J. J. Mohr, R. C. Nichol, R. L. C. Ogando, A. A. Plazas, A. K. Romer, A. Roodman, E. S. Rykoff, E. Sanchez, V. Scarpine, R. Schindler, M. Schubnell, I. Sevilla-Noarbe, E. Sheldon, M. Smith, R. C. Smith, A. Stebbins, E. Suchyta, M. E. C. Swanson, G. Tarle, R. C. Thomas, M. A. Troxel, D. L. Tucker, V. Vikram, A. R. Walker, R. H. Wechsler, J. Weller, J. L. Carlin, M. S. S. Gill, T. S. Li, J. Marriner, E. Neilsen, The Dark Energy Camera GW- EM Collaboration, the DES Collaboration, J. B. Haislip, V. V. Kouprianov, D. E. Reichart, D. J. Sand, L. Tartaglia, S. Valenti, S. Yang, The DLT40 Collaboration, S. Benetti, E. Brocato, S. Campana, E. Cappellaro, S. Covino, P. D'Avanzo, V. D'Elia, F. Getman, G. Ghirlanda, G. Ghisellini, L. Limatola, L. Nicastro, E. Palazzi, E. Pian, S. Piranomonte, A. Possenti, A. Rossi, O. S. Salafia, L. Tomasella, L. Amati, L. A. Antonelli, M. G. Bernardini, F. Bufano, M. Capaccioli, P. Casella, M. Dadina, G. De Cesare, A. Di Paola, G. Giuffrida, A. Giunta, G. L. Israel, M. Lisi, E. Maiorano, M. Mapelli, N. Masetti, A. Pescalli, L. Pulone, R. Salvaterra, P. Schipani, M. Spera,

A. Stamerra, L. Stella, V. Testa, M. Turatto, D. Vergani, G. Aresu, M. Bachetti, F. Buffa, M. Burgay, M. Buttu, T. Caria, E. Carretti, V. Casasola, P. Castangia, G. Carboni, S. Casu, R. Concu, A. Corongiu, G. L. Deiana, E. Egron, A. Fara, F. Gaudiomonte, V. Gusai, A. Ladu, S. Loru, S. Leurini, L. Marongiu, A. Melis, G. Melis, C. Migoni, S. Milia, A. Navarrini, A. Orlati, P. Ortu, S. Palmas, A. Pellizzoni, D. Perrodin, T. Pisanu, S. Poppi, S. Righini, A. Saba, G. Serra, M. Serrau, M. Stagni, G. Surcis, V. Vacca, G. P. Vargiu, L. K. Hunt, Z. P. Jin, S. Klose, C. Kouveliotou, P. A. Mazzali, P. Møller, L. Nava, T. Piran, J. Selsing, S. D. Vergani, K. Wiersema, K. Toma, A. B. Higgins, C. G. Mundell, S. di Serego Alighieri, D. Gótz, W. Gao, A. Gomboc, L. Kaper, S. Kobayashi, D. Kopac, J. Mao, R. L. C. Starling, I. Steele, A. J. van der Horst, GRAWITA: GRAvitational Wave Inaf TeAm, F. Acero, W. B. Atwood, L. Baldini, G. Barbiellini, D. Bastieri, B. Berenji, R. Bellazzini, E. Bissaldi, R. D. Blandford, E. D. Bloom, R. Bonino, E. Bottacini, J. Bregeon, R. Buehler, S. Buson, R. A. Cameron, R. Caputo, P. A. Caraveo, E. Cavazzuti, A. Chekhtman, C. C. Cheung, J. Chiang, S. Ciprini, J. Cohen-Tanugi, L. R. Cominsky, D. Costantin, A. Cuoco, F. D'Ammando, F. de Palma, S. W. Digel, N. Di Lalla, M. Di Mauro, L. Di Venere, R. Dubois, S. J. Fegan, W. B. Focke, A. Franckowiak, Y. Fukazawa, S. Funk, P. Fusco, F. Gargano, D. Gasparrini, N. Giglietto, F. Giordano, M. Giroletti, T. Glanzman, D. Green, M. H. Grondin, L. Guillemot, S. Guiriec, A. K. Harding, D. Horan, G. Jóhannesson, T. Kamae, S. Kensei, M. Kuss, G. La Mura, L. Latronico, M. Lemoine-Goumard, F. Longo, F. Loparco, M. N. Lovellette, P. Lubrano, J. D. Magill, S. Maldera, A. Manfreda, M. N. Mazziotta, J. E. McEnery, M. Meyer, P. F. Michelson, N. Mirabal, M. E. Monzani, E. Moretti, A. Morselli, I. V. Moskalenko, M. Negro, E. Nuss, R. Ojha, N. Omodei, M. Orienti, E. Orlando, M. Palatiello, V. S. Paliya, D. Paneque, M. Pesce-Rollins, F. Piron, T. A. Porter, G. Principe, S. Rainò, R. Rando, M. Razzano, S. Razzaque, A. Reimer, O. Reimer, T. Reposeur, L. S. Rochester, P. M. Saz Parkinson, C. Sgrò, E. J. Siskind, F. Spada, G. Spandre, D. J. Suson, M. Takahashi, Y. Tanaka, J. G. Thayer, J. B. Thayer, D. J. Thompson, L. Tibaldo, D. F. Torres, E. Torresi, E. Troja, T. M. Venters, G. Vianello, G. Zaharijas, The Fermi Large Area Telescope Collaboration, J. R. Allison, K. W. Bannister, D. Dobie, D. L. Kaplan, E. Lenc, C. Lynch, T. Murphy, E. M. Sadler, A. Australia Telescope Compact Array, A. Hotan, C. W. James, S. Oslowski, W. Raja, R. M. Shannon, M. Whiting, A. Australian SKA Pathfinder, I. Arcavi, D. A. Howell, C. McCully, G. Hosseinzadeh, D. Hiramatsu, D. Poznanski, J. Barnes, M. Zaltzman, S. Vasylyev, D. Maoz, Las Cumbres Observatory Group, J. Cooke, M. Bailes, C. Wolf, A. T. Deller, C. Lidman, L. Wang, B. Gendre, I. Andreoni, K. Ackley, T. A. Pritchard, M. S. Bessell, S. W. Chang, A. Möller, C. A. Onken, R. A. Scalzo, R. Ridden-Harper, R. G. Sharp, B. E. Tucker, T. J. Farrell, E. Elmer, S. Johnston, V. Venkatraman Krishnan, E. F. Keane, J. A. Green, A. Jameson, L. Hu, B. Ma, T. Sun, X. Wu, X. Wang, Z. Shang, Y. Hu, M. C. B. Ashley, X. Yuan, X. Li, C. Tao, Z. Zhu, H. Zhang, N. B. Suntzeff, J. Zhou, J. Yang, B. Orange, D. Morris, A. Cucchiara, T. Giblin, A. Klotz, J. Staff, P. Thierry, B. P. Schmidt, OzGrav, D. (Deeper, Wider, F. program, AST3, CAASTRO Collaborations, N. R. Tanvir, A. J. Levan, Z. Cano, A. de Ugarte-Postigo, C. González-Fernández, J. Greiner, J. Hjorth, M. Irwin, T. Krühler, I. Mandel, B. Milvang-Jensen, P. O'Brien, E. Rol, S. Rosetti, S. Rosswog, A. Rowlinson, D. T. H. Steeghs, C. C. Thöne, K. Ulaczyk,

D. Watson, S. H. Bruun, R. Cutter, R. Figuera Jaimes, Y. I. Fujii, A. S. Fruchter, B. Gompertz, P. Jakobsson, G. Hodosan, U. G. Jèrgensen, T. Kangas, D. A. Kann, M. Rabus, S. L. Schrøder, E. R. Stanway, R. A. M. J. Wijers, The VINROUGE Collaboration, V. M. Lipunov, E. S. Gorbovskoy, V. G. Kornilov, N. V. Tyurina, P. V. Balanutsa, A. S. Kuznetsov, D. M. Vlasenko, R. C. Podesta, C. Lopez, F. Podesta, H. O. Levato, C. Saffe, C. C. Mallamaci, N. M. Budnev, O. A. Gress, D. A. Kuvshinov, I. A. Gorbunov, V. V. Vladimirov, D. S. Zimnukhov, A. V. Gabovich, V. V. Yurkov, Y. P. Sergienko, R. Rebolo, M. Serra-Ricart, A. G. Tlatov, Y. V. Ishmuhametova, MASTER Collaboration, F. Abe, K. Aoki, W. Aoki, Y. Asakura, S. Baar, S. Barway, I. A. Bond, M. Doi, F. Finet, T. Fujiyoshi, H. Furusawa, S. Honda, R. Itoh, N. Kanda, K. S. Kawabata, M. Kawabata, J. H. Kim, S. Koshida, D. Kuroda, C. H. Lee, W. Liu, K. Matsubayashi, S. Miyazaki, K. Morihana, T. Morokuma, K. Motohara, K. L. Murata, H. Nagai, H. Nagashima, T. Nagayama, T. Nakaoka, F. Nakata, R. Ohsawa, T. Ohshima, K. Ohta, H. Okita, T. Saito, Y. Saito, S. Sako, Y. Sekiguchi, T. Sumi, A. Tajitsu, J. Takahashi, M. Takayama, Y. Tamura, I. Tanaka, M. Tanaka, T. Terai, N. Tominaga, P. J. Tristram, M. Uemura, Y. Utsumi, M. S. Yamaguchi, N. Yasuda, M. Yoshida, T. Zenko, J-GEM, S. M. Adams, G. C. Anupama, J. Bally, S. Barway, E. Bellm, N. Blagorodnova, C. Cannella, P. Chandra, D. Chatterjee, T. E. Clarke, B. E. Cobb, D. O. Cook, C. Copperwheat, K. De, S. W. K. Emery, U. Feindt, K. Foster, O. D. Fox, D. A. Frail, C. Fremling, C. Frohmaier, J. A. Garcia, S. Ghosh, S. Giacintucci, A. Goobar, O. Gottlieb, B. W. Grefenstette, G. Hallinan, F. Harrison, M. Heida, G. Helou, A. Y. Q. Ho, A. Horesh, K. Hotokezaka, W. H. Ip, R. Itoh, B. Jacobs, J. E. Jencson, D. Kasen, M. M. Kasliwal, N. E. Kassim, H. Kim, B. S. Kiran, N. P. M. Kuin, S. R. Kulkarni, T. Kupfer, R. M. Lau, K. Madsen, P. A. Mazzali, A. A. Miller, H. Miyasaka, K. Mooley, S. T. Myers, E. Nakar, C. C. Ngeow, P. Nugent, E. O. Ofek, N. Palliyaguru, M. Pavana, D. A. Perley, W. M. Peters, S. Pike, T. Piran, H. Qi, R. M. Quimby, J. Rana, S. Rosswog, F. Rusu, E. M. Sadler, A. Van Sistine, J. Sollerman, Y. Xu, L. Yan, Y. Yatsu, P. C. Yu, C. Zhang, W. Zhao, GROWTH, JAGWAR, Caltech-NRAO, TTU-NRAO, NuSTAR Collaborations, K. C. Chambers, M. E. Huber, A. S. B. Schultz, J. Bulger, H. Flewelling, E. A. Magnier, T. B. Lowe, R. J. Wainscoat, C. Waters, M. Willman, Pan-STARRS, K. Ebisawa, C. Hanyu, S. Harita, T. Hashimoto, K. Hidaka, T. Hori, M. Ishikawa, N. Isobe, W. Iwakiri, H. Kawai, N. Kawai, T. Kawamuro, T. Kawase, Y. Kitaoka, K. Makishima, M. Matsuoka, T. Mihara, T. Morita, K. Morita, S. Nakahira, M. Nakajima, Y. Nakamura, H. Negoro, S. Oda, A. Sakamaki, R. Sasaki, M. Serino, M. Shidatsu, R. Shimomukai, Y. Sugawara, S. Sugita, M. Sugizaki, Y. Tachibana, Y. Takao, A. Tanimoto, H. Tomida, Y. Tsuboi, H. Tsunemi, Y. Ueda, S. Ueno, S. Yamada, K. Yamaoka, M. Yamauchi, F. Yatabe, T. Yoneyama, T. Yoshii, The MAXI Team, D. M. Coward, H. Crisp, D. Macpherson, I. Andreoni, R. Laugier, K. Noysena, A. Klotz, B. Gendre, P. Thierry, D. Turpin, T. Consortium, M. Im, C. Choi, J. Kim, Y. Yoon, G. Lim, S. K. Lee, C. U. Lee, S. L. Kim, S. W. Ko, J. Joe, M. K. Kwon, P. J. Kim, S. K. Lim, J. S. Choi, KU Collaboration, J. P. U. Fynbo, D. Malesani, D. Xu, N. Optical Telescope, S. J. Smartt, A. Jerkstrand, E. Kankare, S. A. Sim, M. Fraser, C. Inserra, K. Maguire, G. Leloudas, M. Magee, L. J. Shingles, K. W. Smith, D. R. Young, R. Kotak, A. Gal-Yam, J. D. Lyman, D. S. Homan, C. Agliozzo, J. P. Anderson, C. R. Angus, C. Ashall, C. Barbarino, F. E. Bauer,

M. Berton, M. T. Botticella, M. Bulla, G. Cannizzaro, R. Cartier, A. Cikota, P. Clark, A. De Cia, M. Della Valle, M. Dennefeld, L. Dessart, G. Dimitriadis, N. Elias-Rosa, R. E. Firth, A. Flörs, C. Frohmaier, L. Galbany, S. González-Gaitán, M. Gromadzki, C. P. Gutiérrez, A. Hamanowicz, J. Harmanen, K. E. Heintz, M. S. Hernandez, S. T. Hodgkin, I. M. Hook, L. Izzo, P. A. James, P. G. Jonker, W. E. Kerzendorf, Z. Kostrzewa-Rutkowska, M. Kromer, H. Kuncarayakti, A. Lawrence, I. Manulis, S. Mattila, O. McBrien, A. Müller, J. Nordin, D. O'Neill, F. Onori, J. T. Palmerio, A. Pastorello, F. Patat, G. Pignata, P. Podsiadlowski, A. Razza, T. Reynolds, R. Roy, A. J. Ruiter, K. A. Rybicki, L. Salmon, M. L. Pumo, S. J. Prentice, I. R. Seitenzahl, M. Smith, J. Sollerman, M. Sullivan, H. Szegedi, F. Taddia, S. Taubenberger, G. Terreran, B. Van Soelen, J. Vos, N. A. Walton, D. E. Wright, Ł. Wyrzykowski, O. Yaron, a. pre=”(”¿ePESSTO, T. W. Chen, T. Krühler, P. Schady, P. Wiseman, J. Greiner, A. Rau, T. Schweyer, S. Klose, A. Nicuesa Guelbenzu, GROND, N. T. Palliyaguru, T. Tech University, M. M. Shara, T. Williams, P. Vaisanen, S. B. Potter, E. Romero Colmenero, S. Crawford, D. A. H. Buckley, J. Mao, SALT Group, M. C. Díaz, L. M. Macri, D. García Lambas, C. Mendes de Oliveira, J. L. Nilo Castellón, T. Ribeiro, B. Sánchez, W. Schoenell, L. R. Abramo, S. Akras, J. S. Alcaniz, R. Artola, M. Beroiz, S. Bonoli, J. Cabral, R. Camuccio, V. Chavushyan, P. Coelho, C. Colazo, M. V. Costa- Duarte, H. Cuevas Larenas, M. Domínguez Romero, D. Dultzin, D. Fernández, J. García, C. Girardini, D. R. Gonçalves, T. S. Gonçalves, S. Gurovich, Y. Jiménez-Teja, A. Kanaan, M. Lares, R. Lopes de Oliveira, O. López-Cruz, R. Melia, A. Molino, N. Padilla, T. Peñuela, V. M. Placco, C. Quiñones, A. Ramírez Rivera, V. Renzi, L. Riguccini, E. Ríos-López, H. Rodriguez, L. Sampedro, M. Schneiter, L. Sodré, M. Starck, S. Torres-Flores, M. Tornatore, A. Zadrożny, M. Castillo, TOROS: Transient Robotic Observatory of the South Collaboration, A. J. Castro-Tirado, J. C. Tello, Y. D. Hu, B. B. Zhang, R. Cunniffe, A. Castellón, D. Hiriart, M. D. Caballero-García, M. Jelínek, P. Kubánek, C. Pérez del Pulgar, I. H. Park, S. Jeong, J. M. Castro Cerón, S. B. Pandey, P. C. Yock, R. Querel, Y. Fan, C. Wang, The BOOTES Collaboration, A. Beardsley, I. S. Brown, B. Crosse, D. Emrich, T. Franzen, B. M. Gaensler, L. Horsley, M. Johnston-Hollitt, D. Kenney, M. F. Morales, D. Pallot, M. Sokolowski, K. Steele, S. J. Tingay, C. M. Trott, M. Walker, R. Wayth, A. Williams, C. Wu, M. Murchison Widefield Array, A. Yoshida, T. Sakamoto, Y. Kawakubo, K. Yamaoka, I. Takahashi, Y. Asaoka, S. Ozawa, S. Torii, Y. Shimizu, T. Tamura, W. Ishizaki, M. L. Cherry, S. Ricciarini, A. V. Penacchioni, P. S. Marrocchesi, The CALET Collaboration, A. S. Pozanenko, A. A. Volnova, E. D. Mazaeva, P. Y. Minaev, M. A. Krugov, A. V. Kusakin, I. V. Reva, A. S. Moskvitin, V. V. Rumyantsev, R. Inasaridze, E. V. Klunko, N. Tungalag, S. E. Schmalz, O. Burhonov, IKI-GW Follow-up Collaboration, H. Abdalla, A. Abramowski, F. Aharonian, F. Ait Benkhali, E. O. Angüner, M. Arakawa, M. Arrieta, P. Aubert, M. Backes, A. Balzer, M. Barnard, Y. Becherini, J. Becker Tjus, D. Berge, S. Bernhard, K. Bernlöhr, R. Blackwell, M. Böttcher, C. Boisson, J. Bolmont, S. Bonnefoy, P. Bordas, J. Bregeon, F. Brun, P. Brun, M. Bryan, M. Büchele, T. Bulik, M. Capasso, S. Caroff, A. Carosi, S. Casanova, M. Cerruti, N. Chakraborty, R. C. G. Chaves, A. Chen, J. Chevalier, S. Colafrancesco, B. Condon, J. Conrad, I. D. Davids, J. Decock, C. Deil, J. Devin, P. deWilt, L. Dirson, A. Djannati-Ataï, A. Donath, L. O'C. Drury, K. Dutson, J. Dyks, T. Edwards,

K. Egberts, G. Emery, J. P. Ernenwein, S. Eschbach, C. Farnier, S. Fegan, M. V. Fernandes, A. Fiasson, G. Fontaine, S. Funk, M. Füssling, S. Gabici, Y. A. Gallant, T. Garrigoux, F. Gaté, G. Giavitto, B. Giebels, D. Glawion, J. F. Glicenstein, D. Gottschall, M. H. Grondin, J. Hahn, M. Haupt, J. Hawkes, G. Heinzelmann, G. Henri, G. Hermann, J. A. Hinton, W. Hofmann, C. Hoischen, T. L. Holch, M. Holler, D. Horns, A. Ivascenko, H. Iwasaki, A. Jacholkowska, M. Jamrozy, D. Jankowsky, F. Jankowsky, M. Jingo, L. Jouvin, I. Jung-Richardt, M. A. Kastendieck, K. Katarzyński, M. Katsuragawa, D. Kerszberg, D. Khangulyan, B. Khélifi, J. King, S. Klepser, D. Klochkov, W. Kluźniak, N. Komin, K. Kosack, S. Krakau, M. Kraus, P. P. Krüger, H. Laffon, G. Lamanna, J. Lau, J. P. Lees, J. Lefaucheur, A. Lemière, M. Lemoine-Goumard, J. P. Lenain, E. Leser, T. Lohse, M. Lorentz, R. Liu, I. Lypova, D. Malyshev, V. Marandon, A. Marcowith, C. Mariaud, R. Marx, G. Maurin, N. Maxted, M. Mayer, P. J. Meintjes, M. Meyer, A. M. W. Mitchell, R. Moderski, M. Mohamed, L. Mohrmann, K. Morå, E. Moulin, T. Murach, S. Nakashima, M. de Naurois, H. Ndiyavala, F. Niederwanger, J. Niemiec, L. Oakes, P. O'Brien, H. Odaka, S. Ohm, M. Ostrowski, I. Oya, M. Padovani, M. Panter, R. D. Parsons, N. W. Pekeur, G. Pelletier, C. Perennes, P. O. Petrucci, B. Peyaud, Q. Piel, S. Pita, V. Poireau, H. Poon, D. Prokhorov, H. Prokoph, G. Pühlhofer, M. Punch, A. Quirrenbach, S. Raab, R. Rauth, A. Reimer, O. Reimer, M. Renaud, R. de los Reyes, F. Rieger, L. Rinchiuso, C. Romoli, G. Rowell, B. Rudak, C. B. Rulten, V. Sahakian, S. Saito, D. A. Sanchez, A. Santangelo, M. Sasaki, R. Schlickeiser, F. Schüssler, A. Schulz, U. Schwanke, S. Schwemmer, M. Seglar-Arroyo, M. Settimo, A. S. Seyffert, N. Shafi, I. Shilon, K. Shiningayamwe, R. Simoni, H. Sol, F. Spanier, M. Spir-Jacob, Ł. Stawarz, R. Steenkamp, C. Stegmann, C. Steppa, I. Sushch, T. Takahashi, J. P. Tavernet, T. Tavernier, A. M. Taylor, R. Terrier, L. Tibaldo, D. Tiziani, M. Tluczykont, C. Trichard, M. Tsirou, N. Tsuji, R. Tuffs, Y. Uchiyama, D. J. van der Walt, C. van Eldik, C. van Rensburg, B. van Soelen, G. Vasileiadis, J. Veh, C. Venter, A. Viana, P. Vincent, J. Vink, F. Voisin, H. J. Völk, T. Vuillaume, Z. Wadiasingh, S. J. Wagner, P. Wagner, R. M. Wagner, R. White, A. Wierzcholska, P. Willmann, A. Wörnlein, D. Wouters, R. Yang, D. Zaborov, M. Zacharias, R. Zanin, A. A. Zdziarski, A. Zech, F. Zefi, A. Ziegler, J. Zorn, N. Żywucka, H. E. S. S. Collaboration, R. P. Fender, J. W. Broderick, A. Rowlinson, R. A. M. J. Wijers, A. J. Stewart, S. ter Veen, A. Shulevski, LOFAR Collaboration, M. Kavic, J. H. Simonetti, C. League, J. Tsai, K. S. Obenberger, K. Nathaniel, G. B. Taylor, J. D. Dowell, S. L. Liebling, J. A. Estes, M. Lippert, I. Sharma, P. Vincent, B. Farella, L. L. Wavelength Array, A. U. Abeysekara, A. Albert, R. Alfaro, C. Alvarez, R. Arceo, J. C. Arteaga- Velázquez, D. Avila Rojas, H. A. Ayala Solares, A. S. Barber, J. Becerra Gonzalez, A. Becerril, E. Belmont-Moreno, S. Y. BenZvi, D. Berley, A. Bernal, J. Braun, C. Brisbois, K. S. Caballero-Mora, T. Capistrán, A. Carramiñana, S. Casanova, M. Castillo, U. Cotti, J. Cotzomi, S. Coutiño de León, C. De León, E. De la Fuente, R. Diaz Hernandez, S. Dichiara, B. L. Dingus, M. A. DuVernois, J. C. Díaz-Vélez, R. W. Ellsworth, K. Engel, O. Enríquez-Rivera, D. W. Fiorino, H. Fleischhack, N. Fraija, J. A. García-González, F. Garfias, M. Gerhardt, A. Gonzõlez Muñoz, M. M. González, J. A. Goodman, Z. Hampel-Arias, J. P. Harding, S. Hernandez, A. Hernandez- Almada, B. Hona, P. Hüntemeyer, A. Iriarte, A. Jardin-Blicq, V. Joshi, S. Kaufmann, D. Kieda, A. Lara, R. J.

Lauer, D. Lennarz, H. León Vargas, J. T. Linnemann, A. L. Longinotti, G. L. Raya, R. Luna- García, R. López-Coto, K. Malone, S. S. Marinelli, O. Martinez, I. Martinez- Castellanos, J. Martínez-Castro, H. Martínez-Huerta, J. A. Matthews, P. Miranda-Romagnoli, E. Moreno, M. Mostafá, L. Nellen, M. Newbold, M. U. Nisa, R. Noriega-Papaqui, R. Pelayo, J. Pretz, E. G. Pérez-Pérez, Z. Ren, C. D. Rho, C. Rivière, D. Rosa- González, M. Rosenberg, E. Ruiz-Velasco, H. Salazar, F. Salesa Greus, A. Sandoval, M. Schneider, H. Schoorlemmer, G. Sinnis, A. J. Smith, R. W. Springer, P. Surajbali, O. Tibolla, K. Tollefson, I. Torres, T. N. Ukwatta, T. Weisgarber, S. Westerhoff, I. G. Wisher, J. Wood, T. Yapici, G. B. Yodh, P. W. Younk, H. Zhou, J. D. Álvarez, HAWC Collaboration, A. Aab, P. Abreu, M. Aglietta, I. F. M. Albuquerque, J. M. Albury, I. Allekotte, A. Almela, J. Alvarez Castillo, J. Alvarez-Muñiz, G. A. Anastasi, L. Anchordoqui, B. Andrada, S. Andringa, C. Aramo, N. Arsene, H. Asorey, P. Assis, G. Avila, A. M. Badescu, A. Balaceanu, F. Barbato, R. J. Barreira Luz, K. H. Becker, J. A. Bellido, C. Berat, M. E. Bertaina, X. Bertou, P. L. Biermann, J. Biteau, S. G. Blaess, A. Blanco, J. Blazek, C. Bleve, M. Boháčová, C. Bonifazi, N. Borodai, A. M. Botti, J. Brack, I. Brancus, T. Bretz, A. Bridgeman, F. L. Briechle, P. Buchholz, A. Bueno, S. Buitink, M. Buscemi, K. S. Caballero-Mora, L. Caccianiga, A. Cancio, F. Canfora, R. Caruso, A. Castellina, F. Catalani, G. Cataldi, L. Cazon, A. G. Chavez, J. A. Chinellato, J. Chudoba, R. W. Clay, A. C. Cobos Cerutti, R. Colalillo, A. Coleman, L. Collica, M. R. Coluccia, R. Conceição, G. Consolati, F. Contreras, M. J. Cooper, S. Coutu, C. E. Covault, J. Cronin, S. D'Amico, B. Daniel, S. Dasso, K. Daumiller, B. R. Dawson, J. A. Day, R. M. de Almeida, S. J. de Jong, G. De Mauro, J. R. T. de Mello Neto, I. De Mitri, J. de Oliveira, V. de Souza, J. Debatin, O. Deligny, M. L. Díaz Castro, F. Diogo, C. Dobrigkeit, J. C. D'Olivo, Q. Dorosti, R. C. Dos Anjos, M. T. Dova, A. Dundovic, J. Ebr, R. Engel, M. Erdmann, M. Erfani, C. O. Escobar, J. Espadanal, A. Etchegoyen, H. Falcke, J. Farmer, G. Farrar, A. C. Fauth, N. Fazzini, F. Feldbusch, F. Fenu, B. Fick, J. M. Figueira, A. Filipčič, M. M. Freire, T. Fujii, A. Fuster, R. Gaïor, B. García, F. Gaté, H. Gemmeke, A. Gherghel-Lascu, P. L. Ghia, U. Giaccari, M. Giammarchi, M. Giller, D. Głas, C. Glaser, G. Golup, M. Gómez Berisso, P. F. Gómez Vitale, N. González, A. Gorgi, M. Gottowik, A. F. Grillo, T. D. Grubb, F. Guarino, G. P. Guedes, R. Halliday, M. R. Hampel, P. Hansen, D. Harari, T. A. Harrison, V. M. Harvey, A. Haungs, T. Hebbeker, D. Heck, P. Heimann, A. E. Herve, G. C. Hill, C. Hojvat, E. Holt, P. Homola, J. R. Hörandel, P. Horvath, M. Hrabovský, T. Huege, J. Hulsman, A. Insolia, P. G. Isar, I. Jandt, J. A. Johnsen, M. Josebachuili, J. Jurysek, A. Kääpä, K. H. Kampert, B. Keilhauer, N. Kemmerich, J. Kemp, R. M. Kieckhafer, H. O. Klages, M. Kleifges, J. Kleinfeller, R. Krause, N. Krohm, D. Kuempel, G. Kukec Mezek, N. Kunka, A. Kuotb Awad, B. L. Lago, D. LaHurd, R. G. Lang, M. Lauscher, R. Legumina, M. A. Leigui de Oliveira, A. Letessier-Selvon, I. Lhenry-Yvon, K. Link, D. Lo Presti, L. Lopes, R. López, A. López Casado, R. Lorek, Q. Luce, A. Lucero, M. Malacari, M. Mallamaci, D. Mandat, P. Mantsch, A. G. Mariazzi, I. C. Maris, G. Marsella, D. Martello, H. Martinez, O. Martínez Bravo, J. J. Masías Meza, H. J. Mathes, S. Mathys, J. Matthews, G. Matthiae, E. Mayotte, P. O. Mazur, C. Medina, G. Medina-Tanco, D. Melo, A. Menshikov, K. D. Merenda, S. Michal, M. I. Micheletti, L. Middendorf, L. Miramonti, B. Mitrica, D. Mockler, S. Mollerach, F. Montanet, C. Morello,

G. Morlino, A. L. Müller, G. Müller, M. A. Muller, S. Müller, R. Mussa, I. Naranjo, P. H. Nguyen, M. Niculescu-Oglinzanu, M. Niechciol, L. Niemietz, T. Niggemann, D. Nitz, D. Nosek, V. Novotny, L. Nožka, L. A. Núñez, F. Oikonomou, A. Olinto, M. Palatka, J. Pallotta, P. Papenbreer, G. Parente, A. Parra, T. Paul, M. Pech, F. Pedreira, J. Pękala, J. Peña-Rodriguez, L. A. S. Pereira, M. Perlin, L. Perrone, C. Peters, S. Petrera, J. Phuntsok, T. Pierog, M. Pimenta, V. Pirronello, M. Platino, M. Plum, J. Poh, C. Porowski, R. R. Prado, P. Privitera, M. Prouza, E. J. Quel, S. Querchfeld, S. Quinn, R. Ramos-Pollan, J. Rautenberg, D. Ravignani, J. Ridky, F. Riehn, M. Risse, P. Ristori, V. Rizi, W. Rodrigues de Carvalho, G. Rodriguez Fernandez, J. Rodriguez Rojo, M. J. Roncoroni, M. Roth, E. Roulet, A. C. Rovero, P. Ruehl, S. J. Saffi, A. Saftoiu, F. Salamida, H. Salazar, A. Saleh, G. Salina, F. Sánchez, P. Sanchez-Lucas, E. M. Santos, E. Santos, F. Sarazin, R. Sarmento, C. Sarmiento-Cano, R. Sato, M. Schauer, V. Scherini, H. Schieler, M. Schimp, D. Schmidt, O. Scholten, P. Schovánek, F. G. Schröder, S. Schröder, A. Schulz, J. Schumacher, S. J. Sciutto, A. Segreto, A. Shadkam, R. C. Shellard, G. Sigl, G. Silli, R. Šmída, G. R. Snow, P. Sommers, S. Sonntag, J. F. Soriano, R. Squartini, D. Stanca, S. Stanič, J. Stasielak, P. Stassi, M. Stolpovskiy, F. Strafella, A. Streich, F. Suarez, M. Suarez-Durán, T. Sudholz, T. Suomijärvi, A. D. Supanitsky, J. Šupík, J. Swain, Z. Szadkowski, A. Taboada, O. A. Taborda, C. Timmermans, C. J. Todero Peixoto, L. Tomankova, B. Tomé, G. Torralba Elipe, P. Travnicek, M. Trini, M. Tueros, R. Ulrich, M. Unger, M. Urban, J. F. Valdés Galicia, I. Valiño, L. Valore, G. van Aar, P. van Bodegom, A. M. van den Berg, A. van Vliet, E. Varela, B. Vargas Cárdenas, R. A. Vázquez, D. Veberič, C. Ventura, I. D. Vergara Quispe, V. Verzi, J. Vicha, L. Villaseñor, S. Vorobiov, H. Wahlberg, O. Wainberg, D. Walz, A. A. Watson, M. Weber, A. Weindl, M. Wiedeński, L. Wiencke, H. Wilczyński, M. Wirtz, D. Wittkowski, B. Wundheiler, L. Yang, A. Yushkov, E. Zas, D. Zavrtanik, M. Zavrtanik, A. Zepeda, B. Zimmermann, M. Ziolkowski, Z. Zong, F. Zuccarello, The Pierre Auger Collaboration, S. Kim, S. Schulze, F. E. Bauer, J. M. Corral-Santana, I. de Gregorio- Monsalvo, J. González-López, D. H. Hartmann, C. H. Ishwara-Chandra, S. Martín, A. Mehner, K. Misra, M. J. Michałowski, L. Resmi, ALMA Collaboration, Z. Paragi, I. Agudo, T. An, R. Beswick, C. Casadio, S. Frey, P. Jonker, M. Kettenis, B. Marcote, J. Moldon, A. Szomoru, H. J. van Langevelde, J. Yang, Euro VLBI Team, A. Cwiek, M. Cwiok, H. Czyrkowski, R. Dabrowski, G. Kasprowicz, L. Mankiewicz, K. Nawrocki, R. Opiela, L. W. Piotrowski, G. Wrochna, M. Zaremba, A. F. Żarnecki, Pi of the Sky Collaboration, D. Haggard, M. Nynka, J. J. Ruan, The Chandra Team at McGill University, P. A. Bland, T. Booler, H. A. R. Devillepoix, J. S. de Gois, P. J. Hancock, R. M. Howie, J. Paxman, E. K. Sansom, M. C. Towner, D. Desert Fireball Network, J. Tonry, M. Coughlin, C. W. Stubbs, L. Denneau, A. Heinze, B. Stalder, H. Weiland, ATLAS, R. P. Eatough, M. Kramer, A. Kraus, H. Time Resolution Universe Survey, E. Troja, L. Piro, J. Becerra González, N. R. Butler, O. D. Fox, H. G. Khandrika, A. Kutyrev, W. H. Lee, R. Ricci, J. Ryan, R. E., R. Sánchez-Ramírez, S. Veilleux, A. M. Watson, M. H. Wieringa, J. M. Burgess, H. van Eerten, C. J. Fontes, C. L. Fryer, O. Korobkin, R. T. Wollaeger, RIMAS, RATIR, F. Camilo, A. R. Foley, S. Goedhart, S. Makhathini, N. Oozeer, O. M. Smirnov, R. P. Fender, P. A. Woudt and S. South Africa/MeerKAT, "Multi-messenger Observations of a Binary Neutron

Star Merger", *ApJ* **848**, L12 (2017a).

Abbott, B. P., R. Abbott, T. D. Abbott, F. Acernese, K. Ackley, C. Adams, T. Adams, P. Addesso, R. X. Adhikari, V. B. Adya and et al., "GW170817: Observation of Gravitational Waves from a Binary Neutron Star Inspiral", *Phys. Rev. L.* **119**, 16, 161101 (2017b).

Abbott, R., T. D. Abbott, S. Abraham, F. Acernese, K. Ackley, C. Adams, R. X. Adhikari, V. B. Adya, C. Affeldt, M. Agathos and et al., "GW190814: Gravitational Waves from the Coalescence of a 23 Solar Mass Black Hole with a 2.6 Solar Mass Compact Object", *ApJ* **896**, 2, L44 (2020).

Abe, K., Y. Haga, Y. Hayato, M. Ikeda, K. Iyogi, J. Kameda, Y. Kishimoto, M. Miura, S. Moriyama, M. Nakahata, Y. Nakano, S. Nakayama, H. Sekiya, M. Shiozawa, Y. Suzuki, A. Takeda, H. Tanaka, T. Tomura, K. Ueno, R. A. Wendell, T. Yokozawa, T. Irvine, T. Kajita, I. Kametani, K. Kaneyuki, K. P. Lee, T. McLachlan, Y. Nishimura, E. Richard, K. Okumura, L. Labarga, P. Fernandez, S. Berkman, H. A. Tanaka, S. Tobayama, J. Gustafson, E. Kearns, J. L. Raaf, J. L. Stone, L. R. Sulak, M. Goldhaber, G. Carminati, W. R. Kropp, S. Mine, P. Weatherly, A. Renshaw, M. B. Smy, H. W. Sobel, V. Takhistov, K. S. Ganezer, B. L. Hartfiel, J. Hill, W. E. Keig, N. Hong, J. Y. Kim, I. T. Lim, T. Akiri, A. Himmel, K. Scholberg, C. W. Walter, T. Wongjirad, T. Ishizuka, S. Tasaka, J. S. Jang, J. G. Learned, S. Matsuno, S. N. Smith, T. Hasegawa, T. Ishida, T. Ishii, T. Kobayashi, T. Nakadaira, K. Nakamura, Y. Oyama, K. Sakashita, T. Sekiguchi, T. Tsukamoto, A. T. Suzuki, Y. Takeuchi, C. Bronner, S. Hirota, K. Huang, K. Ieki, T. Kikawa, A. Minamino, A. Murakami, T. Nakaya, K. Suzuki, S. Takahashi, K. Tateishi, Y. Fukuda, K. Choi, Y. Itow, G. Mitsuka, P. Mijakowski, J. Hignight, J. Imber, C. K. Jung, C. Yanagisawa, M. J. Wilking, H. Ishino, A. Kibayashi, Y. Koshio, T. Mori, M. Sakuda, R. Yamaguchi, T. Yano, Y. Kuno, R. Tacik, S. B. Kim, H. Okazawa, Y. Choi, K. Nishijima, M. Koshiba, Y. Suda, Y. Totsuka, M. Yokoyama, K. Martens, L. Marti, M. R. Vagins, J. F. Martin, P. de Perio, A. Konaka, S. Chen, Y. Zhang, K. Connolly and R. J. Wilkes, "Real-time supernova neutrino burst monitor at Super-Kamiokande", Astroparticle Physics **81**, 39–48 (2016).

Abe, S., S. Asami, M. Eizuka, S. Futagi, A. Gando, Y. Gando, T. Gima, A. Goto, T. Hachiya, K. Hata, S. Hayashida, K. Hosokawa, K. Ichimura, S. Ieki, H. Ikeda, K. Inoue, K. Ishidoshiro, Y. Kamei, N. Kawada, Y. Kishimoto, M. Koga, M. Kurasawa, N. Maemura, T. Mitsui, H. Miyake, T. Nakahata, K. Nakamura, K. Nakamura, R. Nakamura, H. Ozaki, T. Sakai, H. Sambonsugi, I. Shimizu, J. Shirai, K. Shiraishi, A. Suzuki, Y. Suzuki, A. Takeuchi, K. Tamae, K. Ueshima, H. Watanabe, Y. Yoshida, S. Obara, A. K. Ichikawa, D. Chernyak, A. Kozlov, K. Z. Nakamura, S. Yoshida, Y. Takemoto, S. Umehara, K. Fushimi, K. Kotera, Y. Urano, B. E. Berger, B. K. Fujikawa, J. G. Learned, J. Maricic, S. N. Axani, J. Smolsky, Z. Fu, L. A. Winslow, Y. Efremenko, H. J. Karwowski, D. M. Markoff, W. Tornow, S. Dell'Oro, T. O'Donnell, J. A. Detwiler, S. Enomoto, M. P. Decowski, C. Grant, A. Li, H. Song and KamLAND-Zen Collaboration, "Search for the Majorana Nature of Neutrinos in the Inverted Mass Ordering Region with KamLAND-Zen", *Phys. Rev. L.* **130**, 5, 051801 (2023).

Acciarri, R., M. A. Acero, M. Adamowski, C. Adams, P. Adamson, S. Adhikari, Z. Ahmad, C. H. Albright, T. Alion, E. Amador and et al., "Long-Baseline Neutrino Facility (LBNF) and Deep Underground Neutrino Experiment (DUNE) Conceptual Design Report, Volume 4 The DUNE Detectors at LBNF", arXiv e-prints p. arXiv:1601.02984 (2016).

Acernese, F., M. Agathos, K. Agatsuma, D. Aisa, N. Allemandou, A. Allocca, J. Amarni, P. Astone, G. Balestri, G. Ballardin and et al., "Advanced Virgo: a second-generation interferometric gravitational wave detector", Classical and Quantum Gravity **32**, 2, 024001 (2015).

Ackermann, M., M. Bustamante, L. Lu, N. Otte, M. H. Reno, S. Wissel, M. Ackermann, S. K. Agarwalla, J. Alvarez-Muñiz, R. Alves Batista, C. A. Argüelles, M. Bustamante, B. A. Clark, A. Cummings, S. Das, V. Decoene, P. B. Denton, D. Dornic, Z.-A. Dzhilkibaev, Y. Farzan, A. Garcia, M. V. Garzelli, C. Glaser, A. Heijboer, J. R. Hörandel, G. Illuminati, Y. Seon Jeong, J. L. Kelley, K. J. Kelly, A. Kheirandish, S. R. Klein, J. F. Krizmanic, M. J. Larson, L. Lu, K. Murase, A. Narang, N. Otte, R. L. Prechelt, S. Prohira, M. H. Reno, E. Resconi, M. Santander, V. B. Valera, J. Vandenbroucke, O. Vasil'evna Suvorova, L. Wiencke, S. Wissel, S. Yoshida, T. Yuan, E. Zas, P. Zhelnin, B. Zhou, L. A. Anchordoqui, Y. Ashida, M. Bagheri, A. Balagopal, V. Basu, J. Beatty, K. Bechtol, N. Bell, A. Bishop, J. Book, A. Brown, A. Burgman, M. Campana, N. Chau, T. Y. Chen, A. Coleman, A. Connolly, J. M. Conrad, P. Correa, C. Creque-Sarbinowski, A. Cummings, Z. Curtis-Ginsberg, P. Dasgupta, S. De Kockere, K. de Vries, C. Deaconu, A. Desai, T. DeYoung, A. di Matteo, D. Elsaesser, P. Fürst, K. L. Fan, A. Fedynitch, D. Fox, E. Ganster, M. H. Minh, C. Haack, S. Hallman, F. Halzen, A. Haungs, A. Ishihara, E. Judd, T. Karg, A. Karle, T. Katori, A. Kochocki, C. Kopper, M. Kowalski, I. Kravchenko, N. Kurahashi, M. Lamoureux, H. León Vargas, M. Lincetto, Q. Liu, J. Madsen, Y. Makino, J. Mammo, Z. Marka, E. Mayotte, K. Meagher, M. Meier, M. H. Minh, L. Miramonti, M. Moulai, K. Mulrey, M. Muzio, R. Naab, A. Nelles, W. Nichols, A. Nozdrina, E. O'Sullivan, V. O´Dell, J. Osborne, V. Pandey, E. N. Paudel, A. Pizzuto, M. Plum, C. Pobes Aranda, L. Pyras, C. Raab, Z. Rechav, J. Rojo, O. Romero Matamala, M. Santander, P. Savina, F. Schroeder, L. Schumacher, S. Sciutto, S. Sclafani, M. Ful Hossain Seikh, M. Silva, R. Singh, D. Smith, S. T. Spencer, R. W. Springer, J. Stachurska, O. Suvorova, I. Taboada, S. Toscano, M. Tueros, J. P. Twagirayezu, N. van Eijndhoven, P. Veres, A. Vieregg, W. Wang, N. Whitehorn, W. Winter, E. Yildizci and S. Yu, "High-energy and ultra-high-energy neutrinos: A Snowmass white paper", Journal of High Energy Astrophysics **36**, 55–110 (2022).

Ahmad, Q. R., R. C. Allen, T. C. Andersen, J. D. Anglin, J. C. Barton, E. W. Beier, M. Bercovitch, J. Bigu, S. D. Biller, R. A. Black, I. Blevis, R. J. Boardman, J. Boger, E. Bonvin, M. G. Boulay, M. G. Bowler, T. J. Bowles, S. J. Brice, M. C. Browne, T. V. Bullard, G. Bühler, J. Cameron, Y. D. Chan, H. H. Chen, M. Chen, X. Chen, B. T. Cleveland, E. T. Clifford, J. H. Cowan, D. F. Cowen, G. A. Cox, X. Dai, F. Dalnoki-Veress, W. F. Davidson, P. J. Doe, G. Doucas, M. R. Dragowsky, C. A. Duba, F. A. Duncan, M. Dunford, J. A. Dunmore, E. D. Earle, S. R. Elliott, H. C. Evans, G. T. Ewan, J. Farine, H. Fergani, A. P. Ferraris, R. J.

Ford, J. A. Formaggio, M. M. Fowler, K. Frame, E. D. Frank, W. Frati, N. Gagnon, J. V. Germani, S. Gil, K. Graham, D. R. Grant, R. L. Hahn, A. L. Hallin, E. D. Hallman, A. S. Hamer, A. A. Hamian, W. B. Handler, R. U. Haq, C. K. Hargrove, P. J. Harvey, R. Hazama, K. M. Heeger, W. J. Heintzelman, J. Heise, R. L. Helmer, J. D. Hepburn, H. Heron, J. Hewett, A. Hime, M. Howe, J. G. Hykawy, M. C. Isaac, P. Jagam, N. A. Jelley, C. Jillings, G. Jonkmans, K. Kazkaz, P. T. Keener, J. R. Klein, A. B. Knox, R. J. Komar, R. Kouzes, T. Kutter, C. C. Kyba, J. Law, I. T. Lawson, M. Lay, H. W. Lee, K. T. Lesko, J. R. Leslie, I. Levine, W. Locke, S. Luoma, J. Lyon, S. Majerus, H. B. Mak, J. Maneira, J. Manor, A. D. Marino, N. McCauley, A. B. McDonald, D. S. McDonald, K. McFarlane, G. McGregor, R. Meijer Drees, C. Mifflin, G. G. Miller, G. Milton, B. A. Moffat, M. Moorhead, C. W. Nally, M. S. Neubauer, F. M. Newcomer, H. S. Ng, A. J. Noble, E. B. Norman, V. M. Novikov, M. O'Neill, C. E. Okada, R. W. Ollerhead, M. Omori, J. L. Orrell, S. M. Oser, A. W. Poon, T. J. Radcliffe, A. Roberge, B. C. Robertson, R. G. Robertson, S. S. Rosendahl, J. K. Rowley, V. L. Rusu, E. Saettler, K. K. Schaffer, M. H. Schwendener, A. Schülke, H. Seifert, M. Shatkay, J. J. Simpson, C. J. Sims, D. Sinclair, P. Skensved, A. R. Smith, M. W. Smith, T. Spreitzer, N. Starinsky, T. D. Steiger, R. G. Stokstad, L. C. Stonehill, R. S. Storey, B. Sur, R. Tafirout, N. Tagg, N. W. Tanner, R. K. Taplin, M. Thorman, P. M. Thornewell, P. T. Trent, Y. I. Tserkovnyak, R. van Berg, R. G. van de Water, C. J. Virtue, C. E. Waltham, J. X. Wang, D. L. Wark, N. West, J. B. Wilhelmy, J. F. Wilkerson, J. R. Wilson, P. Wittich, J. M. Wouters and M. Yeh, "Direct Evidence for Neutrino Flavor Transformation from Neutral-Current Interactions in the Sudbury Neutrino Observatory", *Phys. Rev. L.***89**, 1, 011301 (2002).

Akutsu, T., M. Ando, K. Arai, Y. Arai, S. Araki, A. Araya, N. Aritomi, H. Asada, Y. Aso, S. Bae and et al., "Overview of KAGRA: Calibration, detector characterization, physical environmental monitors, and the geophysics interferometer", Progress of Theoretical and Experimental Physics **2021**, 5, 05A102 (2021).

Al Kharusi, S., S. Y. BenZvi, J. S. Bobowski, W. Bonivento, V. Brdar, T. Brunner, E. Caden, M. Clark, A. Coleiro, M. Colomer-Molla, J. I. Crespo-Anadón, A. Depoian, D. Dornic, V. Fischer, D. Franco, W. Fulgione, A. Gallo Rosso, M. Geske, S. Griswold, M. Gromov, D. Haggard, A. Habig, O. Halim, A. Higuera, R. Hill, S. Horiuchi, K. Ishidoshiro, C. Kato, E. Katsavounidis, D. Khaitan, J. P. Kneller, A. Kopec, V. Kulikovskiy, M. Lai, M. Lamoureux, R. F. Lang, H. L. Li, M. Lincetto, C. Lunardini, J. Migenda, D. Milisavljevic, M. E. McCarthy, E. O Connor, E. O Sullivan, G. Pagliaroli, D. Patel, R. Peres, B. W. Pointon, J. Qin, N. Raj, A. Renshaw, A. Roeth, J. Rumleskie, K. Scholberg, A. Sheshukov, T. Sonley, M. Strait, V. Takhistov, I. Tamborra, J. Tseng, C. D. Tunnell, J. Vasel, C. F. Vigorito, B. Viren, C. J. Virtue, J. S. Wang, L. J. Wen, L. Winslow, F. L. H. Wolfs, X. J. Xu and Y. Xu, "SNEWS 2.0: a next-generation supernova early warning system for multi-messenger astronomy", New Journal of Physics **23**, 3, 031201 (2021).

Alastuey, A. and B. Jancovici, "Nuclear reaction rate enhancement in dense stellar matter", *ApJ***226**, 1034–1040 (1978).

Albert, A., M. André, M. Anghinolfi, M. Ardid, J. J. Aubert, J. Aublin, T. Avgitas, B. Baret, J. Barrios-Martí, S. Basa, B. Belhorma, V. Bertin, S. Biagi, R. Bor-

muth, S. Bourret, M. C. Bouwhuis, H. Brânzaș, R. Bruijn, J. Brunner, J. Busto, A. Capone, L. Caramete, J. Carr, S. Celli, R. Cherkaoui El Moursli, T. Chiarusi, M. Circella, J. A. B. Coelho, A. Coleiro, R. Coniglione, H. Costantini, P. Coyle, A. Creusot, A. F. Díaz, A. Deschamps, G. De Bonis, C. Distefano, I. Di Palma, A. Domi, C. Donzaud, D. Dornic, D. Drouhin, T. Eberl, I. El Bojaddaini, N. El Khayati, D. Elsässer, A. Enzenhöfer, A. Ettahiri, F. Fassi, I. Felis, L. A. Fusco, P. Gay, V. Giordano, H. Glotin, T. Grégoire, R. G. Ruiz, K. Graf, S. Hallmann, H. van Haren, A. J. Heijboer, Y. Hello, J. J. Hernández-Rey, J. Hößl, J. Hofestädt, G. Illuminati, C. W. James, M. de Jong, M. Jongen, M. Kadler, O. Kalekin, U. Katz, D. Kießling, A. Kouchner, M. Kreter, I. Kreykenbohm, V. Kulikovskiy, C. Lachaud, R. Lahmann, D. Lefèvre, E. Leonora, M. Lotze, S. Loucatos, M. Marcelin, A. Margiotta, A. Marinelli, J. A. Martínez-Mora, R. Mele, K. Melis, T. Michael, P. Migliozzi, A. Moussa, S. Navas, E. Nezri, M. Organokov, G. E. Păvălaș, C. Pellegrino, C. Perrina, P. Piattelli, V. Popa, T. Pradier, L. Quinn, C. Racca, G. Riccobene, A. Sánchez-Losa, M. Saldaña, I. Salvadori, D. F. E. Samtleben, M. Sanguineti, P. Sapienza, F. Schüssler, C. Sieger, M. Spurio, T. Stolarczyk, M. Taiuti, Y. Tayalati, A. Trovato, D. Turpin, C. Tönnis, B. Vallage, V. Van Elewyck, F. Versari, D. Vivolo, A. Vizzoca, J. Wilms, J. D. Zornoza, J. Zúñiga, ANTARES Collaboration, M. G. Aartsen, M. Ackermann, J. Adams, J. A. Aguilar, M. Ahlers, M. Ahrens, I. A. Samarai, D. Altmann, K. Andeen, T. Anderson, I. Ansseau, G. Anton, C. Argüelles, J. Auffenberg, S. Axani, H. Bagherpour, X. Bai, J. P. Barron, S. W. Barwick, V. Baum, R. Bay, J. J. Beatty, J. Becker Tjus, K. H. Becker, S. BenZvi, D. Berley, E. Bernardini, D. Z. Besson, G. Binder, D. Bindig, E. Blaufuss, S. Blot, C. Bohm, M. Börner, F. Bos, D. Bose, S. Böser, O. Botner, E. Bourbeau, J. Bourbeau, F. Bradascio, J. Braun, L. Brayeur, M. Brenzke, H. P. Bretz, S. Bron, J. Brostean-Kaiser, A. Burgman, T. Carver, J. Casey, M. Casier, E. Cheung, D. Chirkin, A. Christov, K. Clark, L. Classen, S. Coenders, G. H. Collin, J. M. Conrad, D. F. Cowen, R. Cross, M. Day, J. P. A. M. de André, C. De Clercq, J. J. DeLaunay, H. Dembinski, S. De Ridder, P. Desiati, K. D. de Vries, G. de Wasseige, M. de With, T. DeYoung, J. C. Díaz-Vélez, V. di Lorenzo, H. Dujmovic, J. P. Dumm, M. Dunkman, E. Dvorak, B. Eberhardt, T. Ehrhardt, B. Eichmann, P. Eller, P. A. Evenson, S. Fahey, A. R. Fazely, J. Felde, K. Filimonov, C. Finley, S. Flis, A. Franckowiak, E. Friedman, T. Fuchs, T. K. Gaisser, J. Gallagher, L. Gerhardt, K. Ghorbani, W. Giang, T. Glauch, T. Glüsenkamp, A. Goldschmidt, J. G. Gonzalez, D. Grant, Z. Griffith, C. Haack, A. Hallgren, F. Halzen, K. Hanson, D. Hebecker, D. Heereman, K. Helbing, R. Hellauer, S. Hickford, J. Hignight, G. C. Hill, K. D. Hoffman, R. Hoffmann, B. Hokanson-Fasig, K. Hoshina, F. Huang, M. Huber, K. Hultqvist, M. Hünnefeld, S. In, A. Ishihara, E. Jacobi, G. S. Japaridze, M. Jeong, K. Jero, B. J. P. Jones, P. Kalaczynski, W. Kang, A. Kappes, T. Karg, A. Karle, U. Katz, M. Kauer, A. Keivani, J. L. Kelley, A. Kheirand ish, J. Kim, M. Kim, T. Kintscher, J. Kiryluk, T. Kittler, S. R. Klein, G. Kohnen, R. Koirala, H. Kolanoski, L. Köpke, C. Kopper, S. Kopper, J. P. Koschinsky, D. J. Koskinen, M. Kowalski, K. Krings, M. Kroll, G. Krückl, J. Kunnen, S. Kunwar, N. Kurahashi, T. Kuwabara, A. Kyriacou, M. Labare, J. L. Lanfranchi, M. J. Larson, F. Lauber, M. Lesiak-Bzdak, M. Leuermann, Q. R. Liu, L. Lu, J. Lünemann, W. Luszczak, J. Madsen, G. Maggi, K. B. M. Mahn, S. Mancina, R. Maruyama, K. Mase, R. Maunu, F. McNally, K. Meagher,

M. Medici, M. Meier, T. Menne, G. Merino, T. Meures, S. Miarecki, J. Micallef, G. Momenté, T. Montaruli, R. W. Moore, M. Moulai, R. Nahnhauer, P. Nakarmi, U. Naumann, G. Neer, H. Niederhausen, S. C. Nowicki, D. R. Nygren, A. Obertacke Pollmann, A. Olivas, A. O'Murchadha, T. Palczewski, H. Pand ya, D. V. Pankova, P. Peiffer, J. A. Pepper, C. Pérez de los Heros, D. Pieloth, E. Pinat, M. Plum, D. Pranav, P. B. Price, G. T. Przybylski, C. Raab, L. Rädel, M. Rameez, K. Rawlins, I. C. Rea, R. Reimann, B. Relethford, M. Relich, E. Resconi, W. Rhode, M. Richman, S. Robertson, M. Rongen, C. Rott, T. Ruhe, D. Ryckbosch, D. Rysewyk, T. Sälzer, S. E. Sanchez Herrera, A. Sand rock, J. Sandroos, M. Santander, S. Sarkar, S. Sarkar, K. Satalecka, P. Schlunder, T. Schmidt, A. Schneider, S. Schoenen, S. Schöneberg, L. Schumacher, D. Seckel, S. Seunarine, J. Soedingrekso, D. Soldin, M. Song, G. M. Spiczak, C. Spiering, J. Stachurska, M. Stamatikos, T. Stanev, A. Stasik, J. Stettner, A. Steuer, T. Stezelberger, R. G. Stokstad, A. Stößl, N. L. Strotjohann, T. Stuttard, G. W. Sullivan, M. Sutherland, I. Taboada, J. Tatar, F. Tenholt, S. Ter-Antonyan, A. Terliuk, G. Tešić, S. Tilav, P. A. Toale, M. N. Tobin, S. Toscano, D. Tosi, M. Tselengidou, C. F. Tung, A. Turcati, C. F. Turley, B. Ty, E. Unger, M. Usner, J. Vandenbroucke, W. Van Driessche, N. van Eijndhoven, S. Vanheule, J. van Santen, M. Vehring, E. Vogel, M. Vraeghe, C. Walck, A. Wallace, M. Wallraff, F. D. Wandler, N. Wandkowsky, A. Waza, C. Weaver, M. J. Weiss, C. Wendt, J. Werthebach, S. Westerhoff, B. J. Whelan, K. Wiebe, C. H. Wiebusch, L. Wille, D. R. Williams, L. Wills, M. Wolf, J. Wood, T. R. Wood, E. Woolsey, K. Woschnagg, D. L. Xu, X. W. Xu, Y. Xu, J. P. Yanez, G. Yodh, S. Yoshida, T. Yuan, M. Zoll, IceCube Collaboration, A. Aab, P. Abreu, M. Aglietta, I. F. M. Albuquerque, J. M. Albury, I. Allekotte, A. Almela, J. Alvarez Castillo, J. Alvarez-Muñiz, G. A. Anastasi, L. Anchordoqui, B. Andrada, S. Andringa, C. Aramo, N. Arsene, H. Asorey, P. Assis, G. Avila, A. M. Badescu, A. Balaceanu, F. Barbato, R. J. Barreira Luz, J. J. Beatty, K. H. Becker, J. A. Bellido, C. Berat, M. E. Bertaina, X. Bertou, P. L. Biermann, J. Biteau, S. G. Blaess, A. Blanco, J. Blazek, C. Bleve, M. Boháčová, C. Bonifazi, N. Borodai, A. M. Botti, J. Brack, I. Brancus, T. Bretz, A. Bridgeman, F. L. Briechle, P. Buchholz, A. Bueno, S. Buitink, M. Buscemi, K. S. Caballero-Mora, L. Caccianiga, A. Cancio, F. Canfora, R. Caruso, A. Castellina, F. Catalani, G. Cataldi, L. Cazon, A. G. Chavez, J. A. Chinellato, J. Chudoba, R. W. Clay, A. C. Cobos Cerutti, R. Colalillo, A. Coleman, L. Collica, M. R. Coluccia, R. Conceição, G. Consolati, F. Contreras, M. J. Cooper, S. Coutu, C. E. Covault, J. Cronin, S. D'Amico, B. Daniel, S. Dasso, K. Daumiller, B. R. Dawson, J. A. Day, R. M. de Almeida, S. J. de Jong, G. De Mauro, J. R. T. de Mello Neto, I. De Mitri, J. de Oliveira, V. de Souza, J. Debatin, O. Deligny, M. L. Díaz Castro, F. Diogo, C. Dobrigkeit, J. C. D'Olivo, Q. Dorosti, R. C. dos Anjos, M. T. Dova, A. Dundovic, J. Ebr, R. Engel, M. Erdmann, M. Erfani, C. O. Escobar, J. Espadanal, A. Etchegoyen, H. Falcke, J. Farmer, G. Farrar, A. C. Fauth, N. Fazzini, F. Feldbusch, F. Fenu, B. Fick, J. M. Figueira, A. Filipčič, M. M. Freire, T. Fujii, A. Fuster, R. Gaïor, B. García, F. Gaté, H. Gemmeke, A. Gherghel-Lascu, P. L. Ghia, U. Giaccari, M. Giammarchi, M. Giller, D. Głas, C. Glaser, G. Golup, M. Gómez Berisso, P. F. Gómez Vitale, N. González, A. Gorgi, M. Gottowik, A. F. Grillo, T. D. Grubb, F. Guarino, G. P. Guedes, R. Halliday, M. R. Hampel, P. Hansen, D. Harari, T. A. Harrison, V. M. Harvey, A. Haungs, T. Hebbeker, D. Heck, P. Heimann, A. E. Herve, G. C. Hill, C. Hojvat,

E. Holt, P. Homola, J. R. Hörandel, P. Horvath, M. Hrabovský, T. Huege, J. Hulsman, A. Insolia, P. G. Isar, I. Jandt, J. A. Johnsen, M. Josebachuili, J. Jurysek, A. Kääpä, K. H. Kampert, B. Keilhauer, N. Kemmerich, J. Kemp, R. M. Kieckhafer, H. O. Klages, M. Kleifges, J. Kleinfeller, R. Krause, N. Krohm, D. Kuempel, G. Kukec Mezek, N. Kunka, A. Kuotb Awad, B. L. Lago, D. LaHurd, R. G. Lang, M. Lauscher, R. Legumina, M. A. Leigui de Oliveira, A. Letessier-Selvon, I. Lhenry-Yvon, K. Link, D. Lo Presti, L. Lopes, R. López, A. López Casado, R. Lorek, Q. Luce, A. Lucero, M. Malacari, M. Mallamaci, D. Mandat, P. Mantsch, A. G. Mariazzi, I. C. Mariş, G. Marsella, D. Martello, H. Martinez, O. Martínez Bravo, J. J. Masías Meza, H. J. Mathes, S. Mathys, J. Matthews, G. Matthiae, E. Mayotte, P. O. Mazur, C. Medina, G. Medina-Tanco, D. Melo, A. Menshikov, K. D. Merenda, S. Michal, M. I. Micheletti, L. Middendorf, L. Miramonti, B. Mitrica, D. Mockler, S. Mollerach, F. Montanet, C. Morello, G. Morlino, M. Mostafá, A. L. Müller, G. Müller, M. A. Muller, S. Müller, R. Mussa, I. Naranjo, L. Nellen, P. H. Nguyen, M. Niculescu-Oglinzanu, M. Niechciol, L. Niemietz, T. Niggemann, D. Nitz, D. Nosek, V. Novotny, L. Nožka, L. A. Núñez, F. Oikonomou, A. Olinto, M. Palatka, J. Pallotta, P. Papenbreer, G. Parente, A. Parra, T. Paul, M. Pech, F. Pedreira, J. Pękala, R. Pelayo, J. Peña-Rodriguez, L. A. S. Pereira, M. Perlin, L. Perrone, C. Peters, S. Petrera, J. Phuntsok, T. Pierog, M. Pimenta, V. Pirronello, M. Platino, M. Plum, J. Poh, C. Porowski, R. R. Prado, P. Privitera, M. Prouza, E. J. Quel, S. Querchfeld, S. Quinn, R. Ramos-Pollan, J. Rautenberg, D. Ravignani, J. Ridky, F. Riehn, M. Risse, P. Ristori, V. Rizi, W. Rodrigues de Carvalho, G. Rodriguez Fernandez, J. Rodriguez Rojo, M. J. Roncoroni, M. Roth, E. Roulet, A. C. Rovero, P. Ruehl, S. J. Saffi, A. Saftoiu, F. Salamida, H. Salazar, A. Saleh, G. Salina, F. Sánchez, P. Sanchez-Lucas, E. M. Santos, E. Santos, F. Sarazin, R. Sarmento, C. Sarmiento-Cano, R. Sato, M. Schauer, V. Scherini, H. Schieler, M. Schimp, D. Schmidt, O. Scholten, P. Schovánek, F. G. Schröder, S. Schröder, A. Schulz, J. Schumacher, S. J. Sciutto, A. Segreto, A. Shadkam, R. C. Shellard, G. Sigl, G. Silli, R. Šmída, G. R. Snow, P. Sommers, S. Sonntag, J. F. Soriano, R. Squartini, D. Stanca, S. Stanič, J. Stasielak, P. Stassi, M. Stolpovskiy, F. Strafella, A. Streich, F. Suarez, M. Suarez Durán, T. Sudholz, T. Suomijärvi, A. D. Supanitsky, J. Šupík, J. Swain, Z. Szadkowski, A. Taboada, O. A. Taborda, C. Timmermans, C. J. Todero Peixoto, L. Tomankova, B. Tomé, G. Torralba Elipe, P. Travnicek, M. Trini, M. Tueros, R. Ulrich, M. Unger, M. Urban, J. F. Valdés Galicia, I. Valiño, L. Valore, G. van Aar, P. van Bodegom, A. M. van den Berg, A. van Vliet, E. Varela, B. Vargas Cárdenas, R. A. Vázquez, D. Veberič, C. Ventura, I. D. Vergara Quispe, V. Verzi, J. Vicha, L. Villaseñor, S. Vorobiov, H. Wahlberg, O. Wainberg, D. Walz, A. A. Watson, M. Weber, A. Weindl, M. Wiedeński, L. Wiencke, H. Wilczyński, M. Wirtz, D. Wittkowski, B. Wundheiler, L. Yang, A. Yushkov, E. Zas, D. Zavrtanik, M. Zavrtanik, A. Zepeda, B. Zimmermann, M. Ziolkowski, Z. Zong, F. Zuccarello, Pierre Auger Collaboration, B. P. Abbott, R. Abbott, T. D. Abbott, F. Acernese, K. Ackley, C. Adams, T. Adams, P. Addesso, R. X. Adhikari, V. B. Adya, C. Affeldt, M. Afrough, B. Agarwal, M. Agathos, K. Agatsuma, N. Aggarwal, O. D. Aguiar, L. Aiello, A. Ain, P. Ajith, B. Allen, G. Allen, A. Allocca, P. A. Altin, A. Amato, A. Ananyeva, S. B. Anderson, W. G. Anderson, S. V. Angelova, S. Antier, S. Appert, K. Arai, M. C. Araya, J. S. Areeda, N. Arnaud, K. G. Arun, S. Ascenzi, G. Ashton, M. Ast, S. M. Aston, P. Astone,

D. V. Atallah, P. Aufmuth, C. Aulbert, K. AultONeal, C. Austin, A. Avila-Alvarez, S. Babak, P. Bacon, M. K. M. Bader, S. Bae, P. T. Baker, F. Baldaccini, G. Ballardin, S. W. Ballmer, S. Banagiri, J. C. Barayoga, S. E. Barclay, B. C. Barish, D. Barker, K. Barkett, F. Barone, B. Barr, L. Barsotti, M. Barsuglia, D. Barta, J. Bartlett, I. Bartos, R. Bassiri, A. Basti, J. C. Batch, M. Bawaj, J. C. Bayley, M. Bazzan, B. Bécsy, C. Beer, M. Bejger, I. Belahcene, A. S. Bell, B. K. Berger, G. Bergmann, J. J. Bero, C. P. L. Berry, D. Bersanetti, A. Bertolini, J. Betzwieser, S. Bhagwat, R. Bhandare, I. A. Bilenko, G. Billingsley, C. R. Billman, J. Birch, R. Birney, O. Birnholtz, S. Biscans, S. Biscoveanu, A. Bisht, M. Bitossi, C. Biwer, M. A. Bizouard, J. K. Blackburn, J. Blackman, C. D. Blair, D. G. Blair, R. M. Blair, S. Bloemen, O. Bock, N. Bode, M. Boer, G. Bogaert, A. Bohe, F. Bondu, E. Bonilla, R. Bonnand, B. A. Boom, R. Bork, V. Boschi, S. Bose, K. Bossie, Y. Bouffanais, A. Bozzi, C. Bradaschia, P. R. Brady, M. Branchesi, J. E. Brau, T. Briant, A. Brillet, M. Brinkmann, V. Brisson, P. Brockill, J. E. Broida, A. F. Brooks, D. A. Brown, D. D. Brown, S. Brunett, C. C. Buchanan, A. Buikema, T. Bulik, H. J. Bulten, A. Buonanno, D. Buskulic, C. Buy, R. L. Byer, M. Cabero, L. Cadonati, G. Cagnoli, C. Cahillane, J. Calderón Bustillo, T. A. Callister, E. Calloni, J. B. Camp, M. Canepa, P. Canizares, K. C. Cannon, H. Cao, J. Cao, C. D. Capano, E. Capocasa, F. Carbognani, S. Caride, M. F. Carney, J. Casanueva Diaz, C. Casentini, S. Caudill, M. Cavaglià, F. Cavalier, R. Cavalieri, G. Cella, C. B. Cepeda, P. Cerdá-Durán, G. Cerretani, E. Cesarini, S. J. Chamberlin, M. Chan, S. Chao, P. Charlton, E. Chase, E. Chassand e-Mottin, D. Chatterjee, B. D. Cheeseboro, H. Y. Chen, X. Chen, Y. Chen, H. P. Cheng, H. Chia, A. Chincarini, A. Chiummo, T. Chmiel, H. S. Cho, M. Cho, J. H. Chow, N. Christensen, Q. Chu, A. J. K. Chua, S. Chua, A. K. W. Chung, S. Chung, G. Ciani, R. Ciolfi, C. E. Cirelli, A. Cirone, F. Clara, J. A. Clark, P. Clearwater, F. Cleva, C. Cocchieri, E. Coccia, P. F. Cohadon, D. Cohen, A. Colla, C. G. Collette, L. R. Cominsky, J. Constancio, M., L. Conti, S. J. Cooper, P. Corban, T. R. Corbitt, I. Cordero-Carrión, K. R. Corley, N. Cornish, A. Corsi, S. Cortese, C. A. Costa, M. W. Coughlin, S. B. Coughlin, J. P. Coulon, S. T. Countryman, P. Couvares, P. B. Covas, E. E. Cowan, D. M. Coward, M. J. Cowart, D. C. Coyne, R. Coyne, J. D. E. Creighton, T. D. Creighton, J. Cripe, S. G. Crowder, T. J. Cullen, A. Cumming, L. Cunningham, E. Cuoco, T. Dal Canton, G. Dálya, S. L. Danilishin, S. D'Antonio, K. Danzmann, A. Dasgupta, C. F. Da Silva Costa, V. Dattilo, I. Dave, M. Davier, D. Davis, E. J. Daw, B. Day, S. De, D. DeBra, J. Degallaix, M. De Laurentis, S. Deléglise, W. Del Pozzo, N. Demos, T. Denker, T. Dent, R. De Pietri, V. Dergachev, R. De Rosa, R. T. DeRosa, C. De Rossi, R. DeSalvo, O. de Varona, J. Devenson, S. Dhurandhar, M. C. Díaz, L. Di Fiore, M. Di Giovanni, T. Di Girolamo, A. Di Lieto, S. Di Pace, I. Di Palma, F. Di Renzo, Z. Doctor, V. Dolique, F. Donovan, K. L. Dooley, S. Doravari, I. Dorrington, R. Douglas, M. Dovale Álvarez, T. P. Downes, M. Drago, C. Dreissigacker, J. C. Driggers, Z. Du, M. Ducrot, P. Dupej, S. E. Dwyer, T. B. Edo, M. C. Edwards, A. Effler, H. B. Eggenstein, P. Ehrens, J. Eichholz, S. S. Eikenberry, R. A. Eisenstein, R. C. Essick, D. Estevez, Z. B. Etienne, T. Etzel, M. Evans, T. M. Evans, M. Factourovich, V. Fafone, H. Fair, S. Fairhurst, X. Fan, S. Farinon, B. Farr, W. M. Farr, E. J. Fauchon-Jones, M. Favata, M. Fays, C. Fee, H. Fehrmann, J. Feicht, M. M. Fejer, A. Fernandez-Galiana, I. Ferrante, E. C. Ferreira, F. Ferrini, F. Fidecaro, D. Finstad, I. Fiori, D. Fiorucci, M. Fishbach, R. P. Fisher, M. Fitz-Axen, R. Flaminio, M. Fletcher, H. Fong, J. A. Font, P. W. F. Forsyth, S. S. Forsyth, J. D. Fournier, S. Frasca, F. Frasconi, Z. Frei, A. Freise, R. Frey, V. Frey, E. M. Fries, P. Fritschel, V. V. Frolov, P. Fulda, M. Fyffe, H. Gabbard, B. U. Gadre, S. M. Gaebel, J. R. Gair, L. Gammaitoni, M. R. Ganija, S. G. Gaonkar, C. Garcia-Quiros, F. Garufi, B. Gateley, S. Gaudio, G. Gaur, V. Gayathri, N. Gehrels, G. Gemme, E. Genin, A. Gennai, D. George, J. George, L. Gergely, V. Germain, S. Ghonge, A. Ghosh, A. Ghosh, S. Ghosh, J. A. Giaime, K. D. Giardina, A. Giazotto, K. Gill, L. Glover, E. Goetz, R. Goetz, S. Gomes, B. Goncharov, G. González, J. M. Gonzalez Castro, A. Gopakumar, M. L. Gorodetsky, S. E. Gossan, M. Gosselin, R. Gouaty, A. Grado, C. Graef, M. Granata, A. Grant, S. Gras, C. Gray, G. Greco, A. C. Green, E. M. Gretarsson, P. Groot, H. Grote, S. Grunewald, P. Gruning, G. M. Guidi, X. Guo, A. Gupta, M. K. Gupta, K. E. Gushwa, E. K. Gustafson, R. Gustafson, O. Halim, B. R. Hall, E. D. Hall, E. Z. Hamilton, G. Hammond, M. Haney, M. M. Hanke, J. Hanks, C. Hanna, M. D. Hannam, O. A. Hannuksela, J. Hanson, T. Hardwick, J. Harms, G. M. Harry, I. W. Harry, M. J. Hart, C. J. Haster, K. Haughian, J. Healy, A. Heidmann, M. C. Heintze, H. Heitmann, P. Hello, G. Hemming, M. Hendry, I. S. Heng, J. Hennig, A. W. Heptonstall, M. Heurs, S. Hild, T. Hinderer, D. Hoak, D. Hofman, K. Holt, D. E. Holz, P. Hopkins, C. Horst, J. Hough, E. A. Houston, E. J. Howell, A. Hreibi, Y. M. Hu, E. A. Huerta, D. Huet, B. Hughey, S. Husa, S. H. Huttner, T. Huynh-Dinh, N. Indik, R. Inta, G. Intini, H. N. Isa, J. M. Isac, M. Isi, B. R. Iyer, K. Izumi, T. Jacqmin, K. Jani, P. Jaranowski, S. Jawahar, F. Jiménez-Forteza, W. W. Johnson, D. I. Jones, R. Jones, R. J. G. Jonker, L. Ju, J. Junker, C. V. Kalaghatgi, V. Kalogera, B. Kamai, S. Kand hasamy, G. Kang, J. B. Kanner, S. J. Kapadia, S. Karki, K. S. Karvinen, M. Kasprzack, M. Katolik, E. Katsavounidis, W. Katzman, S. Kaufer, K. Kawabe, F. Kéfélian, D. Keitel, A. J. Kemball, R. Kennedy, C. Kent, J. S. Key, F. Y. Khalili, I. Khan, S. Khan, Z. Khan, E. A. Khazanov, N. Kijbunchoo, C. Kim, J. C. Kim, K. Kim, W. Kim, W. S. Kim, Y. M. Kim, S. J. Kimbrell, E. J. King, P. J. King, M. Kinley-Hanlon, R. Kirchhoff, J. S. Kissel, L. Kleybolte, S. Klimenko, T. D. Knowles, P. Koch, S. M. Koehlenbeck, S. Koley, V. Kondrashov, A. Kontos, M. Korobko, W. Z. Korth, I. Kowalska, D. B. Kozak, C. Krämer, V. Kringel, B. Krishnan, A. Królak, G. Kuehn, P. Kumar, R. Kumar, S. Kumar, L. Kuo, A. Kutynia, S. Kwang, B. D. Lackey, K. H. Lai, M. Landry, R. N. Lang, J. Lange, B. Lantz, R. K. Lanza, A. Lartaux-Vollard, P. D. Lasky, M. Laxen, A. Lazzarini, C. Lazzaro, P. Leaci, S. Leavey, C. H. Lee, H. K. Lee, H. M. Lee, H. W. Lee, K. Lee, J. Lehmann, A. Lenon, M. Leonardi, N. Leroy, N. Letendre, Y. Levin, T. G. F. Li, S. D. Linker, T. B. Littenberg, J. Liu, R. K. L. Lo, N. A. Lockerbie, L. T. London, J. E. Lord, M. Lorenzini, V. Loriette, M. Lormand, G. Losurdo, J. D. Lough, C. O. Lousto, G. Lovelace, H. Lück, D. Lumaca, A. P. Lundgren, R. Lynch, Y. Ma, R. Macas, S. Macfoy, B. Machenschalk, M. MacInnis, D. M. Macleod, I. Magaña Hernandez, F. Magaña-Sand oval, L. Magaña Zertuche, R. M. Magee, E. Majorana, I. Maksimovic, N. Man, V. Mandic, V. Mangano, G. L. Mansell, M. Manske, M. Mantovani, F. Marchesoni, F. Marion, S. Márka, Z. Márka, C. Markakis, A. S. Markosyan, A. Markowitz, E. Maros, A. Marquina, F. Martelli, L. Martellini, I. W. Martin, R. M. Martin, D. V. Martynov, K. Mason, E. Massera, A. Masserot, T. J. Massinger, M. Masso-Reid, S. Mastrogiovanni, A. Matas, F. Matichard, L. Matone, N. Mavalvala, N. Mazumder, R. McCarthy, D. E. McClelland, S. McCormick, L. McCuller, S. C. McGuire, G. McIntyre, J. McIver, D. J. McManus, L. McNeill, T. McRae, S. T. McWilliams, D. Meacher, G. D. Meadors, M. Mehmet, J. Meidam, E. Mejuto-Villa, A. Melatos, G. Mendell, R. A. Mercer, E. L. Merilh, M. Merzougui, S. Meshkov, C. Messenger, C. Messick, R. Metzdorff, P. M. Meyers, H. Miao, C. Michel, H. Middleton, E. E. Mikhailov, L. Milano, A. L. Miller, B. B. Miller, J. Miller, M. Millhouse, M. C. Milovich-Goff, O. Minazzoli, Y. Minenkov, J. Ming, C. Mishra, S. Mitra, V. P. Mitrofanov, G. Mitselmakher, R. Mittleman, D. Moffa, A. Moggi, K. Mogushi, M. Mohan, S. R. P. Mohapatra, M. Montani, C. J. Moore, D. Moraru, G. Moreno, S. R. Morriss, B. Mours, C. M. Mow-Lowry, G. Mueller, A. W. Muir, A. Mukherjee, D. Mukherjee, S. Mukherjee, N. Mukund, A. Mullavey, J. Munch, E. A. Muñiz, M. Muratore, P. G. Murray, K. Napier, I. Nardecchia, L. Naticchioni, R. K. Nayak, J. Neilson, G. Nelemans, T. J. N. Nelson, M. Nery, A. Neunzert, L. Nevin, J. M. Newport, G. Newton, K. K. Y. Ng, T. T. Nguyen, D. Nichols, A. B. Nielsen, S. Nissanke, A. Nitz, A. Noack, F. Nocera, D. Nolting, C. North, L. K. Nuttall, J. Oberling, G. D. O'Dea, G. H. Ogin, J. J. Oh, S. H. Oh, F. Ohme, M. A. Okada, M. Oliver, P. Oppermann, R. J. Oram, B. O'Reilly, R. Ormiston, L. F. Ortega, R. O'Shaughnessy, S. Ossokine, D. J. Ottaway, H. Overmier, B. J. Owen, A. E. Pace, J. Page, M. A. Page, A. Pai, S. A. Pai, J. R. Palamos, O. Palashov, C. Palomba, A. Pal-Singh, H. Pan, H.-W. Pan, B. Pang, P. T. H. Pang, C. Pankow, F. Pannarale, B. C. Pant, F. Paoletti, A. Paoli, M. A. Papa, A. Parida, W. Parker, D. Pascucci, A. Pasqualetti, R. Passaquieti, D. Passuello, M. Patil, B. Patricelli, B. L. Pearlstone, M. Pedraza, R. Pedurand, L. Pekowsky, A. Pele, S. Penn, C. J. Perez, A. Perreca, L. M. Perri, H. P. Pfeiffer, M. Phelps, O. J. Piccinni, M. Pichot, F. Piergiovanni, V. Pierro, G. Pillant, L. Pinard, I. M. Pinto, M. Pirello, M. Pitkin, M. Poe, R. Poggiani, P. Popolizio, E. K. Porter, A. Post, J. Powell, J. Prasad, J. W. W. Pratt, G. Pratten, V. Predoi, T. Prestegard, M. Prijatelj, M. Principe, S. Privitera, G. A. Prodi, L. G. Prokhorov, O. Puncken, M. Punturo, P. Puppo, M. Pürrer, H. Qi, V. Quetschke, E. A. Quintero, R. Quitzow-James, F. J. Raab, D. S. Rabeling, H. Radkins, P. Raffai, S. Raja, C. Rajan, B. Rajbhandari, M. Rakhmanov, K. E. Ramirez, A. Ramos-Buades, P. Rapagnani, V. Raymond, M. Razzano, J. Read, T. Regimbau, L. Rei, S. Reid, D. H. Reitze, W. Ren, S. D. Reyes, F. Ricci, P. M. Ricker, S. Rieger, K. Riles, M. Rizzo, N. A. Robertson, R. Robie, F. Robinet, A. Rocchi, L. Rolland, J. G. Rollins, V. J. Roma, R. Romano, C. L. Romel, J. H. Romie, D. Rosińska, M. P. Ross, S. Rowan, A. Rüdiger, P. Ruggi, G. Rutins, K. Ryan, S. Sachdev, T. Sadecki, L. Sadeghian, M. Sakellariadou, L. Salconi, M. Saleem, F. Salemi, A. Samajdar, L. Sammut, L. M. Sampson, E. J. Sanchez, L. E. Sanchez, N. Sanchis-Gual, V. Sand berg, J. R. Sanders, B. Sassolas, P. R. Saulson, O. Sauter, R. L. Savage, A. Sawadsky, P. Schale, M. Scheel, J. Scheuer, J. Schmidt, P. Schmidt, R. Schnabel, R. M. S. Schofield, A. Schönbeck, E. Schreiber, D. Schuette, B. W. Schulte, B. F. Schutz, S. G. Schwalbe, J. Scott, S. M. Scott, E. Seidel, D. Sellers, A. S. Sengupta, D. Sentenac, V. Sequino, A. Sergeev, D. A. Shaddock, T. J. Shaffer, A. A. Shah, M. S. Shahriar, M. B. Shaner, L. Shao, B. Shapiro, P. Shawhan, A. Sheperd, D. H. Shoemaker, D. M. Shoemaker, K. Siellez, X. Siemens, M. Sieniawska, D. Sigg, A. D. Silva, L. P. Singer, A. Singh, A. Singhal, A. M. Sintes, B. J. J. Slagmolen, B. Smith, J. R. Smith, R. J. E. Smith, S. Somala, E. J. Son, J. A. Sonnenberg, B. Sorazu,

F. Sorrentino, T. Souradeep, A. P. Spencer, A. K. Srivastava, K. Staats, A. Staley, M. Steinke, J. Steinlechner, S. Steinlechner, D. Steinmeyer, S. P. Stevenson, R. Stone, D. J. Stops, K. A. Strain, G. Stratta, S. E. Strigin, A. Strunk, R. Sturani, A. L. Stuver, T. Z. Summerscales, L. Sun, S. Sunil, J. Suresh, P. J. Sutton, B. L. Swinkels, M. J. Szczepańczyk, M. Tacca, S. C. Tait, C. Talbot, D. Talukder, D. B. Tanner, M. Tápai, A. Taracchini, J. D. Tasson, J. A. Taylor, R. Taylor, S. V. Tewari, T. Theeg, F. Thies, E. G. Thomas, M. Thomas, P. Thomas, K. A. Thorne, E. Thrane, S. Tiwari, V. Tiwari, K. V. Tokmakov, K. Toland, M. Tonelli, Z. Tornasi, A. Torres-Forné, C. I. Torrie, D. Töyrä, F. Travasso, G. Traylor, J. Trinastic, M. C. Tringali, L. Trozzo, K. W. Tsang, M. Tse, R. Tso, L. Tsukada, D. Tsuna, D. Tuyenbayev, K. Ueno, D. Ugolini, C. S. Unnikrishnan, A. L. Urban, S. A. Usman, H. Vahlbruch, G. Vajente, G. Valdes, N. van Bakel, M. van Beuzekom, J. F. J. van den Brand, C. Van Den Broeck, D. C. Vander-Hyde, L. van der Schaaf, J. V. van Heijningen, A. A. van Veggel, M. Vardaro, V. Varma, S. Vass, M. Vasúth, A. Vecchio, G. Vedovato, J. Veitch, P. J. Veitch, K. Venkateswara, G. Venugopalan, D. Verkindt, F. Vetrano, A. Viceré, A. D. Viets, S. Vinciguerra, D. J. Vine, J. Y. Vinet, S. Vitale, T. Vo, H. Vocca, C. Vorvick, S. P. Vyatchanin, A. R. Wade, L. E. Wade, M. Wade, R. Walet, M. Walker, L. Wallace, S. Walsh, G. Wang, H. Wang, J. Z. Wang, W. H. Wang, Y. F. Wang, R. L. Ward, J. Warner, M. Was, J. Watchi, B. Weaver, L. W. Wei, M. Weinert, A. J. Weinstein, R. Weiss, L. Wen, E. K. Wessel, P. Weßels, J. Westerweck, T. Westphal, K. Wette, J. T. Whelan, B. F. Whiting, C. Whittle, D. Wilken, D. Williams, R. D. Williams, A. R. Williamson, J. L. Willis, B. Willke, M. H. Wimmer, W. Winkler, C. C. Wipf, H. Wittel, G. Woan, J. Woehler, J. Wofford, K. W. K. Wong, J. Worden, J. L. Wright, D. S. Wu, D. M. Wysocki, S. Xiao, H. Yamamoto, C. C. Yancey, L. Yang, M. J. Yap, M. Yazback, H. Yu, H. Yu, M. Yvert, A. Zadrożny, M. Zanolin, T. Zelenova, J. P. Zendri, M. Zevin, L. Zhang, M. Zhang, T. Zhang, Y. H. Zhang, C. Zhao, M. Zhou, Z. Zhou, S. J. Zhu, X. J. Zhu, M. E. Zucker, J. Zweizig, LIGO Scientific Collaboration and Virgo Collaboration, "Search for High-energy Neutrinos from Binary Neutron Star Merger GW170817 with ANTARES, IceCube, and the Pierre Auger Observatory", *ApJ* **850**, 2, L35 (2017).

Alekseev, E. N., L. N. Alekseeva, V. I. Volchenko and I. V. Krivosheina, "Possible detection of a neutrino signal on 23 February 1987 at the Baksan underground scintillation telescope of the Institute of Nuclear Research", Soviet Journal of Experimental and Theoretical Physics Letters **45**, 589 (1987).

Aliotta, M., R. Buompane, M. Couder, A. Couture, R. J. deBoer, A. Formicola, L. Gialanella, J. Glorius, G. Imbriani, M. Junker, C. Langer, A. Lennarz, Y. A. Litvinov, W. P. Liu, M. Lugaro, C. Matei, Z. Meisel, L. Piersanti, R. Reifarth, D. Robertson, A. Simon, O. Straniero, A. Tumino, M. Wiescher and Y. Xu, "The status and future of direct nuclear reaction measurements for stellar burning", Journal of Physics G Nuclear Physics **49**, 1, 010501 (2022).

Allega, A., M. R. Anderson, S. Andringa, J. Antunes, M. Askins, D. J. Auty, A. Bacon, N. Barros, F. Barão, R. Bayes, E. W. Beier, T. S. Bezerra, A. Bialek, S. D. Biller, E. Blucher, E. Caden, E. J. Callaghan, S. Cheng, M. Chen, B. Cleveland, D. Cookman, J. Corning, M. A. Cox, R. Dehghani, J. Deloye, C. Deluce, M. M. Depatie, J. Dittmer, K. H. Dixon, F. Di Lodovico, E. Falk, N. Fatemighomi, R. Ford, K. Frankiewicz, A. Gaur, O. I. González-Reina, D. Gooding, C. Grant, J. Grove, A. L. Hallin, D. Hallman, W. J. Heintzelman, R. L. Helmer, J. Hu, R. Hunt-Stokes, S. M. A. Hussain, A. S. Inácio, C. J. Jillings, S. Kaluzienski, T. Kaptanoglu, P. Khaghani, H. Khan, J. R. Klein, L. L. Kormos, B. Krar, C. Kraus, C. B. Krauss, T. Kroupová, I. Lam, B. J. Land, I. Lawson, L. Lebanowski, J. Lee, C. Lefebvre, J. Lidgard, Y. H. Lin, V. Lozza, M. Luo, A. Maio, S. Manecki, J. Maneira, R. D. Martin, N. McCauley, A. B. McDonald, C. Mills, I. Morton-Blake, S. Naugle, L. J. Nolan, H. M. O'Keeffe, G. D. Orebi Gann, J. Page, W. Parker, J. Paton, S. J. M. Peeters, L. Pickard, P. Ravi, A. Reichold, S. Riccetto, R. Richardson, M. Rigan, J. Rose, R. Rosero, J. Rumleskie, I. Semenec, P. Skensved, M. Smiley, R. Svoboda, B. Tam, J. Tseng, E. Turner, S. Valder, C. J. Virtue, E. Vázquez-Jáuregui, J. Wang, M. Ward, J. R. Wilson, J. D. Wilson, A. Wright, J. P. Yanez, S. Yang, M. Yeh, S. Yu, Y. Zhang, K. Zuber, A. Zummo and SNO + Collaboration, "Evidence of Antineutrinos from Distant Reactors using Pure Water at SNO +", *Phys. Rev. L.***130**, 9, 091801 (2023).

Almeida-Fernandes, F., V. M. Placco, H. J. Rocha-Pinto, M. B. Fernandes, G. Limberg, L. Beraldo e Silva, J. A. S. Amarante, H. D. Perottoni, R. Overzier, W. Schoenell, T. Ribeiro, A. Kanaan and C. Mendes de Oliveira, "Chemodynamical properties and ages of metal-poor stars in S-PLUS", *MNRAS***523**, 2, 2934–2951 (2023).

Althaus, L. G. and A. H. Córsico, "New DA white dwarf models for asteroseismology of ZZ Ceti stars", *A&A***663**, A167 (2022).

Althaus, L. G., A. H. Córsico, J. Isern and E. García-Berro, "Evolutionary and pulsational properties of white dwarf stars", *The Astronomy and Astrophysics Review***18**, 4, 471–566 (2010).

Alves, D. R. and A. Sarajedini, "The Age-dependent Luminosities of the Red Giant Branch Bump, Asymptotic Giant Branch Bump, and Horizontal Branch Red Clump", *ApJ***511**, 1, 225–234 (1999).

An, F. P., W. D. Bai, A. B. Balantekin, M. Bishai, S. Blyth, G. F. Cao, J. Cao, J. F. Chang, Y. Chang, H. S. Chen and et al., "Precision Measurement of Reactor Antineutrino Oscillation at Kilometer-Scale Baselines by Daya Bay", *Phys. Rev. L.***130**, 16, 161802 (2023).

Anandagoda, S., D. H. Hartmann, M. Ajello and A. Desai, "The Diffuse Supernova Neutrino Background", Research Notes of the American Astronomical Society **4**, 1, 4 (2020).

Anandagoda, S., D. H. Hartmann, C. L. Fryer, M. Ajello, A. Desai, A. L. Hungerford and L.-S. The, "Cosmic Supernova Neutrino and Gamma-Ray Backgrounds in the MeV Regime", *ApJ***950**, 1, 29 (2023).

Ando, S. and K. Sato, "Relic neutrino background from cosmological supernovae", New Journal of Physics **6**, 1, 170 (2004).

Angulo, C., M. Arnould, M. Rayet, P. Descouvemont, D. Baye, C. Leclercq-Willain, A. Coc, S. Barhoumi, P. Aguer, C. Rolfs, R. Kunz, J. Hammer, A. Mayer, T. Paradellis, S. Kossionides, C. Chronidou, K. Spyrou, S. Degl'Innocenti, G. Fiorentini, B. Ricci, S. Zavatarelli, C. Providencia, H. Wolters, J. Soares, C. Grama, J. Rahighi, A. Shotter and M. L. Rachti, "A compilation of charged-particle induced thermonuclear reaction rates", Nuclear Physics A **656**, 1, 3 – 183, URL `http://www.sciencedirect.com/science/article/pii/S0375947499000305` (1999).

Antoniadis, J., P. C. C. Freire, N. Wex, T. M. Tauris, R. S. Lynch, M. H. van Kerkwijk, M. Kramer, C. Bassa, V. S. Dhillon, T. Driebe, J. W. T. Hessels, V. M. Kaspi, V. I. Kondratiev, N. Langer, T. R. Marsh, M. A. McLaughlin, T. T. Pennucci, S. M. Ransom, I. H. Stairs, J. van Leeuwen, J. P. W. Verbiest and D. G. Whelan, "A Massive Pulsar in a Compact Relativistic Binary", Science **340**, 6131, 448 (2013).

Antonini, F. and H. B. Perets, "Secular Evolution of Compact Binaries near Massive Black Holes: Gravitational Wave Sources and Other Exotica", *ApJ***757**, 1, 27 (2012).

Arnett, W. D., "Advanced Evolution of Massive Stars. II. Carbon Burning", *ApJ***176**, 699 (1972).

Arnould, M., S. Goriely and A. Jorissen, "Non-explosive hydrogen and helium burnings: abundance predictions from the NACRE reaction rate compilation", *A&A***347**, 572–582 (1999).

Asplund, M., N. Grevesse, A. J. Sauval and P. Scott, "The Chemical Composition of the Sun", *ARA&A***47**, 1, 481–522 (2009).

Aufderheide, M. B., "Convection and Neutrino Emission in the Late Stages of Massive Star Evolution", *ApJ***411**, 813 (1993).

Austin, S. M., C. West and A. Heger, "Effective Helium Burning Rates and the Production of the Neutrino Nuclei", *Phys. Rev. L.***112**, 11, 111101 (2014).

Bahcall, J. N., *Neutrino Astrophysics* (Cambridge, UK: Cambridge Univ. Press. , 1989).

Bahcall, J. N. and M. H. Pinsonneault, "Standard solar models, with and without helium diffusion, and the solar neutrino problem", Reviews of Modern Physics **64**, 885–926 (1992).

Bahcall, J. N., A. M. Serenelli and S. Basu, "New Solar Opacities, Abundances, Helioseismology, and Neutrino Fluxes", *ApJ***621**, 1, L85–L88 (2005).

Bahcall, J. N. and A. Ulmer, "Temperature dependence of solar neutrino fluxes", *Phys. Rev. D.***53**, 8, 4202–4210 (1996).

Bailyn, C. D., R. K. Jain, P. Coppi and J. A. Orosz, "The Mass Distribution of Stellar Black Holes", *ApJ***499**, 1, 367–374 (1998).

Banik, S., M. Hempel and D. Bandyopadhyay, "New Hyperon Equations of State for Supernovae and Neutron Stars in Density-dependent Hadron Field Theory", *ApJS* **214**, 2, 22 (2014).

Barkat, Z., "Neutrino processes in stellar interiors.", *ARA&A* **13**, 45–68 (1975).

Barkat, Z., G. Rakavy and N. Sack, "Dynamics of Supernova Explosion Resulting from Pair Formation", *Phys. Rev. L.* **18**, 10, 379–381 (1967).

Bartos, I., B. Kocsis, Z. Haiman and S. Márka, "Rapid and Bright Stellar-mass Binary Black Hole Mergers in Active Galactic Nuclei", *ApJ* **835**, 2, 165 (2017).

Basu, S., W. J. Chaplin, Y. Elsworth, R. New and A. M. Serenelli, "Fresh Insights on the Structure of the Solar Core", *ApJ* **699**, 2, 1403–1417 (2009).

Bauer, E. B., "Carbon-Oxygen Phase Separation in Modules for Experiments in Stellar Astrophysics (MESA) White Dwarf Models", *ApJ* **950**, 2, 115 (2023).

Bauer, E. B., J. Schwab, L. Bildsten and S. Cheng, "Multi-gigayear White Dwarf Cooling Delays from Clustering-enhanced Gravitational Sedimentation", *ApJ* **902**, 2, 93 (2020).

Beacom, J. F., "The Diffuse Supernova Neutrino Background", Annual Review of Nuclear and Particle Science **60**, 439–462 (2010).

Beacom, J. F. and P. Vogel, "Can a supernova be located by its neutrinos?", *Phys. Rev. D.* **60**, 3, 033007 (1999).

Beaudet, G., V. Petrosian and E. E. Salpeter, "Energy Losses due to Neutrino Processes", *ApJ* **150**, 979 (1967).

Becker, S. A. and I. Iben, Jr., "The asymptotic giant branch evolution of intermediate-mass stars as a function of mass and composition. I - Through the second dredge-up phase", *ApJ* **232**, 831–853 (1979).

Becker, S. A. and I. Iben, Jr., "The asymptotic giant branch evolution of intermediate-mass stars as a function of mass and composition. II - Through the first major thermal pulse and the consequences of convective dredge-up", *ApJ* **237**, 111–129 (1980).

Belczynski, K., "The Most Ordinary Formation of the Most Unusual Double Black Hole Merger", *ApJ* **905**, 2, L15 (2020).

Belczynski, K., G. Wiktorowicz, C. L. Fryer, D. E. Holz and V. Kalogera, "Missing Black Holes Unveil the Supernova Explosion Mechanism", *ApJ* **757**, 1, 91 (2012).

Bennett, M. E., R. Hirschi, M. Pignatari, S. Diehl, C. Fryer, F. Herwig, A. Hungerford, K. Nomoto, G. Rockefeller, F. X. Timmes and M. Wiescher, "The effect of ^{12}C $+^{12}$C rate uncertainties on the evolution and nucleosynthesis of massive stars", *MNRAS* **420**, 4, 3047–3070 (2012).

Bergemann, M. and A. Serenelli, *Solar Abundance Problem*, pp. 245–258 (Springer, Cham Switzerland, 2014).

Bildsten, L., "MESA Summer School: Approaching the Main Sequence", http://doi.org/10.5281/zenodo.3374948, Private Communication (2019).

Bildsten, L., B. Paxton, K. Moore and P. J. Macias, "Acoustic Signatures of the Helium Core Flash", *ApJ* **744**, 1, L6 (2012).

Bionta, R. M., G. Blewitt, C. B. Bratton, D. Casper, A. Ciocio, R. Claus, B. Cortez, M. Crouch, S. T. Dye, S. Errede, G. W. Foster, W. Gajewski, K. S. Ganezer, M. Goldhaber, T. J. Haines, T. W. Jones, D. Kielczewska, W. R. Kropp, J. G. Learned, J. M. Losecco, J. Matthews, R. Miller, M. S. Mudan, H. S. Park, L. R. Price, F. Reines, J. Schultz, S. Seidel, E. Shumard, D. Sinclair, H. W. Sobel, J. L. Stone, L. R. Sulak, R. Svoboda, G. Thornton, J. C. van der Velde and C. Wuest, "Observation of a neutrino burst in coincidence with supernova 1987A in the Large Magellanic Cloud", *Phys. Rev. L.* **58**, 14, 1494–1496 (1987).

Birkl, R., M. A. Aloy, H. T. Janka and E. Müller, "Neutrino pair annihilation near accreting, stellar-mass black holes", *A&A* **463**, 1, 51–67 (2007).

Bischoff-Kim, A. and M. H. Montgomery, "WDEC: A Code for Modeling White Dwarf Structure and Pulsations", *AJ* **155**, 187 (2018).

Bisnovatyi-Kogan, G. S. and Z. F. Seidov, "Supernovae, neutrino rest mass, and the middle-energy neutrino background in the universe.", Annals of the New York Academy of Sciences **422**, 319–327 (1984).

Blöcker, T., "Evolution on the AGB and beyond: on the formation of H-deficient post-AGB stars", *Ap&SS* **275**, 1–14 (2001).

Bloecker, T. and D. Schoenberner, "Stellar evolution of low and intermediate-mass stars. III. an application of evolutionary post-AGB models: the variable central star FG Sagittae.", *A&A* **324**, 991–997 (1997).

Blouin, S., N. R. Shaffer, D. Saumon and C. E. Starrett, "New Conductive Opacities for White Dwarf Envelopes", *ApJ* **899**, 1, 46 (2020).

Boeltzig, A., R. J. deBoer, Y. Chen, A. Best, M. Couder, A. Di Leva, B. Frentz, J. Görres, G. Gyürky, G. Imbriani, M. Junker, Q. Liu, S. Lyons, K. Manukyan, K. T. Macon, L. Morales, M. T. Moran, D. Odell, C. Seymour, G. Seymour, E. Stech, B. Vande Kolk and M. Wiescher, "Investigation of direct capture in the ^{23}Na(p ,γ)^{24}Mg reaction", *Phys. Rev. C.* **106**, 4, 045801 (2022).

Bond, J. R., W. D. Arnett and B. J. Carr, "The evolution and fate of Very Massive Objects", *ApJ* **280**, 825–847 (1984).

Borexino Collaboration, M. Agostini, K. Altenmüller, S. Appel, V. Atroshchenko, Z. Bagdasarian, D. Basilico, G. Bellini, J. Benziger, D. Bick, G. Bonfini, D. Bravo, B. Caccianiga, F. Calaprice, A. Caminata, S. Caprioli, M. Carlini, P. Cavalcante, A. Chepurnov, K. Choi, L. Collica, D. D'Angelo, S. Davini, A. Derbin,

X. F. Ding, A. Di Ludovico, L. Di Noto, I. Drachnev, K. Fomenko, A. Formozov, D. Franco, F. Gabriele, C. Galbiati, C. Ghiano, M. Giammarchi, A. Goretti, M. Gromov, D. Guffanti, C. Hagner, T. Houdy, E. Hungerford, A. Ianni, A. Ianni, A. Jany, D. Jeschke, V. Kobychev, D. Korablev, G. Korga, D. Kryn, M. Laubenstein, E. Litvinovich, F. Lombardi, P. Lombardi, L. Ludhova, G. Lukyanchenko, L. Lukyanchenko, I. Machulin, G. Manuzio, S. Marcocci, J. Martyn, E. Meroni, M. Meyer, L. Miramonti, M. Misiaszek, V. Muratova, B. Neumair, L. Oberauer, B. Opitz, V. Orekhov, F. Ortica, M. Pallavicini, L. Papp, Ö. Penek, N. Pilipenko, A. Pocar, A. Porcelli, G. Raikov, G. Ranucci, A. Razeto, A. Re, M. Redchuk, A. Romani, R. Roncin, N. Rossi, S. Schönert, D. Semenov, M. Skorokhvatov, O. Smirnov, A. Sotnikov, L. F. F. Stokes, Y. Suvorov, R. Tartaglia, G. Testera, J. Thurn, M. Toropova, E. Unzhakov, F. L. Villante, A. Vishneva, R. B. Vogelaar, F. von Feilitzsch, H. ang, S. Weinz, M. Wojcik, M. Wurm, Z. Yokley, O. Zaimidoroga, S. Zavatarelli, K. Zuber and G. Zuzel, "Comprehensive measurement of pp-chain solar neutrinos", *Nature***562**, 7728, 505–510 (2018).

Borexino Collaboration, M. Agostini, K. Altenmüller, S. Appel, V. Atroshchenko, Z. Bagdasarian, D. Basilico, G. Bellini, J. Benziger, D. Bick, G. Bonfini, D. Bravo, B. Caccianiga, F. Calaprice, A. Caminata, S. Caprioli, M. Carlini, P. Cavalcante, A. Chepurnov, K. Choi, L. Collica, D. D'Angelo, S. Davini, A. Derbin, X. F. Ding, A. Di Ludovico, L. Di Noto, I. Drachnev, K. Fomenko, A. Formozov, D. Franco, F. Gabriele, C. Galbiati, C. Ghiano, M. Giammarchi, A. Goretti, M. Gromov, D. Guffanti, C. Hagner, T. Houdy, E. Hungerford, A. Ianni, A. Ianni, A. Jany, D. Jeschke, V. Kobychev, D. Korablev, G. Korga, D. Kryn, M. Laubenstein, E. Litvinovich, F. Lombardi, P. Lombardi, L. Ludhova, G. Lukyanchenko, L. Lukyanchenko, I. Machulin, G. Manuzio, S. Marcocci, J. Martyn, E. Meroni, M. Meyer, L. Miramonti, M. Misiaszek, V. Muratova, B. Neumair, L. Oberauer, B. Opitz, V. Orekhov, F. Ortica, M. Pallavicini, L. Papp, Ö. Penek, N. Pilipenko, A. Pocar, A. Porcelli, G. Raikov, G. Ranucci, A. Razeto, A. Re, M. Redchuk, A. Romani, R. Roncin, N. Rossi, S. Schönert, D. Semenov, M. Skorokhvatov, O. Smirnov, A. Sotnikov, L. F. F. Stokes, Y. Suvorov, R. Tartaglia, G. Testera, J. Thurn, M. Toropova, E. Unzhakov, F. L. Villante, A. Vishneva, R. B. Vogelaar, F. von Feilitzsch, H. ang, S. Weinz, M. Wojcik, M. Wurm, Z. Yokley, O. Zaimidoroga, S. Zavatarelli, K. Zuber and G. Zuzel, "Experimental evidence of neutrinos produced in the CNO fusion cycle in the Sun", *Nature***587**, 7728, 577–582 (2020).

Borexino Collaboration, G. Bellini, J. Benziger, D. Bick, G. Bonfini, D. Bravo, B. Caccianiga, L. Cadonati, F. Calaprice, A. Caminata, P. Cavalcante, A. Chavarria, A. Chepurnov, D. D'Angelo, S. Davini, A. Derbin, A. Empl, A. Etenko, K. Fomenko, D. Franco, F. Gabriele, C. Galbiati, S. Gazzana, C. Ghiano, M. Giammarchi, M. Göger-Neff, A. Goretti, M. Gromov, C. Hagner, E. Hungerford, A. Ianni, A. Ianni, V. Kobychev, D. Korablev, G. Korga, D. Kryn, M. Laubenstein, B. Lehnert, T. Lewke, E. Litvinovich, F. Lombardi, P. Lombardi, L. Ludhova, G. Lukyanchenko, I. Machulin, S. Manecki, W. Maneschg, S. Marcocci, Q. Meindl, E. Meroni, M. Meyer, L. Miramonti, M. Misiaszek, M. Montuschi, P. Mosteiro, V. Muratova, L. Oberauer, M. Obolensky, F. Ortica, K. Otis, M. Pallavicini, L. Papp, L. Perasso, A. Pocar, G. Ranucci, A. Razeto, A. Re, A. Romani, N. Rossi, R. Saldanha, C. Salvo, S. Schönert, H. Simgen, M. Skorokhvatov, O. Smirnov,

A. Sotnikov, S. Sukhotin, Y. Suvorov, R. Tartaglia, G. Testera, D. Vignaud, R. B. Vogelaar, F. von Feilitzsch, H. Wang, J. Winter, M. Wojcik, A. Wright, M. Wurm, O. Zaimidoroga, S. Zavatarelli, K. Zuber and G. Zuzel, "Neutrinos from the primary proton-proton fusion process in the Sun", *Nature* **512**, 383–386 (2014).

Bouvier, A. and M. Wadhwa, "The age of the Solar System redefined by the oldest Pb-Pb age of a meteoritic inclusion", Nature Geoscience **3**, 9, 637–641 (2010).

Branch, D. and J. C. Wheeler, *Supernova Explosions* (Springer-Verlag GmbH Germany, 2017).

Bravo, E., I. Domínguez, C. Badenes, L. Piersanti and O. Straniero, "Metallicity as a Source of Dispersion in the SNIa Bolometric Light Curve Luminosity-Width Relationship", *ApJ* **711**, L66–L70 (2010).

Breivik, K., S. Coughlin, M. Zevin, C. L. Rodriguez, K. Kremer, C. S. Ye, J. J. Andrews, M. Kurkowski, M. C. Digman, S. L. Larson and F. A. Rasio, "COSMIC Variance in Binary Population Synthesis", *ApJ* **898**, 1, 71 (2020).

Brugière, T., "The Jiangmen underground neutrino observatory experiment", Nuclear Instruments and Methods in Physics Research A **845**, 326–329 (2017).

Burrows, A. and D. Vartanyan, "Core-collapse supernova explosion theory", *Nature* **589**, 7840, 29–39 (2021).

Campante, T. L., M. Schofield, J. S. Kuszlewicz, L. Bouma, W. J. Chaplin, D. Huber, J. Christensen-Dalsgaard, H. Kjeldsen, D. Bossini and T. S. H. North, "The Asteroseismic Potential of TESS: Exoplanet-host Stars", *ApJ* **830**, 2, 138 (2016).

Capozzi, F. and G. Raffelt, "Axion and neutrino bounds improved with new calibrations of the tip of the red-giant branch using geometric distance determinations", *Phys. Rev. D.* **102**, 8, 083007 (2020).

Casamiquela, L., C. Soubiran, P. Jofré, C. Chiappini, N. Lagarde, Y. Tarricq, R. Carrera, C. Jordi, L. Balaguer-Núñez, J. Carbajo-Hijarrubia and S. Blanco-Cuaresma, "Abundance-age relations with red clump stars in open clusters", *A&A* **652**, A25 (2021).

Cassisi, S., A. Y. Potekhin, A. Pietrinferni, M. Catelan and M. Salaris, "Updated Electron-Conduction Opacities: The Impact on Low-Mass Stellar Models", *ApJ* **661**, 1094–1104 (2007).

Cassisi, S. and M. Salaris, *Old Stellar Populations: How to Study the Fossil Record of Galaxy Formation* (Wiley-VCH, 2013).

Catelan, M., J. A. de Freitas Pacheco and J. E. Horvath, "The Helium-Core Mass at the Helium Flash in Low-Mass Red Giant Stars: Observations and Theory", *ApJ* **461**, 231 (1996).

Caughlan, G. R. and W. A. Fowler, "Thermonuclear Reaction Rates V", Atomic Data and Nuclear Data Tables **40**, 283 (1988).

Chidester, M. T., E. Farag and F. X. Timmes, “On Trapped Modes in Variable White Dwarfs as Probes of the $^{12}C(\alpha, \gamma)^{16}O$ Reaction Rate”, *ApJ* **935**, 1, 21 (2022).

Chidester, M. T., F. X. Timmes, J. Schwab, R. H. D. Townsend, E. Farag, A. Thoul, C. E. Fields, E. B. Bauer and M. H. Montgomery, “On the Impact of ^{22}Ne on the Pulsation Periods of Carbon-Oxygen White Dwarfs with Helium-dominated Atmospheres”, *ApJ* **910**, 1, 24 (2021).

Choi, J., A. Dotter, C. Conroy, M. Cantiello, B. Paxton and B. D. Johnson, “Mesa Isochrones and Stellar Tracks (MIST). I. Solar-scaled Models”, *ApJ* **823**, 2, 102 (2016a).

Choi, J., A. Dotter, C. Conroy, M. Cantiello, B. Paxton and B. D. Johnson, “Mesa Isochrones and Stellar Tracks (MIST). I. Solar-scaled Models”, *ApJ* **823**, 102 (2016b).

Choplin, A., R. Hirschi, G. Meynet, S. Ekström, C. Chiappini and A. Laird, “Non-standard s-process in massive rotating stars. Yields of 10-150 $M_\odot$ models at $Z = 10^{-3}$”, *A&A* **618**, A133 (2018).

Christensen-Dalsgaard, J., M. J. P. F. G. Monteiro, M. Rempel and M. J. Thompson, “A more realistic representation of overshoot at the base of the solar convective envelope as seen by helioseismology”, *MNRAS* **414**, 2, 1158–1174 (2011).

Chugunov, A. I., H. E. Dewitt and D. G. Yakovlev, “Coulomb tunneling for fusion reactions in dense matter: Path integral MonteCarlo versus mean field”, *Phys. Rev. D.* **76**, 2, 025028 (2007).

Clayton, G. C. and O. De Marco, “The Evolution of the Final Helium Shell Flash Star V605 Aquilae From 1917 to 1997”, *AJ* **114**, 2679 (1997).

Colpi, M., S. L. Shapiro and S. A. Teukolsky, “Exploding Neutron Stars near the Minimum Mass”, *ApJ* **339**, 318 (1989).

Colpi, M., S. L. Shapiro and S. A. Teukolsky, “A Hydrodynamical Model for the Explosion of a Neutron Star Just below the Minimum Mass”, *ApJ* **414**, 717 (1993).

Cook, K. J., A. Chevis, T. K. Eriksen, E. C. Simpson, T. Kibédi, L. T. Bezzina, A. C. Berriman, J. Buete, I. P. Carter, M. Dasgupta, D. J. Hinde, D. Y. Jeung, P. McGlynn, S. Parker-Steele, B. M. A. Swinton-Bland, T. Tanaka and W. Wojtaczka, “High-precision proton angular distribution measurements of $^{12}C(p\ ,p^{'})$ for the determination of the E 0 decay branching ratio of the Hoyle state”, *Phys. Rev. C.* **104**, 2, 024620 (2021).

Córsico, A. H., L. G. Althaus, M. M. Miller Bertolami and S. O. Kepler, “Pulsating white dwarfs: new insights”, *The Astronomy and Astrophysics Review* **27**, 1, 7 (2019).

Costa, G., A. Bressan, M. Mapelli, P. Marigo, G. Iorio and M. Spera, "Formation of GW190521 from stellar evolution: the impact of the hydrogen-rich envelope, dredge-up, and $^{12}C(\alpha, \gamma)^{16}O$ rate on the pair-instability black hole mass gap", *MNRAS* **501**, 3, 4514–4533 (2021).

Couch, R. G., A. B. Schmiedekamp and W. D. Arnett, "S-PROCESS Nucleosynthesis in Massive Stars: Core Helium Burning", *ApJ* **190**, 95–100 (1974).

Couch, S. M., E. Chatzopoulos, W. D. Arnett and F. X. Timmes, "The Three-dimensional Evolution to Core Collapse of a Massive Star", *ApJ* **808**, L21 (2015).

Cristini, A., R. Hirschi, C. Meakin, D. Arnett, C. Georgy and I. Walkington, "Dependence of convective boundary mixing on boundary properties and turbulence strength", *MNRAS* **484**, 4, 4645–4664 (2019).

Cristini, A., C. Meakin, R. Hirschi, D. Arnett, C. Georgy, M. Viallet and I. Walkington, "3D hydrodynamic simulations of carbon burning in massive stars", *MNRAS* **471**, 279–300 (2017).

Cromartie, H. T., E. Fonseca, S. M. Ransom, P. B. Demorest, Z. Arzoumanian, H. Blumer, P. R. Brook, M. E. DeCesar, T. Dolch, J. A. Ellis, R. D. Ferdman, E. C. Ferrara, N. Garver-Daniels, P. A. Gentile, M. L. Jones, M. T. Lam, D. R. Lorimer, R. S. Lynch, M. A. McLaughlin, C. Ng, D. J. Nice, T. T. Pennucci, R. Spiewak, I. H. Stairs, K. Stovall, J. K. Swiggum and W. W. Zhu, "Relativistic Shapiro delay measurements of an extremely massive millisecond pulsar", Nature Astronomy **4**, 72–76 (2020).

Cyburt, R. H., A. M. Amthor, R. Ferguson, Z. Meisel, K. Smith, S. Warren, A. Heger, R. D. Hoffman, T. Rauscher, A. Sakharuk, H. Schatz, F. K. Thielemann and M. Wiescher, "The JINA REACLIB Database: Its Recent Updates and Impact on Type-I X-ray Bursts", *ApJS* **189**, 240–252 (2010a).

Cyburt, R. H., A. M. Amthor, R. Ferguson, Z. Meisel, K. Smith, S. Warren, A. Heger, R. D. Hoffman, T. Rauscher, A. Sakharuk, H. Schatz, F. K. Thielemann and M. Wiescher, "The JINA REACLIB Database: Its Recent Updates and Impact on Type-I X-ray Bursts", *ApJS* **189**, 240–252 (2010b).

Da Costa, G. S. and T. E. Armandroff, "Standard Globular Cluster Giant Branches in the (M(I), (V - I)o) Plane", *AJ* **100**, 162 (1990).

Davies, B. and E. R. Beasor, "The 'red supergiant problem': the upper luminosity boundary of Type II supernova progenitors", *MNRAS* **493**, 1, 468–476 (2020).

Davies, B., P. A. Crowther and E. R. Beasor, "The luminosities of cool supergiants in the Magellanic Clouds, and the Humphreys-Davidson limit revisited", *MNRAS* **478**, 3, 3138–3148 (2018).

Dayras, R., Z. E. Switkowski and S. E. Woosley, "Neutron branching in the reaction $^{12}C + ^{12}C$", *Nuclear Physics A* **279**, 1, 70–84 (1977).

De Gerónimo, F. C., M. M. Miller Bertolami, F. Plaza and M. Catelan, "The composition of massive white dwarfs and their dependence on C-burning modeling", *A&A* **659**, A150 (2022).

de Mink, S. E. and I. Mandel, "The chemically homogeneous evolutionary channel for binary black hole mergers: rates and properties of gravitational-wave events detectable by advanced LIGO", *MNRAS* **460**, 4, 3545–3553 (2016).

deBoer, R. J., J. Görres, M. Wiescher, R. E. Azuma, A. Best, C. R. Brune, C. E. Fields, S. Jones, M. Pignatari, D. Sayre, K. Smith, F. X. Timmes and E. Uberseder, "The $^{12}C(\alpha,\gamma)^{16}O$ reaction and its implications for stellar helium burning", Reviews of Modern Physics **89**, 3, 035007 (2017).

Deinzer, W. and E. E. Salpeter, "Models for Carbon-Burning Stars", *ApJ* **142**, 813 (1965).

Demarque, P., "The Structure of Population II Stars.", *ApJ* **132**, 366 (1960).

Demarque, P., "The Early Evolution of Population II Stars", *ApJ* **149**, 117 (1967).

Denissenkov, P. A., J. W. Truran, F. Herwig, S. Jones, B. Paxton, K. Nomoto, T. Suzuki and H. Toki, "Hybrid C-O-Ne white dwarfs as progenitors of Type Ia supernovae: dependence on Urca process and mixing assumptions", *MNRAS* **447**, 2696–2705 (2015).

Dewitt, H. E., H. C. Graboske and M. S. Cooper, "Screening Factors for Nuclear Reactions. General Theory", *ApJ* **181**, 439–456 (1973).

Di Carlo, U. N., M. Mapelli, N. Giacobbo, M. Spera, Y. Bouffanais, S. Rastello, F. Santoliquido, M. Pasquato, A. Ballone, A. A. Trani, S. Torniamenti and F. Haardt, "Binary black holes in young star clusters: the impact of metallicity", *MNRAS* **498**, 1, 495–506 (2020).

Dondoglio, E., A. P. Milone, E. P. Lagioia, A. F. Marino, M. Tailo, G. Cordoni, S. Jang and M. Carlos, "Multiple Stellar Populations along the Red Horizontal Branch and Red Clump of Globular Clusters", *ApJ* **906**, 2, 76 (2021).

Dutta, S. I., S. Ratković and M. Prakash, "Photoneutrino process in astrophysical systems", *Phys. Rev. D.* **69**, 2, 023005 (2004).

Dzhioev, A. A., A. V. Yudin, N. V. Dunina-Barkovskaya and A. I. Vdovin, "Neutrino spectrum and energy loss rates due to weak processes on hot ^{56}Fe in pre-supernova environment", arXiv e-prints p. arXiv:2306.16055 (2023).

Edvardsson, B., J. Andersen, B. Gustafsson, D. L. Lambert, P. E. Nissen and J. Tomkin, "The Chemical Evolution of the Galactic Disk - Part One - Analysis and Results", *A&A* **275**, 101–+ (1993).

El Eid, M. F., B. S. Meyer and L.-S. The, "Evolution of Massive Stars Up to the End of Central Oxygen Burning", *ApJ* **611**, 452–465 (2004).

Eriksen, T. K., T. Kibédi, M. W. Reed, A. E. Stuchbery, K. J. Cook, A. Akber, B. Alshahrani, A. A. Avaa, K. Banerjee, A. C. Berriman, L. T. Bezzina, L. Bignell, J. Buete, I. P. Carter, B. J. Coombes, J. T. H. Dowie, M. Dasgupta, L. J. Evitts, A. B. Garnsworthy, M. S. M. Gerathy, T. J. Gray, D. J. Hinde, T. H. Hoang, S. S. Hota, E. Ideguchi, P. Jones, G. J. Lane, B. P. McCormick, A. J. Mitchell, N. Palalani, T. Palazzo, M. Ripper, E. C. Simpson, J. Smallcombe, B. M. A. Swinton-Bland, T. Tanaka, T. G. Tornyi and M. O. de Vries, "Improved precision on the experimental E 0 decay branching ratio of the Hoyle state", *Phys. Rev. C.***102**, 2, 024320 (2020).

Farag, E., M. Renzo, R. Farmer, M. T. Chidester and F. X. Timmes, "Resolving the Peak of the Black Hole Mass Spectrum", *ApJ***937**, 2, 112 (2022).

Farag, E., F. X. Timmes, M. T. Chidester, S. Anandagoda and D. H. Hartmann, "Stellar Neutrino Emission across the Mass-Metallicity Plane", *ApJS***270**, 1, 5 (2024).

Farag, E., F. X. Timmes, M. Taylor, K. M. Patton and R. Farmer, "On Stellar Evolution in a Neutrino Hertzsprung-Russell Diagram", *ApJ***893**, 2, 133 (2020).

Farmer, R., C. E. Fields, I. Petermann, L. Dessart, M. Cantiello, B. Paxton and F. X. Timmes, "On Variations Of Pre-supernova Model Properties", *ApJS***227**, 22 (2016).

Farmer, R., C. E. Fields and F. X. Timmes, "On Carbon Burning in Super Asymptotic Giant Branch Stars", *ApJ***807**, 184 (2015).

Farmer, R., M. Renzo, S. E. de Mink, M. Fishbach and S. Justham, "Constraints from Gravitational-wave Detections of Binary Black Hole Mergers on the ^{12}C(α, γ)^{16}O Rate", *ApJ***902**, 2, L36 (2020).

Farmer, R., M. Renzo, S. E. de Mink, P. Marchant and S. Justham, "Mind the Gap: The Location of the Lower Edge of the Pair-instability Supernova Black Hole Mass Gap", *ApJ***887**, 1, 53 (2019).

Farr, W. M. and K. Chatziioannou, "A Population-Informed Mass Estimate for Pulsar J0740+6620", Research Notes of the American Astronomical Society **4**, 5, 65 (2020).

Farr, W. M., N. Sravan, A. Cantrell, L. Kreidberg, C. D. Bailyn, I. Mandel and V. Kalogera, "The Mass Distribution of Stellar-mass Black Holes", *ApJ***741**, 2, 103 (2011).

Ferguson, J. W., D. R. Alexander, F. Allard, T. Barman, J. G. Bodnarik, P. H. Hauschildt, A. Heffner-Wong and A. Tamanai, "Low-Temperature Opacities", *ApJ***623**, 585–596 (2005).

Ferguson, J. W. and A. Dotter, "Changing Abundances, Changing Opacities", in "The Art of Modeling Stars in the 21st Century", edited by L. Deng and K. L. Chan, vol. 252, pp. 1–11 (2008).

Fernández, R., E. Quataert, K. Kashiyama and E. R. Coughlin, "Mass ejection in failed supernovae: variation with stellar progenitor", *MNRAS* **476**, 2, 2366–2383 (2018).

Ferreira, M. and C. Providência, "Constraints on high density equation of state from maximum neutron star mass", *Phys. Rev. D.* **104**, 6, 063006 (2021).

Fields, C. E. and S. Couch, "In preparation", (2020).

Fields, C. E. and S. M. Couch, "Three-dimensional Hydrodynamic Simulations of Convective Nuclear Burning in Massive Stars Near Iron Core Collapse", *ApJ* **921**, 1, 28 (2021).

Fields, C. E., F. X. Timmes, R. Farmer, I. Petermann, W. M. Wolf and S. M. Couch, "The Impact of Nuclear Reaction Rate Uncertainties on the Evolution of Core-collapse Supernova Progenitors", *ApJS* **234**, 19 (2018).

Fonseca, E., H. T. Cromartie, T. T. Pennucci, P. S. Ray, A. Y. Kirichenko, S. M. Ransom, P. B. Demorest, I. H. Stairs, Z. Arzoumanian, L. Guillemot, A. Parthasarathy, M. Kerr, I. Cognard, P. T. Baker, H. Blumer, P. R. Brook, M. DeCesar, T. Dolch, F. A. Dong, E. C. Ferrara, W. Fiore, N. Garver-Daniels, D. C. Good, R. Jennings, M. L. Jones, V. M. Kaspi, M. T. Lam, D. R. Lorimer, J. Luo, A. McEwen, J. W. McKee, M. A. McLaughlin, N. McMann, B. W. Meyers, A. Naidu, C. Ng, D. J. Nice, N. Pol, H. A. Radovan, B. Shapiro-Albert, C. M. Tan, S. P. Tendulkar, J. K. Swiggum, H. M. Wahl and W. W. Zhu, "Refined Mass and Geometric Measurements of the High-mass PSR J0740+6620", *ApJ* **915**, 1, L12 (2021).

Fontaine, G., P. Brassard and P. Bergeron, "The Potential of White Dwarf Cosmochronology", *PASP* **113**, 409–435 (2001).

Fowler, W. A. and F. Hoyle, "Neutrino Processes and Pair Formation in Massive Stars and Supernovae.", *ApJS* **9**, 201 (1964).

Fragione, G., B. Kocsis, F. A. Rasio and J. Silk, "Repeated Mergers, Mass-gap Black Holes, and Formation of Intermediate-mass Black Holes in Dense Massive Star Clusters", *ApJ* **927**, 2, 231 (2022).

Fraley, G. S., "Supernovae Explosions Induced by Pair-Production Instability", *Ap&SS* **2**, 96–114 (1968).

Franz, N., M. Dennis and J. Sakstein, "Tip of the Red Giant Branch Bounds on the Neutrino Magnetic Dipole Moment Revisited", arXiv e-prints p. arXiv:2307.13050 (2023).

Freer, M. and H. O. U. Fynbo, "The Hoyle state in ^{12}C", Progress in Particle and Nuclear Physics **78**, 1–23 (2014).

Fröhlich, C., G. Martínez-Pinedo, M. Liebendörfer, F. Thielemann, E. Bravo, W. R. Hix, K. Langanke and N. T. Zinner, "Neutrino-Induced Nucleosynthesis of A>64 Nuclei: The νp Process", Physical Review Letters **96**, 14, 142502–+ (2006).

Fryer, C., W. Benz, M. Herant and S. A. Colgate, "What Can the Accretion-induced Collapse of White Dwarfs Really Explain?", *ApJ* **516**, 2, 892–899 (1999).

Fryer, C. L., K. Belczynski, G. Wiktorowicz, M. Dominik, V. Kalogera and D. E. Holz, "Compact Remnant Mass Function: Dependence on the Explosion Mechanism and Metallicity", *ApJ* **749**, 1, 91 (2012).

Fryer, C. L., A. Olejak and K. Belczynski, "The Effect of Supernova Convection On Neutron Star and Black Hole Masses", *ApJ* **931**, 2, 94 (2022).

Fryer, C. L., J. A. Rueda and R. Ruffini, "Hypercritical Accretion, Induced Gravitational Collapse, and Binary-Driven Hypernovae", *ApJ* **793**, 2, L36 (2014).

Fryer, C. L., S. E. Woosley and A. Heger, "Pair-Instability Supernovae, Gravity Waves, and Gamma-Ray Transients", *ApJ* **550**, 1, 372–382 (2001).

Fujimoto, M. Y., M. Sztajno, W. H. G. Lewin and J. van Paradijs, "On the Theory of Type I X-Ray Bursts. The Energetics of Bursts and the Nuclear Fuel Reservoir in the Envelope", *ApJ* **319**, 902 (1987).

Fuller, G. M., W. A. Fowler and M. J. Newman, "Stellar weak-interaction rates for sd-shell nuclei. I - Nuclear matrix element systematics with application to Al-26 and selected nuclei of importance to the supernova problem", *ApJS* **42**, 447–473 (1980).

Fuller, G. M., W. A. Fowler and M. J. Newman, "Stellar weak interaction rates for intermediate-mass nuclei. II - A = 21 to A = 60", *ApJ* **252**, 715–740 (1982a).

Fuller, G. M., W. A. Fowler and M. J. Newman, "Stellar weak interaction rates for intermediate mass nuclei. III - Rate tables for the free nucleons and nuclei with A = 21 to A = 60", *ApJS* **48**, 279–319 (1982b).

Fuller, G. M., W. A. Fowler and M. J. Newman, "Stellar weak interaction rates for intermediate-mass nuclei. IV - Interpolation procedures for rapidly varying lepton capture rates using effective log (ft)-values", *ApJ* **293**, 1–16 (1985).

Fuller, J. and W. Lu, "The spins of compact objects born from helium stars in binary systems", *MNRAS* **511**, 3, 3951–3964 (2022).

Gallino, R., C. Arlandini, M. Busso, M. Lugaro, C. Travaglio, O. Straniero, A. Chieffi and M. Limongi, "Evolution and Nucleosynthesis in Low-Mass Asymptotic Giant Branch Stars. II. Neutron Capture and the S-Process", *ApJ* **497**, 1, 388–403 (1998).

García-Berro, E., C. Ritossa and I. Iben, Jr., "On the Evolution of Stars that Form Electron-Degenerate Cores Processed by Carbon Burning. III. The Inward Propagation of a Carbon-Burning Flame and Other Properties of a 9 Msun Model Star", *ApJ* **485**, 2, 765, URL `http://stacks.iop.org/0004-637X/485/i=2/a=765` (1997).

Gautschy, A., "Helium Ignition in the Cores of Low-Mass Stars", ArXiv e-prints (2012).

Gautschy, A., "The Thermal Pulses of Very-Low-Mass Stars", arXiv e-prints p. arXiv:1303.6652 (2013).

Georgy, C., S. Ekström, P. Eggenberger, G. Meynet, L. Haemmerlé, A. Maeder, A. Granada, J. H. Groh, R. Hirschi, N. Mowlavi, N. Yusof, C. Charbonnel, T. Decressin and F. Barblan, "Grids of stellar models with rotation. III. Models from 0.8 to 120 $M_\odot$ at a metallicity Z = 0.002", *A&A* **558**, A103 (2013).

Ghosh, S., N. Wolfe and C. Fröhlich, "PUSHing Core-collapse Supernovae to Explosions in Spherical Symmetry. V. Equation of State Dependency of Explosion Properties, Nucleosynthesis Yields, and Compact Remnants", *ApJ* **929**, 1, 43 (2022).

Giannone, P. and A. Weigert, "Entwicklung in engen Doppelsternsystemen III.", *Zeitschrift fuer Astrophysik* **67**, 41 (1967).

Girardi, L., "A secondary clump of red giant stars: why and where", *MNRAS* **308**, 3, 818–832 (1999).

Glatzel, W., K. J. Fricke and M. F. El Eid, "The fate of rotating pair-unstable carbon-oxygen cores", *A&A* **149**, 2, 413–422 (1985).

Glebbeek, E., E. Gaburov, S. E. de Mink, O. R. Pols and S. F. Portegies Zwart, "The evolution of runaway stellar collision products", *A&A* **497**, 255–264 (2009).

Goodwin, A. J., A. Heger and D. K. Galloway, "Neutrino Losses in Type I Thermonuclear X-Ray Bursts: An Improved Nuclear Energy Generation Approximation", *ApJ* **870**, 2, 64 (2019).

Graboske, H. C., H. E. Dewitt, A. S. Grossman and M. S. Cooper, "Screening Factors for Nuclear Reactions. 11. Intermediate Screen-Ing and Astrophysical Applications", *ApJ* **181**, 457–474 (1973).

Grevesse, N. and A. J. Sauval, "Standard Solar Composition", *Space Science Reviews* **85**, 161–174 (1998).

Groh, J. H., S. Ekström, C. Georgy, G. Meynet, A. Choplin, P. Eggenberger, R. Hirschi, A. Maeder, L. J. Murphy, I. Boian and E. J. Farrell, "Grids of stellar models with rotation. IV. Models from 1.7 to 120 $M_\odot$ at a metallicity Z = 0.0004", *A&A* **627**, A24 (2019).

Grohs, E., A. R. Howe and F. C. Adams, "Universes without the weak force: Astrophysical processes with stable neutrons", *Phys. Rev. D.* **97**, 4, 043003 (2018).

Gupta, A., D. Gerosa, K. G. Arun, E. Berti, W. M. Farr and B. S. Sathyaprakash, "Black holes in the low-mass gap: Implications for gravitational-wave observations", *Phys. Rev. D.* **101**, 10, 103036 (2020).

Haensel, P., J. L. Zdunik and F. Douchin, "Equation of state of dense matter and the minimum mass of cold neutron stars", *A&A* **385**, 301–307 (2002).

Hajduk, M., H. Todt, W.-R. Hamann, K. Borek, P. A. M. van Hoof and A. A. Zijlstra, "The cooling-down central star of the planetary nebula SwSt 1: a late thermal pulse in a massive post-AGB star?", *MNRAS* **498**, 1, 1205–1220 (2020).

Hamers, A. S. and J. Samsing, "Analytic computation of the secular effects of encounters on a binary: features arising from second-order perturbation theory", *MNRAS* **487**, 4, 5630–5648 (2019).

Hansen, C. J., S. D. Kawaler and V. Trimble, *Stellar interiors : physical principles, structure, and evolution* (New York: Springer-Verlag, 2004).

Harada, M., K. Abe, C. Bronner, Y. Hayato, K. Hiraide, K. Hosokawa, K. Ieki, M. Ikeda, J. Kameda, Y. Kanemura and et al., "Search for astrophysical electron antineutrinos in Super-Kamiokande with 0.01wt% gadolinium-loaded water", arXiv e-prints p. arXiv:2305.05135 (2023).

Hartmann, D. H. and S. E. Woosley, "The cosmic supernova neutrino background", Astroparticle Physics **7**, 1-2, 137–146 (1997).

Hawkins, K., B. Leistedt, J. Bovy and D. W. Hogg, "Red clump stars and Gaia: calibration of the standard candle using a hierarchical probabilistic model", *MNRAS* **471**, 1, 722–729 (2017).

Haxton, W. C., R. G. Hamish Robertson and A. M. Serenelli, "Solar Neutrinos: Status and Prospects", *ARA&A* **51**, 1, 21–61 (2013).

Hayashi, C., R. Hōshi and D. Sugimoto, "Evolution of the Stars", Progress of Theoretical Physics Supplement **22**, 1–183 (1962).

Heger, A., C. L. Fryer, S. E. Woosley, N. Langer and D. H. Hartmann, "How Massive Single Stars End Their Life", *ApJ* **591**, 288–300 (2003).

Heger, A., S. E. Woosley, G. Martínez-Pinedo and K. Langanke, "Presupernova Evolution with Improved Rates for Weak Interactions", *ApJ* **560**, 307–325 (2001).

Herwig, F., "The evolution of AGB stars with convective overshoot", *A&A* **360**, 952–968 (2000a).

Herwig, F., "The evolution of AGB stars with convective overshoot", *A&A* **360**, 952–968 (2000b).

Herwig, F., "Modeling the evolution of Sakurai's Object", *Ap&SS* **279**, 103–113 (2002).

Herwig, F., "Evolution of Asymptotic Giant Branch Stars", *ARA&A* **43**, 435–479 (2005).

Higgins, E. R., A. A. C. Sander, J. S. Vink and R. Hirschi, "Evolution of Wolf-Rayet stars as black hole progenitors", *MNRAS* **505**, 4, 4874–4889 (2021).

Hirata, K., T. Kajita, M. Koshiba, M. Nakahata and Y. Oyama, "Observation of a neutrino burst from the supernova SN1987A", *Phys. Rev. L.***58**, 1490–1493 (1987).

Hirata, K. S., T. Kajita, M. Koshiba, M. Nakahata, Y. Oyama, N. Sato, A. Suzuki, M. Takita, Y. Totsuka, T. Kifune, T. Suda, K. Takahashi, T. Tanimori, K. Miyano, M. Yamada, E. W. Beier, L. R. Feldscher, W. Frati, S. B. Kim, A. K. Mann, F. M. Newcomer, R. van Berg, W. Zhang and B. G. Cortez, "Observation in the Kamiokande-II detector of the neutrino burst from supernova SN1987A", *Phys. Rev. D.***38**, 2, 448–458 (1988).

Hofmeister, E., R. Kippenhahn and A. Weigert, "Sternentwicklung III. Die Helium-brennende Phase und die Cepheidenstadien eines Sterns von 7.0 Sonnenmassen. Mit 6 Textabbildungen", *Zeitschrift fuer Astrophysik***60**, 57 (1964).

Horiuchi, S., J. F. Beacom and E. Dwek, "Diffuse supernova neutrino background is detectable in Super-Kamiokande", *Phys. Rev. D.***79**, 8, 083013 (2009).

Hoyle, F., "On Nuclear Reactions Occuring in Very Hot STARS.I. the Synthesis of Elements from Carbon to Nickel.", *ApJS***1**, 121 (1954).

Humphreys, R. M. and K. Davidson, "Studies of luminous stars in nearby galaxies. III. Comments on the evolution of the most massive stars in the Milky Way and the Large Magellanic Cloud.", *ApJ***232**, 409–420 (1979).

Iben, J., I., J. B. Kaler, J. W. Truran and A. Renzini, "On the evolution of those nuclei of planetary nebulae that experiencea final helium shell flash.", *ApJ***264**, 605–612 (1983).

Iben, J., Icko, "A Comparison Between Homogeneous Stellar Models and the Observations.", *ApJ***138**, 452 (1963).

Iben, J., Icko, "Stellar Evolution. I. The Approach to the Main Sequence.", *ApJ***141**, 993 (1965).

Iben, J., Icko and R. T. Rood, "Metal-Poor Stars. I. Evolution from the Main Sequence to the Giant Branch", *ApJ***159**, 605 (1970).

IceCube Collaboration, "Observation of high-energy neutrinos from the Galactic plane", Science **380**, 6652, 1338–1343 (2023).

IceCube Collaboration, M. G. Aartsen, M. Ackermann, J. Adams, J. A. Aguilar, M. Ahlers, M. Ahrens, I. Al Samarai, D. Altmann, K. Andeen, T. Anderson, I. Ansseau, G. Anton, C. Argüelles, J. Auffenberg, S. Axani, H. Bagherpour, X. Bai, J. P. Barron, S. W. Barwick, V. Baum, R. Bay, J. J. Beatty, J. Becker Tjus, K. H. Becker, S. BenZvi, D. Berley, E. Bernardini, D. Z. Besson, G. Binder, D. Bindig, E. Blaufuss, S. Blot, C. Bohm, M. Börner, F. Bos, S. Böser, O. Botner, E. Bourbeau, J. Bourbeau, F. Bradascio, J. Braun, M. Brenzke, H. P. Bretz, S. Bron, J. Brostean-Kaiser, A. Burgman, R. S. Busse, T. Carver, E. Cheung, D. Chirkin, A. Christov, K. Clark, L. Classen, S. Coenders, G. H. Collin, J. M. Conrad, P. Coppin, P. Correa, D. F. Cowen, R. Cross, P. Dave, M. Day, J. P. A. M. de André, C. De Clercq,

J. J. DeLaunay, H. Dembinski, S. De Ridder, P. Desiati, K. D. de Vries, G. de Wasseige, M. de With, T. DeYoung, J. C. Díaz-Vélez, V. di Lorenzo, H. Dujmovic, J. P. Dumm, M. Dunkman, E. Dvorak, B. Eberhardt, T. Ehrhardt, B. Eichmann, P. Eller, P. A. Evenson, S. Fahey, A. R. Fazely, J. Felde, K. Filimonov, C. Finley, S. Flis, A. Franckowiak, E. Friedman, A. Fritz, T. K. Gaisser, J. Gallagher, L. Gerhardt, K. Ghorbani, T. Glauch, T. Glüsenkamp, A. Goldschmidt, J. G. Gonzalez, D. Grant, Z. Griffith, C. Haack, A. Hallgren, F. Halzen, K. Hanson, D. Hebecker, D. Heereman, K. Helbing, R. Hellauer, S. Hickford, J. Hignight, G. C. Hill, K. D. Hoffman, R. Hoffmann, T. Hoinka, B. Hokanson-Fasig, K. Hoshina, F. Huang, M. Huber, K. Hultqvist, M. Hünnefeld, R. Hussain, S. In, N. Iovine, A. Ishihara, E. Jacobi, G. S. Japaridze, M. Jeong, K. Jero, B. J. P. Jones, P. Kalaczynski, W. Kang, A. Kappes, D. Kappesser, T. Karg, A. Karle, U. Katz, M. Kauer, A. Keivani, J. L. Kelley, A. Kheirandish, J. Kim, M. Kim, T. Kintscher, J. Kiryluk, T. Kittler, S. R. Klein, R. Koirala, H. Kolanoski, L. Köpke, C. Kopper, S. Kopper, J. P. Koschinsky, D. J. Koskinen, M. Kowalski, K. Krings, M. Kroll, G. Krückl, S. Kunwar, N. Kurahashi, T. Kuwabara, A. Kyriacou, M. Labare, J. L. Lanfranchi, M. J. Larson, F. Lauber, K. Leonard, M. Lesiak-Bzdak, M. Leuermann, Q. R. Liu, C. J. Lozano Mariscal, L. Lu, J. Lünemann, W. Luszczak, J. Madsen, G. Maggi, K. B. M. Mahn, S. Mancina, R. Maruyama, K. Mase, R. Maunu, K. Meagher, M. Medici, M. Meier, T. Menne, G. Merino, T. Meures, S. Miarecki, J. Micallef, G. Momenté, T. Montaruli, R. W. Moore, S, R. Morse, M. Moulai, R. Nahnhauer, P. Nakarmi, U. Naumann, G. Neer, H. Niederhausen, S. C. Nowicki, D. R. Nygren, A. Obertacke Pollmann, A. Olivas, A. O'Murchadha, E. O'Sullivan, T. Palczewski, H. Pandya, D. V. Pankova, P. Peiffer, J. A. Pepper, C. Pérez de los Heros, D. Pieloth, E. Pinat, M. Plum, P. B. Price, G. T. Przybylski, C. Raab, L. Rädel, M. Rameez, L. Rauch, K. Rawlins, I. C. Rea, R. Reimann, B. Relethford, M. Relich, E. Resconi, W. Rhode, M. Richman, S. Robertson, M. Rongen, C. Rott, T. Ruhe, D. Ryckbosch, D. Rysewyk, I. Safa, T. Sälzer, S. E. Sanchez Herrera, A. Sandrock, J. Sandroos, M. Santander, S. Sarkar, S. Sarkar, K. Satalecka, P. Schlunder, T. Schmidt, A. Schneider, S. Schoenen, S. Schöneberg, L. Schumacher, S. Sclafani, D. Seckel, S. Seunarine, J. Soedingrekso, D. Soldin, M. Song, G. M. Spiczak, C. Spiering, J. Stachurska, M. Stamatikos, T. Stanev, A. Stasik, R. Stein, J. Stettner, A. Steuer, T. Stezelberger, R. G. Stokstad, A. Stößl, N. L. Strotjohann, T. Stuttard, G. W. Sullivan, M. Sutherland, I. Taboada, J. Tatar, F. Tenholt, S. Ter-Antonyan, A. Terliuk, S. Tilav, P. A. Toale, M. N. Tobin, C. Toennis, S. Toscano, D. Tosi, M. Tselengidou, C. F. Tung, A. Turcati, C. F. Turley, B. Ty, E. Unger, M. Usner, J. Vandenbroucke, W. Van Driessche, D. van Eijk, N. van Eijndhoven, S. Vanheule, J. van Santen, E. Vogel, M. Vraeghe, C. Walck, A. Wallace, M. Wallraff, F. D. Wandler, N. Wandkowsky, A. Waza, C. Weaver, M. J. Weiss, C. Wendt, J. Werthebach, S. Westerhoff, B. J. Whelan, N. Whitehorn, K. Wiebe, C. H. Wiebusch, L. Wille, D. R. Williams, L. Wills, M. Wolf, J. Wood, T. R. Wood, K. Woschnagg, D. L. Xu, X. W. Xu, Y. Xu, J. P. Yanez, G. Yodh, S. Yoshida, T. Yuan, Fermi-LAT Collaboration, S. Abdollahi, M. Ajello, R. Angioni, L. Baldini, J. Ballet, G. Barbiellini, D. Bastieri, K. Bechtol, R. Bellazzini, B. Berenji, E. Bissaldi, R. D. Blandford, R. Bonino, E. Bottacini, J. Bregeon, P. Bruel, R. Buehler, T. H. Burnett, E. Burns, S. Buson, R. A. Cameron, R. Caputo, P. A. Caraveo, E. Cavazzuti, E. Charles, S. Chen, C. C. Cheung, J. Chi-

ang, G. Chiaro, S. Ciprini, J. Cohen-Tanugi, J. Conrad, D. Costantin, S. Cutini, F. D'Ammando, F. de Palma, S. W. Digel, N. Di Lalla, M. Di Mauro, L. Di Venere, A. Domínguez, C. Favuzzi, A. Franckowiak, Y. Fukazawa, S. Funk, P. Fusco, F. Gargano, D. Gasparrini, N. Giglietto, M. Giomi, P. Giommi, F. Giordano, M. Giroletti, T. Glanzman, D. Green, I. A. Grenier, M. H. Grondin, S. Guiriec, A. K. Harding, M. Hayashida, E. Hays, J. W. Hewitt, D. Horan, G. Jóhannesson, M. Kadler, S. Kensei, D. Kocevski, F. Krauss, M. Kreter, M. Kuss, G. La Mura, S. Larsson, L. Latronico, M. Lemoine-Goumard, J. Li, F. Longo, F. Loparco, M. N. Lovellette, P. Lubrano, J. D. Magill, S. Maldera, D. Malyshev, A. Manfreda, M. N. Mazziotta, J. E. McEnery, M. Meyer, P. F. Michelson, T. Mizuno, M. E. Monzani, A. Morselli, I. V. Moskalenko, M. Negro, E. Nuss, R. Ojha, N. Omodei, M. Orienti, E. Orlando, M. Palatiello, V. S. Paliya, J. S. Perkins, M. Persic, M. Pesce-Rollins, F. Piron, T. A. Porter, G. Principe, S. Rainò, R. Rando, B. Rani, M. Razzano, S. Razzaque, A. Reimer, O. Reimer, N. Renault-Tinacci, S. Ritz, L. S. Rochester, P. M. Saz Parkinson, C. Sgrò, E. J. Siskind, G. Spandre, P. Spinelli, D. J. Suson, H. Tajima, M. Takahashi, Y. Tanaka, J. B. Thayer, D. J. Thompson, L. Tibaldo, D. F. Torres, E. Torresi, G. Tosti, E. Troja, J. Valverde, G. Vianello, M. Vogel, K. Wood, M. Wood, G. Zaharijas, MAGIC Collaboration, M. L. Ahnen, S. Ansoldi, L. A. Antonelli, C. Arcaro, D. Baack, A. Babić, B. Banerjee, P. Bangale, U. Barres de Almeida, J. A. Barrio, J. Becerra González, W. Bednarek, E. Bernardini, A. Berti, W. Bhattacharyya, A. Biland, O. Blanch, G. Bonnoli, A. Carosi, R. Carosi, G. Ceribella, A. Chatterjee, S. M. Colak, P. Colin, E. Colombo, J. L. Contreras, J. Cortina, S. Covino, P. Cumani, P. Da Vela, F. Dazzi, A. De Angelis, B. De Lotto, M. Delfino, J. Delgado, F. Di Pierro, A. Domínguez, D. Dominis Prester, D. Dorner, M. Doro, S. Einecke, D. Elsaesser, V. Fallah Ramazani, A. Fernández-Barral, D. Fidalgo, L. Foffano, K. Pfrang, M. V. Fonseca, L. Font, A. Franceschini, C. Fruck, D. Galindo, S. Gallozzi, R. J. García López, M. Garczarczyk, M. Gaug, P. Giammaria, N. Godinović, D. Gora, D. Guberman, D. Hadasch, A. Hahn, T. Hassan, M. Hayashida, J. Herrera, J. Hose, D. Hrupec, S. Inoue, K. Ishio, Y. Konno, H. Kubo, J. Kushida, D. Lelas, E. Lindfors, S. Lombardi, F. Longo, M. López, C. Maggio, P. Majumdar, M. Makariev, G. Maneva, M. Manganaro, K. Mannheim, L. Maraschi, M. Mariotti, M. Martínez, S. Masuda, D. Mazin, M. Minev, J. M. M, R. Mirzoyan, A. Moralejo, V. Moreno, E. Moretti, T. Nagayoshi, V. Neustroev, A. Niedzwiecki, M. Nievas Rosillo, C. Nigro, K. Nilsson, D. Ninci, K. Nishijima, K. Noda, L. Nogués, S. Paiano, J. Palacio, D. Paneque, R. Paoletti, J. M. Paredes, G. Pedaletti, M. Peresano, M. Persic, P. G. Prada Moroni, E. Prandini, I. Puljak, J. Rodriguez Garcia, I. Reichardt, W. Rhode, M. Ribó, J. Rico, C. Righi, A. Rugliancich, T. Saito, K. Satalecka, T. Schweizer, J. Sitarek, I. Šnidaric´, D. Sobczynska, A. Stamerra, M. Strzys, T. Surić, M. Takahashi, F. Tavecchio, P. Temnikov, T. Terzić, M. Teshima, N. Torres-Albà, A. Treves, S. Tsujimoto, G. Vanzo, M. Vazquez Acosta, I. Vovk, J. E. Ward, M. Will, S, D. Zaric ´, AGILE Team, F. Lucarelli, M. Tavani, G. Piano, I. Donnarumma, C. Pittori, F. Verrecchia, G. Barbiellini, A. Bulgarelli, P. Caraveo, P. W. Cattaneo, S. Colafrancesco, E. Costa, G. Di Cocco, A. Ferrari, F. Gianotti, A. Giuliani, P. Lipari, S. Mereghetti, A. Morselli, L. Pacciani, F. Paoletti, N. Parmiggiani, A. Pellizzoni, P. Picozza, M. Pilia, A. Rappoldi, A. Trois, S. Vercellone, V. Vittorini, ASAS-SN Team, A. F. K. Z. Stanek, C. S. Kochanek, J. F.

Beacom, T. A. Thompson, T. W. S. Holoien, S. Dong, J. L. Prieto, B. J. Shappee, S. Holmbo, HAWC Collaboration, A. U. Abeysekara, A. Albert, R. Alfaro, C. Alvarez, R. Arceo, J. C. Arteaga-Velázquez, D. Avila Rojas, H. A. Ayala Solares, A. Becerril, E. Belmont-Moreno, A. Bernal, K. S. Caballero-Mora, T. Capistrán, A. Carramiñana, S. Casanova, M. Castillo, U. Cotti, J. Cotzomi, S. Coutiño de León, C. De León, E. De la Fuente, R. Diaz Hernandez, S. Dichiara, B. L. Dingus, M. A. DuVernois, J. C. Díaz-Vélez, R. W. Ellsworth, K. Engel, D. W. Fiorino, H. Fleischhack, N. Fraija, J. A. García-González, F. Garfias, A. González Muñoz, M. M. González, J. A. Goodman, Z. Hampel-Arias, J. P. Harding, S. Hernand ez, B. Hona, F. Hueyotl-Zahuantitla, C. M. Hui, P. Hüntemeyer, A. Iriarte, A. Jardin-Blicq, V. Joshi, S. Kaufmann, G. J. Kunde, A. Lara, R. J. Lauer, W. H. Lee, D. Lennarz, H. León Vargas, J. T. Linnemann, A. L. Longinotti, G. Luis-Raya, R. Luna-García, K. Malone, S. S. Marinelli, O. Martinez, I. Martinez-Castellanos, J. Martínez-Castro, H. Martínez-Huerta, J. A. Matthews, P. Miranda-Romagnoli, E. Moreno, M. Mostafá, A. Nayerhoda, L. Nellen, M. Newbold, M. U. Nisa, R. Noriega-Papaqui, R. Pelayo, J. Pretz, E. G. Pérez-Pérez, Z. Ren, C. D. Rho, C. Rivière, D. Rosa-González, M. Rosenberg, E. Ruiz-Velasco, E. Ruiz-Velasco, F. Salesa Greus, A. Sandoval, M. Schneider, H. Schoorlemmer, G. Sinnis, A. J. Smith, R. W. Springer, P. Surajbali, O. Tibolla, K. Tollefson, I. Torres, L. Villaseñor, T. Weisgarber, F. Werner, T. Yapici, Y. Gaurang, A. Zepeda, H. Zhou, J. D. Álvarez, H. E. S. S. Collaboration, H. Abdalla, E. O. Angüner, C. Armand, M. Backes, Y. Becherini, D. Berge, M. Böttcher, C. Boisson, J. Bolmont, S. Bonnefoy, P. Bordas, F. Brun, M. Büchele, T. Bulik, S. Caroff, A. Carosi, S. Casanova, M. Cerruti, N. Chakraborty, S. Chandra, A. Chen, S. Colafrancesco, I. D. Davids, C. Deil, J. Devin, A. Djannati-Ataï, K. Egberts, G. Emery, S. Eschbach, A. Fiasson, G. Fontaine, S. Funk, M. Füßling, Y. A. Gallant, F. Gaté, G. Giavitto, D. Glawion, J. F. Glicenstein, D. Gottschall, M. H. Grondin, M. Haupt, G. Henri, J. A. Hinton, C. Hoischen, T. L. Holch, D. Huber, M. Jamrozy, D. Jankowsky, F. Jankowsky, L. Jouvin, I. Jung-Richardt, D. Kerszberg, B. Khélifi, J. King, S. Klepser, W. Kluz´niak, N. Komin, M. Kraus, J. Lefaucheur, A. Lemière, M. Lemoine-Goumard, J. P. Lenain, E. Leser, T. Lohse, R. López-Coto, M. Lorentz, I. Lypova, V. Marandon, G. Guillem Martí-Devesa, G. Maurin, A. M. W. Mitchell, R. Moderski, M. Mohamed, L. Mohrmann, E. Moulin, T. Murach, M. de Naurois, F. Niederwanger, J. Niemiec, L. Oakes, P. O'Brien, S. Ohm, M. Ostrowski, I. Oya, M. Panter, R. D. Parsons, C. Perennes, Q. Piel, S. Pita, V. Poireau, A. Priyana Noel, H. Prokoph, G. Pühlhofer, A. Quirrenbach, S. Raab, R. Rauth, M. Renaud, F. Rieger, L. Rinchiuso, C. Romoli, G. Rowell, B. Rudak, D. A. Sasaki, M. Sanchez, R. Schlickeiser, F. Schüssler, A. Schulz, U. Schwanke, M. Seglar-Arroyo, N. Shafi, R. Simoni, H. Sol, C. Stegmann, C. Steppa, T. Tavernier, A. M. Taylor, D. Tiziani, C. Trichard, M. Tsirou, C. van Eldik, C. van Rensburg, B. van Soelen, J. Veh, P. Vincent, F. Voisin, S. J. Wagner, R. M. Wagner, A. Wierzcholska, R. Zanin, A. A. Zdziarski, A. Zech, A. Ziegler, J. Zorn, N. Żywucka, INTEGRAL Team, V. Savchenko, C. Ferrigno, A. Bazzano, R. Diehl, E. Kuulkers, P. Laurent, S. Mereghetti, L. Natalucci, F. Panessa, J. Rodi, P. Ubertini, K. Kanata, S. O. Teams, T. Morokuma, K. Ohta, Y. T. Tanaka, H. Mori, M. Yamanaka, K. S. Kawabata, Y. Utsumi, T. Nakaoka, M. Kawabata, H. Nagashima, M. Yoshida, Y. Matsuoka, R. Itoh, Kapteyn Team, W. Keel, Liverpool Telescope

Team, C. Copperwheat, I. Steele, Swift/NuSTAR Team, S. B. Cenko, D. F. Cowen, J. J. DeLaunay, P. A. Evans, D. B. Fox, A. Keivani, J. A. Kennea, F. E. Marshall, J. P. Osborne, M. Santander, A. Tohuvavohu, C. F. Turley, VERITAS Collaboration, A. U. Abeysekara, A. Archer, W. Benbow, R. Bird, A. Brill, R. Brose, M. Buchovecky, J. H. Buckley, V. Bugaev, J. L. Christiansen, M. P. Connolly, W. Cui, M. K. Daniel, M. Errando, A. Falcone, Q. Feng, J. P. Finley, L. Fortson, A. Furniss, O. Gueta, M. Hütten, O. Hervet, G. Hughes, T. B. Humensky, C. A. Johnson, P. Kaaret, P. Kar, N. Kelley-Hoskins, M. Kertzman, D. Kieda, M. Krause, F. Krennrich, S. Kumar, M. J. Lang, T. T. Y. Lin, G. Maier, S. McArthur, P. Moriarty, R. Mukherjee, D. Nieto, S. O'Brien, R. A. Ong, A. N. Otte, N. Park, A. Petrashyk, M. Pohl, A. Popkow, S. E. Pueschel, J. Quinn, K. Ragan, P. T. Reynolds, G. T. Richards, E. Roache, C. Rulten, I. Sadeh, M. Santander, S. S. Scott, G. H. Sembroski, K. Shahinyan, I. Sushch, S. Trépanier, J. Tyler, V. V. Vassiliev, S. P. Wakely, A. Weinstein, R. M. Wells, P. Wilcox, A. Wilhelm, D. A. Williams, B. Zitzer, VLA/B Team, A. J. Tetarenko, A. E. Kimball, J. C. A. Miller-Jones and G. R. Sivakoff, "Multimessenger observations of a flaring blazar coincident with high-energy neutrino IceCube-170922A", Science **361**, 6398, eaat1378 (2018a).

IceCube Collaboration, M. G. Aartsen, M. Ackermann, J. Adams, J. A. Aguilar, M. Ahlers, M. Ahrens, I. A. Samarai, D. Altmann, K. Andeen, T. Anderson, I. Ansseau, G. Anton, C. Argüelles, B. Arsioli, J. Auffenberg, S. Axani, H. Bagherpour, X. Bai, J. P. Barron, S. W. Barwick, V. Baum, R. Bay, J. J. Beatty, J. Becker Tjus, K. H. Becker, S. BenZvi, D. Berley, E. Bernardini, D. Z. Besson, G. Binder, D. Bindig, E. Blaufuss, S. Blot, C. Bohm, M. Börner, F. Bos, S. Böser, O. Botner, E. Bourbeau, J. Bourbeau, F. Bradascio, J. Braun, M. Brenzke, H. P. Bretz, S. Bron, J. Brostean-Kaiser, A. Burgman, R. S. Busse, T. Carver, E. Cheung, D. Chirkin, A. Christov, K. Clark, L. Classen, S. Coenders, G. H. Collin, J. M. Conrad, P. Coppin, P. Correa, D. F. Cowen, R. Cross, P. Dave, M. Day, J. P. A. M. de André, C. De Clercq, J. J. DeLaunay, H. Dembinski, S. DeRidder, P. Desiati, K. D. de Vries, G. de Wasseige, M. de With, T. DeYoung, J. C. Díaz-Vélez, V. di Lorenzo, H. Dujmovic, J. P. Dumm, M. Dunkman, E. Dvorak, B. Eberhardt, T. Ehrhardt, B. Eichmann, P. Eller, P. A. Evenson, S. Fahey, A. R. Fazely, J. Felde, K. Filimonov, C. Finley, S. Flis, A. Franckowiak, E. Friedman, A. Fritz, T. K. Gaisser, J. Gallagher, L. Gerhardt, K. Ghorbani, P. Giommi, T. Glauch, T. Glüsenkamp, A. Goldschmidt, J. G. Gonzalez, D. Grant, Z. Griffith, C. Haack, A. Hallgren, F. Halzen, K. Hanson, D. Hebecker, D. Heereman, K. Helbing, R. Hellauer, S. Hickford, J. Hignight, G. C. Hill, K. D. Hoffman, R. Hoffmann, T. Hoinka, B. Hokanson-Fasig, K. Hoshina, F. Huang, M. Huber, K. Hultqvist, M. Hünnefeld, R. Hussain, S. In, N. Iovine, A. Ishihara, E. Jacobi, G. S. Japaridze, M. Jeong, K. Jero, B. J. P. Jones, P. Kalaczynski, W. Kang, A. Kappes, D. Kappesser, T. Karg, A. Karle, U. Katz, M. Kauer, A. Keivani, J. L. Kelley, A. Kheirandish, J. Kim, M. Kim, T. Kintscher, J. Kiryluk, T. Kittler, S. R. Klein, R. Koirala, H. Kolanoski, L. Köpke, C. Kopper, S. Kopper, J. P. Koschinsky, D. J. Koskinen, M. Kowalski, B. Krammer, K. Krings, M. Kroll, G. Krückl, S. Kunwar, N. Kurahashi, T. Kuwabara, A. Kyriacou, M. Labare, J. L. Lanfranchi, M. J. Larson, F. Lauber, K. Leonard, M. Lesiak-Bzdak, M. Leuermann, Q. R. Liu, C. J. Lozano Mariscal, L. Lu, J. Lünemann, W. Luszczak, J. Madsen, G. Maggi,

K. B. M. Mahn, S. Mancina, R. Maruyama, K. Mase, R. Maunu, K. Meagher, M. Medici, M. Meier, T. Menne, G. Merino, T. Meures, S. Miarecki, J. Micallef, G. Momenté, T. Montaruli, R. W. Moore, R. Morse, M. Moulai, R. Nahnhauer, P. Nakarmi, U. Naumann, G. Neer, H. Niederhausen, S. C. Nowicki, D. R. Nygren, A. Obertacke Pollmann, A. Olivas, A. O'Murchadha, E. O'Sullivan, P. Padovani, T. Palczewski, H. Pand ya, D. V. Pankova, P. Peiffer, J. A. Pepper, C. Pérez de los Heros, D. Pieloth, E. Pinat, M. Plum, P. B. Price, G. T. Przybylski, C. Raab, L. Rädel, M. Rameez, K. Rawlins, I. C. Rea, R. Reimann, B. Relethford, M. Relich, E. Resconi, W. Rhode, M. Richman, S. Robertson, M. Rongen, C. Rott, T. Ruhe, D. Ryckbosch, D. Rysewyk, I. Safa, N. Sahakyan, T. Sälzer, S. E. Sanchez Herrera, A. Sandrock, J. Sandroos, M. Santander, S. Sarkar, S. Sarkar, K. Satalecka, P. Schlunder, T. Schmidt, A. Schneider, S. Schoenen, S. Schöneberg, L. Schumacher, S. Sclafani, D. Seckel, S. Seunarine, J. Soedingrekso, D. Soldin, M. Song, G. M. Spiczak, C. Spiering, J. Stachurska, M. Stamatikos, T. Stanev, A. Stasik, J. Stettner, A. Steuer, T. Stezelberger, R. G. Stokstad, A. Stößl, N. L. Strotjohann, T. Stuttard, G. W. Sullivan, M. Sutherland, I. Taboada, J. Tatar, F. Tenholt, S. Ter-Antonyan, A. Terliuk, S. Tilav, P. A. Toale, M. N. Tobin, C. Toennis, S. Toscano, D. Tosi, M. Tselengidou, C. F. Tung, A. Turcati, C. F. Turley, B. Ty, E. Unger, M. Usner, J. Vandenbroucke, W. Van Driessche, D. van Eijk, N. van Eijndhoven, S. Vanheule, J. van Santen, E. Vogel, M. Vraeghe, C. Walck, A. Wallace, M. Wallraff, F. D. Wandler, N. Wand kowsky, A. Waza, C. Weaver, M. J. Weiss, C. Wendt, J. Werthebach, S. Westerhoff, B. J. Whelan, N. Whitehorn, K. Wiebe, C. H. Wiebusch, L. Wille, D. R. Williams, L. Wills, M. Wolf, J. Wood, T. R. Wood, K. Woschnagg, D. L. Xu, X. W. Xu, Y. Xu, J. P. Yanez, G. Yodh, S. Yoshida and T. Yuan, "Neutrino emission from the direction of the blazar TXS 0506+056 prior to the IceCube-170922A alert", Science **361**, 6398, 147–151 (2018b).

Iglesias, C. A. and F. J. Rogers, "Radiative opacities for carbon- and oxygen-rich mixtures", *ApJ***412**, 752–760 (1993).

Iglesias, C. A. and F. J. Rogers, "Updated Opal Opacities", *ApJ***464**, 943 (1996a).

Iglesias, C. A. and F. J. Rogers, "Updated Opal Opacities", *ApJ***464**, 943 (1996b).

Imbriani, G., M. Limongi, L. Gialanella, F. Terrasi, O. Straniero and A. Chieffi, "The ^{12}C(α, γ)^{16}O Reaction Rate and the Evolution of Stars in the Mass Range 0.8¡=M/M$_{solar}$¡=25", *ApJ***558**, 2, 903–915 (2001).

Irwin, A. W., "The FreeEOS Code for Calculating the Equation of State for Stellar Interiors", http://freeeos.sourceforge.net/, (2004).

Itoh, N., T. Adachi, M. Nakagawa, Y. Kohyama and H. Munakata, "Neutrino Energy Loss in Stellar Interiors. III. Pair, Photo-, Plasma, and Bremsstrahlung Processes", *ApJ***339**, 354 (1989).

Itoh, N., H. Hayashi, A. Nishikawa and Y. Kohyama, "Neutrino Energy Loss in Stellar Interiors. VII. Pair, Photo-, Plasma, Bremsstrahlung, and Recombination Neutrino Processes", *ApJS***102**, 411–+ (1996a).

Itoh, N., H. Mutoh, A. Hikita and Y. Kohyama, "Neutrino Energy Loss in Stellar Interiors. IV. Plasma Neutrino Process for Strongly Degenerate Electrons", *ApJ* **395**, 622 (1992).

Itoh, N., A. Nishikawa and Y. Kohyama, "Neutrino Energy Loss in Stellar Interiors. VIII. Braaten-Segel Approximation for the Plasma Neutrino Process", *ApJ* **470**, 1015 (1996b).

Itoh, N., H. Totsuji, S. Ichimaru and H. E. Dewitt, "Enhancement of thermonuclear reaction rate due to strong screening. II - Ionic mixtures", *ApJ* **234**, 1079–1084 (1979).

Ivanov, M. and R. Fernández, "Mass Ejection in Failed Supernovae: Equation of State and Neutrino Loss Dependence", *ApJ* **911**, 1, 6 (2021).

Izzard, R. G., M. Lugaro, A. I. Karakas, C. Iliadis and M. van Raai, "Reaction rate uncertainties and the operation of the NeNa and MgAl chains during HBB in intermediate-mass AGB stars", *A&A* **466**, 2, 641–648 (2007).

Jacobson-Galán, W. V., L. Dessart, D. O. Jones, R. Margutti, D. L. Coppejans, G. Dimitriadis, R. J. Foley, C. D. Kilpatrick, D. J. Matthews, S. Rest, G. Terreran, P. D. Aleo, K. Auchettl, P. K. Blanchard, D. A. Coulter, K. W. Davis, T. J. L. de Boer, L. DeMarchi, M. R. Drout, N. Earl, A. Gagliano, C. Gall, J. Hjorth, M. E. Huber, A. L. Ibik, D. Milisavljevic, Y. C. Pan, A. Rest, R. Ridden-Harper, C. Rojas-Bravo, M. R. Siebert, K. W. Smith, K. Taggart, S. Tinyanont, Q. Wang and Y. Zenati, "Final Moments. I. Precursor Emission, Envelope Inflation, and Enhanced Mass Loss Preceding the Luminous Type II Supernova 2020tlf", *ApJ* **924**, 1, 15 (2022).

Janka, H.-T., "Neutrino Emission from Supernovae", ArXiv e-prints (2017).

Jermyn, A. S., E. B. Bauer, J. Schwab, R. Farmer, W. H. Ball, E. P. Bellinger, A. Dotter, M. Joyce, P. Marchant, J. S. G. Mombarg, W. M. Wolf, T. L. Sunny Wong, G. C. Cinquegrana, E. Farrell, R. Smolec, A. Thoul, M. Cantiello, F. Herwig, O. Toloza, L. Bildsten, R. H. D. Townsend and F. X. Timmes, "Modules for Experiments in Stellar Astrophysics (MESA): Time-dependent Convection, Energy Conservation, Automatic Differentiation, and Infrastructure", *ApJS* **265**, 1, 15 (2023).

Jermyn, A. S., E. B. Bauer, J. Schwab, R. Farmer, W. H. Ball, E. P. Bellinger, A. Dotter, M. Joyce, P. Marchant, J. S. G. Mombarg, W. M. Wolf, T. L. S. Wong, G. C. Cinquegrana, E. Farrell, R. Smolec, A. Thoul, M. Cantiello, F. Herwig, O. Toloza, L. Bildsten, R. H. D. Townsend and F. X. Timmes, "Modules for Experiments in Stellar Astrophysics (MESA): Time-Dependent Convection, Energy Conservation, Automatic Differentiation, and Infrastructure", arXiv e-prints p. arXiv:2208.03651 (2022).

Jermyn, A. S., J. Schwab, E. Bauer, F. X. Timmes and A. Y. Potekhin, "Skye: A Differentiable Equation of State", *ApJ* **913**, 1, 72 (2021).

Jones, S., R. Hirschi, K. Nomoto, T. Fischer, F. X. Timmes, F. Herwig, B. Paxton, H. Toki, T. Suzuki, G. Martínez-Pinedo, Y. H. Lam and M. G. Bertolli, "Advanced Burning Stages and Fate of 8-10 $M_\odot$ Stars", *ApJ* **772**, 150 (2013).

Jones, S., R. Hirschi, M. Pignatari, A. Heger, C. Georgy, N. Nishimura, C. Fryer and F. Herwig, "Code dependencies of pre-supernova evolution and nucleosynthesis in massive stars: evolution to the end of core helium burning", *MNRAS* **447**, 4, 3115–3129 (2015).

José, J., A. Coc and M. Hernanz, "Nuclear Uncertainties in the NeNa-MgAl Cycles and Production of ^{22}Na and ^{26}Al during Nova Outbursts", *ApJ* **520**, 1, 347–360 (1999).

Kajino, T., W. Aoki, A. B. Balantekin, R. Diehl, M. A. Famiano and G. J. Mathews, "Current status of r-process nucleosynthesis", Progress in Particle and Nuclear Physics **107**, 109–166 (2019).

Kantor, E. M. and M. E. Gusakov, "The neutrino emission due to plasmon decay and neutrino luminosity of white dwarfs", *MNRAS* **381**, 4, 1702–1710 (2007).

Kappeler, F., H. Beer and K. Wisshak, "s-process nucleosynthesis-nuclear physics and the classical model", Reports on Progress in Physics **52**, 945–1013 (1989).

Käppeler, F., R. Gallino, S. Bisterzo and W. Aoki, "The s process: Nuclear physics, stellar models, and observations", Reviews of Modern Physics **83**, 157–194 (2011).

Kato, C., M. Delfan Azari, S. Yamada, K. Takahashi, H. Umeda, T. Yoshida and K. Ishidoshiro, "Pre-supernova Neutrino Emissions from ONe Cores in the Progenitors of Core-collapse Supernovae: Are They Distinguishable from Those of Fe Cores?", *ApJ* **808**, 2, 168 (2015).

Kato, C., R. Hirai and H. Nagakura, "The sensitivity of presupernova neutrinos to stellar evolution models", *MNRAS* **496**, 3, 3961–3972 (2020a).

Kato, C., K. Ishidoshiro and T. Yoshida, "Theoretical Prediction of Presupernova Neutrinos and Their Detection", Annual Review of Nuclear and Particle Science **70**, 121–145 (2020b).

Kato, C., H. Nagakura, S. Furusawa, K. Takahashi, H. Umeda, T. Yoshida, K. Ishidoshiro and S. Yamada, "Neutrino Emissions in All Flavors up to the Pre-bounce of Massive Stars and the Possibility of Their Detections", *ApJ* **848**, 1, 48 (2017).

Kawaler, S. D., D. E. Winget, J. Iben, I. and C. J. Hansen, "Evolutionary Period Changes in Variable Helium-rich White Dwarfs", *ApJ* **302**, 530 (1986).

Kemp, A. J., A. I. Karakas, A. R. Casey, C. Kobayashi and R. G. Izzard, "The impact of metallicity on nova populations", *MNRAS* **509**, 1, 1175–1193 (2022).

Kibédi, T., B. Alshahrani, A. E. Stuchbery, A. C. Larsen, A. Görgen, S. Siem, M. Guttormsen, F. Giacoppo, A. I. Morales, E. Sahin, G. M. Tveten, F. L. B. Garrote, L. C. Campo, T. K. Eriksen, M. Klintefjord, S. Maharramova, H. T. Nyhus, T. G. Tornyi, T. Renstrøm and W. Paulsen, "Radiative Width of the Hoyle State from γ -Ray Spectroscopy", *Phys. Rev. L.***125**, 18, 182701 (2020).

Koliogiannis, P. S. and C. C. Moustakidis, "Thermodynamical Description of Hot, Rapidly Rotating Neutron Stars, Protoneutron Stars, and Neutron Star Merger Remnants", *ApJ***912**, 1, 69 (2021).

Kosmas, T. S., I. Tsoulos, O. Kosmas and P. G. Giannaka, "Evolution of Hot and Dense Stellar Interiors: The Role of the Weak Interaction Processes", Frontiers in Astronomy and Space Sciences **8**, 763276 (2022).

Krauss, L. M., S. L. Glashow and D. N. Schramm, "Antineutrino astronomy and geophysics", *Nature***310**, 5974, 191–198 (1984).

Kroupa, P., "On the variation of the initial mass function", *MNRAS***322**, 2, 231–246 (2001).

Kunz, R., M. Fey, M. Jaeger, A. Mayer, J. W. Hammer, G. Staudt, S. Harissopulos and T. Paradellis, "Astrophysical Reaction Rate of ^{12}C(α, γ)^{16}O", *ApJ***567**, 1, 643–650 (2002).

Kupka, F., F. Ahlborn and A. Weiss, "Stellar evolution models with overshooting based on 3-equation non-local theories I. Physical basis and the computation of the dissipation rate", arXiv e-prints p. arXiv:2207.12296 (2022).

Kutschera, M., A. Odrzywołek and M. Misiaszek, "Presupernovae as Powerful Neutrino Sources", Acta Physica Polonica B **40**, 11, 3063 (2009).

Kutter, G. S. and M. P. Savedoff, "Evolution of Initially Pure ˆ{12}C Stars and the Production of Planetary Nebulae", *ApJ***156**, 1021 (1969).

Kyutoku, K. and K. Kashiyama, "Detectability of thermal neutrinos from binary neutron-star mergers and implications for neutrino physics", *Phys. Rev. D.***97**, 10, 103001 (2018a).

Kyutoku, K. and K. Kashiyama, "Detectability of thermal neutrinos from binary neutron-star mergers and implications for neutrino physics", *Phys. Rev. D.***97**, 10, 103001 (2018b).

Lamb, S. A., I. Iben, Jr. and W. M. Howard, "On the evolution of massive stars through the core carbon-burning phase", *ApJ***207**, 209–232 (1976).

Langanke, K. and G. Martínez-Pinedo, "Shell-model calculations of stellar weak interaction rates: II. Weak rates for nuclei in the mass range /A=45-65 in supernovae environments", Nuclear Physics A **673**, 481–508 (2000).

Langanke, K. and G. Martínez-Pinedo, "The role of electron capture in core-collapse supernovae", Nuclear Physics A **928**, 305–312 (2014).

Lattimer, J., "Neutron stars and the nuclear matter equation of state", Annual Review of Nuclear and Particle Science **71**, 1, 433–464, URL `https://doi.org/10.1146/annurev-nucl-102419-124827` (2021).

Lawlor, T. M., "A closer look at low-mass post-AGB late thermal pulses", *MNRAS* **519**, 4, 5373–5383 (2023).

Lecoanet, D., J. Schwab, E. Quataert, L. Bildsten, F. X. Timmes, K. J. Burns, G. M. Vasil, J. S. Oishi and B. P. Brown, "Turbulent Chemical Diffusion in Convectively Bounded Carbon Flames", *ApJ* **832**, 71 (2016).

Lee, M. G., W. L. Freedman and B. F. Madore, "The Tip of the Red Giant Branch as a Distance Indicator for Resolved Galaxies", *ApJ* **417**, 553 (1993).

Lejeune, T., F. Cuisinier and R. Buser, "A standard stellar library for evolutionary synthesis. II. The M dwarf extension", *A&AS* **130**, 65–75 (1998).

Leung, S.-C., S. Blinnikov, K. Ishidoshiro, A. Kozlov and K. Nomoto, "Pulsational Pair-instability Supernovae. II. Neutrino Signals from Pulsations and Their Detection by Terrestrial Neutrino Detectors", *ApJ* **889**, 2, 75 (2020).

Li, Y.-F., "Overview of the Jiangmen Underground Neutrino Observatory (JUNO)", in "International Journal of Modern Physics Conference Series", vol. 31 of *International Journal of Modern Physics Conference Series*, p. 1460300 (2014).

LIGO Scientific Collaboration, J. Aasi, B. P. Abbott, R. Abbott, T. Abbott, M. R. Abernathy, K. Ackley, C. Adams, T. Adams, P. Addesso and et al., "Advanced LIGO", Classical and Quantum Gravity **32**, 7, 074001 (2015).

Limongi, M. and A. Chieffi, "Presupernova Evolution and Explosive Nucleosynthesis of Rotating Massive Stars in the Metallicity Range $-3 \leq$ [Fe/H] ≤ 0", *ApJS* **237**, 13 (2018).

Lin, Z. and C. Lunardini, "Observing cosmological binary mergers with next generation neutrino and gravitational wave detectors", *Phys. Rev. D.* **101**, 2, 023016 (2020).

Liu, B. and D. Lai, "Black Hole and Neutron Star Binary Mergers in Triple Systems: Merger Fraction and Spin-Orbit Misalignment", *ApJ* **863**, 1, 68 (2018).

Lunardini, C. and W. Winter, "High energy neutrinos from the tidal disruption of stars", *Phys. Rev. D.* **95**, 12, 123001 (2017).

Madore, B. F., W. L. Freedman, K. A. Owens and I. S. Jang, "Quantifying Uncertainties on the Tip of the Red Giant Branch Method", *AJ* **166**, 1, 2 (2023).

Mandel, I. and F. S. Broekgaarden, "Rates of compact object coalescences", Living Reviews in Relativity **25**, 1, 1 (2022).

Mandel, I. and A. Farmer, "Merging stellar-mass binary black holes", *Phys. Reports* **955**, 1–24 (2022).

Mapelli, M., "Formation Channels of Single and Binary Stellar-Mass Black Holes", in "Handbook of Gravitational Wave Astronomy", p. 16 (Springer Nature Singapore, 2021).

Marchant, P. and T. J. Moriya, "The impact of stellar rotation on the black hole mass-gap from pair-instability supernovae", *A&A* **640**, L18 (2020).

Marchant, P., M. Renzo, R. Farmer, K. M. W. Pappas, R. E. Taam, S. E. de Mink and V. Kalogera, "Pulsational Pair-instability Supernovae in Very Close Binaries", *ApJ* **882**, 1, 36 (2019).

Marion, J. B. and W. A. Fowler, "Nuclear Reactions with the Neon Isotopes in Stars.", *ApJ* **125**, 221 (1957).

Marques, M., M. Oertel, M. Hempel and J. Novak, "New temperature dependent hyperonic equation of state: Application to rotating neutron star models and I -Q relations", *Phys. Rev. C.* **96**, 4, 045806 (2017).

Matzner, C. D. and S. Ro, "Wave-driven Shocks in Stellar Outbursts: Dynamics, Envelope Heating, and Nascent Blast Waves", *ApJ* **908**, 1, 23 (2021).

McLaughlin, G. C. and G. M. Fuller, "Neutrino Capture on Heavy Nuclei", *ApJ* **455**, 202–+ (1995).

Meakin, C. A. and D. Arnett, "Turbulent Convection in Stellar Interiors. I. Hydrodynamic Simulation", *ApJ* **667**, 448–475 (2007).

Mehta, A. K., A. Buonanno, J. Gair, M. C. Miller, E. Farag, R. J. deBoer, M. Wiescher and F. X. Timmes, "Observing Intermediate-mass Black Holes and the Upper Stellar-mass gap with LIGO and Virgo", *ApJ* **924**, 1, 39 (2022).

Miller, M. C., F. K. Lamb, A. J. Dittmann, S. Bogdanov, Z. Arzoumanian, K. C. Gendreau, S. Guillot, W. C. G. Ho, J. M. Lattimer, M. Loewenstein, S. M. Morsink, P. S. Ray, M. T. Wolff, C. L. Baker, T. Cazeau, S. Manthripragada, C. B. Markwardt, T. Okajima, S. Pollard, I. Cognard, H. T. Cromartie, E. Fonseca, L. Guillemot, M. Kerr, A. Parthasarathy, T. T. Pennucci, S. Ransom and I. Stairs, "The Radius of PSR J0740+6620 from NICER and XMM-Newton Data", *ApJ* **918**, 2, L28 (2021).

Miller Bertolami, M. M. and L. G. Althaus, "The born-again (very late thermal pulse) scenario revisited: the mass of the remnants and implications for V4334 Sgr", *MNRAS* **380**, 2, 763–770 (2007).

Misch, G. W., Y. Sun and G. M. Fuller, "Neutrino Spectra from Nuclear Weak Interactions in sd-Shell Nuclei under Astrophysical Conditions", *ApJ* **852**, 1, 43 (2018).

Misiaszek, M., A. Odrzywołek and M. Kutschera, "Neutrino spectrum from the pair-annihilation process in the hot stellar plasma", *Phys. Rev. D.* **74**, 4, 043006 (2006a).

Misiaszek, M., A. Odrzywołek and M. Kutschera, "Neutrino spectrum from the pair-annihilation process in the hot stellar plasma", *Phys. Rev. D.***74**, 4, 043006 (2006b).

Mitalas, R., "Unconventional C-12 production in population III stars", *ApJ***290**, 273–275 (1985).

Monpribat, E., S. Martinet, S. Courtin, M. Heine, S. Ekström, D. G. Jenkins, A. Choplin, P. Adsley, D. Curien, M. Moukaddam, J. Nippert, S. Tsiatsiou and G. Meynet, "A new $^{12}C + ^{12}C$ nuclear reaction rate: Impact on stellar evolution", *A&A***660**, A47 (2022).

Mukhopadhyay, M., C. Lunardini, F. X. Timmes and K. Zuber, "Presupernova Neutrinos: Directional Sensitivity and Prospects for Progenitor Identification", *ApJ***899**, 2, 153 (2020).

Müller, B., T. Melson, A. Heger and H.-T. Janka, "Supernova simulations from a 3D progenitor model - Impact of perturbations and evolution of explosion properties", *MNRAS***472**, 491–513 (2017).

Murai, T., D. Sugimoto, R. Hōshi and C. Hayashi, "Evolution of Carbon Stars. I —Gravitational Contraction and Onset of Carbon Burning—", Progress of Theoretical Physics **39**, 619–634 (1968).

Nabi, J.-U., A. Ullah and A. A. Khan, "Investigation of Important Weak Interaction Nuclei in Presupernova Evolution", *ApJ***911**, 2, 93 (2021).

Nadezhin, D. K., "Some Secondary Indications of Gravitational Collapse", *Ap&SS***69**, 1, 115–125 (1980).

Naumov, V. A., "Solar neutrinos. Astrophysical aspects", Physics of Particles and Nuclei Letters **8**, 7, 683–703 (2011).

Newstead, J. L., L. E. Strigari and R. F. Lang, "Detecting CNO solar neutrinos in next-generation xenon dark matter experiments", *Phys. Rev. D.***99**, 4, 043006 (2019).

Nieuwenhuijzen, H. and C. de Jager, "Parametrization of stellar rates of mass loss as functions of the fundamental stellar parameters M, L, and R", *A&A***231**, 134–136 (1990).

Nixon, C. J., E. R. Coughlin and J. E. Pringle, "Short Gamma-Ray Bursts and the Decompression of Neutron Star Matter in Tidal Streams", *ApJ***900**, 1, L12 (2020).

Nomoto, K. and M. Hashimoto, "Presupernova evolution of massive stars.", *Phys. Reports***163**, 13–36 (1988).

Nomoto, K., F.-K. Thielemann and S. Miyaji, "The triple alpha reaction at low temperatures in accreting white dwarfs and neutron stars", *A&A***149**, 239–245 (1985).

Nomoto, K. and S. Tsuruta, “Cooling of young neutron stars and Einstein X-ray observartions.”, *ApJ* **250**, L19–L23 (1981).

Nugis, T. and H. J. G. L. M. Lamers, “Mass-loss rates of Wolf-Rayet stars as a function of stellar parameters”, *A&A* **360**, 227–244 (2000).

Ober, W. W., M. F. El Eid and K. J. Fricke, “Evolution of Massive Pregalactic Stars - Part Two - Nucleosynthesis in Pair Creation Supernovae and Pregalactic Enrichment”, *A&A* **119**, 61 (1983).

Oda, T., M. Hino, K. Muto, M. Takahara and K. Sato, “Rate Tables for the Weak Processes of sd-Shell Nuclei in Stellar Matter”, Atomic Data and Nuclear Data Tables **56**, 231–403 (1994).

Odrzywołek, A., “Plasmaneutrino spectrum”, European Physical Journal C **52**, 2, 425–434 (2007).

Odrzywolek, A., “Nuclear statistical equilibrium neutrino spectrum”, *Phys. Rev. C.* **80**, 4, 045801 (2009).

Odrzywolek, A. and A. Heger, “Neutrino signatures of dying massive stars: From main sequence to the neutron star”, Acta Phys. Polon. B **41**, 1611–1628 (2010).

Odrzywolek, A., M. Misiaszek and M. Kutschera, “Detection possibility of the pair-annihilation neutrinos from the neutrino-cooled pre-supernova star”, Astroparticle Physics **21**, 3, 303–313 (2004).

O’Leary, R. M., B. Kocsis and A. Loeb, “Gravitational waves from scattering of stellar-mass black holes in galactic nuclei”, *MNRAS* **395**, 4, 2127–2146 (2009).

OpenAI, “GPT-4 Technical Report”, arXiv e-prints p. arXiv:2303.08774 (2023).

Oppenheimer, J. R. and R. Serber, “On the Stability of Stellar Neutron Cores”, Physical Review **54**, 7, 540–540 (1938).

Özel, F., D. Psaltis, R. Narayan and J. E. McClintock, “The Black Hole Mass Distribution in the Galaxy”, *ApJ* **725**, 2, 1918–1927 (2010).

Page, D. N., “Neutron star explosions?”, Physics Letters A **91**, 4, 201–202 (1982).

Patton, K. M., C. Lunardini and R. J. Farmer, “Presupernova Neutrinos: Realistic Emissivities from Stellar Evolution”, *ApJ* **840**, 2 (2017a).

Patton, K. M., C. Lunardini, R. J. Farmer and F. X. Timmes, “Neutrinos from Beta Processes in a Presupernova: Probing the Isotopic Evolution of a Massive Star”, *ApJ* **851**, 1, 6 (2017b).

Patton, R. A. and T. Sukhbold, “Towards a realistic explosion landscape for binary population synthesis”, *MNRAS* **499**, 2, 2803–2816 (2020).

Patton, R. A., T. Sukhbold and J. J. Eldridge, "Comparing compact object distributions from mass- and presupernova core structure-based prescriptions", *MNRAS* **511**, 1, 903–913 (2022).

Paxton, B., L. Bildsten, A. Dotter, F. Herwig, P. Lesaffre and F. Timmes, "Modules for Experiments in Stellar Astrophysics (MESA)", *ApJS* **192**, 3 (2011).

Paxton, B., M. Cantiello, P. Arras, L. Bildsten, E. F. Brown, A. Dotter, C. Mankovich, M. H. Montgomery, D. Stello, F. X. Timmes and R. Townsend, "Modules for Experiments in Stellar Astrophysics (MESA): Planets, Oscillations, Rotation, and Massive Stars", *ApJS* **208**, 1, 4 (2013).

Paxton, B., P. Marchant, J. Schwab, E. B. Bauer, L. Bildsten, M. Cantiello, L. Dessart, R. Farmer, H. Hu, N. Langer, R. H. D. Townsend, D. M. Townsley and F. X. Timmes, "Modules for Experiments in Stellar Astrophysics (MESA): Binaries, Pulsations, and Explosions", *ApJS* **220**, 15 (2015).

Paxton, B., J. Schwab, E. B. Bauer, L. Bildsten, S. Blinnikov, P. Duffell, R. Farmer, J. A. Goldberg, P. Marchant, E. Sorokina, A. Thoul, R. H. D. Townsend and F. X. Timmes, "Modules for Experiments in Stellar Astrophysics (MESA): Convective Boundaries, Element Diffusion, and Massive Star Explosions", *ApJS* **234**, 34 (2018).

Paxton, B., R. Smolec, J. Schwab, A. Gautschy, L. Bildsten, M. Cantiello, A. Dotter, R. Farmer, J. A. Goldberg, A. S. Jermyn, S. M. Kanbur, P. Marchant, A. Thoul, R. H. D. Townsend, W. M. Wolf, M. Zhang and F. X. Timmes, "Modules for Experiments in Stellar Astrophysics (MESA): Pulsating Variable Stars, Rotation, Convective Boundaries, and Energy Conservation", *ApJS* **243**, 1, 10 (2019).

Peña, M., M. Parthasarathy, F. Ruiz-Escobedo and R. Manick, "Evolution of Hen 3-1357, the Stingray Nebula", *MNRAS* **515**, 1, 1459–1468 (2022).

Perna, R., Y.-H. Wang, W. M. Farr, N. Leigh and M. Cantiello, "Constraining the Black Hole Initial Mass Function with LIGO/Virgo Observations", *ApJ* **878**, 1, L1 (2019).

Peters, J. G., "Nucleosynthesis by the s-PROCESS in Stars of 9 and 15 Solar Masses", *ApJ* **154**, 225 (1968).

Piersanti, L., E. Bravo, O. Straniero, S. Cristallo and I. Domínguez, "Pre-explosive Accretion and Simmering Phases of SNe Ia", *ApJ* **926**, 1, 103 (2022).

Pignatari, M., R. Gallino, M. Heil, M. Wiescher, F. Käppeler, F. Herwig and S. Bisterzo, "The Weak s-Process in Massive Stars and its Dependence on the Neutron Capture Cross Sections", *ApJ* **710**, 1557–1577 (2010).

Pignatari, M., R. Hirschi, M. Wiescher, R. Gallino, M. Bennett, M. Beard, C. Fryer, F. Herwig, G. Rockefeller and F. X. Timmes, "The ^{12}C + ^{12}C Reaction and the Impact on Nucleosynthesis in Massive Stars", *ApJ* **762**, 1, 31 (2013).

Piro, A. L., B. Giacomazzo and R. Perna, "The Fate of Neutron Star Binary Mergers", *ApJ* **844**, L19 (2017).

Planck Collaboration, P. A. R. Ade, N. Aghanim, M. Arnaud, M. Ashdown, J. Aumont, C. Baccigalupi, A. J. Banday, R. B. Barreiro, J. G. Bartlett and et al., "Planck 2015 results. XIII. Cosmological parameters", *A&A* **594**, A13 (2016).

Portegies Zwart, S. F. and S. L. W. McMillan, "Black Hole Mergers in the Universe", *ApJ* **528**, 1, L17–L20 (2000).

Potekhin, A. Y. and G. Chabrier, "Thermodynamic Functions of Dense Plasmas: Analytic Approximations for Astrophysical Applications", Contributions to Plasma Physics **50**, 82–87 (2010).

Potekhin, A. Y., J. A. Pons and D. Page, "Neutron Stars—Cooling and Transport", *Space Science Reviews* **191**, 1-4, 239–291 (2015).

Poutanen, J., "Rosseland and Flux Mean Opacities for Compton Scattering", *ApJ* **835**, 2, 119 (2017).

Prantzos, N., M. Hashimoto and K. Nomoto, "The s-process in massive stars : yields as a function of stellar mass and metallicity.", *A&A* **234**, 211 (1990).

Prša, A., P. Harmanec, G. Torres, E. Mamajek, M. Asplund, N. Capitaine, J. Christensen-Dalsgaard, É. Depagne, M. Haberreiter, S. Hekker, J. Hilton, G. Kopp, V. Kostov, D. W. Kurtz, J. Laskar, B. D. Mason, E. F. Milone, M. Montgomery, M. Richards, W. Schmutz, J. Schou and S. G. Stewart, "Nominal Values for Selected Solar and Planetary Quantities: IAU 2015 Resolution B3", *AJ* **152**, 2, 41 (2016a).

Prša, A., P. Harmanec, G. Torres, E. Mamajek, M. Asplund, N. Capitaine, J. Christensen-Dalsgaard, É. Depagne, M. Haberreiter, S. Hekker, J. Hilton, G. Kopp, V. Kostov, D. W. Kurtz, J. Laskar, B. D. Mason, E. F. Milone, M. Montgomery, M. Richards, W. Schmutz, J. Schou and S. G. Stewart, "Nominal Values for Selected Solar and Planetary Quantities: IAU 2015 Resolution B3", *AJ* **152**, 2, 41 (2016b).

Quataert, E. and J. Shiode, "Wave-driven mass loss in the last year of stellar evolution: setting the stage for the most luminous core-collapse supernovae", *MNRAS* **423**, L92–L96 (2012).

Raffelt, G. and A. Weiss, "Non-standard neutrino interactions and the evolution of red giants", *A&A* **264**, 2, 536–546 (1992).

Rahman, N., H. T. Janka, G. Stockinger and S. E. Woosley, "Pulsational pair-instability supernovae: gravitational collapse, black hole formation, and beyond", *MNRAS* **512**, 3, 4503–4540 (2022).

Raiteri, C. M., M. Busso, R. Gallino and G. Picchio, "S-Process Nucleosynthesis in Massive Stars and the Weak Component. II. Carbon Burning and Galactic Enrichment", *ApJ* **371**, 665 (1991a).

Raiteri, C. M., M. Busso, R. Gallino, G. Picchio and L. Pulone, “S-Process Nucleosynthesis in Massive Stars and the Weak Component. I. Evolution and Neutron Captures in a 25 M_{sun} Star”, *ApJ* **367**, 228 (1991b).

Rakavy, G. and G. Shaviv, “Instabilities in Highly Evolved Stellar Models”, *ApJ* **148**, 803 (1967).

Ramadurai, S., “Neutral current and the onset of the helium flash.”, *MNRAS* **176**, 9–13 (1976).

Ramadurai, S., “Evolution of a 16-solar mass star”, *MNRAS* **206**, 849–857 (1984).

Ratcliffe, B., I. Minchev, F. Anders, S. Khoperskov, G. Guiglion, T. Buck, K. Cunha, A. Queiroz, C. Nitschelm, S. Meszaros, M. Steinmetz, R. S. de Jong, S. Nepal, R. R. Lane and J. Sobeck, “Unveiling the time evolution of chemical abundances across the Milky Way disk with APOGEE”, *MNRAS*(2023).

Ratković, S., S. Iyer Dutta and M. Prakash, “Differential neutrino rates and emissivities from the plasma process in astrophysical systems”, *Phys. Rev. D.* **67**, 12, 123002 (2003).

Ray, A., S. M. Chitre and K. Kar, “Electron capture supernovae - One-zone collapse calculation for stars with masses 10 solar masses and 15 solar masses”, *ApJ* **285**, 766–777 (1984).

Reimers, D., “On the absolute scale of mass-loss in red giants. I. Circumstellar absorption lines in the spectrum of the visual companion of alpha [1]Her.”, *A&A* **61**, 217–224 (1977).

Reindl, N., T. Rauch, M. M. Miller Bertolami, H. Todt and K. Werner, “Breaking news from the HST: the central star of the Stingray Nebula is now returning towards the AGB”, *MNRAS* **464**, 1, L51–L55 (2017).

Renzo, M., T. Callister, K. Chatziioannou, L. A. C. van Son, C. M. F. Mingarelli, M. Cantiello, K. E. S. Ford, B. McKernan and G. Ashton, “Prospects of Gravitational Wave Detections from Common Envelope Evolution with LISA”, *ApJ* **919**, 2, 128 (2021).

Renzo, M., M. Cantiello, B. D. Metzger and Y. F. Jiang, “The Stellar Merger Scenario for Black Holes in the Pair-instability Gap”, *ApJ* **904**, 2, L13 (2020a).

Renzo, M., R. Farmer, S. Justham, Y. Götberg, S. E. de Mink, E. Zapartas, P. Marchant and N. Smith, “Predictions for the hydrogen-free ejecta of pulsational pair-instability supernovae”, *A&A* **640**, A56 (2020b).

Renzo, M., R. J. Farmer, S. Justham, S. E. de Mink, Y. Götberg and P. Marchant, “Sensitivity of the lower edge of the pair-instability black hole mass gap to the treatment of time-dependent convection”, *MNRAS* **493**, 3, 4333–4341 (2020c).

Renzo, M., D. D. Hendriks, L. A. C. van Son and R. Farmer, "Pair-instability Mass Loss for Top-down Compact Object Mass Calculations", Research Notes of the American Astronomical Society **6**, 2, 25 (2022).

Renzo, M., C. D. Ott, S. N. Shore and S. E. de Mink, "Systematic survey of the effects of wind mass loss algorithms on the evolution of single massive stars", *A&A* **603**, A118 (2017).

Reusch, S., R. Stein, M. Kowalski, S. van Velzen, A. Franckowiak, C. Lunardini, K. Murase, W. Winter, J. C. A. Miller-Jones, M. M. Kasliwal, M. Gilfanov, S. Garrappa, V. S. Paliya, T. Ahumada, S. Anand, C. Barbarino, E. C. Bellm, V. Brinnel, S. Buson, S. B. Cenko, M. W. Coughlin, K. De, R. Dekany, S. Frederick, A. Gal-Yam, S. Gezari, M. Giroletti, M. J. Graham, V. Karambelkar, S. S. Kimura, A. K. H. Kong, E. C. Kool, R. R. Laher, P. Medvedev, J. Necker, J. Nordin, D. A. Perley, M. Rigault, B. Rusholme, S. Schulze, T. Schweyer, L. P. Singer, J. Sollerman, N. L. Strotjohann, R. Sunyaev, J. van Santen, R. Walters, B. T. Zhang and E. Zimmerman, "Candidate Tidal Disruption Event AT2019fdr Coincident with a High-Energy Neutrino", *Phys. Rev. L.* **128**, 22, 221101 (2022).

Rezzolla, L., E. R. Most and L. R. Weih, "Using Gravitational-wave Observations and Quasi-universal Relations to Constrain the Maximum Mass of Neutron Stars", *ApJ* **852**, 2, L25 (2018).

Richers, S., C. D. Ott, E. Abdikamalov, E. O'Connor and C. Sullivan, "Equation of state effects on gravitational waves from rotating core collapse", *Phys. Rev. D.* **95**, 6, 063019 (2017).

Riley, T. E., A. L. Watts, P. S. Ray, S. Bogdanov, S. Guillot, S. M. Morsink, A. V. Bilous, Z. Arzoumanian, D. Choudhury, J. S. Deneva, K. C. Gendreau, A. K. Harding, W. C. G. Ho, J. M. Lattimer, M. Loewenstein, R. M. Ludlam, C. B. Markwardt, T. Okajima, C. Prescod-Weinstein, R. A. Remillard, M. T. Wolff, E. Fonseca, H. T. Cromartie, M. Kerr, T. T. Pennucci, A. Parthasarathy, S. Ransom, I. Stairs, L. Guillemot and I. Cognard, "A NICER View of the Massive Pulsar PSR J0740+6620 Informed by Radio Timing and XMM-Newton Spectroscopy", *ApJ* **918**, 2, L27 (2021).

Ritter, C., R. Andrassy, B. Côté, F. Herwig, P. R. Woodward, M. Pignatari and S. Jones, "Convective-reactive nucleosynthesis of K, Sc, Cl and p-process isotopes in O-C shell mergers", *MNRAS* **474**, 1, L1–L6 (2018).

Rogers, F. J. and A. Nayfonov, "Updated and Expanded OPAL Equation-of-State Tables: Implications for Helioseismology", *ApJ* **576**, 1064–1074 (2002).

Rolfs, C. E. and W. S. Rodney, *Cauldrons in the cosmos : nuclear astrophysics* (Chicago: University of Chicago Press, 1988).

Sabhahit, G. N., J. S. Vink, E. R. Higgins and A. A. C. Sander, "Superadiabaticity and the metallicity independence of the Humphreys-Davidson limit", *MNRAS* **506**, 3, 4473–4487 (2021).

Sallaska, A. L., C. Iliadis, A. E. Champange, S. Goriely, S. Starrfield and F. X. Timmes, "STARLIB: A Next-generation Reaction-rate Library for Nuclear Astrophysics", *ApJS* **207**, 18 (2013).

Salpeter, E. E., "Nuclear Reactions in Stars. II. Protons on Light Nuclei", Physical Review **97**, 5, 1237–1244 (1955).

Sana, H., S. E. de Mink, A. de Koter, N. Langer, C. J. Evans, M. Gieles, E. Gosset, R. G. Izzard, J. B. Le Bouquin and F. R. N. Schneider, "Binary Interaction Dominates the Evolution of Massive Stars", Science **337**, 6093, 444 (2012).

Sana, H. and C. J. Evans, "The multiplicity of massive stars", in "Active OB Stars: Structure, Evolution, Mass Loss, and Critical Limits", edited by C. Neiner, G. Wade, G. Meynet and G. Peters, vol. 272, pp. 474–485 (2011).

Sandage, A., "The population concept, globular clusters, subdwarfs, ages, and the collapse of the galaxy.", *ARA&A* **24**, 421–458 (1986).

Santoliquido, F., M. Mapelli, N. Giacobbo, Y. Bouffanais and M. C. Artale, "The cosmic merger rate density of compact objects: impact of star formation, metallicity, initial mass function, and binary evolution", *MNRAS* **502**, 4, 4877–4889 (2021).

Sanyal, D., N. Langer, D. Szécsi, S. -C Yoon and L. Grassitelli, "Metallicity dependence of envelope inflation in massive stars", *A&A* **597**, A71 (2017).

Sarajedini, A., "WIYN Open Cluster Study. III. The Observed Variation of the Red Clump Luminosity and Color with Metallicity and Age", *AJ* **118**, 5, 2321–2326 (1999).

Saumon, D., G. Chabrier and H. M. van Horn, "An Equation of State for Low-Mass Stars and Giant Planets", *ApJS* **99**, 713–+ (1995).

Schinder, P. J., D. N. Schramm, P. J. Wiita, S. H. Margolis and D. L. Tubbs, "Neutrino Emission by the Pair, Plasma, and Photo Processes in the Weinberg-Salam Model", *ApJ* **313**, 531 (1987).

Schwab, J., "Evolutionary Models for the Remnant of the Merger of Two Carbon-Oxygen Core White Dwarfs", *ApJ* **906**, 1, 53 (2021).

Schwab, J., R. Farmer and F. X. Timmes, "Laminar Flame Speeds in Degenerate Oxygen-Neon Mixtures", arXiv e-prints p. arXiv:2001.07733 (2020).

Schwarzschild, M. and R. Härm, "Thermal Instability in Non-Degenerate Stars.", *ApJ* **142**, 855 (1965).

Serenelli, A., "Alive and well: A short review about standard solar models", European Physical Journal A **52**, 4, 78 (2016).

Serenelli, A. and A. Weiss, "On constructing horizontal branch models", *A&A* **442**, 3, 1041–1048 (2005).

Serenelli, A., A. Weiss, S. Cassisi, M. Salaris and A. Pietrinferni, "The brightness of the red giant branch tip. Theoretical framework, a set of reference models, and predicted observables", *A&A* **606**, A33 (2017).

Serenelli, A. M. and M. Fukugita, "Burst Neutrinos from the Nitrogen Flash", *ApJ* **632**, 1, L33–L36 (2005).

Shiode, J. H. and E. Quataert, "Setting the Stage for Circumstellar Interaction in Core-Collapse Supernovae. II. Wave-driven Mass Loss in Supernova Progenitors", *ApJ* **780**, 96 (2014).

Siegel, D. M., A. Agarwal, J. Barnes, B. D. Metzger, M. Renzo and V. A. Villar, ""Super-Kilonovae" from Massive Collapsars as Signatures of Black-Hole Birth in the Pair-instability Mass Gap", arXiv e-prints p. arXiv:2111.03094 (2021).

Siess, L., "Evolution of massive AGB stars. II. model properties at non-solar metallicity and the fate of Super-AGB stars", *A&A* **476**, 893–909 (2007).

Siess, L., "Evolution of massive AGB stars. III. the thermally pulsing super-AGB phase", *A&A* **512**, A10 (2010).

Simpson, C., K. Abe, C. Bronner, Y. Hayato, M. Ikeda, H. Ito, K. Iyogi, J. Kameda, Y. Kataoka, Y. Kato, Y. Kishimoto, L. Marti, M. Miura, S. Moriyama, T. Mochizuki, M. Nakahata, Y. Nakajima, S. Nakayama, T. Okada, K. Okamoto, A. Orii, G. Pronost, H. Sekiya, M. Shiozawa, Y. Sonoda, A. Takeda, A. Takenaka, H. Tanaka, T. Yano, R. Akutsu, T. Kajita, K. Okumura, R. Wang, J. Xia, D. Bravo-Berguño, L. Labarga, P. Fernandez, F. d. M. Blaszczyk, C. Kachulis, E. Kearns, J. L. Raaf, J. L. Stone, L. Wan, T. Wester, S. Sussman, S. Berkman, J. Bian, N. J. Griskevich, W. R. Kropp, S. Locke, S. Mine, M. B. Smy, H. W. Sobel, V. Takhistov, P. Weatherly, K. S. Ganezer, J. Hill, J. Y. Kim, I. T. Lim, R. G. Park, B. Bodur, K. Scholberg, C. W. Walter, A. Coffani, O. Drapier, M. Gonin, J. Imber, T. A. Mueller, P. Paganini, T. Ishizuka, T. Nakamura, J. S. Jang, K. Choi, J. G. Learned, S. Matsuno, R. P. Litchfield, A. A. Sztuc, Y. Uchida, M. O. Wascko, V. Berardi, N. F. Calabria, M. G. Catanesi, R. A. Intonti, E. Radicioni, G. De Rosa, G. Collazuol, F. Iacob, L. Ludovici, Y. Nishimura, S. Cao, M. Friend, T. Hasegawa, T. Ishida, T. Kobayashi, T. Nakadaira, K. Nakamura, Y. Oyama, K. Sakashita, T. Sekiguchi, T. Tsukamoto, K. Abe, M. Hasegawa, Y. Isobe, H. Miyabe, Y. Nakano, T. Shiozawa, T. Sugimoto, A. T. Suzuki, Y. Takeuchi, A. Ali, Y. Ashida, T. Hayashino, S. Hirota, M. Jiang, T. Kikawa, M. Mori, K. Nakamura, T. Nakaya, R. A. Wendell, L. H. V. Anthony, N. McCauley, A. Pritchard, K. M. Tsui, Y. Fukuda, Y. Itow, M. Murrase, T. Niwa, M. Taani, M. Tsukada, P. Mijakowski, K. Frankiewicz, C. K. Jung, X. Li, J. L. Palomino, G. Santucci, C. Vilela, M. J. Wilking, C. Yanagisawa, D. Fukuda, M. Harada, K. Hagiwara, T. Horai, H. Ishino, S. Ito, Y. Koshio, M. Sakuda, Y. Takahira, C. Xu, Y. Kuno, L. Cook, D. Wark, F. Di Lodovico, S. Molina Sedgwick, B. Richards, S. Zsoldos, S. B. Kim, R. Tacik, M. Thiesse, L. Thompson, H. Okazawa, Y. Choi, K. Nishijima, M. Koshiba, M. Yokoyama, A. Goldsack, K. Martens, M. Murdoch, B. Quilain,

Y. Suzuki, M. R. Vagins, M. Kuze, Y. Okajima, M. Tanaka, T. Yoshida, M. Ishitsuka, R. Matsumoto, K. Ohta, J. F. Martin, C. M. Nantais, H. A. Tanaka, T. Towstego, M. Hartz, A. Konaka, P. de Perio, S. Chen, B. Jamieson, J. Walker, A. Minamino, K. Okamoto, G. Pintaudi and Super-Kamiokande Collaboration, "Sensitivity of Super-Kamiokande with Gadolinium to Low Energy Antineutrinos from Pre-supernova Emission", *ApJ* **885**, 2, 133 (2019).

Smith, R., M. Gai, S. R. Stern, D. K. Schweitzer and M. W. Ahmed, "Precision measurements on oxygen formation in stellar helium burning with gamma-ray beams and a Time Projection Chamber", Nature Communications **12**, 5920 (2021).

Spera, M., M. Mapelli and A. Bressan, "The mass spectrum of compact remnants from the PARSEC stellar evolution tracks", *MNRAS* **451**, 4, 4086–4103 (2015).

Spera, M., M. Mapelli, N. Giacobbo, A. A. Trani, A. Bressan and G. Costa, "Merging black hole binaries with the SEVN code", *MNRAS* **485**, 1, 889–907 (2019).

Spera, M., A. A. Trani and M. Mencagli, "Compact Binary Coalescences: Astrophysical Processes and Lessons Learned", Galaxies **10**, 4, 76 (2022).

Stonehill, L. C., J. A. Formaggio and R. G. Robertson, "Solar neutrinos from CNO electron capture", *Phys. Rev. C.* **69**, 1, 015801 (2004).

Stothers, R. B., "Criterion for the dynamical stability of a non-adiabatic spherical self-gravitating body", *MNRAS* **305**, 2, 365–372 (1999).

Sukhbold, T. and S. Adams, "Missing red supergiants and carbon burning", *MNRAS* **492**, 2, 2578–2587 (2020).

Sukhbold, T., T. Ertl, S. E. Woosley, J. M. Brown and H.-T. Janka, "Core-collapse Supernovae from 9 to 120 Solar Masses Based on Neutrino-powered Explosions", *ApJ* **821**, 38 (2016).

Sukhbold, T. and S. E. Woosley, "The Compactness of Presupernova Stellar Cores", *ApJ* **783**, 1, 10 (2014).

Sukhbold, T., S. E. Woosley and A. Heger, "A High-resolution Study of Presupernova Core Structure", *ApJ* **860**, 93 (2018).

Suliga, A. M., "Diffuse supernova neutrino background", arXiv e-prints p. arXiv:2207.09632 (2022).

Sumiyoshi, K., S. Yamada, H. Suzuki and W. Hillebrandt, "The fate of a neutron star just below the minimum mass: does it explode?", *A&A* **334**, 159–168 (1998).

Sweigart, A. V. and P. G. Gross, "Evolutionary sequences for red giant stars.", *ApJS* **36**, 405–437 (1978).

Takahashi, K., "The Low Detection Rate of Pair-instability Supernovae and the Effect of the Core Carbon Fraction", *ApJ* **863**, 2, 153 (2018).

Takahashi, K., T. Takiwaki and T. Yoshida, "Monotonicity of the Cores of Massive Stars", *ApJ* **945**, 1, 19 (2023).

Tan, W. P., A. Boeltzig, C. Dulal, R. J. deBoer, B. Frentz, S. Henderson, K. B. Howard, R. Kelmar, J. J. Kolata, J. Long, K. T. Macon, S. Moylan, G. F. Peaslee, M. Renaud, C. Seymour, G. Seymour, B. Vande Kolk, M. Wiescher, E. F. Aguilera, P. Amador-Valenzuela, D. Lizcano and E. Martinez-Quiroz, "New Measurement of C 12 +C 12 Fusion Reaction at Astrophysical Energies", *Phys. Rev. L.* **124**, 19, 192702 (2020).

Tanikawa, A., T. Kinugawa, T. Yoshida, K. Hijikawa and H. Umeda, "Population III binary black holes: effects of convective overshooting on formation of GW190521", *MNRAS* **505**, 2, 2170–2176 (2021).

The, L.-S., M. F. El Eid and B. S. Meyer, "s-Process Nucleosynthesis in Advanced Burning Phases of Massive Stars", *ApJ* **655**, 2, 1058–1078 (2007).

The LIGO Scientific Collaboration, the Virgo Collaboration, the KAGRA Collaboration, R. Abbott, T. D. Abbott, F. Acernese, K. Ackley, C. Adams, N. Adhikari, R. X. Adhikari, V. B. Adya, C. Affeldt, D. Agarwal, M. Agathos, K. Agatsuma, N. Aggarwal, O. D. Aguiar, L. Aiello, A. Ain, P. Ajith, T. Akutsu, S. Albanesi, A. Allocca, P. A. Altin, A. Amato, C. Anand, S. Anand, A. Ananyeva, S. B. Anderson, W. G. Anderson, M. Ando, T. Andrade, N. Andres, T. Andrić, S. V. Angelova, S. Ansoldi, J. M. Antelis, S. Antier, F. Antonini, S. Appert, K. Arai, K. Arai, Y. Arai, S. Araki, A. Araya, M. C. Araya, J. S. Areeda, M. Arène, N. Aritomi, N. Arnaud, S. M. Aronson, K. G. Arun, H. Asada, Y. Asali, G. Ashton, Y. Aso, M. Assiduo, S. M. Aston, P. Astone, F. Aubin, C. Austin, S. Babak, F. Badaracco, M. K. M. Bader, C. Badger, S. Bae, Y. Bae, A. M. Baer, S. Bagnasco, Y. Bai, L. Baiotti, J. Baird, R. Bajpai, M. Ball, G. Ballardin, S. W. Ballmer, A. Balsamo, G. Baltus, S. Banagiri, D. Bankar, J. C. Barayoga, C. Barbieri, B. C. Barish, D. Barker, P. Barneo, F. Barone, B. Barr, L. Barsotti, M. Barsuglia, D. Barta, J. Bartlett, M. A. Barton, I. Bartos, R. Bassiri, A. Basti, M. Bawaj, J. C. Bayley, A. C. Baylor, M. Bazzan, B. Bécsy, V. M. Bedakihale, M. Bejger, I. Belahcene, V. Benedetto, D. Beniwal, T. F. Bennett, J. D. Bentley, M. BenYaala, F. Bergamin, B. K. Berger, S. Bernuzzi, C. P. L. Berry, D. Bersanetti, A. Bertolini, J. Betzwieser, D. Beveridge, R. Bhandare, U. Bhardwaj, D. Bhattacharjee, S. Bhaumik, I. A. Bilenko, G. Billingsley, S. Bini, R. Birney, O. Birnholtz, S. Biscans, M. Bischi, S. Biscoveanu, A. Bisht, B. Biswas, M. Bitossi, M. A. Bizouard, J. K. Blackburn, C. D. Blair, D. G. Blair, R. M. Blair, F. Bobba, N. Bode, M. Boer, G. Bogaert, M. Boldrini, L. D. Bonavena, F. Bondu, E. Bonilla, R. Bonnand, P. Booker, B. A. Boom, R. Bork, V. Boschi, N. Bose, S. Bose, V. Bossilkov, V. Boudart, Y. Bouffanais, A. Bozzi, C. Bradaschia, P. R. Brady, A. Bramley, A. Branch, M. Branchesi, J. E. Brau, M. Breschi, T. Briant, J. H. Briggs, A. Brillet, M. Brinkmann, P. Brockill, A. F. Brooks, J. Brooks, D. D. Brown, S. Brunett, G. Bruno, R. Bruntz, J. Bryant, T. Bulik, H. J. Bulten, A. Buonanno, R. Buscicchio, D. Buskulic, C. Buy, R. L. Byer, L. Cadonati, G. Cagnoli, C. Cahillane, J. Calderón Bustillo, J. D. Callaghan, T. A. Callister, E. Calloni, J. Cameron, J. B. Camp, M. Canepa, S. Canevarolo, M. Cannavacciuolo, K. C. Cannon, H. Cao, Z. Cao, E. Capocasa,

E. Capote, G. Carapella, F. Carbognani, J. B. Carlin, M. F. Carney, M. Carpinelli, G. Carrillo, G. Carullo, T. L. Carver, J. Casanueva Diaz, C. Casentini, G. Castaldi, S. Caudill, M. Cavaglià, F. Cavalier, R. Cavalieri, M. Ceasar, G. Cella, P. Cerdá-Durán, E. Cesarini, W. Chaibi, K. Chakravarti, S. Chalathadka Subrahmanya, E. Champion, C. H. Chan, C. Chan, C. L. Chan, K. Chan, M. Chan, K. Chandra, P. Chanial, S. Chao, P. Charlton, E. A. Chase, E. Chassande-Mottin, C. Chatterjee, D. Chatterjee, D. Chatterjee, M. Chaturvedi, S. Chaty, K. Chatziioannou, C. Chen, H. Y. Chen, J. Chen, K. Chen, X. Chen, Y. B. Chen, Y. R. Chen, Z. Chen, H. Cheng, C. K. Cheong, H. Y. Cheung, H. Y. Chia, F. Chiadini, C.-Y. Chiang, G. Chiarini, R. Chierici, A. Chincarini, M. L. Chiofalo, A. Chiummo, G. Cho, H. S. Cho, R. K. Choudhary, S. Choudhary, N. Christensen, H. Chu, Q. Chu, Y.-K. Chu, S. Chua, K. W. Chung, G. Ciani, P. Ciecielag, M. Cieślar, M. Cifaldi, A. A. Ciobanu, R. Ciolfi, F. Cipriano, A. Cirone, F. Clara, E. N. Clark, J. A. Clark, L. Clarke, P. Clearwater, S. Clesse, F. Cleva, E. Coccia, E. Codazzo, P. F. Cohadon, D. E. Cohen, L. Cohen, M. Colleoni, C. G. Collette, A. Colombo, M. Colpi, C. M. Compton, J. Constancio, M., L. Conti, S. J. Cooper, P. Corban, T. R. Corbitt, I. Cordero-Carrión, S. Corezzi, K. R. Corley, N. Cornish, D. Corre, A. Corsi, S. Cortese, C. A. Costa, R. Cotesta, M. W. Coughlin, J. P. Coulon, S. T. Countryman, B. Cousins, P. Couvares, D. M. Coward, M. J. Cowart, D. C. Coyne, R. Coyne, J. D. E. Creighton, T. D. Creighton, A. W. Criswell, M. Croquette, S. G. Crowder, J. R. Cudell, T. J. Cullen, A. Cumming, R. Cummings, L. Cunningham, E. Cuoco, M. Curyło, P. Dabadie, T. Dal Canton, S. Dall'Osso, G. Dálya, A. Dana, L. M. DaneshgaranBajastani, B. D'Angelo, S. Danilishin, S. D'Antonio, K. Danzmann, C. Darsow-Fromm, A. Dasgupta, L. E. H. Datrier, S. Datta, V. Dattilo, I. Dave, M. Davier, G. S. Davies, D. Davis, M. C. Davis, E. J. Daw, R. Dean, D. DeBra, M. Deenadayalan, J. Degallaix, M. De Laurentis, S. Deléglise, V. Del Favero, F. De Lillo, N. De Lillo, W. Del Pozzo, L. M. DeMarchi, F. De Matteis, V. D'Emilio, N. Demos, T. Dent, A. Depasse, R. De Pietri, R. De Rosa, C. De Rossi, R. DeSalvo, R. De Simone, S. Dhurandhar, M. C. Díaz, J. Diaz-Ortiz, M., N. A. Didio, T. Dietrich, L. Di Fiore, C. Di Fronzo, C. Di Giorgio, F. Di Giovanni, M. Di Giovanni, T. Di Girolamo, A. Di Lieto, B. Ding, S. Di Pace, I. Di Palma, F. Di Renzo, A. K. Divakarla, A. Dmitriev, Z. Doctor, L. D'Onofrio, F. Donovan, K. L. Dooley, S. Doravari, I. Dorrington, M. Drago, J. C. Driggers, Y. Drori, J. G. Ducoin, P. Dupej, O. Durante, D. D'Urso, P. A. Duverne, S. E. Dwyer, C. Eassa, P. J. Easter, M. Ebersold, T. Eckhardt, G. Eddolls, B. Edelman, T. B. Edo, O. Edy, A. Effler, S. Eguchi, J. Eichholz, S. S. Eikenberry, M. Eisenmann, R. A. Eisenstein, A. Ejlli, E. Engelby, Y. Enomoto, L. Errico, R. C. Essick, H. Estellés, D. Estevez, Z. Etienne, T. Etzel, M. Evans, T. M. Evans, B. E. Ewing, V. Fafone, H. Fair, S. Fairhurst, A. M. Farah, S. Farinon, B. Farr, W. M. Farr, N. W. Farrow, E. J. Fauchon-Jones, G. Favaro, M. Favata, M. Fays, M. Fazio, J. Feicht, M. M. Fejer, E. Fenyvesi, D. L. Ferguson, A. Fernandez-Galiana, I. Ferrante, T. A. Ferreira, F. Fidecaro, P. Figura, I. Fiori, M. Fishbach, R. P. Fisher, R. Fittipaldi, V. Fiumara, R. Flaminio, E. Floden, H. Fong, J. A. Font, B. Fornal, P. W. F. Forsyth, A. Franke, S. Frasca, F. Frasconi, C. Frederick, J. P. Freed, Z. Frei, A. Freise, R. Frey, P. Fritschel, V. V. Frolov, G. G. Fronzé, Y. Fujii, Y. Fujikawa, M. Fukunaga, M. Fukushima, P. Fulda, M. Fyffe, H. A. Gabbard, B. U. Gadre, J. R. Gair, J. Gais, S. Galaudage, R. Gamba, D. Ganapathy, A. Ganguly, D. Gao, S. G. Gaonkar, B. Garaventa, C. García-Núñez, C. García-Quirós, F. Garufi, B. Gateley, S. Gaudio, V. Gayathri, G. G. Ge, G. Gemme, A. Gennai, J. George, O. Gerberding, L. Gergely, P. Gewecke, S. Ghonge, A. Ghosh, A. Ghosh, S. Ghosh, S. Ghosh, B. Giacomazzo, L. Giacoppo, J. A. Giaime, K. D. Giardina, D. R. Gibson, C. Gier, M. Giesler, P. Giri, F. Gissi, J. Glanzer, A. E. Gleckl, P. Godwin, E. Goetz, R. Goetz, N. Gohlke, J. Golomb, B. Goncharov, G. González, A. Gopakumar, M. Gosselin, R. Gouaty, D. W. Gould, B. Grace, A. Grado, M. Granata, V. Granata, A. Grant, S. Gras, P. Grassia, C. Gray, R. Gray, G. Greco, A. C. Green, R. Green, A. M. Gretarsson, E. M. Gretarsson, D. Griffith, W. Griffiths, H. L. Griggs, G. Grignani, A. Grimaldi, S. J. Grimm, H. Grote, S. Grunewald, P. Gruning, D. Guerra, G. M. Guidi, A. R. Guimaraes, G. Guixé, H. K. Gulati, H. K. Guo, Y. Guo, A. Gupta, A. Gupta, P. Gupta, E. K. Gustafson, R. Gustafson, F. Guzman, S. Ha, L. Haegel, A. Hagiwara, S. Haino, O. Halim, E. D. Hall, E. Z. Hamilton, G. Hammond, W. B. Han, M. Haney, J. Hanks, C. Hanna, M. D. Hannam, O. Hannuksela, H. Hansen, T. J. Hansen, J. Hanson, T. Harder, T. Hardwick, K. Haris, J. Harms, G. M. Harry, I. W. Harry, D. Hartwig, K. Hasegawa, B. Haskell, R. K. Hasskew, C. J. Haster, K. Hattori, K. Haughian, H. Hayakawa, K. Hayama, F. J. Hayes, J. Healy, A. Heidmann, A. Heidt, M. C. Heintze, J. Heinze, J. Heinzel, H. Heitmann, F. Hellman, P. Hello, A. F. Helmling-Cornell, G. Hemming, M. Hendry, I. S. Heng, E. Hennes, J. Hennig, M. H. Hennig, A. G. Hernandez, F. Hernandez Vivanco, M. Heurs, S. Hild, P. Hill, Y. Himemoto, A. S. Hines, Y. Hiranuma, N. Hirata, E. Hirose, S. Hochheim, D. Hofman, J. N. Hohmann, D. G. Holcomb, N. A. Holland, I. J. Hollows, Z. J. Holmes, K. Holt, D. E. Holz, Z. Hong, P. Hopkins, J. Hough, S. Hourihane, E. J. Howell, C. G. Hoy, D. Hoyland, A. Hreibi, B.-H. Hsieh, Y. Hsu, G.-Z. Huang, H.-Y. Huang, P. Huang, Y.-C. Huang, Y. J. Huang, Y. Huang, M. T. Hübner, A. D. Huddart, B. Hughey, D. C. Y. Hui, V. Hui, S. Husa, S. H. Huttner, R. Huxford, T. Huynh-Dinh, S. Ide, B. Idzkowski, A. Iess, B. Ikenoue, S. Imam, K. Inayoshi, C. Ingram, Y. Inoue, K. Ioka, M. Isi, K. Isleif, K. Ito, Y. Itoh, B. R. Iyer, K. Izumi, V. JaberianHamedan, T. Jacqmin, S. J. Jadhav, S. P. Jadhav, A. L. James, A. Z. Jan, K. Jani, J. Janquart, K. Janssens, N. N. Janthalur, P. Jaranowski, D. Jariwala, R. Jaume, A. C. Jenkins, K. Jenner, C. Jeon, M. Jeunon, W. Jia, H. B. Jin, G. R. Johns, A. W. Jones, D. I. Jones, J. D. Jones, P. Jones, R. Jones, R. J. G. Jonker, L. Ju, P. Jung, k. Jung, J. Junker, V. Juste, K. Kaihotsu, T. Kajita, M. Kakizaki, C. V. Kalaghatgi, V. Kalogera, B. Kamai, M. Kamiizumi, N. Kanda, S. Kandhasamy, G. Kang, J. B. Kanner, Y. Kao, S. J. Kapadia, D. P. Kapasi, S. Karat, C. Karathanasis, S. Karki, R. Kashyap, M. Kasprzack, W. Kastaun, S. Katsanevas, E. Katsavounidis, W. Katzman, T. Kaur, K. Kawabe, K. Kawaguchi, N. Kawai, T. Kawasaki, F. Kéfélian, D. Keitel, J. S. Key, S. Khadka, F. Y. Khalili, S. Khan, E. A. Khazanov, N. Khetan, M. Khursheed, N. Kijbunchoo, C. Kim, J. C. Kim, J. Kim, K. Kim, W. S. Kim, Y. M. Kim, C. Kimball, N. Kimura, M. Kinley-Hanlon, R. Kirchhoff, J. S. Kissel, N. Kita, H. Kitazawa, L. Kleybolte, S. Klimenko, A. M. Knee, T. D. Knowles, E. Knyazev, P. Koch, G. Koekoek, Y. Kojima, K. Kokeyama, S. Koley, P. Kolitsidou, M. Kolstein, K. Komori, V. Kondrashov, A. K. H. Kong, A. Kontos, N. Koper, M. Korobko, K. Kotake, M. Kovalam, D. B. Kozak, C. Kozakai, R. Kozu, V. Kringel, N. V. Krishnendu, A. Królak, G. Kuehn, F. Kuei, P. Kuijer, A. Kumar, P. Kumar, R. Kumar, R. Kumar, J. Kume, K. Kuns, C. Kuo, H.-S. Kuo, Y. Kuromiya, S. Kuroyanagi, K. Kusayanagi, S. Kuwahara, K. Kwak, P. Lagabbe, D. Laghi, E. Lalande, T. L. Lam, A. Lamberts, M. Landry, P. Landry, B. B. Lane, R. N. Lang, J. Lange, B. Lantz, I. La Rosa, A. Lartaux-Vollard, P. D. Lasky, M. Laxen, A. Lazzarini, C. Lazzaro, P. Leaci, S. Leavey, Y. K. Lecoeuche, H. K. Lee, H. M. Lee, H. W. Lee, J. Lee, K. Lee, R. Lee, J. Lehmann, A. Lemaître, M. Leonardi, N. Leroy, N. Letendre, C. Levesque, Y. Levin, J. N. Leviton, K. Leyde, A. K. Y. Li, B. Li, J. Li, K. L. Li, T. G. F. Li, X. Li, C.-Y. Lin, F.-K. Lin, F.-L. Lin, H. L. Lin, L. C. C. Lin, F. Linde, S. D. Linker, J. N. Linley, T. B. Littenberg, G. C. Liu, J. Liu, K. Liu, X. Liu, F. Llamas, M. Llorens-Monteagudo, R. K. L. Lo, A. Lockwood, L. T. London, A. Longo, D. Lopez, M. Lopez Portilla, M. Lorenzini, V. Loriette, M. Lormand, G. Losurdo, T. P. Lott, J. D. Lough, C. O. Lousto, G. Lovelace, J. F. Lucaccioni, H. Lück, D. Lumaca, A. P. Lundgren, L. W. Luo, J. E. Lynam, R. Macas, M. MacInnis, D. M. Macleod, I. A. O. MacMillan, A. Macquet, I. Magaña Hernandez, C. Magazzù, R. M. Magee, R. Maggiore, M. Magnozzi, S. Mahesh, E. Majorana, C. Makarem, I. Maksimovic, S. Maliakal, A. Malik, N. Man, V. Mandic, V. Mangano, J. L. Mango, G. L. Mansell, M. Manske, M. Mantovani, M. Mapelli, F. Marchesoni, M. Marchio, F. Marion, Z. Mark, S. Márka, Z. Márka, C. Markakis, A. S. Markosyan, A. Markowitz, E. Maros, A. Marquina, S. Marsat, F. Martelli, I. W. Martin, R. M. Martin, M. Martinez, V. A. Martinez, V. Martinez, K. Martinovic, D. V. Martynov, E. J. Marx, H. Masalehdan, K. Mason, E. Massera, A. Masserot, T. J. Massinger, M. Masso-Reid, S. Mastrogiovanni, A. Matas, M. Mateu-Lucena, F. Matichard, M. Matiushechkina, N. Mavalvala, J. J. McCann, R. McCarthy, D. E. McClelland, P. K. McClincy, S. McCormick, L. McCuller, G. I. McGhee, S. C. McGuire, C. McIsaac, J. McIver, T. McRae, S. T. McWilliams, D. Meacher, M. Mehmet, A. K. Mehta, Q. Meijer, A. Melatos, D. A. Melchor, G. Mendell, A. Menendez-Vazquez, C. S. Menoni, R. A. Mercer, L. Mereni, K. Merfeld, E. L. Merilh, J. D. Merritt, M. Merzougui, S. Meshkov, C. Messenger, C. Messick, P. M. Meyers, F. Meylahn, A. Mhaske, A. Miani, H. Miao, I. Michaloliakos, C. Michel, Y. Michimura, H. Middleton, L. Milano, A. L. Miller, A. Miller, B. Miller, S. Miller, M. Millhouse, J. C. Mills, E. Milotti, O. Minazzoli, Y. Minenkov, N. Mio, L. M. Mir, M. Miravet-Tenés, C. Mishra, T. Mishra, T. Mistry, S. Mitra, V. P. Mitrofanov, G. Mitselmakher, R. Mittleman, O. Miyakawa, A. Miyamoto, Y. Miyazaki, K. Miyo, S. Miyoki, G. Mo, E. Moguel, K. Mogushi, S. R. P. Mohapatra, S. R. Mohite, I. Molina, M. Molina-Ruiz, M. Mondin, M. Montani, C. J. Moore, D. Moraru, F. Morawski, A. More, C. Moreno, G. Moreno, Y. Mori, S. Morisaki, Y. Moriwaki, B. Mours, C. M. Mow-Lowry, S. Mozzon, F. Muciaccia, A. Mukherjee, D. Mukherjee, S. Mukherjee, S. Mukherjee, S. Mukherjee, N. Mukund, A. Mullavey, J. Munch, E. A. Muñiz, P. G. Murray, R. Musenich, S. Muusse, S. L. Nadji, K. Nagano, S. Nagano, A. Nagar, K. Nakamura, H. Nakano, M. Nakano, R. Nakashima, Y. Nakayama, V. Napolano, I. Nardecchia, T. Narikawa, L. Naticchioni, B. Nayak, R. K. Nayak, R. Negishi, B. F. Neil, J. Neilson, G. Nelemans, T. J. N. Nelson, M. Nery, P. Neubauer, A. Neunzert, K. Y. Ng, S. W. S. Ng, C. Nguyen, P. Nguyen, T. Nguyen, L. Nguyen Quynh, W. T. Ni, S. A. Nichols, A. Nishizawa, S. Nissanke, E. Nitoglia, F. Nocera, M. Norman, C. North, S. Nozaki, L. K. Nuttall, J. Oberling, B. D. O'Brien, Y. Obuchi, J. O'Dell, E. Oelker, W. Ogaki, G. Oganesyan, J. J. Oh, K. Oh, S. H. Oh, M. Ohashi, N. Ohishi, M. Ohkawa, F. Ohme, H. Ohta, M. A. Okada, Y. Okutani, K. Okutomi, C. Olivetto, K. Oohara, C. Ooi, R. Oram, B. O'Reilly, R. G. Ormiston, N. D. Ormsby, L. F. Ortega, R. O'Shaughnessy, E. O'Shea, S. Oshino, S. Ossokine, C. Osthelder, S. Otabe, D. J. Ottaway, H. Overmier, A. E. Pace, G. Pagano, M. A. Page, G. Pagliaroli, A. Pai, S. A. Pai, J. R. Palamos, O. Palashov, C. Palomba, H. Pan, K. Pan, P. K. Panda, H. Pang, P. T. H. Pang, C. Pankow, F. Pannarale, B. C. Pant, F. H. Panther, F. Paoletti, A. Paoli, A. Paolone, A. Parisi, H. Park, J. Park, W. Parker, D. Pascucci, A. Pasqualetti, R. Passaquieti, D. Passuello, M. Patel, M. Pathak, B. Patricelli, A. S. Patron, S. Paul, E. Payne, M. Pedraza, M. Pegoraro, A. Pele, F. E. Peña Arellano, S. Penn, A. Perego, A. Pereira, T. Pereira, C. J. Perez, C. Périgois, C. C. Perkins, A. Perreca, S. Perriès, J. Petermann, D. Petterson, H. P. Pfeiffer, K. A. Pham, K. S. Phukon, O. J. Piccinni, M. Pichot, M. Piendibene, F. Piergiovanni, L. Pierini, V. Pierro, G. Pillant, M. Pillas, F. Pilo, L. Pinard, I. M. Pinto, M. Pinto, K. Piotrzkowski, M. Pirello, M. D. Pitkin, E. Placidi, L. Planas, W. Plastino, C. Pluchar, R. Poggiani, E. Polini, D. Y. T. Pong, S. Ponrathnam, P. Popolizio, E. K. Porter, R. Poulton, J. Powell, M. Pracchia, T. Pradier, A. K. Prajapati, K. Prasai, R. Prasanna, G. Pratten, M. Principe, G. A. Prodi, L. Prokhorov, P. Prosposito, L. Prudenzi, A. Puecher, M. Punturo, F. Puosi, P. Puppo, M. Pürrer, H. Qi, V. Quetschke, R. Quitzow-James, F. J. Raab, G. Raaijmakers, H. Radkins, N. Radulesco, P. Raffai, S. X. Rail, S. Raja, C. Rajan, K. E. Ramirez, T. D. Ramirez, A. Ramos-Buades, J. Rana, P. Rapagnani, U. D. Rapol, A. Ray, V. Raymond, N. Raza, M. Razzano, J. Read, L. A. Rees, T. Regimbau, L. Rei, S. Reid, S. W. Reid, D. H. Reitze, P. Relton, A. Renzini, P. Rettegno, M. Rezac, F. Ricci, D. Richards, J. W. Richardson, L. Richardson, G. Riemenschneider, K. Riles, S. Rinaldi, K. Rink, M. Rizzo, N. A. Robertson, R. Robie, F. Robinet, A. Rocchi, S. Rodriguez, L. Rolland, J. G. Rollins, M. Romanelli, R. Romano, C. L. Romel, A. Romero-Rodríguez, I. M. Romero-Shaw, J. H. Romie, S. Ronchini, L. Rosa, C. A. Rose, D. Rosińska, M. P. Ross, S. Rowan, S. J. Rowlinson, S. Roy, S. Roy, S. Roy, D. Rozza, P. Ruggi, K. Ryan, S. Sachdev, T. Sadecki, J. Sadiq, N. Sago, S. Saito, Y. Saito, K. Sakai, Y. Sakai, M. Sakellariadou, Y. Sakuno, O. S. Salafia, L. Salconi, M. Saleem, F. Salemi, A. Samajdar, E. J. Sanchez, J. H. Sanchez, L. E. Sanchez, N. Sanchis-Gual, J. R. Sanders, A. Sanuy, T. R. Saravanan, N. Sarin, B. Sassolas, H. Satari, B. S. Sathyaprakash, S. Sato, T. Sato, O. Sauter, R. L. Savage, T. Sawada, D. Sawant, H. L. Sawant, S. Sayah, D. Schaetzl, M. Scheel, J. Scheuer, M. Schiworski, P. Schmidt, S. Schmidt, R. Schnabel, M. Schneewind, R. M. S. Schofield, A. Schönbeck, B. W. Schulte, B. F. Schutz, E. Schwartz, J. Scott, S. M. Scott, M. Seglar-Arroyo, T. Sekiguchi, Y. Sekiguchi, D. Sellers, A. S. Sengupta, D. Sentenac, E. G. Seo, V. Sequino, A. Sergeev, Y. Setyawati, T. Shaffer, M. S. Shahriar, B. Shams, L. Shao, A. Sharma, P. Sharma, P. Shawhan, N. S. Shcheblanov, S. Shibagaki, M. Shikauchi, R. Shimizu, T. Shimoda, K. Shimode, H. Shinkai, T. Shishido, A. Shoda, D. H. Shoemaker, D. M. Shoemaker, S. ShyamSundar, M. Sieniawska, D. Sigg, L. P. Singer, D. Singh, N. Singh, A. Singha, A. M. Sintes, V. Sipala, V. Skliris, B. J. J. Slagmolen, T. J. Slaven-Blair, J. Smetana, J. R. Smith, R. J. E. Smith, J. Soldateschi, S. N. Somala, K. Somiya, E. J. Son, K. Soni, S. Soni, V. Sordini, F. Sorrentino, N. Sorrentino, H. Sotani, R. Soulard, T. Souradeep, E. Sowell, V. Spagnuolo, A. P. Spencer, M. Spera, R. Srinivasan, A. K. Srivastava, V. Srivastava, K. Staats, C. Stachie, D. A. Steer, J. Steinlechner, S. Steinlechner, D. J. Stops, M. Stover,

K. A. Strain, L. C. Strang, G. Stratta, A. Strunk, R. Sturani, A. L. Stuver, S. Sudhagar, V. Sudhir, R. Sugimoto, H. G. Suh, T. Z. Summerscales, H. Sun, L. Sun, S. Sunil, A. Sur, J. Suresh, P. J. Sutton, T. Suzuki, T. Suzuki, B. L. Swinkels, M. J. Szczepańczyk, P. Szewczyk, M. Tacca, H. Tagoshi, S. C. Tait, H. Takahashi, R. Takahashi, A. Takamori, S. Takano, H. Takeda, M. Takeda, C. J. Talbot, C. Talbot, H. Tanaka, K. Tanaka, K. Tanaka, T. Tanaka, T. Tanaka, A. J. Tanasijczuk, S. Tanioka, D. B. Tanner, D. Tao, L. Tao, E. N. Tapia San Martín, C. Taranto, J. D. Tasson, S. Telada, R. Tenorio, J. E. Terhune, L. Terkowski, M. P. Thirugnanasambandam, M. Thomas, P. Thomas, J. E. Thompson, S. R. Thondapu, K. A. Thorne, E. Thrane, S. Tiwari, S. Tiwari, V. Tiwari, A. M. Toivonen, K. Toland, A. E. Tolley, T. Tomaru, Y. Tomigami, T. Tomura, M. Tonelli, A. Torres-Forné, C. I. Torrie, I. Tosta e Melo, D. Töyrä, A. Trapananti, F. Travasso, G. Traylor, M. Trevor, M. C. Tringali, A. Tripathee, L. Troiano, A. Trovato, L. Trozzo, R. J. Trudeau, D. S. Tsai, D. Tsai, K. W. Tsang, T. Tsang, J.-S. Tsao, M. Tse, R. Tso, K. Tsubono, S. Tsuchida, L. Tsukada, D. Tsuna, T. Tsutsui, T. Tsuzuki, K. Turbang, M. Turconi, D. Tuyenbayev, A. S. Ubhi, N. Uchikata, T. Uchiyama, R. P. Udall, A. Ueda, T. Uehara, K. Ueno, G. Ueshima, C. S. Unnikrishnan, F. Uraguchi, A. L. Urban, T. Ushiba, A. Utina, H. Vahlbruch, G. Vajente, A. Vajpeyi, G. Valdes, M. Valentini, V. Valsan, N. van Bakel, M. van Beuzekom, J. F. J. van den Brand, C. Van Den Broeck, D. C. Vander-Hyde, L. van der Schaaf, J. V. van Heijningen, J. Vanosky, M. H. P. M. van Putten, N. van Remortel, M. Vardaro, A. F. Vargas, V. Varma, M. Vasúth, A. Vecchio, G. Vedovato, J. Veitch, P. J. Veitch, J. Venneberg, G. Venugopalan, D. Verkindt, P. Verma, Y. Verma, D. Veske, F. Vetrano, A. Viceré, S. Vidyant, A. D. Viets, A. Vijaykumar, V. Villa-Ortega, J. Y. Vinet, A. Virtuoso, S. Vitale, T. Vo, H. Vocca, E. R. G. von Reis, J. S. A. von Wrangel, C. Vorvick, S. P. Vyatchanin, L. E. Wade, M. Wade, K. J. Wagner, R. C. Walet, M. Walker, G. S. Wallace, L. Wallace, S. Walsh, J. Wang, J. Z. Wang, W. H. Wang, R. L. Ward, J. Warner, M. Was, T. Washimi, N. Y. Washington, J. Watchi, B. Weaver, S. A. Webster, M. Weinert, A. J. Weinstein, R. Weiss, C. M. Weller, F. Wellmann, L. Wen, P. Weßels, K. Wette, J. T. Whelan, D. D. White, B. F. Whiting, C. Whittle, D. Wilken, D. Williams, M. J. Williams, A. R. Williamson, J. L. Willis, B. Willke, D. J. Wilson, W. Winkler, C. C. Wipf, T. Wlodarczyk, G. Woan, J. Woehler, J. K. Wofford, I. C. F. Wong, C. Wu, D. S. Wu, H. Wu, S. Wu, D. M. Wysocki, L. Xiao, W.-R. Xu, T. Yamada, H. Yamamoto, K. Yamamoto, K. Yamamoto, T. Yamamoto, K. Yamashita, R. Yamazaki, F. W. Yang, L. Yang, Y. Yang, Y. Yang, Z. Yang, M. J. Yap, D. W. Yeeles, A. B. Yelikar, M. Ying, K. Yokogawa, J. Yokoyama, T. Yokozawa, J. Yoo, T. Yoshioka, H. Yu, H. Yu, H. Yuzurihara, A. Zadrożny, M. Zanolin, S. Zeidler, T. Zelenova, J. P. Zendri, M. Zevin, M. Zhan, H. Zhang, J. Zhang, L. Zhang, T. Zhang, Y. Zhang, C. Zhao, G. Zhao, Y. Zhao, Y. Zhao, R. Zhou, Z. Zhou, X. J. Zhu, Z. H. Zhu, A. B. Zimmerman, Y. Zlochower, M. E. Zucker and J. Zweizig, "The population of merging compact binaries inferred using gravitational waves through GWTC-3", arXiv e-prints p. arXiv:2111.03634 (2021a).

The LIGO Scientific Collaboration, the Virgo Collaboration, the KAGRA Collaboration, R. Abbott, T. D. Abbott, F. Acernese, K. Ackley, C. Adams, N. Adhikari, R. X. Adhikari, V. B. Adya, C. Affeldt, D. Agarwal, M. Agathos, K. Agatsuma, N. Aggarwal, O. D. Aguiar, L. Aiello, A. Ain, P. Ajith, T. Akutsu, S. Albanesi,

A. Allocca, P. A. Altin, A. Amato, C. Anand, S. Anand, A. Ananyeva, S. B. Anderson, W. G. Anderson, M. Ando, T. Andrade, N. Andres, T. Andrić, S. V. Angelova, S. Ansoldi, J. M. Antelis, S. Antier, F. Antonini, S. Appert, K. Arai, K. Arai, Y. Arai, S. Araki, A. Araya, M. C. Araya, J. S. Areeda, M. Arène, N. Aritomi, N. Arnaud, S. M. Aronson, K. G. Arun, H. Asada, Y. Asali, G. Ashton, Y. Aso, M. Assiduo, S. M. Aston, P. Astone, F. Aubin, C. Austin, S. Babak, F. Badaracco, M. K. M. Bader, C. Badger, S. Bae, Y. Bae, A. M. Baer, S. Bagnasco, Y. Bai, L. Baiotti, J. Baird, R. Bajpai, M. Ball, G. Ballardin, S. W. Ballmer, A. Balsamo, G. Baltus, S. Banagiri, D. Bankar, J. C. Barayoga, C. Barbieri, B. C. Barish, D. Barker, P. Barneo, F. Barone, B. Barr, L. Barsotti, M. Barsuglia, D. Barta, J. Bartlett, M. A. Barton, I. Bartos, R. Bassiri, A. Basti, M. Bawaj, J. C. Bayley, A. C. Baylor, M. Bazzan, B. Bécsy, V. M. Bedakihale, M. Bejger, I. Belahcene, V. Benedetto, D. Beniwal, T. F. Bennett, J. D. Bentley, M. BenYaala, F. Bergamin, B. K. Berger, S. Bernuzzi, C. P. L. Berry, D. Bersanetti, A. Bertolini, J. Betzwieser, D. Beveridge, R. Bhandare, U. Bhardwaj, D. Bhattacharjee, S. Bhaumik, I. A. Bilenko, G. Billingsley, S. Bini, R. Birney, O. Birnholtz, S. Biscans, M. Bischi, S. Biscoveanu, A. Bisht, B. Biswas, M. Bitossi, M. A. Bizouard, J. K. Blackburn, C. D. Blair, D. G. Blair, R. M. Blair, F. Bobba, N. Bode, M. Boer, G. Bogaert, M. Boldrini, L. D. Bonavena, F. Bondu, E. Bonilla, R. Bonnand, P. Booker, B. A. Boom, R. Bork, V. Boschi, N. Bose, S. Bose, V. Bossilkov, V. Boudart, Y. Bouffanais, A. Bozzi, C. Bradaschia, P. R. Brady, A. Bramley, A. Branch, M. Branchesi, J. E. Brau, M. Breschi, T. Briant, J. H. Briggs, A. Brillet, M. Brinkmann, P. Brockill, A. F. Brooks, J. Brooks, D. D. Brown, S. Brunett, G. Bruno, R. Bruntz, J. Bryant, T. Bulik, H. J. Bulten, A. Buonanno, R. Buscicchio, D. Buskulic, C. Buy, R. L. Byer, L. Cadonati, G. Cagnoli, C. Cahillane, J. Calderón Bustillo, J. D. Callaghan, T. A. Callister, E. Calloni, J. Cameron, J. B. Camp, M. Canepa, S. Canevarolo, M. Cannavacciuolo, K. C. Cannon, H. Cao, Z. Cao, E. Capocasa, E. Capote, G. Carapella, F. Carbognani, J. B. Carlin, M. F. Carney, M. Carpinelli, G. Carrillo, G. Carullo, T. L. Carver, J. Casanueva Diaz, C. Casentini, G. Castaldi, S. Caudill, M. Cavaglià, F. Cavalier, R. Cavalieri, M. Ceasar, G. Cella, P. Cerdá-Durán, E. Cesarini, W. Chaibi, K. Chakravarti, S. Chalathadka Subrahmanya, E. Champion, C. H. Chan, C. Chan, C. L. Chan, K. Chan, M. Chan, K. Chandra, P. Chanial, S. Chao, P. Charlton, E. A. Chase, E. Chassande-Mottin, C. Chatterjee, D. Chatterjee, D. Chatterjee, M. Chaturvedi, S. Chaty, K. Chatziioannou, C. Chen, H. Y. Chen, J. Chen, K. Chen, X. Chen, Y. B. Chen, Y. R. Chen, Z. Chen, H. Cheng, C. K. Cheong, H. Y. Cheung, H. Y. Chia, F. Chiadini, C.-Y. Chiang, G. Chiarini, R. Chierici, A. Chincarini, M. L. Chiofalo, A. Chiummo, G. Cho, H. S. Cho, R. K. Choudhary, S. Choudhary, N. Christensen, H. Chu, Q. Chu, Y.-K. Chu, S. Chua, K. W. Chung, G. Ciani, P. Ciecielag, M. Cieślar, M. Cifaldi, A. A. Ciobanu, R. Ciolfi, F. Cipriano, A. Cirone, F. Clara, E. N. Clark, J. A. Clark, L. Clarke, P. Clearwater, S. Clesse, F. Cleva, E. Coccia, E. Codazzo, P. F. Cohadon, D. E. Cohen, L. Cohen, M. Colleoni, C. G. Collette, A. Colombo, M. Colpi, C. M. Compton, J. Constancio, M., L. Conti, S. J. Cooper, P. Corban, T. R. Corbitt, I. Cordero-Carrión, S. Corezzi, K. R. Corley, N. Cornish, D. Corre, A. Corsi, S. Cortese, C. A. Costa, R. Cotesta, M. W. Coughlin, J. P. Coulon, S. T. Countryman, B. Cousins, P. Couvares, D. M. Coward, M. J. Cowart, D. C. Coyne, R. Coyne, J. D. E. Creighton, T. D. Creighton, A. W. Criswell, M. Croquette, S. G.

Crowder, J. R. Cudell, T. J. Cullen, A. Cumming, R. Cummings, L. Cunningham, E. Cuoco, M. Curyło, P. Dabadie, T. Dal Canton, S. Dall'Osso, G. Dályа, A. Dana, L. M. DaneshgaranBajastani, B. D'Angelo, S. Danilishin, S. D'Antonio, K. Danzmann, C. Darsow-Fromm, A. Dasgupta, L. E. H. Datrier, S. Datta, V. Dattilo, I. Dave, M. Davier, G. S. Davies, D. Davis, M. C. Davis, E. J. Daw, R. Dean, D. DeBra, M. Deenadayalan, J. Degallaix, M. De Laurentis, S. Deléglise, V. Del Favero, F. De Lillo, N. De Lillo, W. Del Pozzo, L. M. DeMarchi, F. De Matteis, V. D'Emilio, N. Demos, T. Dent, A. Depasse, R. De Pietri, R. De Rosa, C. De Rossi, R. DeSalvo, R. De Simone, S. Dhurandhar, M. C. Díaz, J. Diaz-Ortiz, M., N. A. Didio, T. Dietrich, L. Di Fiore, C. Di Fronzo, C. Di Giorgio, F. Di Giovanni, M. Di Giovanni, T. Di Girolamo, A. Di Lieto, B. Ding, S. Di Pace, I. Di Palma, F. Di Renzo, A. K. Divakarla, A. Dmitriev, Z. Doctor, L. D'Onofrio, F. Donovan, K. L. Dooley, S. Doravari, I. Dorrington, M. Drago, J. C. Driggers, Y. Drori, J. G. Ducoin, P. Dupej, O. Durante, D. D'Urso, P. A. Duverne, S. E. Dwyer, C. Eassa, P. J. Easter, M. Ebersold, T. Eckhardt, G. Eddolls, B. Edelman, T. B. Edo, O. Edy, A. Effler, S. Eguchi, J. Eichholz, S. S. Eikenberry, M. Eisenmann, R. A. Eisenstein, A. Ejlli, E. Engelby, Y. Enomoto, L. Errico, R. C. Essick, H. Estellés, D. Estevez, Z. Etienne, T. Etzel, M. Evans, T. M. Evans, B. E. Ewing, V. Fafone, H. Fair, S. Fairhurst, A. M. Farah, S. Farinon, B. Farr, W. M. Farr, N. W. Farrow, E. J. Fauchon-Jones, G. Favaro, M. Favata, M. Fays, M. Fazio, J. Feicht, M. M. Fejer, E. Fenyvesi, D. L. Ferguson, A. Fernandez-Galiana, I. Ferrante, T. A. Ferreira, F. Fidecaro, P. Figura, I. Fiori, M. Fishbach, R. P. Fisher, R. Fittipaldi, V. Fiumara, R. Flaminio, E. Floden, H. Fong, J. A. Font, B. Fornal, P. W. F. Forsyth, A. Franke, S. Frasca, F. Frasconi, C. Frederick, J. P. Freed, Z. Frei, A. Freise, R. Frey, P. Fritschel, V. V. Frolov, G. G. Fronzé, Y. Fujii, Y. Fujikawa, M. Fukunaga, M. Fukushima, P. Fulda, M. Fyffe, H. A. Gabbard, B. U. Gadre, J. R. Gair, J. Gais, S. Galaudage, R. Gamba, D. Ganapathy, A. Ganguly, D. Gao, S. G. Gaonkar, B. Garaventa, C. García-Núñez, C. García-Quirós, F. Garufi, B. Gateley, S. Gaudio, V. Gayathri, G. G. Ge, G. Gemme, A. Gennai, J. George, O. Gerberding, L. Gergely, P. Gewecke, S. Ghonge, A. Ghosh, A. Ghosh, S. Ghosh, S. Ghosh, B. Giacomazzo, L. Giacoppo, J. A. Giaime, K. D. Giardina, D. R. Gibson, C. Gier, M. Giesler, P. Giri, F. Gissi, J. Glanzer, A. E. Gleckl, P. Godwin, E. Goetz, R. Goetz, N. Gohlke, J. Golomb, B. Goncharov, G. González, A. Gopakumar, M. Gosselin, R. Gouaty, D. W. Gould, B. Grace, A. Grado, M. Granata, V. Granata, A. Grant, S. Gras, P. Grassia, C. Gray, R. Gray, G. Greco, A. C. Green, R. Green, A. M. Gretarsson, E. M. Gretarsson, D. Griffith, W. Griffiths, H. L. Griggs, G. Grignani, A. Grimaldi, S. J. Grimm, H. Grote, S. Grunewald, P. Gruning, D. Guerra, G. M. Guidi, A. R. Guimaraes, G. Guixé, H. K. Gulati, H. K. Guo, Y. Guo, A. Gupta, A. Gupta, P. Gupta, E. K. Gustafson, R. Gustafson, F. Guzman, S. Ha, L. Haegel, A. Hagiwara, S. Haino, O. Halim, E. D. Hall, E. Z. Hamilton, G. Hammond, W. B. Han, M. Haney, J. Hanks, C. Hanna, M. D. Hannam, O. Hannuksela, H. Hansen, T. J. Hansen, J. Hanson, T. Harder, T. Hardwick, K. Haris, J. Harms, G. M. Harry, I. W. Harry, D. Hartwig, K. Hasegawa, B. Haskell, R. K. Hasskew, C. J. Haster, K. Hattori, K. Haughian, H. Hayakawa, K. Hayama, F. J. Hayes, J. Healy, A. Heidmann, A. Heidt, M. C. Heintze, J. Heinze, J. Heinzel, H. Heitmann, F. Hellman, P. Hello, A. F. Helmling-Cornell, G. Hemming, M. Hendry, I. S. Heng, E. Hennes, J. Hennig, M. H. Hennig, A. G. Hernandez, F. Hernandez Vivanco, M. Heurs, S. Hild, P. Hill, Y. Himemoto, A. S. Hines, Y. Hiranuma, N. Hirata, E. Hirose, S. Hochheim, D. Hofman, J. N. Hohmann, D. G. Holcomb, N. A. Holland, I. J. Hollows, Z. J. Holmes, K. Holt, D. E. Holz, Z. Hong, P. Hopkins, J. Hough, S. Hourihane, E. J. Howell, C. G. Hoy, D. Hoyland, A. Hreibi, B.-H. Hsieh, Y. Hsu, G.-Z. Huang, H.-Y. Huang, P. Huang, Y.-C. Huang, Y. J. Huang, Y. Huang, M. T. Hübner, A. D. Huddart, B. Hughey, D. C. Y. Hui, V. Hui, S. Husa, S. H. Huttner, R. Huxford, T. Huynh-Dinh, S. Ide, B. Idzkowski, A. Iess, B. Ikenoue, S. Imam, K. Inayoshi, C. Ingram, Y. Inoue, K. Ioka, M. Isi, K. Isleif, K. Ito, Y. Itoh, B. R. Iyer, K. Izumi, V. JaberianHamedan, T. Jacqmin, S. J. Jadhav, S. P. Jadhav, A. L. James, A. Z. Jan, K. Jani, J. Janquart, K. Janssens, N. N. Janthalur, P. Jaranowski, D. Jariwala, R. Jaume, A. C. Jenkins, K. Jenner, C. Jeon, M. Jeunon, W. Jia, H. B. Jin, G. R. Johns, A. W. Jones, D. I. Jones, J. D. Jones, P. Jones, R. Jones, R. J. G. Jonker, L. Ju, P. Jung, k. Jung, J. Junker, V. Juste, K. Kaihotsu, T. Kajita, M. Kakizaki, C. V. Kalaghatgi, V. Kalogera, B. Kamai, M. Kamiizumi, N. Kanda, S. Kandhasamy, G. Kang, J. B. Kanner, Y. Kao, S. J. Kapadia, D. P. Kapasi, S. Karat, C. Karathanasis, S. Karki, R. Kashyap, M. Kasprzack, W. Kastaun, S. Katsanevas, E. Katsavounidis, W. Katzman, T. Kaur, K. Kawabe, K. Kawaguchi, N. Kawai, T. Kawasaki, F. Kéfélian, D. Keitel, J. S. Key, S. Khadka, F. Y. Khalili, S. Khan, E. A. Khazanov, N. Khetan, M. Khursheed, N. Kijbunchoo, C. Kim, J. C. Kim, J. Kim, K. Kim, W. S. Kim, Y. M. Kim, C. Kimball, N. Kimura, M. Kinley-Hanlon, R. Kirchhoff, J. S. Kissel, N. Kita, H. Kitazawa, L. Kleybolte, S. Klimenko, A. M. Knee, T. D. Knowles, E. Knyazev, P. Koch, G. Koekoek, Y. Kojima, K. Kokeyama, S. Koley, P. Kolitsidou, M. Kolstein, K. Komori, V. Kondrashov, A. K. H. Kong, A. Kontos, N. Koper, M. Korobko, K. Kotake, M. Kovalam, D. B. Kozak, C. Kozakai, R. Kozu, V. Kringel, N. V. Krishnendu, A. Królak, G. Kuehn, F. Kuei, P. Kuijer, A. Kumar, P. Kumar, R. Kumar, R. Kumar, J. Kume, K. Kuns, C. Kuo, H.-S. Kuo, Y. Kuromiya, S. Kuroyanagi, K. Kusayanagi, S. Kuwahara, K. Kwak, P. Lagabbe, D. Laghi, E. Lalande, T. L. Lam, A. Lamberts, M. Landry, P. Landry, B. B. Lane, R. N. Lang, J. Lange, B. Lantz, I. La Rosa, A. Lartaux-Vollard, P. D. Lasky, M. Laxen, A. Lazzarini, C. Lazzaro, P. Leaci, S. Leavey, Y. K. Lecoeuche, H. K. Lee, H. M. Lee, H. W. Lee, J. Lee, K. Lee, R. Lee, J. Lehmann, A. Lemaître, M. Leonardi, N. Leroy, N. Letendre, C. Levesque, Y. Levin, J. N. Leviton, K. Leyde, A. K. Y. Li, B. Li, J. Li, K. L. Li, T. G. F. Li, X. Li, C.-Y. Lin, F.-K. Lin, F.-L. Lin, H. L. Lin, L. C. C. Lin, F. Linde, S. D. Linker, J. N. Linley, T. B. Littenberg, G. C. Liu, J. Liu, K. Liu, X. Liu, F. Llamas, M. Llorens-Monteagudo, R. K. L. Lo, A. Lockwood, L. T. London, A. Longo, D. Lopez, M. Lopez Portilla, M. Lorenzini, V. Loriette, M. Lormand, G. Losurdo, T. P. Lott, J. D. Lough, C. O. Lousto, G. Lovelace, J. F. Lucaccioni, H. Lück, D. Lumaca, A. P. Lundgren, L. W. Luo, J. E. Lynam, R. Macas, M. MacInnis, D. M. Macleod, I. A. O. MacMillan, A. Macquet, I. Magaña Hernandez, C. Magazzù, R. M. Magee, R. Maggiore, M. Magnozzi, S. Mahesh, E. Majorana, C. Makarem, I. Maksimovic, S. Maliakal, A. Malik, N. Man, V. Mandic, V. Mangano, J. L. Mango, G. L. Mansell, M. Manske, M. Mantovani, M. Mapelli, F. Marchesoni, M. Marchio, F. Marion, Z. Mark, S. Márka, Z. Márka, C. Markakis, A. S. Markosyan, A. Markowitz, E. Maros, A. Marquina, S. Marsat, F. Martelli, I. W. Martin, R. M. Martin, M. Martinez, V. A. Martinez, V. Martinez, K. Martinovic, D. V. Martynov, E. J. Marx, H. Masalehdan, K. Mason, E. Massera, A. Masserot, T. J. Massinger, M. Masso-Reid, S. Mastrogiovanni, A. Matas, M. Mateu-Lucena, F. Matichard, M. Matiushechkina, N. Mavalvala, J. J. McCann, R. McCarthy, D. E. McClelland, P. K. McClincy, S. McCormick, L. McCuller, G. I. McGhee, S. C. McGuire, C. McIsaac, J. McIver, T. McRae, S. T. McWilliams, D. Meacher, M. Mehmet, A. K. Mehta, Q. Meijer, A. Melatos, D. A. Melchor, G. Mendell, A. Menendez-Vazquez, C. S. Menoni, R. A. Mercer, L. Mereni, K. Merfeld, E. L. Merilh, J. D. Merritt, M. Merzougui, S. Meshkov, C. Messenger, C. Messick, P. M. Meyers, F. Meylahn, A. Mhaske, A. Miani, H. Miao, I. Michaloliakos, C. Michel, Y. Michimura, H. Middleton, L. Milano, A. L. Miller, A. Miller, B. Miller, S. Miller, M. Millhouse, J. C. Mills, E. Milotti, O. Minazzoli, Y. Minenkov, N. Mio, L. M. Mir, M. Miravet-Tenés, C. Mishra, T. Mishra, T. Mistry, S. Mitra, V. P. Mitrofanov, G. Mitselmakher, R. Mittleman, O. Miyakawa, A. Miyamoto, Y. Miyazaki, K. Miyo, S. Miyoki, G. Mo, E. Moguel, K. Mogushi, S. R. P. Mohapatra, S. R. Mohite, I. Molina, M. Molina-Ruiz, M. Mondin, M. Montani, C. J. Moore, D. Moraru, F. Morawski, A. More, C. Moreno, G. Moreno, Y. Mori, S. Morisaki, Y. Moriwaki, B. Mours, C. M. Mow-Lowry, S. Mozzon, F. Muciaccia, A. Mukherjee, D. Mukherjee, S. Mukherjee, S. Mukherjee, S. Mukherjee, N. Mukund, A. Mullavey, J. Munch, E. A. Muñiz, P. G. Murray, R. Musenich, S. Muusse, S. L. Nadji, K. Nagano, S. Nagano, A. Nagar, K. Nakamura, H. Nakano, M. Nakano, R. Nakashima, Y. Nakayama, V. Napolano, I. Nardecchia, T. Narikawa, L. Naticchioni, B. Nayak, R. K. Nayak, R. Negishi, B. F. Neil, J. Neilson, G. Nelemans, T. J. N. Nelson, M. Nery, P. Neubauer, A. Neunzert, K. Y. Ng, S. W. S. Ng, C. Nguyen, P. Nguyen, T. Nguyen, L. Nguyen Quynh, W. T. Ni, S. A. Nichols, A. Nishizawa, S. Nissanke, E. Nitoglia, F. Nocera, M. Norman, C. North, S. Nozaki, L. K. Nuttall, J. Oberling, B. D. O'Brien, Y. Obuchi, J. O'Dell, E. Oelker, W. Ogaki, G. Oganesyan, J. J. Oh, K. Oh, S. H. Oh, M. Ohashi, N. Ohishi, M. Ohkawa, F. Ohme, H. Ohta, M. A. Okada, Y. Okutani, K. Okutomi, C. Olivetto, K. Oohara, C. Ooi, R. Oram, B. O'Reilly, R. G. Ormiston, N. D. Ormsby, L. F. Ortega, R. O'Shaughnessy, E. O'Shea, S. Oshino, S. Ossokine, C. Osthelder, S. Otabe, D. J. Ottaway, H. Overmier, A. E. Pace, G. Pagano, M. A. Page, G. Pagliaroli, A. Pai, S. A. Pai, J. R. Palamos, O. Palashov, C. Palomba, H. Pan, K. Pan, P. K. Panda, H. Pang, P. T. H. Pang, C. Pankow, F. Pannarale, B. C. Pant, F. H. Panther, F. Paoletti, A. Paoli, A. Paolone, A. Parisi, H. Park, J. Park, W. Parker, D. Pascucci, A. Pasqualetti, R. Passaquieti, D. Passuello, M. Patel, M. Pathak, B. Patricelli, A. S. Patron, S. Paul, E. Payne, M. Pedraza, M. Pegoraro, A. Pele, F. E. Peña Arellano, S. Penn, A. Perego, A. Pereira, T. Pereira, C. J. Perez, C. Périgois, C. C. Perkins, A. Perreca, S. Perriès, J. Petermann, D. Petterson, H. P. Pfeiffer, K. A. Pham, K. S. Phukon, O. J. Piccinni, M. Pichot, M. Piendibene, F. Piergiovanni, L. Pierini, V. Pierro, G. Pillant, M. Pillas, F. Pilo, L. Pinard, I. M. Pinto, M. Pinto, K. Piotrzkowski, M. Pirello, M. D. Pitkin, E. Placidi, L. Planas, W. Plastino, C. Pluchar, R. Poggiani, E. Polini, D. Y. T. Pong, S. Ponrathnam, P. Popolizio, E. K. Porter, R. Poulton, J. Powell, M. Pracchia, T. Pradier, A. K. Prajapati, K. Prasai, R. Prasanna, G. Pratten, M. Principe, G. A. Prodi, L. Prokhorov, P. Prosposito, L. Prudenzi, A. Puecher, M. Punturo, F. Puosi, P. Puppo, M. Pürrer, H. Qi, V. Quetschke, R. Quitzow-James, F. J. Raab, G. Raaijmakers, H. Radkins, N. Radulesco, P. Raffai, S. X. Rail, S. Raja, C. Rajan, K. E. Ramirez, T. D. Ramirez, A. Ramos-Buades, J. Rana, P. Rapagnani,

U. D. Rapol, A. Ray, V. Raymond, N. Raza, M. Razzano, J. Read, L. A. Rees, T. Regimbau, L. Rei, S. Reid, S. W. Reid, D. H. Reitze, P. Relton, A. Renzini, P. Rettegno, M. Rezac, F. Ricci, D. Richards, J. W. Richardson, L. Richardson, G. Riemenschneider, K. Riles, S. Rinaldi, K. Rink, M. Rizzo, N. A. Robertson, R. Robie, F. Robinet, A. Rocchi, S. Rodriguez, L. Rolland, J. G. Rollins, M. Romanelli, R. Romano, C. L. Romel, A. Romero-Rodríguez, I. M. Romero-Shaw, J. H. Romie, S. Ronchini, L. Rosa, C. A. Rose, D. Rosińska, M. P. Ross, S. Rowan, S. J. Rowlinson, S. Roy, S. Roy, S. Roy, D. Rozza, P. Ruggi, K. Ryan, S. Sachdev, T. Sadecki, J. Sadiq, N. Sago, S. Saito, Y. Saito, K. Sakai, Y. Sakai, M. Sakellariadou, Y. Sakuno, O. S. Salafia, L. Salconi, M. Saleem, F. Salemi, A. Samajdar, E. J. Sanchez, J. H. Sanchez, L. E. Sanchez, N. Sanchis-Gual, J. R. Sanders, A. Sanuy, T. R. Saravanan, N. Sarin, B. Sassolas, H. Satari, B. S. Sathyaprakash, S. Sato, T. Sato, O. Sauter, R. L. Savage, T. Sawada, D. Sawant, H. L. Sawant, S. Sayah, D. Schaetzl, M. Scheel, J. Scheuer, M. Schiworski, P. Schmidt, S. Schmidt, R. Schnabel, M. Schneewind, R. M. S. Schofield, A. Schönbeck, B. W. Schulte, B. F. Schutz, E. Schwartz, J. Scott, S. M. Scott, M. Seglar-Arroyo, T. Sekiguchi, Y. Sekiguchi, D. Sellers, A. S. Sengupta, D. Sentenac, E. G. Seo, V. Sequino, A. Sergeev, Y. Setyawati, T. Shaffer, M. S. Shahriar, B. Shams, L. Shao, A. Sharma, P. Sharma, P. Shawhan, N. S. Shcheblanov, S. Shibagaki, M. Shikauchi, R. Shimizu, T. Shimoda, K. Shimode, H. Shinkai, T. Shishido, A. Shoda, D. H. Shoemaker, D. M. Shoemaker, S. ShyamSundar, M. Sieniawska, D. Sigg, L. P. Singer, D. Singh, N. Singh, A. Singha, A. M. Sintes, V. Sipala, V. Skliris, B. J. J. Slagmolen, T. J. Slaven-Blair, J. Smetana, J. R. Smith, R. J. E. Smith, J. Soldateschi, S. N. Somala, K. Somiya, E. J. Son, K. Soni, S. Soni, V. Sordini, F. Sorrentino, N. Sorrentino, H. Sotani, R. Soulard, T. Souradeep, E. Sowell, V. Spagnuolo, A. P. Spencer, M. Spera, R. Srinivasan, A. K. Srivastava, V. Srivastava, K. Staats, C. Stachie, D. A. Steer, J. Steinlechner, S. Steinlechner, D. J. Stops, M. Stover, K. A. Strain, L. C. Strang, G. Stratta, A. Strunk, R. Sturani, A. L. Stuver, S. Sudhagar, V. Sudhir, R. Sugimoto, H. G. Suh, T. Z. Summerscales, H. Sun, L. Sun, S. Sunil, A. Sur, J. Suresh, P. J. Sutton, T. Suzuki, T. Suzuki, B. L. Swinkels, M. J. Szczepańczyk, P. Szewczyk, M. Tacca, H. Tagoshi, S. C. Tait, H. Takahashi, R. Takahashi, A. Takamori, S. Takano, H. Takeda, M. Takeda, C. J. Talbot, C. Talbot, H. Tanaka, K. Tanaka, K. Tanaka, T. Tanaka, T. Tanaka, A. J. Tanasijczuk, S. Tanioka, D. B. Tanner, D. Tao, L. Tao, E. N. Tapia San Martín, C. Taranto, J. D. Tasson, S. Telada, R. Tenorio, J. E. Terhune, L. Terkowski, M. P. Thirugnanasambandam, M. Thomas, P. Thomas, J. E. Thompson, S. R. Thondapu, K. A. Thorne, E. Thrane, S. Tiwari, S. Tiwari, V. Tiwari, A. M. Toivonen, K. Toland, A. E. Tolley, T. Tomaru, Y. Tomigami, T. Tomura, M. Tonelli, A. Torres-Forné, C. I. Torrie, I. Tosta e Melo, D. Töyrä, A. Trapananti, F. Travasso, G. Traylor, M. Trevor, M. C. Tringali, A. Tripathee, L. Troiano, A. Trovato, L. Trozzo, R. J. Trudeau, D. S. Tsai, D. Tsai, K. W. Tsang, T. Tsang, J.-S. Tsao, M. Tse, R. Tso, K. Tsubono, S. Tsuchida, L. Tsukada, D. Tsuna, T. Tsutsui, T. Tsuzuki, K. Turbang, M. Turconi, D. Tuyenbayev, A. S. Ubhi, N. Uchikata, T. Uchiyama, R. P. Udall, A. Ueda, T. Uehara, K. Ueno, G. Ueshima, C. S. Unnikrishnan, F. Uraguchi, A. L. Urban, T. Ushiba, A. Utina, H. Vahlbruch, G. Vajente, A. Vajpeyi, G. Valdes, M. Valentini, V. Valsan, N. van Bakel, M. van Beuzekom, J. F. J. van den Brand, C. Van Den Broeck, D. C. Vander-Hyde, L. van der Schaaf, J. V. van Heijningen,

J. Vanosky, M. H. P. M. van Putten, N. van Remortel, M. Vardaro, A. F. Vargas, V. Varma, M. Vasúth, A. Vecchio, G. Vedovato, J. Veitch, P. J. Veitch, J. Venneberg, G. Venugopalan, D. Verkindt, P. Verma, Y. Verma, D. Veske, F. Vetrano, A. Viceré, S. Vidyant, A. D. Viets, A. Vijaykumar, V. Villa-Ortega, J. Y. Vinet, A. Virtuoso, S. Vitale, T. Vo, H. Vocca, E. R. G. von Reis, J. S. A. von Wrangel, C. Vorvick, S. P. Vyatchanin, L. E. Wade, M. Wade, K. J. Wagner, R. C. Walet, M. Walker, G. S. Wallace, L. Wallace, S. Walsh, J. Wang, J. Z. Wang, W. H. Wang, R. L. Ward, J. Warner, M. Was, T. Washimi, N. Y. Washington, J. Watchi, B. Weaver, S. A. Webster, M. Weinert, A. J. Weinstein, R. Weiss, C. M. Weller, F. Wellmann, L. Wen, P. Weßels, K. Wette, J. T. Whelan, D. D. White, B. F. Whiting, C. Whittle, D. Wilken, D. Williams, M. J. Williams, A. R. Williamson, J. L. Willis, B. Willke, D. J. Wilson, W. Winkler, C. C. Wipf, T. Wlodarczyk, G. Woan, J. Woehler, J. K. Wofford, I. C. F. Wong, C. Wu, D. S. Wu, H. Wu, S. Wu, D. M. Wysocki, L. Xiao, W.-R. Xu, T. Yamada, H. Yamamoto, K. Yamamoto, K. Yamamoto, T. Yamamoto, K. Yamashita, R. Yamazaki, F. W. Yang, L. Yang, Y. Yang, Y. Yang, Z. Yang, M. J. Yap, D. W. Yeeles, A. B. Yelikar, M. Ying, K. Yokogawa, J. Yokoyama, T. Yokozawa, J. Yoo, T. Yoshioka, H. Yu, H. Yu, H. Yuzurihara, A. Zadrożny, M. Zanolin, S. Zeidler, T. Zelenova, J. P. Zendri, M. Zevin, M. Zhan, H. Zhang, J. Zhang, L. Zhang, T. Zhang, Y. Zhang, C. Zhao, G. Zhao, Y. Zhao, Y. Zhao, R. Zhou, Z. Zhou, X. J. Zhu, Z. H. Zhu, A. B. Zimmerman, Y. Zlochower, M. E. Zucker and J. Zweizig, "The population of merging compact binaries inferred using gravitational waves through GWTC-3", arXiv e-prints p. arXiv:2111.03634 (2021b).

Thomas, H.-C., "Sternentwicklung VIII. Der Helium-Flash bei einem Stern von 1. 3 Sonnenmassen", *Zeitschrift fuer Astrophysik* **67**, 420 (1967).

Thompson, T. A., C. S. Kochanek, K. Z. Stanek, C. Badenes, R. S. Post, T. Jayasinghe, D. W. Latham, A. Bieryla, G. A. Esquerdo, P. Berlind, M. L. Calkins, J. Tayar, L. Lindegren, J. A. Johnson, T. W. S. Holoien, K. Auchettl and K. Covey, "A noninteracting low-mass black hole-giant star binary system", Science **366**, 6465, 637–640 (2019).

Thoul, A. A., J. N. Bahcall and A. Loeb, "Element Diffusion in the Solar Interior", *ApJ* **421**, 828 (1994).

Timmes, F. X., E. F. Brown and J. W. Truran, "On Variations in the Peak Luminosity of Type Ia Supernovae", *ApJ* **590**, L83–L86 (2003).

Timmes, F. X. and F. D. Swesty, "The Accuracy, Consistency, and Speed of an Electron-Positron Equation of State Based on Table Interpolation of the Helmholtz Free Energy", *ApJS* **126**, 501–516 (2000).

Timmes, F. X., R. H. D. Townsend, E. B. Bauer, A. Thoul, C. E. Fields and W. M. Wolf, "The Impact of White Dwarf Luminosity Profiles on Oscillation Frequencies", *ApJ* **867**, L30 (2018a).

Timmes, F. X., R. H. D. Townsend, E. B. Bauer, A. Thoul, C. E. Fields and W. M. Wolf, "The Impact of White Dwarf Luminosity Profiles on Oscillation Frequencies", *ApJ* **867**, L30 (2018b).

Timmes, F. X., S. E. Woosley and R. E. Taam, “The conductive propagation of nuclear flames. II: Convectively bounded flames in C + O and O + NE + MG cores”, *ApJ* **420**, 348–363 (1994).

Timmes, F. X., S. E. Woosley and T. A. Weaver, “The Neutron Star and Black Hole Initial Mass Function”, *ApJ* **457**, 834–+ (1996).

Tompkins, S., R. Windhorst, P. Young and F. X. Timmes, “CNO Cycle Burning in Ultra-low Metallicity Solar Mass Stars”, Research Notes of the American Astronomical Society **4**, 9, 172 (2020).

Toro, E. F., M. Spruce and W. Speares, “Restoration of the contact surface in the HLL-Riemann solver”, Shock Waves **4**, 1, 25–34 (1994).

Townsley, D. M., A. P. Jackson, A. C. Calder, D. A. Chamulak, E. F. Brown and F. X. Timmes, “Evaluating Systematic Dependencies of Type Ia Supernovae: The Influence of Progenitor ^{22}Ne Content on Dynamics”, *ApJ* **701**, 1582–1604 (2009).

Uchida, H., M. Shibata, K. Takahashi and T. Yoshida, “Black Hole Formation and Explosion from Rapidly Rotating Very Massive Stars”, *ApJ* **870**, 2, 98 (2019).

Uribe Suárez, J. D. and J. A. Rueda Hernandez, “Neutrino oscillations in a neutrino-dominated accretion disk around a Kerr BH”, arXiv e-prints p. arXiv:1909.01841 (2019).

van Horn, H. M., “Cooling of White Dwarfs”, in “White Dwarfs”, edited by W. J. Luyten, vol. 42 of *IAU Symposium*, p. 97 (Dordrecht: Springer, 1971).

van Son, L. A. C., S. E. De Mink, F. S. Broekgaarden, M. Renzo, S. Justham, E. Laplace, J. Morán-Fraile, D. D. Hendriks and R. Farmer, “Polluting the Pair-instability Mass Gap for Binary Black Holes through Super-Eddington Accretion in Isolated Binaries”, *ApJ* **897**, 1, 100 (2020).

Vandenberg, D. A., “Star clusters and stellar evolution. I. Improved synthetic color-magnitude diagrams for the oldest clusters.”, *ApJS* **51**, 29–66 (1983).

VandenBerg, D. A., L. Casagrande and B. Edvardsson, “Models for metal-poor stars with different initial abundances of C, N, O, Mg, and Si. II. Application to the colour-magnitude diagrams of the globular clusters 47 Tuc, NGC 6362, M 5, M 3, M 55, and M92”, *MNRAS* **509**, 3, 4208–4228 (2022).

Vartanyan, D., A. Burrows, D. Radice, M. A. Skinner and J. Dolence, “Revival of the fittest: exploding core-collapse supernovae from 12 to 25 $M_\odot$”, *MNRAS* **477**, 3091–3108 (2018).

Vila, S. C., “Pre-White-Dwarf Evolution. I”, *ApJ* **146**, 437 (1966).

Villante, F. L., A. M. Serenelli, F. Delahaye and M. H. Pinsonneault, “The Chemical Composition of the Sun from Helioseismic and Solar Neutrino Data”, *ApJ* **787**, 1, 13 (2014).

Vink, J. S., A. de Koter and H. J. G. L. M. Lamers, "Mass-loss predictions for O and B stars as a function of metallicity", *A&A* **369**, 574–588 (2001).

Vink, J. S., A. Heger, M. R. Krumholz, J. Puls, S. Banerjee, N. Castro, K. J. Chen, A. N. Chenè, P. A. Crowther, A. Daminelli, G. Gräfener, J. H. Groh, W. R. Hamann, S. Heap, A. Herrero, L. Kaper, F. Najarro, L. M. Oskinova, A. Roman-Lopes, A. Rosen, A. Sander, M. Shirazi, Y. Sugawara, F. Tramper, D. Vanbeveren, R. Voss, A. Wofford and Y. Zhang, "Very Massive Stars in the local Universe", Highlights of Astronomy **16**, 51–79 (2015).

Vink, J. S., E. R. Higgins, A. A. C. Sander and G. N. Sabhahit, "Maximum black hole mass across cosmic time", *MNRAS* **504**, 1, 146–154 (2021).

Vinyoles, N., A. M. Serenelli, F. L. Villante, S. Basu, J. Bergström, M. C. Gonzalez-Garcia, M. Maltoni, C. Peña-Garay and N. Song, "A New Generation of Standard Solar Models", *ApJ* **835**, 2, 202 (2017).

Vishniac, E. T., "Editorial: On the Use of Chatbots in Writing Scientific Manuscripts", in "Bulletin of the American Astronomical Society", vol. 55, p. 016 (2023).

Vogel, P. and J. F. Beacom, "Angular distribution of neutron inverse beta decay, ν_e+p–>e$^+$+n", *Phys. Rev. D.* **60**, 5, 053003 (1999).

Wang, B., D. Liu and H. Chen, "Formation of millisecond pulsars with long orbital periods by accretion-induced collapse of white dwarfs", *MNRAS* **510**, 4, 6011–6021 (2022).

Wang, H., A. P. Stephan, S. Naoz, B.-M. Hoang and K. Breivik, "Gravitational-wave Signatures from Compact Object Binaries in the Galactic Center", *ApJ* **917**, 2, 76 (2021).

Wang, S. and X. Chen, "3D Parameter Maps of Red Clump Stars in the Milky Way: Absolute Magnitudes and Intrinsic Colors", *ApJ* **923**, 2, 145 (2021).

Weaver, T. A. and S. E. Woosley, "Nucleosynthesis in massive stars and the ^{12}C(α, γ)^{16}O reaction rate", *Phys. Reports* **227**, 65–96 (1993).

Weiss, A., S. Cassisi, H. Schlattl and M. Salaris, "Evolution of Low-Mass Metal-Free Stars including Effects of Diffusion and External Pollution", *ApJ* **533**, 1, 413–423 (2000).

West, C., A. Heger and S. M. Austin, "The Impact of Helium-burning Reaction Rates on Massive Star Evolution and Nucleosynthesis", *ApJ* **769**, 2 (2013).

Wiescher, M., R. J. deBoer and J. Görres, "The resonances in the ^{22}Ne+α fusion reactions", European Physical Journal A **59**, 1, 11 (2023).

Wiescher, M., J. Gorres, S. Graff, L. Buchmann and F. K. Thielemann, "The Hot Proton-Proton Chains in Low-Metallicity Objects", *ApJ* **343**, 352 (1989).

Wiescher, M., J. Görres, E. Uberseder, G. Imbriani and M. Pignatari, "The Cold and Hot CNO Cycles", Annual Review of Nuclear and Particle Science **60**, 381–404 (2010).

Winget, D. E., D. J. Sullivan, T. S. Metcalfe, S. D. Kawaler and M. H. Montgomery, "A Strong Test of Electroweak Theory Using Pulsating DB White Dwarf Stars as Plasmon Neutrino Detectors", *ApJ* **602**, L109–L112 (2004).

Winter, W. and C. Lunardini, "Time-dependent interpretation of the neutrino emission from Tidal Disruption Events", arXiv e-prints p. arXiv:2205.11538 (2022).

Woosley, S. E., "Pulsational Pair-instability Supernovae", *ApJ* **836**, 244 (2017).

Woosley, S. E., "The Evolution of Massive Helium Stars, Including Mass Loss", *ApJ* **878**, 1, 49 (2019).

Woosley, S. E., D. H. Hartmann, R. D. Hoffman and W. C. Haxton, "The nu-process", *ApJ* **356**, 272–301 (1990).

Woosley, S. E. and A. Heger, "The Remarkable Deaths of 9-11 Solar Mass Stars", *ApJ* **810**, 1, 34 (2015).

Woosley, S. E. and A. Heger, "The Pair-instability Mass Gap for Black Holes", *ApJ* **912**, 2, L31 (2021).

Woosley, S. E., A. Heger and T. A. Weaver, "The evolution and explosion of massive stars", Rev. Mod. Phys. **74**, 1015–1071, URL `http://link.aps.org/doi/10.1103/RevModPhys.74.1015` (2002).

Woosley, S. E. and T. A. Weaver, "The physics of supernova explosions", *ARA&A* **24**, 205–253 (1986).

Wu, S. C. and J. Fuller, "Wave-driven Outbursts and Variability of Low-mass Supernova Progenitors", *ApJ* **930**, 2, 119 (2022).

Wyrzykowski, Ł. and I. Mandel, "Constraining the masses of microlensing black holes and the mass gap with Gaia DR2", *A&A* **636**, A20 (2020).

Xu, H. Y. and Y. Li, "Blue loops of intermediate mass stars . I. CNO cycles and blue loops", *A&A* **418**, 213–224 (2004).

Yang, Y., V. Gayathri, I. Bartos, Z. Haiman, M. Safarzadeh and H. Tagawa, "Black Hole Formation in the Lower Mass Gap through Mergers and Accretion in AGN Disks", *ApJ* **901**, 2, L34 (2020).

Yang, Y. and JUNO Collaboration, "Status of the Jiangmen Underground Neutrino Observatory", Nuclear Instruments and Methods in Physics Research A **1042**, 167435 (2022).

Ye, C. and M. Fishbach, "Inferring the neutron star maximum mass and lower mass gap in neutron star-black hole systems with spin", arXiv e-prints p. arXiv:2202.05164 (2022).

Yoshida, T., H. Umeda, K. Maeda and T. Ishii, "Mass ejection by pulsational pair instability in very massive stars and implications for luminous supernovae", *MNRAS* **457**, 351–361 (2016).

Young, P. A., *Stellar Composition, Structure and Evolution: Impact on Habitability*, pp. 1–22 (Springer International Publishing, 2018), URL `https://doi.org/10.1007/978-3-319-30648-3_60-1`.

Zapartas, E., M. Renzo, T. Fragos, A. Dotter, J. J. Andrews, S. S. Bavera, S. Coughlin, D. Misra, K. Kovlakas, J. Román-Garza, J. G. Serra, Y. Qin, K. A. Rocha, N. H. Tran and Z. P. Xing, "Revisiting the explodability of single massive star progenitors of stripped-envelope supernovae", *A&A* **656**, L19 (2021).

Zevin, M., S. S. Bavera, C. P. L. Berry, V. Kalogera, T. Fragos, P. Marchant, C. L. Rodriguez, F. Antonini, D. E. Holz and C. Pankow, "One Channel to Rule Them All? Constraining the Origins of Binary Black Holes Using Multiple Formation Pathways", *ApJ* **910**, 2, 152 (2021).

Zevin, M., M. Spera, C. P. L. Berry and V. Kalogera, "Exploring the Lower Mass Gap and Unequal Mass Regime in Compact Binary Evolution", *ApJ* **899**, 1, L1 (2020).

Zhang, Q.-S., Y. Li and J. Christensen-Dalsgaard, "Solar Models with Convective Overshoot, Solar-wind Mass Loss, and PMS Disk Accretion: Helioseismic Quantities, Li Depletion, and Neutrino Fluxes", *ApJ* **881**, 2, 103 (2019).

Zhang, W., S. E. Woosley and A. Heger, "Fallback and Black Hole Production in Massive Stars", *ApJ* **679**, 639–654 (2008).

Zhao, L., H. Song, G. Meynet, A. Maeder, S. Ekström, R. Zhang, Y. Qin, S. Qi and Q. Zhan, "The evolutionary properties of the blue loop under the influence of rapid rotation and low metallicity", *A&A* **674**, A92 (2023).

Zickefoose, J., A. Di Leva, F. Strieder, L. Gialanella, G. Imbriani, N. De Cesare, C. Rolfs, J. Schweitzer, T. Spillane, O. Straniero and F. Terrasi, "Measurement of the ^{12}C(^{12}C,p)^{23}Na cross section near the Gamow energy", *Phys. Rev. C.* **97**, 6, 065806 (2018).